INFORMATION TO USERS

This manuscript has been reproduced from the microfilm master. UMI films the text directly from the original or copy submitted. Thus, some thesis and dissertation copies are in typewriter face, while others may be from any type of computer printer.

The quality of this reproduction is dependent upon the quality of the copy submitted. Broken or indistinct print, colored or poor quality illustrations and photographs, print bleedthrough, substandard margins, and improper alignment can adversely affect reproduction.

In the unlikely event that the author did not send UMI a complete manuscript and there are missing pages, these will be noted. Also, if unauthorized copyright material had to be removed, a note will indicate the deletion.

Oversize materials (e.g., maps, drawings, charts) are reproduced by sectioning the original, beginning at the upper left-hand corner and continuing from left to right in equal sections with small overlaps.

ProQuest Information and Learning
300 North Zeeb Road, Ann Arbor, MI 48106-1346 USA
800-521-0600

TERNARY PHASE DIAGRAMS INVOLVING III-V ALLOYS

by

Michel F. Gratton

Submitted to the School of Graduate Studies in partial fulfillment of the requirements for the degree of Ph.D. in Physics.

University of Ottawa,
Department of Physics,
Ottawa, Canada,

1978.

"They laughed at Fulton...."

Abstract

Ingots of $GaAs_ySb_{1-y}$ alloys have been prepared by various directional freezing techniques, the rate of freezing being kept sufficiently small (e.g. $\sim$ 0.5cm/day) that equilibrium conditions were obtained in cross-sectional slices. Samples from these slices have then been investigated by powder X-ray photographs and an X-ray fluorescence technique to determine the variation of lattice parameter with composition and the range of single phase solid solution. The results show that this system has a solid miscibility gap of maximum range $0.38 < y < 0.61$ and that this corresponds to a peritectic reaction. In the range $0 < y < 0.38$ the lattice parameter a_o follows the Vegard line, but for $0.61 < y < 1.00$ a_o lies below this line. By annealing samples in the liquid-solid two-phase fields, data have also been obtained on the solidus curve and the peritectic temperature has been shown to be 745 ± 5C.

Solidus isotherms and isoconcentration lines have been experimentally determined for the Ga-In-Sb ternary diagram by means of the technique of annealing samples in the two-phase liquid-solid field and quenching, a method shown previously to give good results for the pseudobinary section. The results are compared with data predicted by the simple solution model. In this analysis, the linear

temperature dependence of the interaction parameters α_{Ga-Sb}, α_{In-Sb}, α_{Ga-In} and $\alpha_{GaSb-InSb}$ has been examined and also the effect on the predicted data of variation in the values of these parameters. It is shown that while the model can give values of liquidus isotherms in good agreement with the available experimental data, the predicted solidus isotherms and isoconcentration lines are very different from the experimental data. No reasonable variation of the α parameters can eliminate this latter discrepancy and it is seen that in the case of this particular ternary system the simple solution model is of no value for prediction of solidus data.

Tie-lines, boundaries of three-phase fields, range of immiscibility of the solid solutions, details of the liquidus sheet have been experimentally determined for the Ga-As-Sb ternary diagram again by means of the technique of annealing and quenching. Samples were annealed to equilibrium in either two-phase liquid-solid fields or three-phase liquid-solid-solid fields then quenched in order to freeze in the solid phase(s) in equilibrium in the solution. The results are compared with the predictions of the simple solution model which is successful in predicting a peritectic behaviour for the pseudobinary section of the diagram. The interaction parameters are treated as linearly dependent on temperature except for $\alpha_{GaAs-GaSb}$ found to be constant. The model shows reasonable agreement with the few

liquidus data available but fails to reproduce the measured range of the miscibility gap except at the peritectic temperature. No variation of the interaction parameters could bring the theoretical predictions in line with the experimental solidus data.

The solid-solid interaction parameters were then tested for a dependence on solidus composition but this latter analysis showed that if any success is to be obtained here, those interaction parameters would have to depend on both the temperature and the solidus composition and in no simple manner.

Originality

To the knowledge of the author, the following aspects of this thesis represent original work performed in the Department of Physics at the University of Ottawa.

The experimental determination of a miscibility gap in the range of solid solutions of the alloy system $GaAs_ySb_{1-y}$. The investigations were carried out on samples with compositions on the pseudobinary section $GaAs_ySb_{1-y}$ as well as off that section of the ternary system Ga-As-Sb. The experimental technique was that of annealing samples to equilibrium, then quenching to freeze in the solid phase in equilibrium.

An energy dispersive X-ray analysis (fluorescence) was used to determine the range of single phase solid solution for $GaAs_ySb_{1-y}$ and investigate the variation of lattice parameter with composition. A departure from Vegard's law was established for the GaAs-rich end of the composition range.

The verification of a peritectic behaviour for $GaAs_ySb_{1-y}$ and the preparation of an ingot from the melt by very slow step-freeze in order to show the abrupt change in composition due to such a peritectic behaviour.

The technique of anneal and quench was also used to characterize the phase diagrams of two ternary systems: Ga-In-Sb and Ga-As-Sb. The investigations were centered on the determination of isothermal sections: tie-lines, boundaries of three-phase fields, solidus isotherms and isoconcentration lines and details of the liquidus sheet.

The simple solution model was used for the theoretical treatment of the data. The emphasis was put on the evaluation of the interaction parameters:

a) the temperature dependence of α_{Ga-Sb}, α_{In-Sb} and α_{Ga-As} was redetermined

b) the parameters $\alpha_{III-III'}$, $\alpha_{V-V'}$ and $\alpha_{III,V-III,V'}$ were taken as linearly dependent of temperature

c) the solid-solid interaction parameters were tested for a solidus composition dependence with the experimental solidus data collected.

Acknowledgements

The constant encouragement and suggestions of Dr. J. C. Woolley have been instrumental in the completion of this research project.

The atmosphere provided by the members of this department, especially Dr. S. D. Rosenbaum for supplying alloy material and passing on his techniques regarding crystal growth, and Dr. R. Boyer for assisting in the development of the computer programme was greatly appreciated.

The cooperation of the workshop staff and especially Mr. J. R. Hart for attending to the various furnaces throughout this work was most helpful.

The financial support was provided by the National Research Council of Canada and the Defence Research Board of Canada, in the form of research grants to Dr. Woolley, and by the Government of Ontario through an Ontario Graduate Fellowship (1974-75).

The manuscript has been typed by Mrs. Loretta T. Leroux.

To those mentioned here, the author expresses his deepest gratitude.

Table of Contents

Abstract		iii
Originality		vi
Acknowledgements		viii
Table of Contents		ix
List of Figures		xi
List of Tables		xviii
Chapter 1	Introduction	1
Chapter 2	Properties of the crystals from the Group III and Group V elements	4
Chapter 3	The III-V pseudobinary system $GaAs_ySb_{1-y}$	28
Chapter 4	Equilibrium diagram: general principles	64
Chapter 5	Theoretical model for III-V ternary systems	86
Chapter 6	Thermodynamic data for the III-V ternary systems Ga-In-Sb and Ga-As-Sb	123
Chapter 7	Phase diagram of the ternary system Ga-In-Sb	145
Chapter 8	Phase diagram of the pseudobinary system $GaAs_ySb_{1-y}$	176
Chapter 9	Theoretical analysis of the ternary system Ga-As-Sb	185

Chapter 10	Experimental investigation of the ternary system Ga-As-Sb	204
Chapter 11	Recent developments and suggestions	226
Chapter 12	Summary	237
Appendix A	Experimental techniques	240
Appendix B	Derivation of Vieland's equation for liquid-solid equilibrium	250
References		257

List of Figures

2-1	Orientation of the base triangle in two interpenetrating tetrahedra.	8
2-2	Zinc-blende lattice.	9
2-3	Zinc-blende lattice observed perpendicular to a [111] -axis and along a [110]- axis.	10
2-4	Occurrence of constitutional supercooling.	20
2-5	Variation of lattice constant with composition for three III-V ternary alloy systems.	24
2-6	Ingot profile of $Ga_xIn_{1-x}Sb$ grown from the horizontal Bridgman technique.	25
2-7	Ingot profile of $InAs_ySb_{1-y}$ grown from the horizontal Bridgman technique.	25
2-8	Ingot profile of $InAs_ySb_{1-y}$ grown from the sequential growth technique.	25
3-1	Ingot profile of $GaAs_ySb_{1-y}$ grown from a step-freeze technique.	34
3-2	Ingot profile of $GaAs_ySb_{1-y}$ grown from a travelling zone technique.	34
3-3	Ingot profile of $GaAs_ySb_{1-y}$ grown from a travelling zone and sequential growth technique.	35
3-4	Ingot profile of $GaAs_ySb_{1-y}$ grown from a travelling zone and sequential growth technique.	35

3-5a	Side view of X-ray fluorescence excitor and detector assembly.	37
3-5b	Side view of sample and source.	38
3-6	Block diagram of detection system.	38
3-7	Typical spectra a) $GaAs_{0.1}Sb_{0.9}$, b) $GaAs_{0.6}Sb_{0.4}$	43
3-8	Spectrum identifying all peaks present.	45
3-9	Typical computer fit of a peak.	48
3-10	Noise and backscattering for no sample.	48
3-11	Noise and backscattering for Si.	49
3-12	Noise and backscattering for H_2O.	50
3-13	$GaAs_ySb_{1-y}$ system. Calibration curves for X-ray fluorescence analysis.	52
3-14	$GaAs_ySb_{1-y}$ - variation of lattice parameter as a function of composition.	56
3-15 a,b	Cross-sectional slice showing the sharp boundary between GaAs-rich and GaSb-rich material.	60
3-16 a,b	Ingot TFF-73-1 showing the sharp change of phase.	60
3-17 a,b	The two faces of a slice from ingot TFF-73-1 showing the sharp boundary.	60
3-18	$GaAs_ySb_{1-y}$ - representation of the limits of the miscibility gap on the pseudobinary section.	63

4-1	Simple hypothetical binary system for two elements A and B.	67
4-2	Hypothetical binary system with closed miscibility gap at low temperatures.	69
4-3	Simple eutectic system.	70
4-4	Simple peritectic system.	70
4-5	Forms of free energy vs. composition curves for two elements with the same crystal structure.	73
4-6	Form of an equilibrium diagram related to the effect of temperature on the free energy curves.	74
4-7	Geometrical construction inside an equilateral triangle.	75
4-8	Corner of a three-dimensional equilibrium diagram showing two partial binary diagrams.	76
4-9	Pictorial view of a ternary system ABC.	77
4-10 a,b c,d	Isothermal sections of a ternary system ABC.	79
4-11	Isothermal section of a hypothetical ternary section WXZ.	83
4-12	Construction for finding the relative amounts of phases inside a three-phase triangle.	83

4-13	Isothermal section of a ternary system showing possible phase boundaries.	84
6-1	Binary phase diagram for the III-V compounds GaSb and InSb.	131
6-2	GaSb. Interaction parameter α_{Ga-Sb} as a function of temperature.	132
6-3	InSb. Interaction parameter α_{In-Sb} as a function of temperature.	135
6-4	Binary phase diagram for the III-V compound GaAs.	138
6-5	GaAs. Interaction parameter α_{Ga-As} as a function of temperature.	139
6-6	Binary phase diagram of the Gallium-Indium system.	142
6-7	Binary phase diagram of the Antimony-Arsenic system.	142
7-1	Phase diagram of pseudobinary system $Ga_xIn_{1-x}Sb$.	147
7-2	Liquidus isotherms and tie-lines of Ga-In-Sb; a) 380°C, b) 430°C.	143
7-3	Liquidus isotherms and tie-lines of Ga-In-Sb; a) 475°C, b) 525°C.	154
7-4	Liquidus isotherms and tie-lines of Ga-In-Sb; a) 550°C, b) 600°C.	155

7-5	The 650°C liquidus isotherm and tie-lines of Ga-In-Sb.	156
7-6	Three-dimensional representation of the phase diagram for Ga-In-Sb.	157
7-7	α_{Ga-In} vs. T.	161
7-8	$\alpha_{GaSb-InSb}$ vs. T.	162
7-9	Relationship between T and N_{Ga} from the theoretical analysis of Ga-In-Sb.	164
7-10	Liquidus isotherms in the Ga-In-Sb ternary phase diagram.	165
7-11	Variation of x_{solid} as a function of N_{Ga} from the theoretical analysis of Ga-In-Sb.	167
7-12	Solidus isotherms of the Ga-In-Sb system; a) 380°C, b) 430°C, c) 475°C, d) 525°C.	168
7-13	Solidus isotherms of the Ga-In-Sb system; a) 550°C, b) 600°C, c) 650°C.	169
7-14	Solidus isotherms of the Ga-In-Sb system; a) 300°C, b) 500°C.	171
7-15	Solidus isoconcentration lines in the Ga-In-Sb ternary phase diagram.	173
8-1	Phase diagram for the pseudobinary system $GaAs_ySb_{1-y}$.	181
9-1	α_{As-Sb} vs. T.	189

9-2	$\alpha_{GaAs-GaSb}$ vs. T.	190
9-3	Relationship between T and N_{As} from the theoretical analysis of Ga-As-Sb.	193
9-4	Theoretical liquidus isotherms in the Ga-As-Sb ternary phase diagram.	194
9-5	Theoretical liquidus isotherms for low temperatures in the Ga-As-Sb ternary phase diagram.	196
9-6	Theoretical solidus compositions vs. N_{As}.	198
9-7	Theoretical solidus compositions vs. N_{As} ($y < 0.50$).	199
9-8	Theoretical solidus compositions vs. N_{As} ($y > 0.50$).	200
9-9	Theoretical position of the cusp $0.10 \leq N_{Ga} \leq 0.50$.	202
9-10	Theoretical position of the cusp $0.55 \leq N_{Ga} \leq 1.0$.	203
10-1	Isothermal sections of the Ga-As-Sb system	
	a) $600^{\circ}C$	208
	b) $625^{\circ}C$	209
	c) $645^{\circ}C$	210
	d) $675^{\circ}C$	211
	e) $700^{\circ}C$	212

10-2	Relations between the GaSb-rich solid phase in equilibrium and the arsenic concentrations for constant values of the gallium concentration.	215
10-3	Phase diagram for the pseudobinary system $GaAs_ySb_{1-y}$.	220
10-4	Theoretical position of the cusp on the liquidus sheet of the Ga-As-Sb system.	223
11-1	$\alpha_{GaAs-GaSb}$ vs. y_{solid}.	235
11-2	$\alpha_{GaSb-InSb}$ vs. x_{solid}.	235
A-1	Annealing furnaces assemblies.	243
A-2	Section of a heating element.	243
A-3	Samples after initial melting.	246
A-4	'Necking' sequence of a quartz ampoule.	246
A-5	X-ray diffraction photograph of a sample of Ga-As-Sb.	246
A-6	Diagram representing the X-ray paths when asymmetry of low angle lines is observed.	248
A-7	Diagram showing the axis of the fiber displaced relative to the axis of rotation.	249
A-8	X-ray diffraction photograph of a sample of Ga-As-Sb.	246

List of Tables

2-I	Section of the periodic table describing elements of the groups III, IV and V respectively.	7
2-II	Lattice constants of four III-V binary compounds.	11
2-III	Temperatures of fusion of four III-V binary compounds.	13
3-I	X-ray fluorescence data.	46
3-II	List of samples used to determine the lattice constant-composition relation for the pseudo-binary system $GaAs_ySb_{1-y}$.	54
5-I	Quantities related to the various kinds of nearest neighbour pairs.	109
6-I	Entropies of fusion and temperatures of fusion of the binary compounds GaSb, InSb and GaAs.	125
6-II	Comparison of the two terms in ΔC_p and ΔS^F of Vieland's treatment.	128
6-III	Binary phase diagram data for GaSb and values of α_{Ga-Sb}.	130
6-IV	Binary phase diagram data for InSb and values of α_{In-Sb}.	134

6-V	Binary phase diagram data for GaAs and values of α_{Ga-As}.	137
6-VI	Various values of the interaction parameters of the binary compounds: GaSb, InSb and GaAs.	141
6-VII	Various values of the interaction parameters of the III-V systems: Ga-In, As-Sb, $Ga_xIn_{1-x}Sb$ and $GaAs_ySb_{1-y}$.	144
7-I	Experimental data for tie-lines and solidus isotherms of Ga-In-Sb.	152
7-II	Interaction parameters for the ternary system Ga-In-Sb.	160
8-I	Experimental solidus data for the pseudobinary system $GaAs_ySb_{1-y}$.	180
8-II	Experimental data for the determination of the miscibility gap in $GaAs_ySb_{1-y}$.	180
9-I	Liquidus-solidus data of $GaAs_ySb_{1-y}$ for the calculation of α_{As-Sb} and $\alpha_{GaAs-GaSb}$.	188
9-II	Interaction parameters for the ternary system Ga-As-Sb.	192

10-I	Compositions of samples with constant N_{Ga} annealed at various temperatures T, and of resulting equilibrium solid phases.	214
10-II	Compositions of samples annealed in a three-phase field at temperature T and of equilibrium solid phases.	218
11-I	Experimental data for the redetermination of the solidus curve of $GaAs_ySb_{1-y}$.	230

Chapter 1 Introduction

In recent years, pseudobinary systems of alloys formed from elements of the group III and V have received considerable attention because of the possibility of obtaining a required band gap value by choice of the composition of the alloy used. Such a possibility is of considerable interest in the application to various devices such as optical detectors, L.E.D.'s and Gunn oscillators. In the selection of suitable alloys, in the production of single crystal samples and in the fabrication of devices, a knowledge of the range of solid solution, of sample composition and of the phase diagram of the appropriate alloy system is essential.

This research project on the characterization of the phase diagram of some III-V ternary systems started from the need to produce homogeneous samples of the pseudobinary alloy system $GaAs_ySb_{1-y}$ for investigations of its electrical and optical properties especially for the middle composition region. There was very little work published on this alloy system and in fact, the range of solid solution was not well defined and the lattice constant-composition relation still very approximate. Once these properties were established satisfactorily it was decided to pursue the investigations into the characterization of the phase diagram of such alloy systems both theoretically and experimentally. The system investigated in this study were the ternary III-V systems: Ga-In-Sb and Ga-As-Sb.

The report of this research project has been divided in such a way as to preserve the chronology in which the various analyses were carried out.

Chapter 2 recalls some of the important properties relative to such alloys and describes the various growth methods used in this laboratory for preparing these alloys.

Chapter 3 describes the technique used to investigate the range of solid solution of $GaAs_ySb_{1-y}$ and the lattice constant-composition relation.

Chapter 4 reviews the properties of ternary phase diagrams and chapter 5 presents a theoretical model developed by Guggenheim in order to predict the equilibrium conditions which hold for such alloy systems.

Chapter 6 gives a reinterpretation of some of the parameters included in the theoretical model.

Chapter 7 presents the experimental and theoretical analyses carried out on the phase diagram of the ternary system Ga-In-Sb.

Chapters 8, 9, and 10 report the various experimental and theoretical analyses on the pseudobinary section $GaAs_ySb_{1-y}$ as well as on the whole phase diagram of the ternary system Ga-As-Sb.

Chapter 11 discusses recent developments and suggestions for improving the theoretical treatment.

The summary contains further suggestions for future work. Appendix A describes various experimental techniques and finally, appendix B shows the detailed calculation leading to one of the important equations of the theoretical model.

Chapter 2 Properties of the crystals from the Group III and the Group V elements

2.1 Introduction

2.2 Elements of the Groups III and V

2.3 III-V Binary Compounds

2.3.1 Crystal structure

2.3.2 Stoichiometry

2.3.3 Temperatures of fusion

2.4 III-V Pseudobinary Alloys

2.4.1 Growth techniques

2.4.1 i) quenching

ii) gradient freeze

iii) step-freeze (or horizontal Bridgman)

iv) zone growth

v) sequential growth

2.4.2 Constitutional supercooling

2.5 III-V Pseudobinary Alloys

2.5.1 Lattice constant as a function of composition

2.5.2 Range of miscibility in solid solutions

2.1 Introduction

As stated previously, the wide variety of applications for crystals of the binary III-V compounds has generated much incentive to pursue fundamental research on the properties of such systems. But to be able to undertake any new research programs it is essential that a knowledge of some of these basic properties already established be acquired so that any profitable advancement be achieved.

Since this study deals with ternary III-V systems, the aim of this chapter is to recall some of the properties of solid solutions formed between various binary III-V compounds. Discussions on elemental properties, binary mixtures, crystalline structure and techniques of crystal growth are also included.

The literature is abundant yet little is known for instance of the physical changes of some III-V compounds as well as of ternary and quaternary alloys involving these same compounds. As an example, the melting point of boron nitride still remains undetermined which goes to prove that there is still progress to be made in the field of III-V compounds.

In this study, the combinations between four particular elements will be discussed: gallium and indium of the group III and arsenic and antimony of the group V. Among the various properties of interest here those pertaining to thermodynamics as for instance free energy, entropy, enthalpy, phase diagram, etc,will be left out as they will be treated at

a later stage in this work. The reason behind this is to present the various properties concurrently with the related experimental investigations.

Various tables and diagrams are inserted in the discussion in order to complete or clarify the discussion of each individual property when justifiable.

2.2 Elements of the Groups III and V

The four elements of interest throughout this work are compared with their neighbours in a section of the periodic table (table 2-I).

From table 2-I, it is readily seen that for an isolated atom, all elements of group III have two '*s*' electrons and one '*p*' electron in the external portion of the electronic shell. Similarly, the isolated atom of a group V element contains two '*s*' electrons and three '*p*' electrons in the external shell.

Another characteristic of interest here is that elements of the group V have high vapour pressures, particularly arsenic which sublimes at normal pressure before reaching the melting temperature. The latter property makes crystal growth involving these elements all the more difficult and special care has to be taken during the growth process which will be discussed later.

Table 2-I Section of the periodic table describing elements of the groups III, IV and V respectively. The temperatures are in degrees Celsius, the specific gravity is quoted with the temperature (^{o}C) and the energy gap values are in eV at room temperature.

Atomic number	32	$4s^2 4p^2$	Electron configuration
Symbol	Ge	937.4	Melting temperature
Atomic weight	72.59	2830	Boiling temperature
Energy gap	0.67	5.323 (25^{o})	Specific gravity

key to chart

5	$2s^2 2p^1$	6	$2s^2 2p^2$	7	$2s^2 2p^3$
B	2300	C	3550	N	-209.86
10.811	a.	12.01115	c.	14.0067	-195.8
1.50 - 1.56	2.34[b.]	5.4	d.		1.2506[e.]
13	$3s^2 3p^1$	14	$3s^2 3p^2$	15	$3s^2 3p^3$
Al	660.2	Si	1410	P	44.1[f.]
26.9815	2467	28.086	2355	30.9738	280.[f.]
	2.6989(20^{o})	1.107	2.33(25^{o})		g.
31	$4s^2 4p^1$	32	$4s^2 4p^2$	33	$4s^2 4p^3$
Ga	29.78	Ge	937.4	As	817[h.]
69.72	2403	72.59	2830	74.9216	i.
	5.907(20^{o})	0.67	5.323(25^{o})		j.
49	$5s^2 5p^1$	50	$5s^2 5p^2$	51	$5s^2 5p^3$
In	156.61	Sn	231.89	Sb	630.5
114.82	2000	118.69	22.70	121.75	1380
	7.31(20^{o})	0.08	k.		6.691(20^{o})
81	$6s^2 6p^1$	82	$6s^2 6p^2$	83	$6s^2 6p^3$
Tl	303.5	Pb	327.5	Bi	271.3
204.37	1457	207.19	1744	208.980	1560
	11.85(20^{o})		11.35(20^{o})		9.747

a. boron sublimes at $2550^{o}C$
b. the specific gravity of amorphous boron is 2.37
c. carbon is reported to sublime above $3550^{o}C$
d. the specific gravities are: 1.8 - 2.1 (amorphous), 1.9 - 2.3 (graphite), 3.15 - 3.53 (diamond).
e. this value is the density of the gas in g/l.
f. these values are for white phosphorus
g. the specific gravities are: 1.82 (white), 2.12 (red), 2.25 - 2.69 (black)
h. at 2.8 MPa of pressure
i. arsenic sublimes at $613^{o}C$
j. the specific gravities are: 1.97 (yellow), 4.73 (black), 5.73 (gray).
k. the specific gravities are: 5.75 (grey or α), 7.31 (white or β).
l. for α-Sn

2.3 III-V Binary Compounds

The charactoristic properties of the III-V binary compounds are certainly most significant when considering alloy systems of these compounds and particularly the pseudobinary solutions. The compounds of interest here all behave as semiconductors.

2.3.1 Crystal structure

Of all the properties to be covered in this chapter regarding III-V semiconductors, it is essential that the crystal structure be discussed first. The crystals of interest here have a tetrahedral structure in which each atom is surrounded by four nearest neighbours situated at the vertices of a tetrahedron. Thus the lattice formed has a coordination number of 4.

The compounds considered in this thesis have a zinc-blende structure: each atom of one element lies in the center of a tetrahedron formed by the four nearest neighbouring atoms of the other element, and the base triangles of two such interpenetrating tetrahedra are rotated 60^{o} with respect to each other (see figure 2-1).

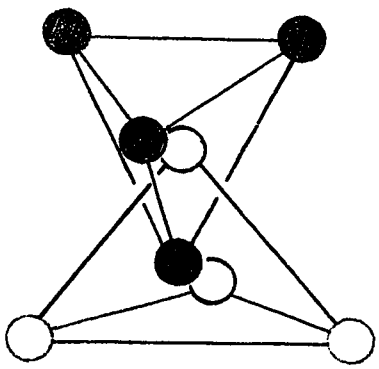

Fig. 2-1 The orientation of the base triangles in two interpenetrating tetrahedra.

A more complete representation of the zinc-blende lattice is given schematically in figure 2-2. It is described as two interpenetrating face-centered cubic sublattices.

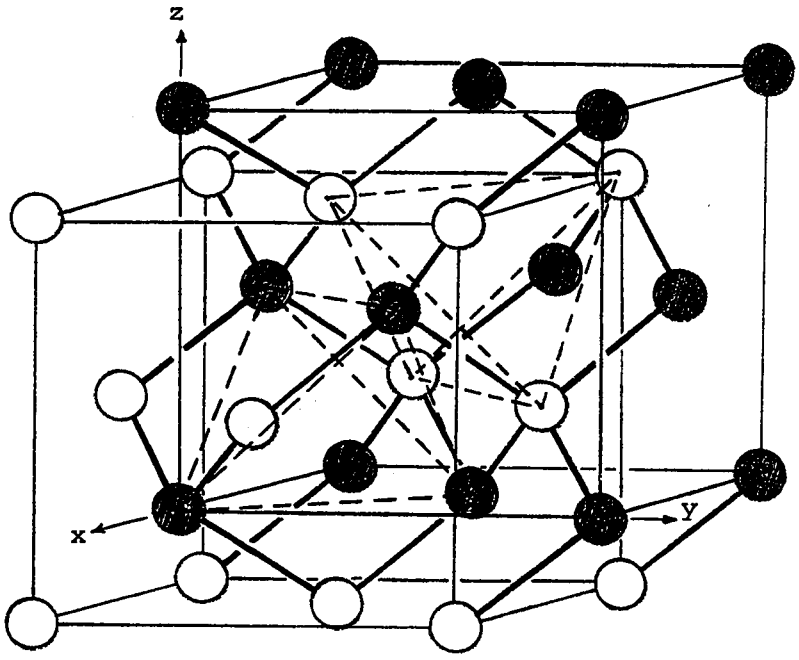

Fig. 2-2 The zinc-blende lattice. Two interpenetrating f.c.c. lattices. Two tetrahedra rotated by 60^{o} are also outlined (they are not interpenetrating here).

The two sublattices are orientated parallel to each other and are displaced by a vector $\vec{\tau}(\ a/4,\ \ a/4,\ \ a/4)$ where 'a' is the length of the edge of the elementary cube forming the unit cell. The length of the vector $\vec{\tau}$ is then found to be $a\sqrt{3}/4$ and it also represents the distance between nearest neighbour atoms.

The positions occupied by the atoms are not those of the points of a Bravais lattice and when the cubic configuration is used, the unit cell contains 8 atoms. The structure is identical to the diamond lattice except that in the latter case, carbon atoms occupy all the lattice sites. Other characteristics of the zinc-blende lattice may be observed upon inspection of figure 2-3.

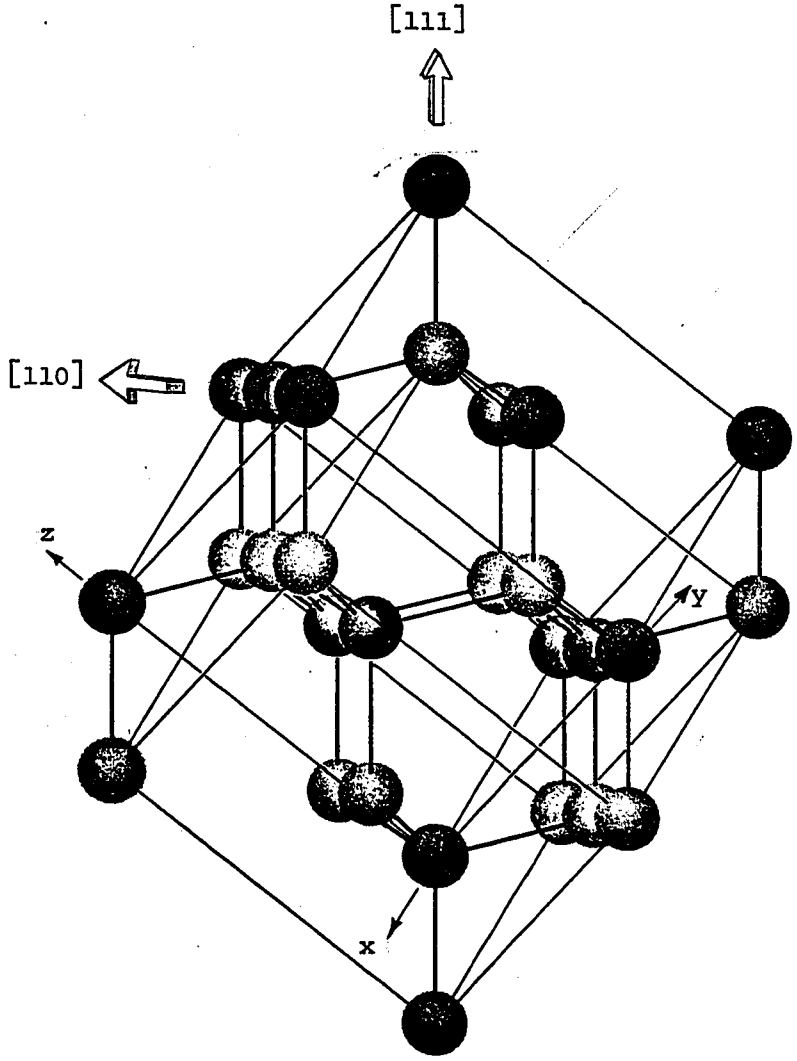

Fig. 2-3 The zinc-blende lattice observed perpendicular to a [111] -axis and along a [110] -axis.

In the [110]-direction, identical hexagonal rings may be observed with alternating kinds of atoms situated at the vertices. Along the [111]-direction, alternating planes of only one kind of atom appear with the distances between them alternating between two different values. If the successive planes are viewed along the [111]-direction, the pattern is inverted when viewed along the $[\bar{1}\bar{1}\bar{1}]$-direction and consequently the two directions are distinguished from one another. This means that the [111]-axis is a 'polar axis' in the zinc-blende structure as a consequence of the absence of an inversion center.

A further characteristic is that the III-V binary compounds with the zinc-blende structure differ in as much as the lattice constants a are different. The value of a for some of the compounds are tabulated in table 2-II.

Table 2-II Lattice constants of four III-V binary compounds

Compound	Lattice constant a	Reference
GaAs	$0.56534 \pm 2 \times 10^{-5}$ nm (18°C)	(58G1)
GaSb	$0.60954 \pm 1 \times 10^{-5}$ nm (18°C)	(58G1)
InAs	$0.60584 \pm 1 \times 10^{-5}$ nm (18°C)	(58G1)
InSb	$0.647877 \pm 5 \times 10^{-6}$ nm (18°C)	(58G1)

2.3.2 Stoichiometry

Among the various properties of semiconductors, the width of the forbidden gap as well as the nobility of electrons and holes are two very important parameters which are characteristic of the band structure which differs for each semiconducting material. It is not the scope of this study to deal in detail with these properties. However, one important factor that can affect the semiconducting properties of the various III-V compounds of interest is their chemical formation. To be more specific, it is the departure from stoichiometry that is considered here.

Deviations from stoichiometry in III-V compounds are very small from a macroscopic chemical point of view. However, the very small deviations that must be possible have a pronounced effect upon semiconducting properties, dopant incorporation and all the properties related to dopant incorporation. The elemental semiconductors, silicon and germanium, do not suffer from chemical deviations but the possibility does arise for compound semiconductors. Among the compounds of interest here, GaSb has shown some evidence of non-stoichiometry.

In a more general sense, non-stoichiometry may be properly considered to result from the presence of native point defects, and these point defects are present in silicon, germanium and compound semiconductors. On the other hand, impurities are incorporation in general in a situation in which there is a dynamic equilibrium between native point defects and the incorporating atoms. They do not tend, in general, to reduce native defect concentrations. The departure from stoichiometry for GaSb is believed to be caused by those native defects

and results in p-type conductivity for this compound.

Therefore, small deviations from stoichiometry can alter considerably the semiconducting properties of III-V compounds and alloys, and in view of the technological importance that these materials are taking, these variations have to be predictable if not controllable.

There remains many more physical properties related to III-V semiconductor materials and the reader is referred to the various texts on the subjects of interest (for instance, Madelung 64M1, Sirota 68S1).

2.3.3 Temperatures of fusion

Finally, another important physical property is the temperature of fusion of the binary compounds and values are tabulated in table 2-III.

Table 2-III Temperatures of fusion of four III-V binary compounds

Compound	T_f K	Reference
GaAs	1511	(55K1)
GaSb	985	(55B1)
InAs	1215	(53L1)
InSb	798	(52L1)

2.4 III-V Pseudobinary Alloys

The previous discussions have been centered around the binary compounds but as mentioned previously, the main interest of this study is the behaviour of ternary systems and particularly the pseudobinary sections of these systems. The III-V ternary alloys crystallize in the zinc-blende structure and the alloying involves the substitution of atoms of one group with other atoms of the same group. It is assumed that the symmetry properties of the zinc-blende structure are conserved because the two types of atoms of the same group which occupy one sublattice do so in a random manner and therefore, over an extended volume, the symmetry is that of the zinc-blende structure.

2.4.1 Growth techniques

The remainder of this chapter is devoted to a discussion on the preparation of such ternary alloys and properties associated with it. A review of the preparation from the melt of such alloy systems was presented by Woolley (62W1); even though it is an old method, it is still one of the better methods of obtaining a wide range of compositions for pseudobinary alloys. In that review, such topics as evidence for solid solution over the whole composition range, phase diagram determinations and growth techniques are covered. Many pseudobinary systems are discussed with reference to the possibility of producing homogeneous material and it was found that in some cases the ternary systems present no more problems than the inherent difficulties in preparing the binary compounds themselves. However, for compounds such as GaSb, GaAs, InSb and InAs new difficulties arose due to the extreme segregation of components asso-

ciated with the wide separation of the liquidus and solidus curves on the phase diagram and thus the difficulty in obtaining equilibrium due to the very low diffusion rates.

In this laboratory, the author and previous workers have used several methods of preparation. In most cases, however, the ternary alloys are grown from a melt of binary compounds and only occasionally are the elements used. The major point of concern in the latter technique is the property of elemental arsenic which sublimes at 613^{o}C. The vapour pressure of the gaseous arsenic can be such that quartz ampoules will crack or blow up therefore releasing harmful vapours and depriving the melt of one component. The former technique of working with the binary compounds eliminates dealing with such high vapour pressures, because these compounds are available commercially.

In many of the techniques used, it is possible to keep the temperatures lower than that of the highest melting compound because all the III-V compounds used here are soluble in one another and solutions can usually become homogeneous relatively fast except in the case when only a small quantity of liquid is present initially. Usually a few hours will be sufficient but for some cases involving the compounds GaAs and GaSb it was found that periods of up to three days were required to obtain equilibrium.

In this laboratory, five techniques have been used for growth from stoichiometric melts. However, no epitaxial growth has as yet been carried out but a project is being set up at the moment.

2.4.1 i) quenching

The stoichiometric mixture is encapsulated in a quartz ampoule under a reduced pressure of argon (approximately 35 kPa) and brought to a temperature which nears the highest melting point or exceeds it when possible. The ampoule is shaken to insure good mixing then it is dropped in a bath of cold oil (room temperature). Oil is used rather than water to avoid the formation of steam pockets that could slow down the freezing process. The technique yields non-homogeneous material and is used mostly to prepare ingots for use with another growth technique or when anneals of quenched ingots are to be used.

ii) gradient freeze

The furnace has a temperature gradient over the length containing the stoichiometric mixture. Initially, the temperature at all points is such as to melt the charge which is then left in long enough for the liquid to become homogeneous. The temperature is then lowered very slowly so that freezing progresses from one end. With this technique, inhomogeneous growth may occur and is due mostly to the effect of constitutional supercooling (see later). The inhomogeneities are characterized by composition fluctuations on a semi-microscopic scale and must not be confused with the actual variation of composition along the length of the ingot which results from the growth method. These inhomogeneities are more readily observable for pseudobinary alloys than for binary compounds: in the case of the alloys which contain three different elements, the random distribution of two kinds of atoms of the same group is confined to one of the two sublattices of the zinc-blende structure while each kind of atoms in a binary compound are distributed on each sublattice thus preserving

the long-range order. The major fault of this growth method therefore remains the difficulty in obtaining homogeneous samples large enough to allow bulk measurements.

iii) step-freeze (or horizontal Bridgman)

The furnace has two zones; a high temperature zone where the charge is completely molten (the properties of solubility are often used in this case in order to avoid too high temperatures), and a second zone kept at temperatures below the lowest melting point but yet high enough to avoid condensation of vapours on the walls of the quartz ampoule containing the charge (e.g. arsenic vapours). The two zones are separated by the smallest distance possible and this narrow section of the furnace is often cooled in order to provide as steep a temperature gradient as possible.

A charge, encapsulated in a quartz ampoule, is left in the hot zone until the solution has liquified completely and then mechanically pulled through the section with the temperature gradient. The rate of crystallization is kept low by pulling the charge through the gradient very slowly (typical pulling speeds are indicated later). The advantage of this technique over the previous one is that homogeneous growth is obtained at faster rates. Inhomogeneities, of course, can still appear but reasonably good quality material can be produced in shorter time and the furnace design is much simpler.

Finally, the rate of variation in composition with length will depend upon the form of the solidus and liquidus curves of the alloy system produced and therefore will vary considerably from one end of the

ingot to the other. When doped material is needed, the movement of impurities, initially introduced in the charge, will behave differently as freezing occurs. Different compositions will then have different amounts of impurities associated with them, thus making the control over composition and impurity very difficult.

iv) zone growth

The furnace consists of two cool zones separated by a short hot zone set at a temperature high enough to initiate and maintain a liquid zone within it. A charge is prepared beforehand by either quenching or a rapid step-freeze of a stoichiometric mixture. A typical rate would be a 10 cm long ingot pulled through in a day or less compared with a rate of 0.5 cm per day in a normal step-freeze. The ampoule containing the charge is then slowly pulled through the zone. As material crystallizes at the freezing interface, the melt is depleted in higher melting component but the later component is being supplied by the charge at the melting interface.

The method yields an ingot with a composition profile resembling that of the initial charge but with local inhomogeneities smoothed out (many inhomogeneities were present because of the rapid treatment given to the initial stoichiometric mixture). Also, the front and the end part of such an ingot will be similar in composition distribution to that of an ingot grown from a step-freeze technique.

v) sequential growth

This technique was used by Rosenbaum of this laboratory and is particularly convenient for alloy systems having a wide separation between liquidus and solidus curves of the phase diagram. Briefly, the ingot is initially treated with a relatively rapid step-freeze, the rate of freezing is chosen so to give a reasonably smooth variation of the averaged cross sectional composition. This is then followed by a slow zone recrystallization. For more details on this method, refer to S. D. Rosenbaum's Ph.D. thesis (72R1).

The various growth techniques described above have the general advantage of yielding equilibrium specimens over a large range of composition from a single ingot, thus providing ideal material for initial investigation of the physical properties of an alloy system. The resulting ingots are polycrystalline with coarse grains but show little evidence of microcracks or porosity and are quite suitable for measurements where polycrystalline samples can be used. Among the alloys of interest however, there is one exception: for GaSb-rich alloys, high resistance barriers at grain boundaries in Te-doped specimens were identified by Rosenbaum (72R1) as the principal reason for erratic apparent mobilities in electrical conductivity measurements.

2.4.2 Constitutional supercooling

As indicated in the previous section, the problem of formation of inhomogeneities is always present in this type of growth and care must be taken to reduce this effect to a minimum. The main factor in this occurence of inhomogeneities is found to be constitutional supercooling.

Constitutional supercooling occurs when the growth rate exceeds a critical value which is characteristic of a particular alloy system and of the temperature gradient at the growth interface. It results from excessive depletion of the higher melting component from the liquid at the growth interface. A hypothetical example is given in figure 2-4.

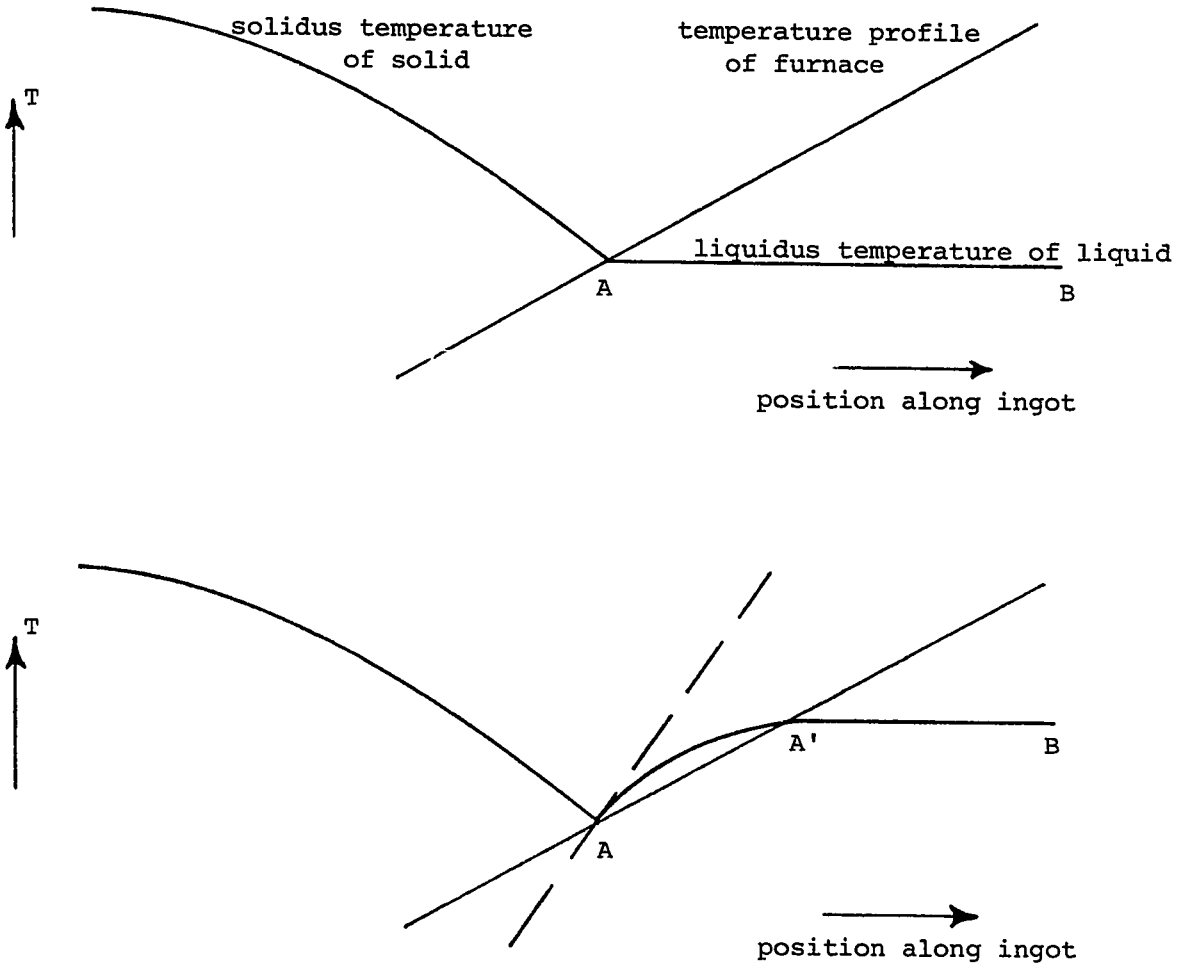

Fig. 2-4. Solidus and liquidus temperatures as a function of length along ingot. The point of interest here is the freezing interface.
a) ideal case,
b) constitutional supercooling.

Figure 2-4a shows the freezing interface (point A) for an ideal case. The solidus temperature profile of the crystallized section of the ingot shows a characteristic variation for a simple case. Line AB indicates the liquidus temperature profile of the remaining liquid; the constant temperature implies that the melt is homogeneous throughout. As the charge progresses across the temperature gradient of the furnace, the temperature represented by AB drops until it reaches the lowest melting point of the alloy. The position along the ingot usually coincides with the end of the ingot for simple systems.

In figure 2-4b , constitutional supercooling occurs: at the freezing interface (point A), there is a marked depletion of the high melting component. The melt at point A is lacking high-melting material because the later is being crystallized faster than it can be supplied via diffusion or stirring from the rest of the liquid solution. The melt is therefore slow in recovering an average composition throughout. This results in a liquidus temperature profile shown by the line AA'B. Between points A and A' the melt is enriched with high-melting component that is moving towards the freezing interface with the result that in this region the liquid has a liquidus temperature profile above the local temperature of the furnace, consequently, crystallization occurs in this region also and inhomogeneous material is produced.

In order to correct the effect of constitutional supercooling, the travelling speed may be reduced to allow more time for the high-melting component to diffuse throughout the entire melt. Stirring may

also be efficient but the vibrations induced at the freezing interface would certainly increase the possibilities of growing faults. An increase in the slope of the temperature profile of the furnace (dashed line in figure 2-4b would also eliminate constitutional supercooling as it would reproduce the ideal situation described in figure 2-4a. It should be underlined that constitutional supercooling is self-curing because as the melt is depleted in high melting component, the average composition drops such that the curved section (AA') would return below the temperature profile of the furnace. Nonetheless, inhomogeneous material would still result from the earlier stages of the growth.

2.5 III-V Pseudobinary Alloys

There are various techniques to check the homogeneity of solid specimens from ingots grown from the methods presented above. The most useful one is the X-ray powder photograph as it yields also the value of the lattice constant if the sample shows single phase behaviour. The alloys dealt with here all crystallize in the cubic zinc-blende structure and it is a matter of routine work to obtain the lattice parameter values of each sample. Only a small piece of material is lost from that test and the accuracy of the measurement is of the order of 0.0002 nm in typical lattice constants of 0.6 nm.

2.5.1 Lattice constant as a function of composition

The next step is to determine the composition of each sample which is usually determined with the help of a lattice constant versus composition relation. It becomes quite simple when the Vegard rule applies to a system as the lattice constant varies linearly with the composition. The variation of lattice parameter with composition for the three pseudobinary sections $Ga_xIn_{1-x}Sb$, $Ga_xIn_{1-x}As$ and $InAs_ySb_{1-y}$ has been determined by Woolley and Smith (62W1). Figure 2-5 shows these relations. Two systems follow Vegard's law, but the third system $InAs_ySb_{1-y}$ differs from it throughout the entire composition range.

With such a simple method of measuring the composition of solid specimens with accuracy, it is useful to present various ingot profiles grown from the techniques described earlier. Figures 2-6 and 2-7 are typical ingot profiles of the alloy systems $Ga_xIn_{1-x}Sb$ and $InAs_ySb_{1-y}$ respectively, grown by the horizontal Bridgman technique.

Here, the shape of the liquidus and solidus curves yields a smoother curve for the profile of the $Ga_xIn_{1-x}Sb$ system and therefore provide better samples of single phase material for bulk analyses. Other characteristics of ingots of this system are: good homogeneity throughout the length of the ingot and a tail end which is composed nearly solely of the lower melting point component, InSb in this case.

The second profile (figure 2-7) for the system $InAs_ySb_{1-y}$ displays a steep section for which homogeneity is usually poor and thick samples

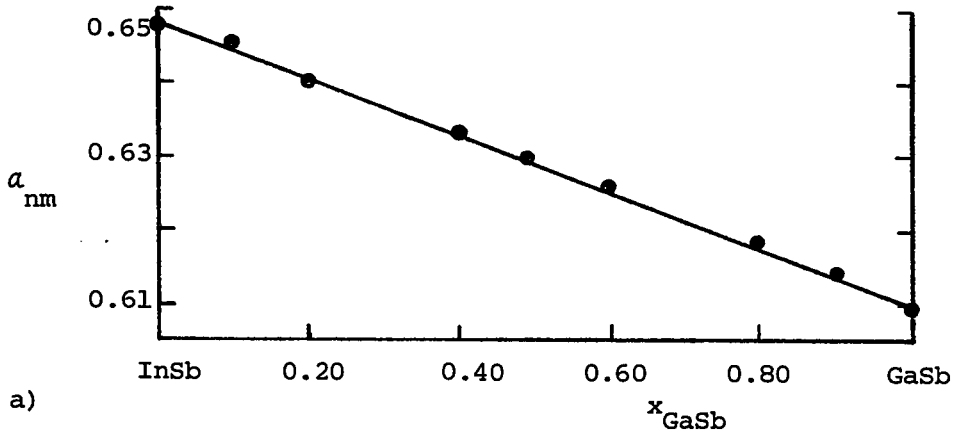

a)

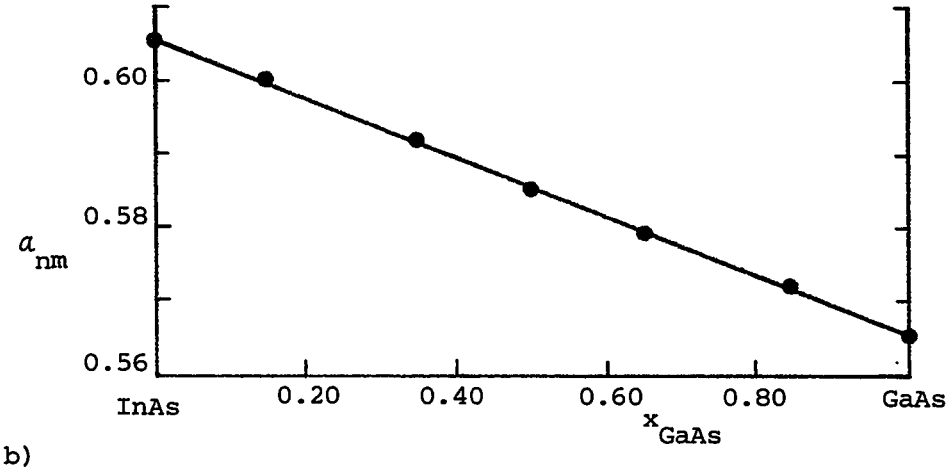

b)

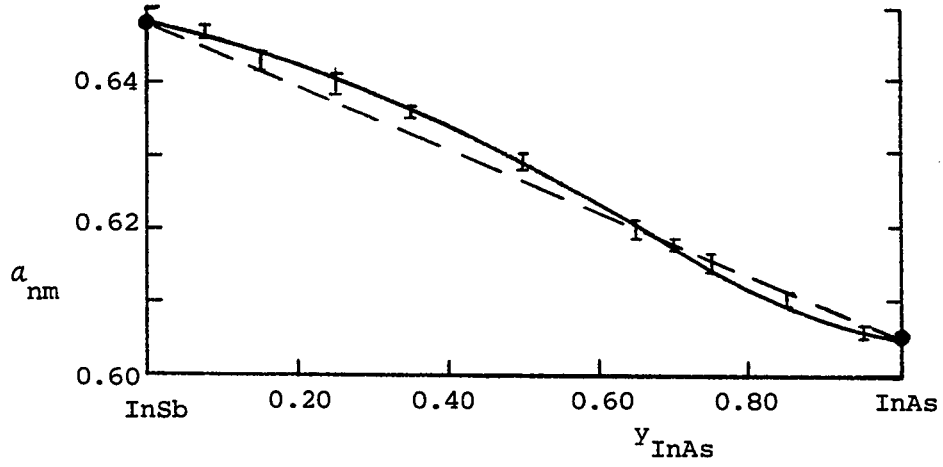

Fig. 2-5 Variation of lattice constant with composition for three III-V ternary alloy systems (62W1).
a) $Ga_xIn_{1-x}Sb$, b) $Ga_xIn_{1-x}As$, c) $InAs_ySb_{1-y}$.

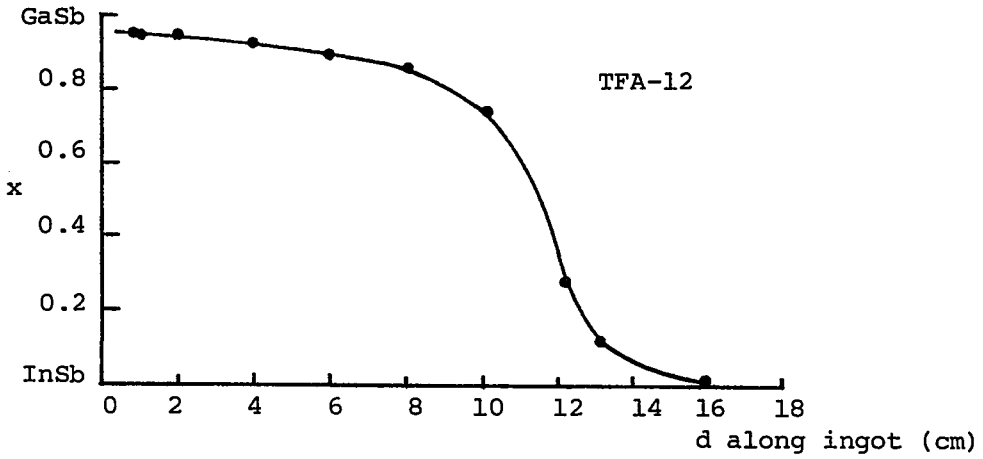

Fig. 2-6. Typical profile of an ingot of $Ga_xIn_{1-x}Sb$ grown from the horizontal Bridgman technique. The variation in composition is smooth over the entire length of the ingot.

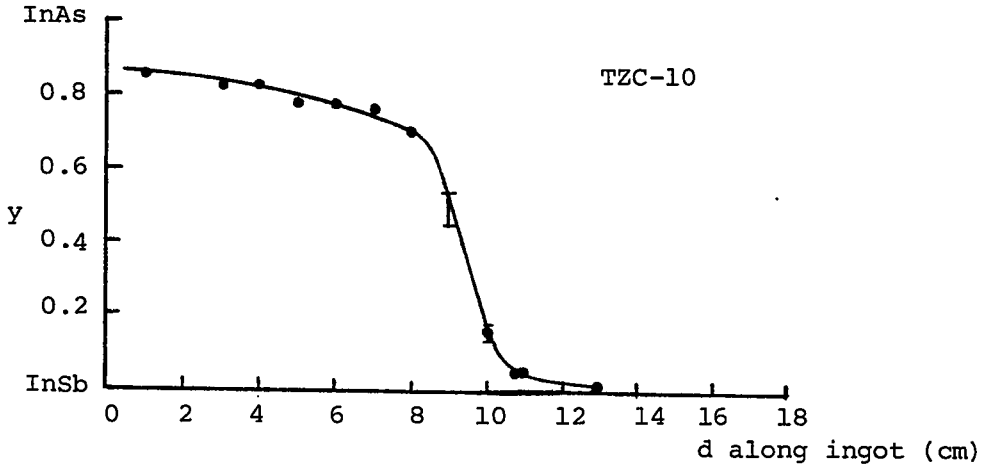

Fig. 2-7. Typical profile of an ingot of $InAs_ySb_{1-y}$ grown from the horizontal Bridgman technique. The sudden change in composition yields single phase specimens that have to be cut very thin.

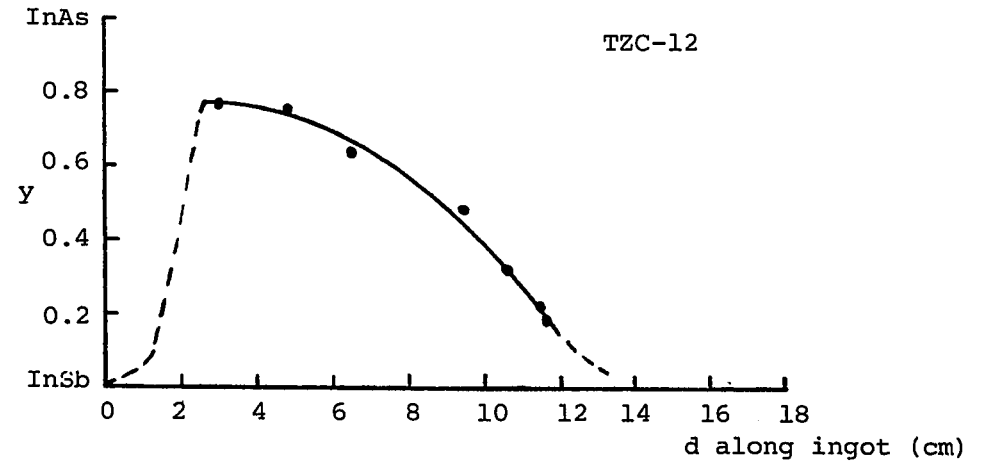

Fig. 2-8. Profile of an ingot of $InAs_ySb_{1-y}$ grown from the sequential growth technique (72R1).

of homogeneous material are hard to obtain. Again the tail end is practically pure InSb. Typical traveling rates used for such alloy systems have been of the order of 0.3 to 0.8 cm per day.

A behaviour such as that displayed by the system $InAs_ySb_{1-y}$ is not particularly convenient and such an ingot can be treated by the sequential growth process. A typical profile of an ingot of $InAs_ySb_{1-y}$ submitted to this last technique is shown in figure 2-8. It is, however, not necessary to present profiles of the system $Ga_xIn_{1-x}As$ as its behaviour is comparable to that of $Ga_xIn_{1-x}Sb$.

2.5.2 Range of miscibility in solid solutions

The final property to be discussed here regarding the III-V pseudobinary alloys is the range of solid solution. It is clear now that the three systems presented above all show total miscibility throughout the whole composition range. There is, however, another combination of binary compounds which yields a fourth ternary system, namely the $GaAs_ySb_{1-y}$ system. Very little has been reported on the growth of this system: the available experimental data of Woolley (62W1) and Inoue et al. (70I1) seem to indicate that the liquidus and solidus curves are quite widely separated thus suggesting increased difficulty in growing alloys of such a pseudobinary section. Rosenbaum had already noticed a high degree of segregation when a few ingots were grown but the results remained fragmentary. The system $InAs_ySb_{1-y}$ also showed a steep section (figure 2-7) which suggested the possibility of non-mixing of the constituents or at best instability of some phases. Sequential growth, however, has for-

tunately eliminated that possibility.

In Chapter 3, the ternary system $GaAs_ySb_{1-y}$ is thoroughly investigated in order to determine the range of solid solution for this alloy.

Chapter 3 The III-V pseudobinary system $GaAs_ySb_{1-y}$

3.1 Introduction

3.2 Review of Literature

3.3 Crystal Growth

3.4 X-ray Fluorescence Analysis

3.4.1 Instrument and method

3.4.2 Sample preparation

3.4.3 Calibration

3.4.4 Analysis and results

3.5 Lattice Constant-Composition Relation

3.6 Solid Solution in $GaAs_ySb_{1-y}$

3.6.1 Evidence of a miscibility gap

3.6.2 Growth of $GaAs_ySb_{1-y}$ with slow step-freeze

3.6.3 A miscibility gap in the range $0.38 < y < 0.61$

3.1 Introduction

Of the four possible ternary systems of the quaternary Ga-In-As-Sb, three have been investigated in considerable detail and particularly the pseudobinary alloys formed within each system (72P1). However, a fourth ternary system, Ga-As-Sb has received until recently very much less attention and there is little published data on its pseudobinary section $GaAs_ySb_{1-y}$. This is due, to some extent, to the difficulty in producing samples in equilibrium for these alloys.

3.2 Review of Literature

Muller and Richards (64M2), using a flash evaporation method of preparation, indicated that complete solid solution occurred over the whole composition range and that, to a reasonable approximation, Vegard's law was satisfied. However, they showed the results for only one alloy sample, that is $y = 0.50$. Potter and Stierwalt (64P1) produced alloy films by vacuum evaporation of the metallic constituents and claimed complete solid solution, but this paper shows some uncertainty in alloy composition close to $y = 0.50$. Straumanis and Kim (65S1), in an investigation of the lattice parameter variation of the alloys, prepared samples by quenching from the melt and then annealing in the solid form. For the GaSb-rich range, that is $0 < y < 0.35$, they obtained reasonably good homogeneous samples, and showed that in this range Vegard's law is obeyed. However, for samples with $y > 0.50$, where they had difficulty in obtaining

equilibrium conditions, their tentative results indicated that the lattice parameter values probably fall below the Vegard line in this range. Clough and Tietjen (69C1) produced alloys by a vapour transport technique but had no samples with composition in the range $0.38 < y < 0.69$. The liquid epitaxy method was used by Antypas and James (70A1) to produce alloys but, again, all of their samples had $y > 0.75$. In measurements of the physical properties, various workers (e.g. Woolley (62W1), Sirota and Matyas (68S2) and Thomas et al. (70T1)), have made the convenient assumption that Vegard's law is satisfied in this system, but in none of these cases did the compositions of alloys they determined lie in the range $0.38 < y < 0.70$.

On the theoretical side, Antypas and James (70A1) calculated the liquidus and solidus curves for the pseudobinary section $GaAs_ySb_{1-y}$ using Darken's (67D1) quadratic formalism for a ternary liquid and assuming a regular solid solution and concluded that single phase solid solution occurred throughout the whole range of composition. Van Vechten (70V1), using the spectroscopic theory of heats of formation to calculate internal energy values, predicted that complete solid solution should occur. However, subsequent phase diagram calculations by Stringfellow (72S1) in which the thermodynamic properties of the liquid are treated from a regular solution model and the properties of the solid are calculated from a spectroscopic theory of chemical bonding, indicated that the system showed a peritectic behaviour and predicted a solid phase miscibility gap of approximately $0.20 < y < 0.65$. Calculations of liquidus and solidus curves by Panish and Ilegems (72P1) also indicated that a miscibility gap exists in this system. They used a method of cal-

culation called 'simple solutions' which is similar to the approach of 'quasi-regular solutions' used by other authors. Brebrick and Panlener (74B1) using an ideal liquid-quasiregular solid model have also shown the possibility of a peritectic behaviour. Thus the collected data up to now are not conclusive as to the range of miscibility in the system or as to whether Vegard's law is satisfied.

3.3 Crystal Growth

The first investigations in this study were orientated towards the lattice constant-composition relation. In order to do so, an X-ray fluorescence technique was used. This technique is fairly standard for detection of trace elements (72L1), but has had much less application for composition analysis as required here. But before going any further it is perhaps more valuable to discuss the type of material that was available and see why and how this technique was utilised.

It has been indicated in chapter 2 that in the case of other mixed III-V systems a very convenient method of obtaining a number of alloy samples of different compositions by a melt growth method is to prepare an ingot by some suitable directional crystallization technique. This has been done here, and polycrystalline ingots of length 15 - 20 centimetres have been produced by the three following techniques, viz. a) step-freeze or horizontal Bridgman, b) zone recrystallization in a uniform ingot, and c) sequential growth. In all cases, the initial charge of 25 - 30 grams was prepared from appropriate amounts of the two compounds in broken ingot form. These were sealed in quartz ampoules. In methods a) and c), the charges were then placed in the hot zone of

the step-freeze furnace and held in the molten state for approximately 48 hours to allow good mixing of the components before the freezing process was initiated. (Of course, with method c) the ingots were further processed as described in chapter 2). The cold zone was held at 600°C to avoid transport of arsenic to that end of the system as the ampoule was pulled through the 'step'. The temperature gradient at the 'step' was 72°C/cm. In method b), a similar initial melting was carried out and the ingot then allowed to solidify in a horizontal position before being passed through the zone furnace. The molten zone width varied with ingot composition, position in ingot, etc. but was normally in the range 5 - 7 centimetres. The liquid zone therefore generally accounted for 25% of the overall length of the ingot.

In all three methods, the rate of movement of the freezing surface was made very slow: 0.3 - 0.8 cm/day, since previous work (62W1) had shown that these very slow rates were necessary if equilibrium were to be attained and homogeneous cross-sections produced. Cross-sectional slices, 0.5 to 0.8 millimetre thick, were then cut from every ingot and samples from each slice checked with a standard powder X-ray photograph to determine whether a single phase condition had been attained in each case. The majority of slices thus investigated were found to be homogeneous and single phase, and the powder photographs were analyzed in the normal way to determine the lattice constant 'a' for future use. Because of the use of directional crystallization techniques, in all cases, the composition of the cross-sectional slices varied with position along the ingot and since no definite lattice constant-composition

relation existed except for the assumption of a Vegard-like system it was found necessary to investigate a mean of determining the composition of the homogeneous samples grown by either one of the three techniques described above.

In figures 3-1 to 3-4, various ingot profiles are presented. The composition is found by obtaining the lattice constants from X-ray powder photographs and assuming a Vegard law for this alloy. It is of interest to underline at this early stage the apparent absence of homogeneous material in the range $0.38 > y > 0.80$.

3.4 X-ray Fluorescence Analysis

3.4.1 Instrument and method

In order to determine the composition of the single phase specimens of $GaAs_ySb_{1-y}$, a method rarely used for that precise purpose was adopted: X-ray fluorescence analysis which is also known as energy dispersive X-ray analysis or spectrochemistry. The method has often been used in quantitative analysis of very small amounts of material in a sample. However, the introduction of improved detectors and high resolution analyzers have made it possible to adapt the technique for accurate determination of large amounts of multicomponent alloys. Basically, the system used here consists of a γ source of Iodine-125 (100 millicuries) used to excite the characteristic K radiations of the three elements to be determined. The essential components of the X-ray fluorescence spectrometer are a Li-drifted silicon detector, held at 77 K,

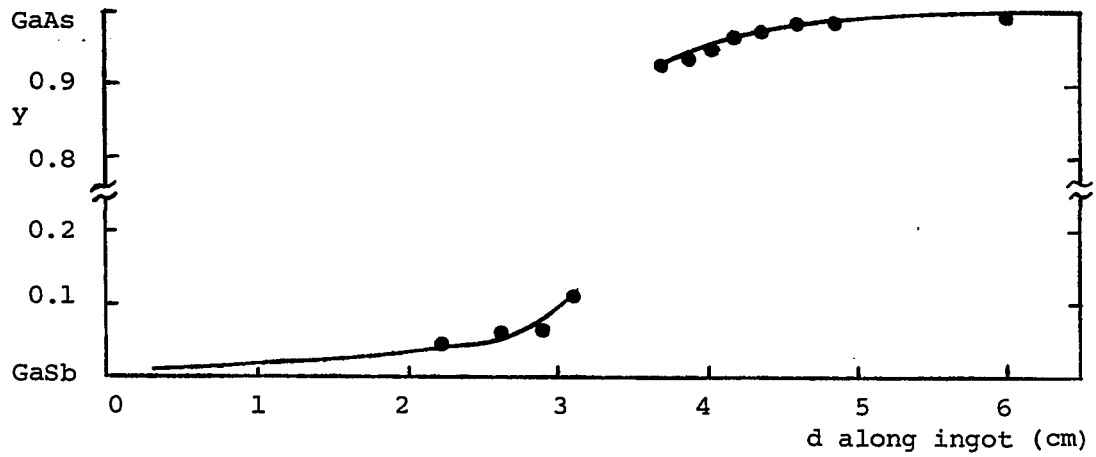

Fig. 3-1. $GaAs_ySb_{1-y}$ - profile of ingot TFF-1 (step-freeze). Composition determination assumes a Vegard law.

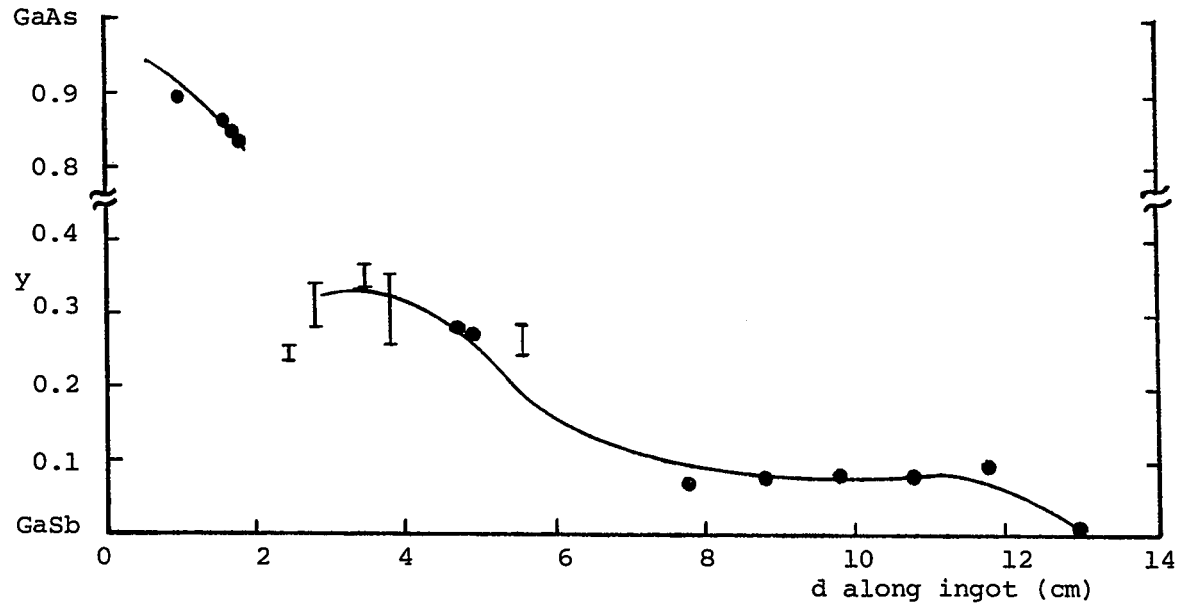

Fig. 3-2 $GaAs_ySb_{1-y}$ - profile of ingot TZF-2 (travelling zone). Composition determination assumes a Vegard law.

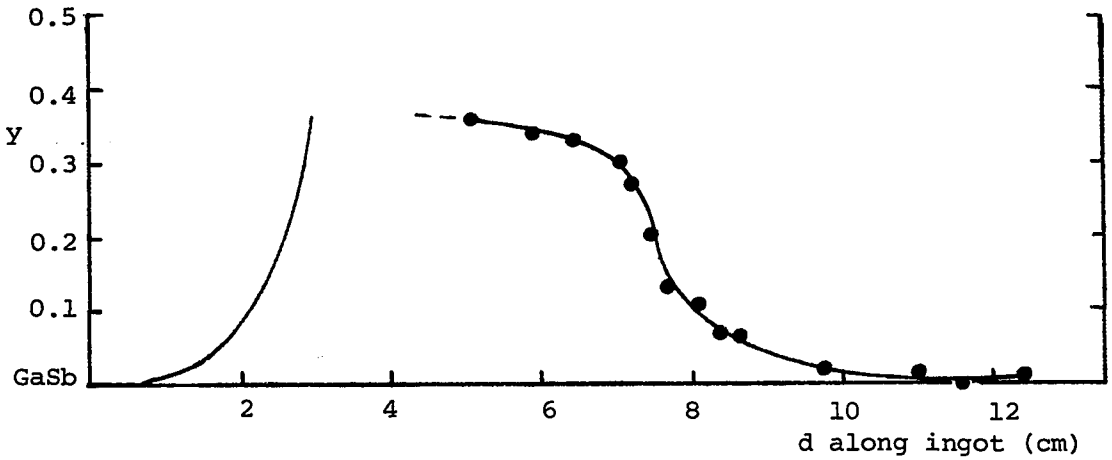

Fig. 3-3 $GaAs_ySb_{1-y}$ - profile of ingot TZF-6 (travelling zone and sequential growth). Composition assumes a Vegard law.

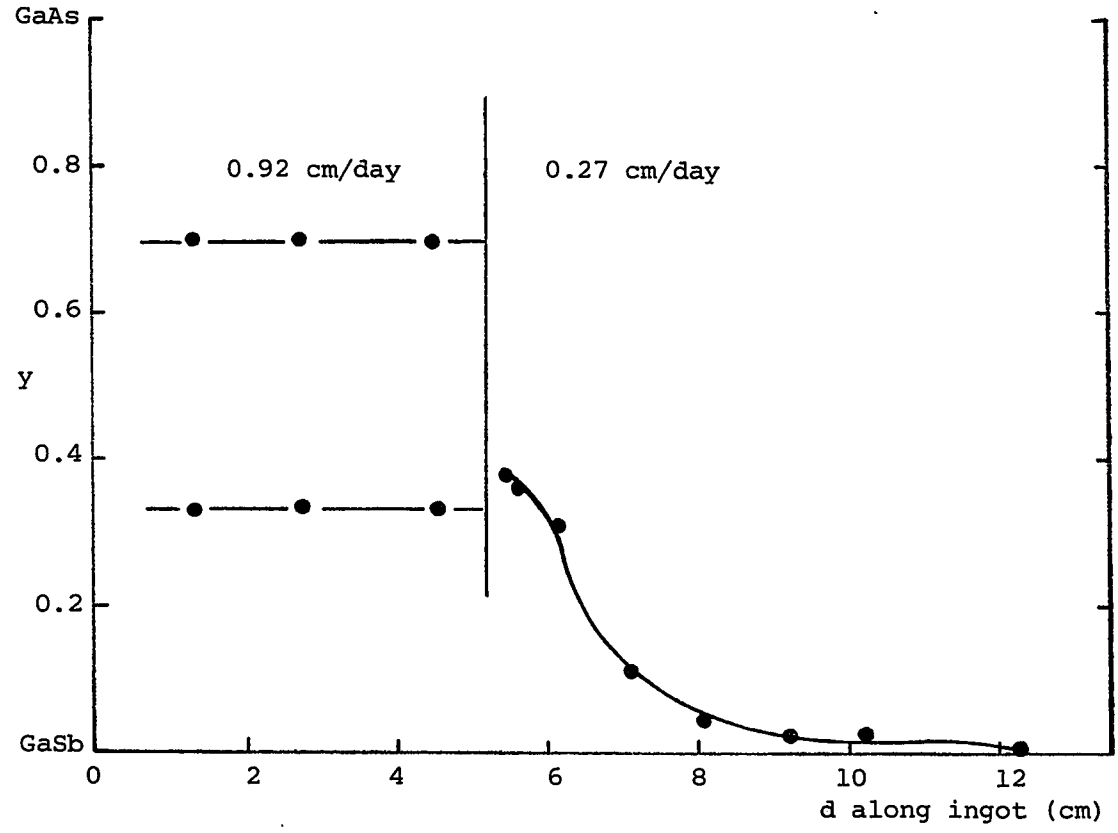

Fig. 3-4 $GaAs_ySb_{1-y}$ - profile of ingot TZF-4 (travelling zone and sequential growth). Composition assumes a Vegard law.

followed by a multichannel pulse height analyzer. (Nuclear Diodes, model 705/706). The system resolution for 5.9 KeV manganese K_α X-rays (taken with a radioactive Fe^{55} source) is 196 eV at FWHM (full width half maximum). The resolution calibration is 20 eV per channel.

The detector, kept at low temperature and under vacuum, is placed behind a beryllium window (0.0075 cm thick). The later is protected by a thin mylar membrane to eliminate the possibility of dust or sample particles falling upon it since the beryllium window breaks easily because of the atmospheric pressure it supports. Specimens are placed on a sample holder which consists of a thin plastic membrane mounted on an acrylic cylinder. All these precautions were taken in order to protect the beryllium window as the presence of these various membranes did not reduce significantly the amount of radiation detected. Figures 3-5 and 3-6 show the various parts of the X-ray fluorescence system.

3.4.2 Sample preparation

The samples were prepared in powder form as it was found to be the most suitable format for this type of analysis. The powder was very fine (less than 5μ -the powdering method is described in Appendix A) but it was later found that such a fine size was not necessary: Claisse (62Cl) has shown that the fluorescent intensity usually increases with decreasing particle size until the absorption in an individual particle is only a few percent, then the dependence on particle size disappears. Studying a system containing fluorescent and non-fluorescent particles (e.g. lead sulphide in silica) excited by Co^{57}, he calculated the ratio of the

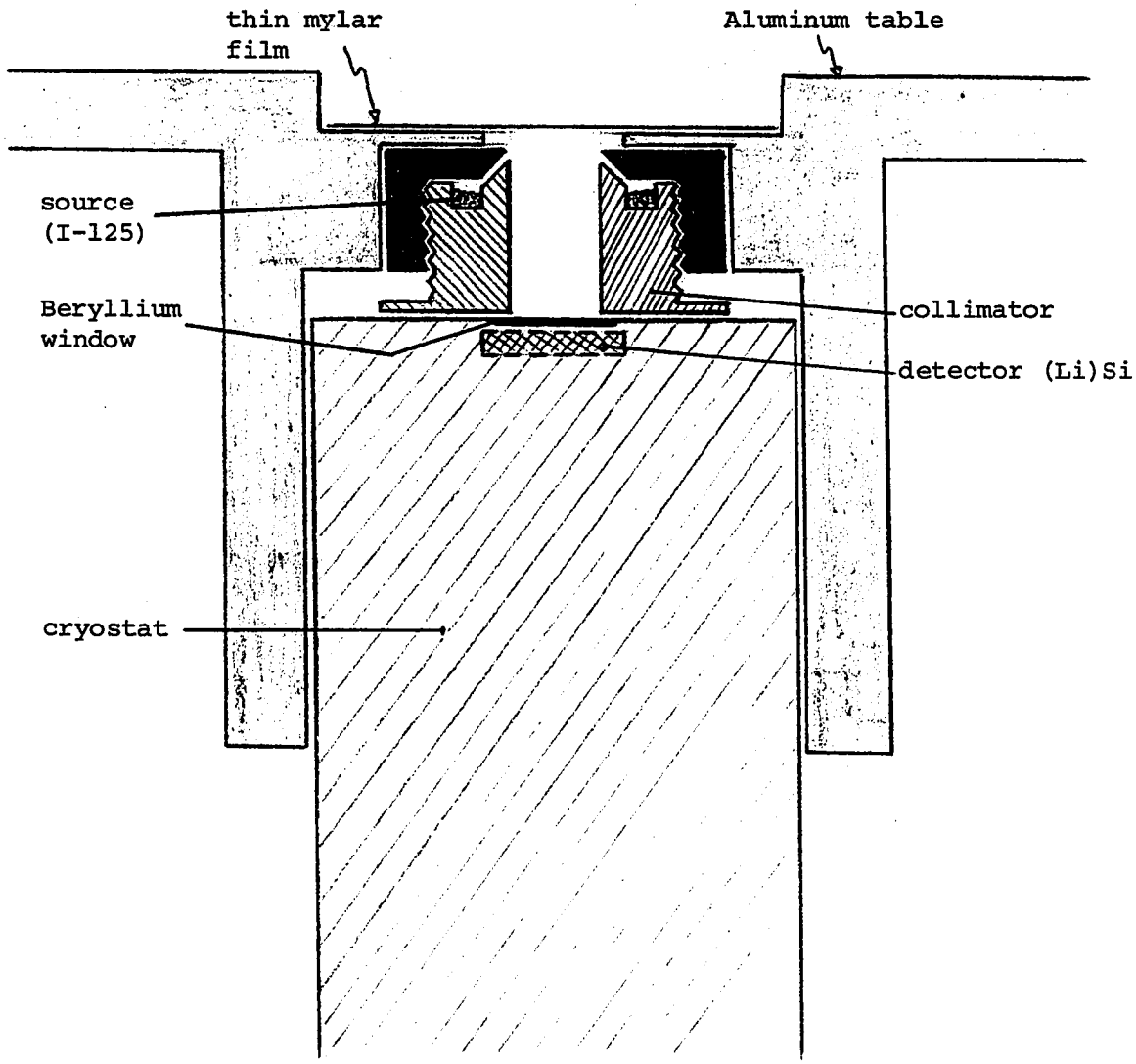

Fig. 3-5a Side view of X-ray fluorescence excitor and detector assembly.

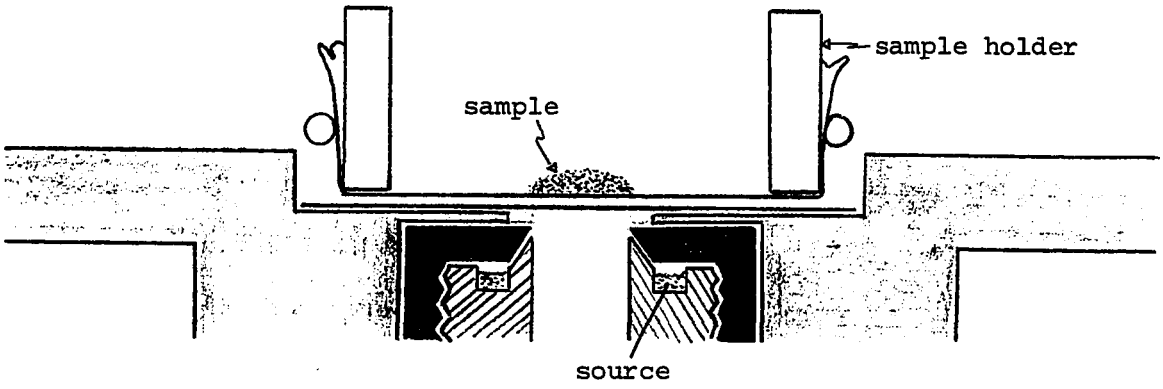

Fig. 3-5b. Side view of sample and source.

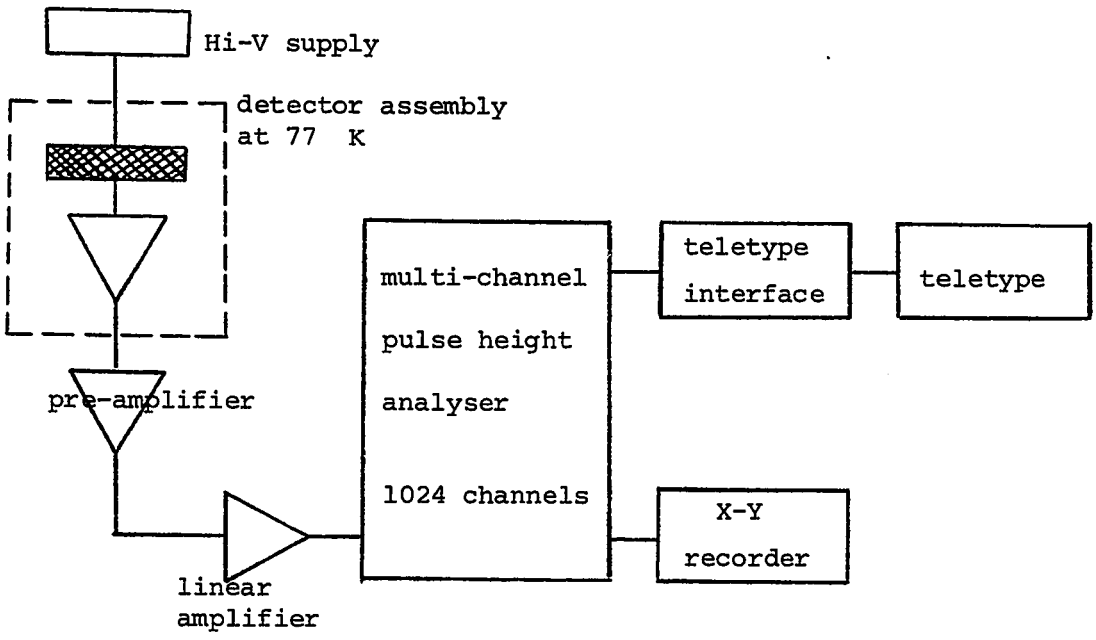

Fig. 3-6. Block diagram of detection system.

intensity of incident radiation over fluorescent radiation and found it to be maximum and constant for particle sizes up to 200 microns. In this case, both exciting and fluorescent radiations are relatively penetrating but when the radiation only penetrates the surface, the fluorescent intensity becomes independent of particle size. Nevertheless, the powdering technique developed here was used for every sample as it did not involve any great difficulties and the fine powder was preferable for X-ray powder photographs when they were required.

3.4.3 Calibration

As is often the case with new instruments, a lot of preliminary work had to be done in order to adjust the equipment to be able to obtain spectra of multi-component alloys*. Once the energy range suitable for analysis of fluorescent radiations from the four elements, gallium, indium, arsenic and antimony was finally adjusted, came the calibration of the instrument for the specific ternary system Ga-As-Sb. The first measurements toward the calibration of the apparatus were made on quenched samples in the composition range 10% to 90% GaAs-rich. The samples were prepared from stoichiometric mixtures of small pieces of polycrystalline GaAs and GaSb, the total weight of each sample being 2 grams. A melting furnace was heated to between 1150^{o}C and 1200^{o}C (temperature determined

* The author wishes to thank Mr. D. Martel who spent a great deal of time in making the system operational while working on an M.Sc. project.

by a Pt-Pt 13% Rh thermocouple). Each mixture was sealed in individual quartz ampoules and introduced directly into the hot zone of the furnace. They were left for 75 minutes with a 3-minute shaking period after the first 15 minutes. Quenching occurred quite rapidly as the ampoules were held in a vertical furnace and then dropped into an oil bath (free fall of about 30 cm).

Each ingot was powdered individually and the total amount of powder was then placed on a thin plastic film mounted on an acrylic cylinder. It was felt at this stage that the multi-phase material could be used adequately for calibration purposes as it was obvious that poly-crystalline material had been formed and the whole ingot retained the overall initial composition which was necessary for the calibration of the instrument. It is important to notice here that the whole powdered ingot was submitted to the radiation source so that the detection and analyzer systems would "see" the initial composition. However, it was found later that this precaution was unnecessary and thorough mixing of the powder insured that a small sampling of the mixed powdered ingot was representative of the initial composition. The sample of powder was then exposed for fixed periods of time (30 minutes in these initial trials).

The paths of the incident and emitted radiations may be followed on figure 3-5 and go as follows: the radioactive material (I^{125}) is mounted in a hollow cylinder and collimated to give a cone of incident radiation. The excited atoms of the sample fluoresce in all directions and a fraction of this emitted radiation reaches the Si(Li) detector.

The detected radiation is then analyzed and recorded via the electronics described in figure 3-6.

The resulting spectrum for each sample thus analyzed was recorded and stored for future analysis.

It was then decided to investigate the possibility of simplifying the preparation of calibration samples as the quenching technique proved to be rather time consuming. A second set of samples was prepared identically with the previous one, that is from pieces of GaAs and GaSb, but was simply mixed then powdered and not melted. Direct synthesis of the three elements Ga, As and Sb could have also produced a stoichiometric mixture but this method was abondoned for two reasons. First, powdering gallium is a difficult operation because of its very low melting point. Second, it is known that the alloy $GaAs_ySb_{1-y}$ crystallizes in the zinc-blende structure; since the new calibration samples are not heat treated, a ternary alloy is never formed, therefore it stands to reason that a mixture of binary compounds with zinc-blende structures and similar nearest neighbour pairs (Ga-Ga, Ga-As, Ga-Sb, As-As, Sb-Sb and As-Sb) will simulate the alloy better than the mixed elements will.

The new samples were exposed to X-rays for 30 minutes each and the resulting spectra compared to those of the quenched samples. Results clearly demonstrated that all differences lay within the range of experimental errors and therefore the second method of preparation was adopted for all subsequent calibration samples. It was also at this time that

tests were carried on small sampling rather than the full amounts of mixture initially prepared. The tests were conducted as follows: for every sample prepared, an amount of powder (approximately 0.5 gram) was exposed for 30 minutes and its spectrum recorded, then the analyzed sample was remixed with the remainder of the powder and again another amount of powder was sampled and subjected to an identical analysis. This procedure was repeated once more so that each initial sample was tested three times for small sampling. Finally, it was possible to compare a set of eight spectra (4 from a quenched sample and 4 from a straight mixture) for each initial composition. The difference remained within the range of experimental errors. A further investigation also revealed that 20-minute exposures were sufficient and provided spectra amply adequate for analysis.

Therefore, the experimental method for calibration purposes can be summarized as follows: preparation of a stoichiometric mixture from the compounds, powdering, and three 20-minute exposures of each sampling with remixing after the first exposure. This process was followed for all samples analyzed thereafter.

3.4.4 Analysis and results

The calibration cannot be completed until the results are analyzed and the type of analysis dictated which characteristics of each spectrum was to be considered. Figure 3-7 shows the spectra of two different compositions and already qualitatively the difference is striking. In the numerical analysis, a computer programme calculates the number of counts under each peak and subtracts the contribution due

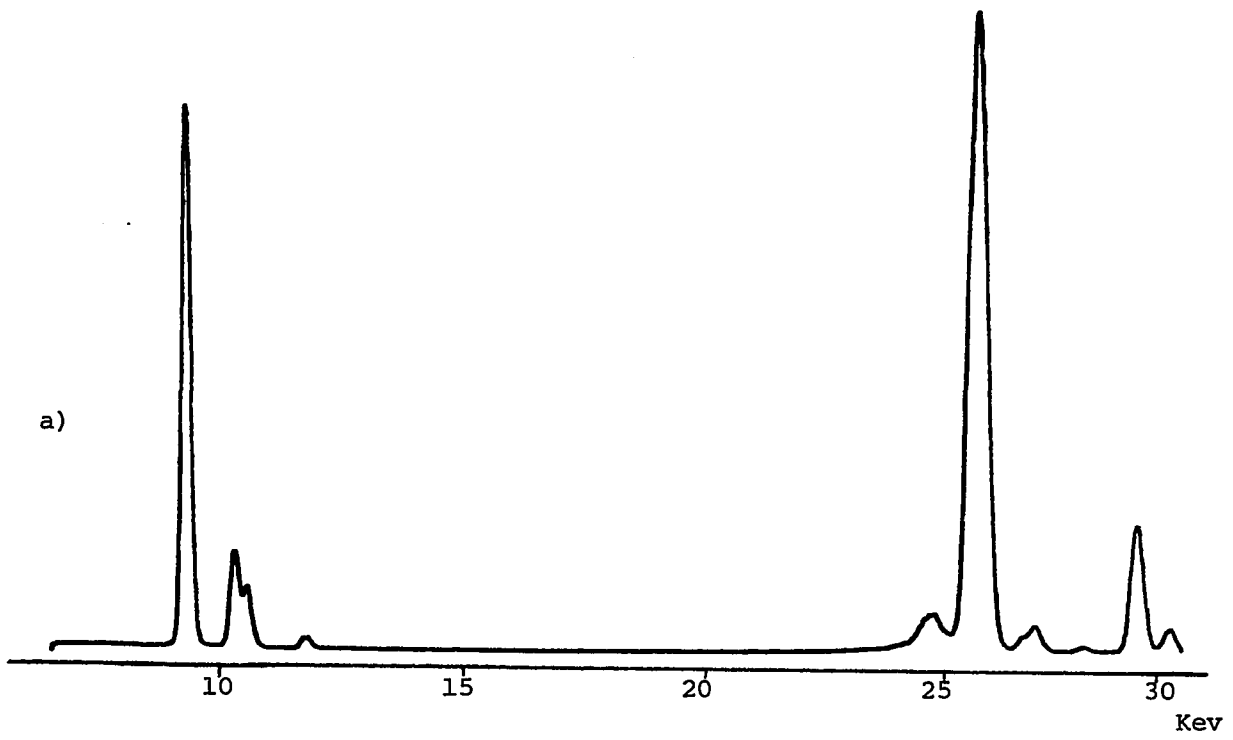

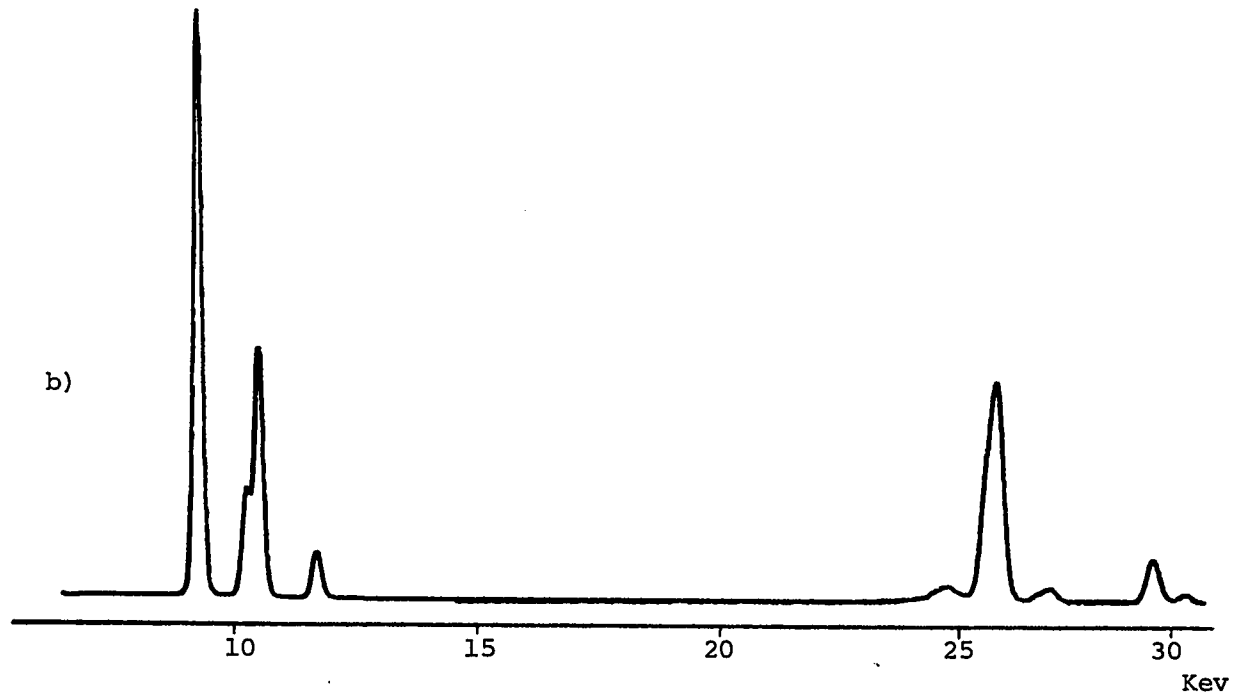

Fig. 3-7. Typical Spectra, a) $GaAs_{0.1}Sb_{0.9}$, b) $GaAs_{0.6}Sb_{0.4}$.

to background noise. It integrates the peaks by fitting them to a gaussian distribution after assuming initial values for position, height and width (a standard technique in Nuclear Physics). Then ratios of relative number of counts between pairs of peaks are calculated. When establishing a calibrating curve, only three of these ratios are retained, namely: Ga_α/As_β, Ga_α/Sb_α and Sb_α/As_β where the α's and β's mean the K_α and K_β radiations characteristic of each element. The contributions due to K_{α_1} and K_{α_2}, as well as K_{β_1} and K_{β_2} radiations of the lower energy elements Ga and As cannot be distinguished here because of the resolution of the analyzer, however, for Sb the K_{α_2} radiations are barely distinguished from the K_{α_1} radiations, but the K_β's are clearly separate. Careful inspection of figure 3-8 where a typical spectrum is recorded on a semi-log scale reveals the situation.

The reason for the choice of As_β over As_α also becomes evident from figure 3-8: the As_α peak overlaps the Ga_β peak and complicates the analysis. At the Sb-end of the spectrum other peaks as well are present due to the radiations associated with various emission and scattering processes. All these peaks are identified in figure 3-8 and table 3-I compares their characteristic energies with those of the three elements of concern here. In the numerical analysis, all peaks present are treated with a gaussian distribution and the background noise is assumed to vary linearly throughout the spectrum. In figure 3-9 the fit between the calculated points (C) and the experimental points (E) is displayed on a computer output for a typical Sb K_α-peak. It is possible to distinguish the K_{α_1} and K_{α_2} contributions within the peak but due to limited resolution

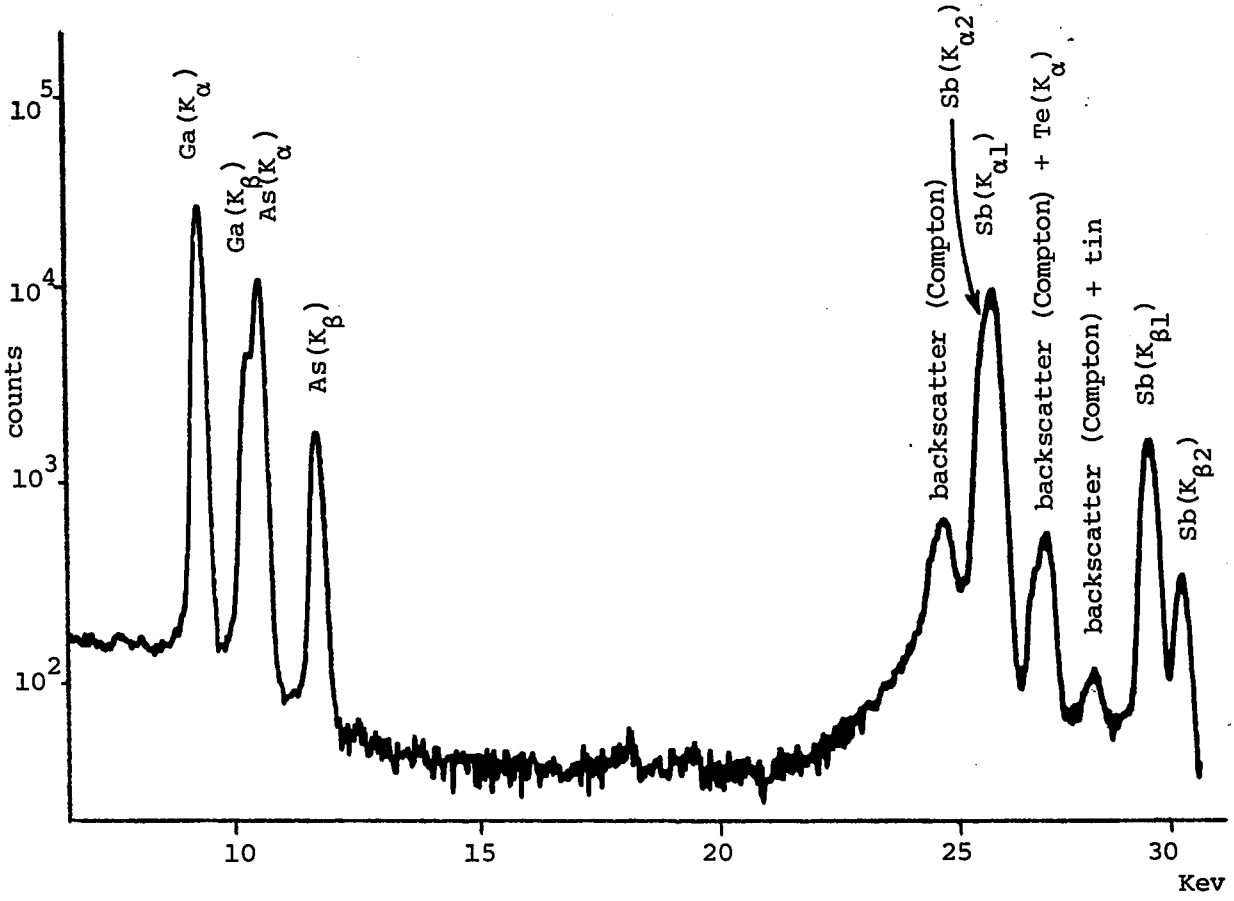

Fig. 3-8. Spectrum identifying all peaks present.

Table 3.I

$_{53}I^{125} + e^{-} \rightarrow {}_{52}Te^{125}$ - electron capture
- lifetime: 60 days

$_{52}Te^{125} \rightarrow {}_{52}Te^{125} + \gamma$ - isomeric transition
- lifetime: 58 days
- gamma energies: 35.48 KeV

Characteristic K X-rays of some elements in KeV

ELEMENT	K_{ab}	$K_{\beta 2}$	$K_{\beta 1}$	$K_{\alpha 1}$	$K_{\alpha 2}$
Ga	10.368	10.365	10.263	9.251	9.234
As	11.863	11.863	11.725	10.543	10.507
In	27.928	27.859	27.274	24.207	24.000
Sn	29.190	29.106	28.483	25.270	25.042
Sb	30.486	30.387	29.273	26.357	16.109
Te	31.809	31.698	30.993	27.471	27.200

Energy of backscattered radiation from source

Compton scattering: $$E' = \frac{E_o}{1 + \frac{E_o}{mc^2}(1 - \cos\theta)}$$

where

E' = scattered radiation (in KeV)

E_o = incident radiation (in KeV)

mc^2 = rest mass of an electron = 511 KeV

$\theta = 180^{\circ}$ for backscattering.

for E_o = 35.48 KeV (γ-ray) → E' = 31.17 KeV
E_o = 27.47 KeV ($K_{\alpha 1}$ X-ray of Te) → E' = 24.80 Kev
E_o = 30.99 KeV ($K_{\beta 1}$ X-ray of Te) → E' = 27.64 KeV
E_o = 31.70 KeV ($K_{\beta 2}$ X-ray of Te) → E' = 28.21 KeV

the whole peak is fitted to a gaussian distribution. The result shown in figure 3-9 confirms the usefulness of the technique used.

Further tests were conducted in order to standardize the calibration of the instrument. Figures 3-10 to 3-12 reveal the inherent problems relative to the geometry of the excitation-detection unit and of the sample itself. Figure 3-10 shows the contribution to the number of counts when only the sample holder and the milar membrane are exposed. The background noise is relatively low but peaks already appear in the high energy end of the spectrum. Figure 3-11 emphasizes the increase in the number of counts and gives a better resolution of the peaks present at the high energy end of the spectrum. These peaks are caused by the Compton backscattering and elastic scattering of the various radiations present (see table 3-I). Here a sample of pure silicon was powdered and analyzed. Silicon was known to fluoresce outside the energy range used in this study and was therefore chosen so that no Si-characteristic peaks would appear in the spectrum. Finally, figure 3-12 shows a spectrum for a layer of water placed in a sample holder. Water also fluoresces outside the chosen range of energy and the increase in counts (compared with figure 3-11) is due to the increased area of sample since the layer of liquid occupies the full area of the sample holder.

Despite these various contributions to the number of counts in the spectrum, it was nevertheless decided to retain the geometry of the instrument and that of the sample holder since they were of a simple design, and to correct for these effects in the numerical analysis,by adjusting

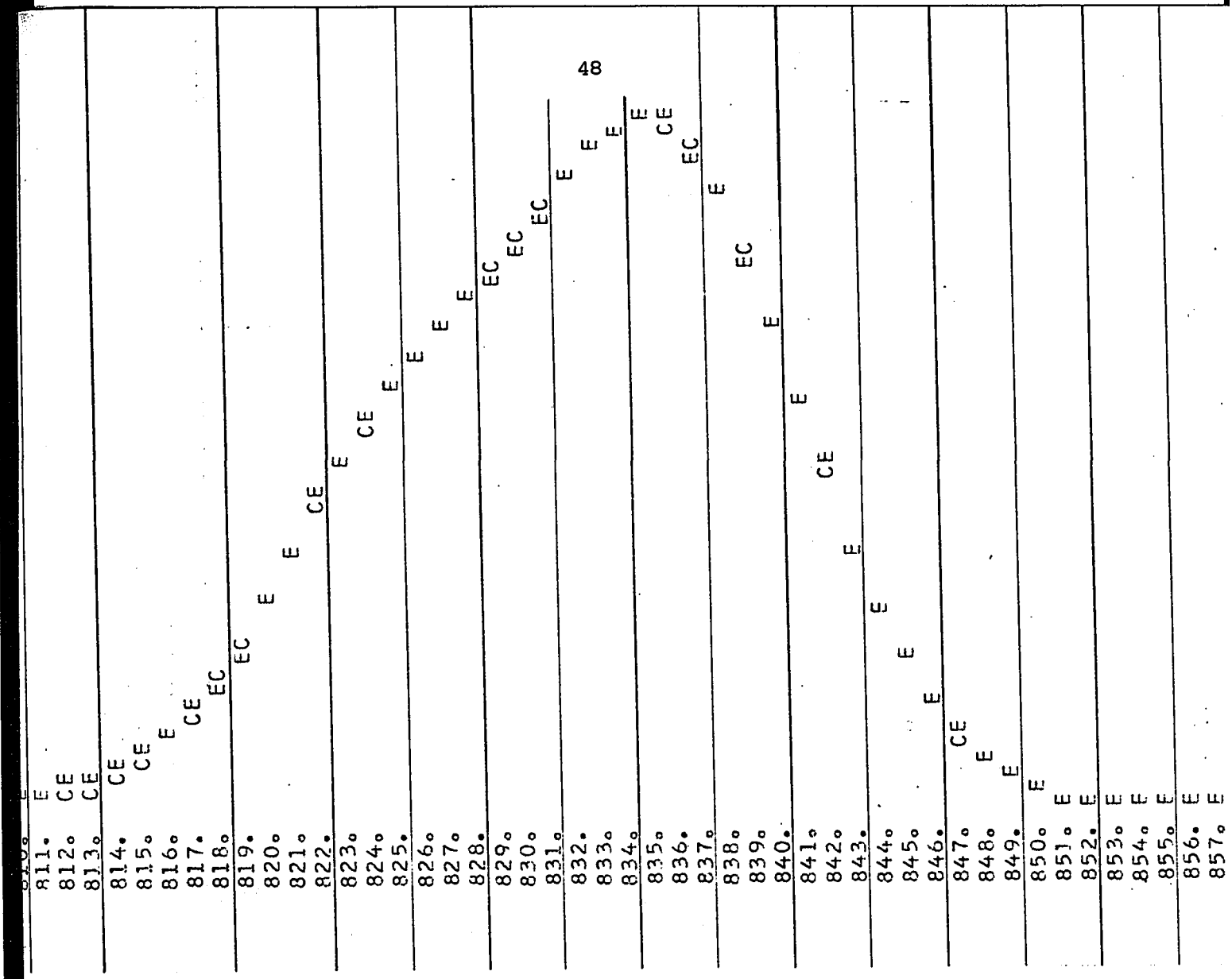

Fig. 3-9. Typical computer fit of a peak. (C) calculated points, (E) experimental points. (When both coincide, E appears only).

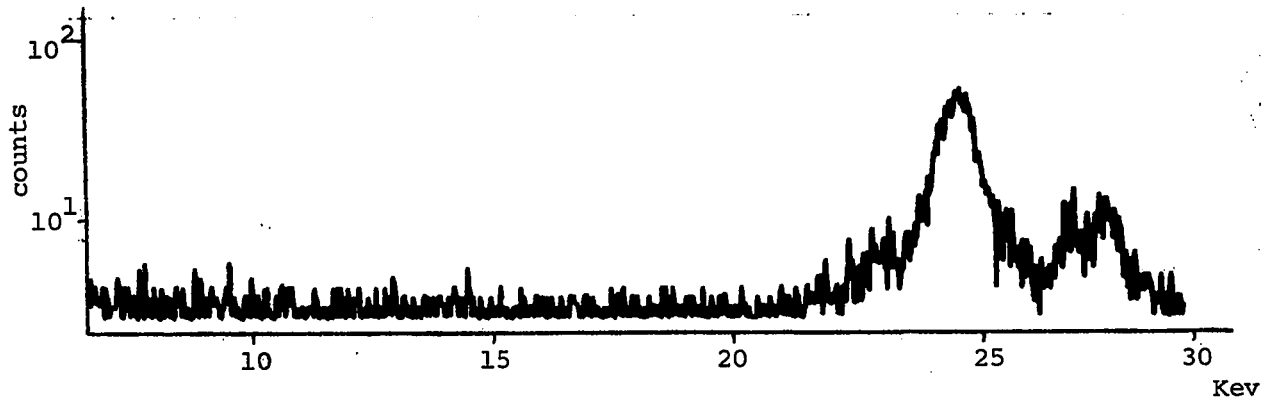

Fig. 3-10. Noise and backscattering for no sample. (Exposure time : 20 minutes).

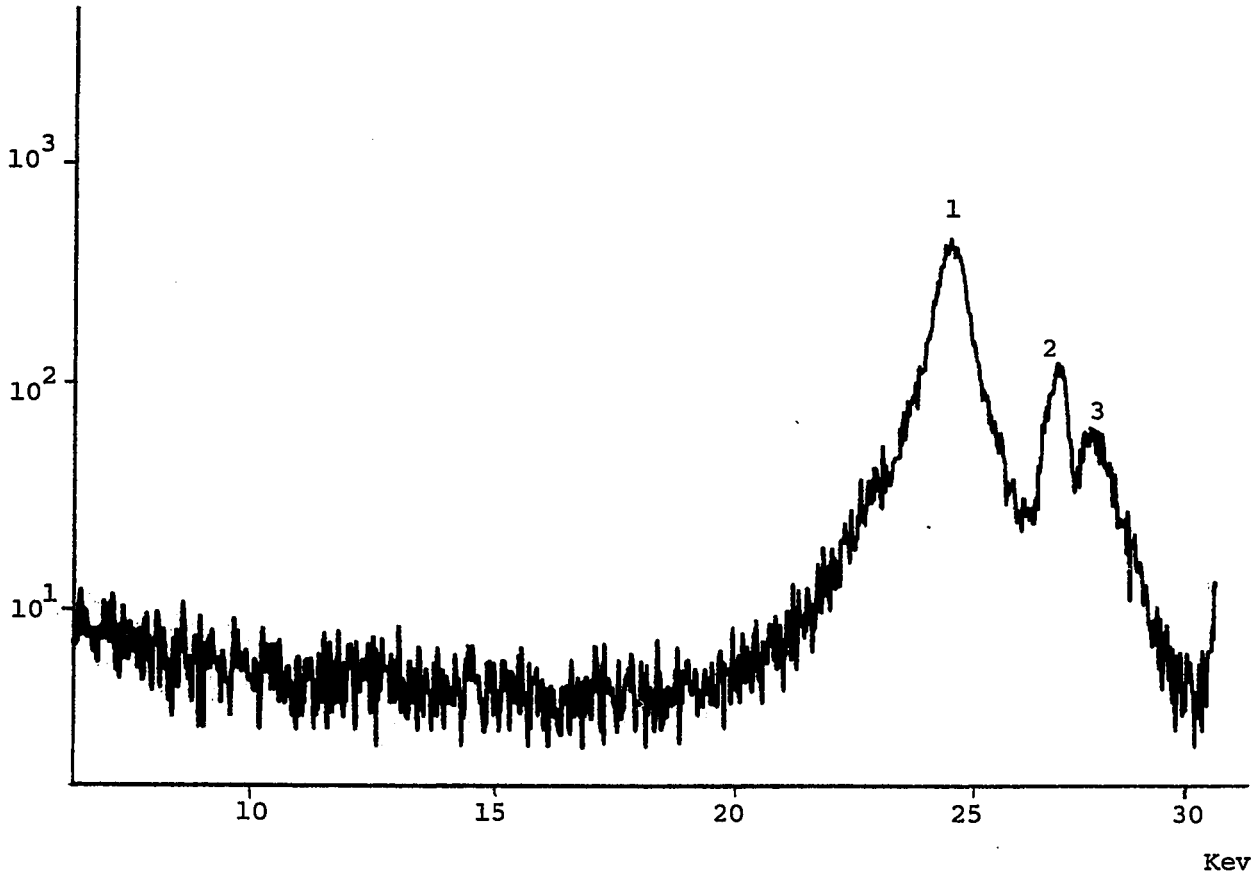

Fig. 3-11. Noise and backscattering for Si. (Exposure time: 20 minutes).

1 : peak due to Compton backscattering of $K_{\alpha 1}$ radiation of Te ($\theta=180^{o}$) and elastic scattering of $K_{\alpha 1}$ radiation of Sn.

2 : peak due to Compton backscattering of $K_{\beta 1}$ radiation of Te and elastic scattering of $K_{\alpha 1}$ radiation of Te.

3 : peak due to Compton backscattering of $K_{\beta 2}$ radiation of Te and elastic scattering of $K_{\beta 1}$ radiation of Sn.

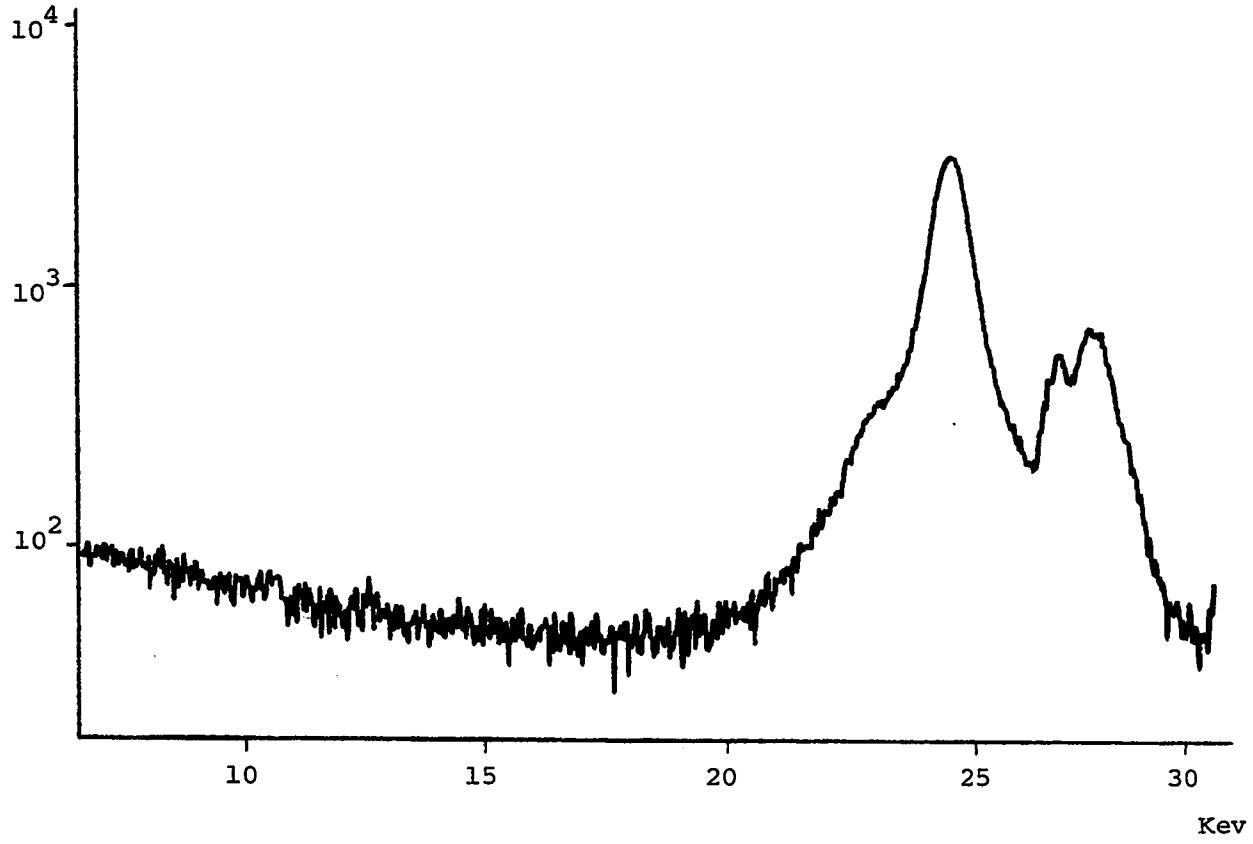

Fig. 3-12. Noise and backscattering for H_2O. (Exposure time: 20 minutes).

the computer programme, was easy. One effect, however, that could not be dealt with numerically when tested, was due to the sample itself: more precisely, to the amount of material to be analyzed. The reason for conducting such a test came from the fact that the samples of single phase material to be analyzed upon completion of calibration were available in very small quantities (up to 0.3 gram but more often between 0.05 and 0.1 gram).

Varying amounts of the standard samples were analyzed (down to 0.05 gram) and results showed that the values of the ratios varied with the masses of sample used if these were less than about half a gram. It is important to note here that every sample then and thereafter was placed over the same area in the sample holder in order to devise a standard procedure for the analysis and avoid effects due to the geometry of the sample in the sample holder as discussed previously.

The variations recorded are due to the effect of the penetration depth of the incident radiation: the absorption coefficients of the K-radiations of gallium and arsenic atoms are both large and similar in the sample, therefore the absorption is practically the same for each element. The ratio Ga_{α}/As_{β} remains almost constant for different quantities of powder (see figure 3-13), and little effect is observed since both types of radiations are affected similarly with varying amounts of sample. However, the absorption coefficient of the K-radiations of antimony is smaller than those of gallium or arsenic in a sample: if, for instance, the amount of sample is increased, the Sb K-radiations suffer less absorption than the Ga K-radiations or the As K-radiations, and results

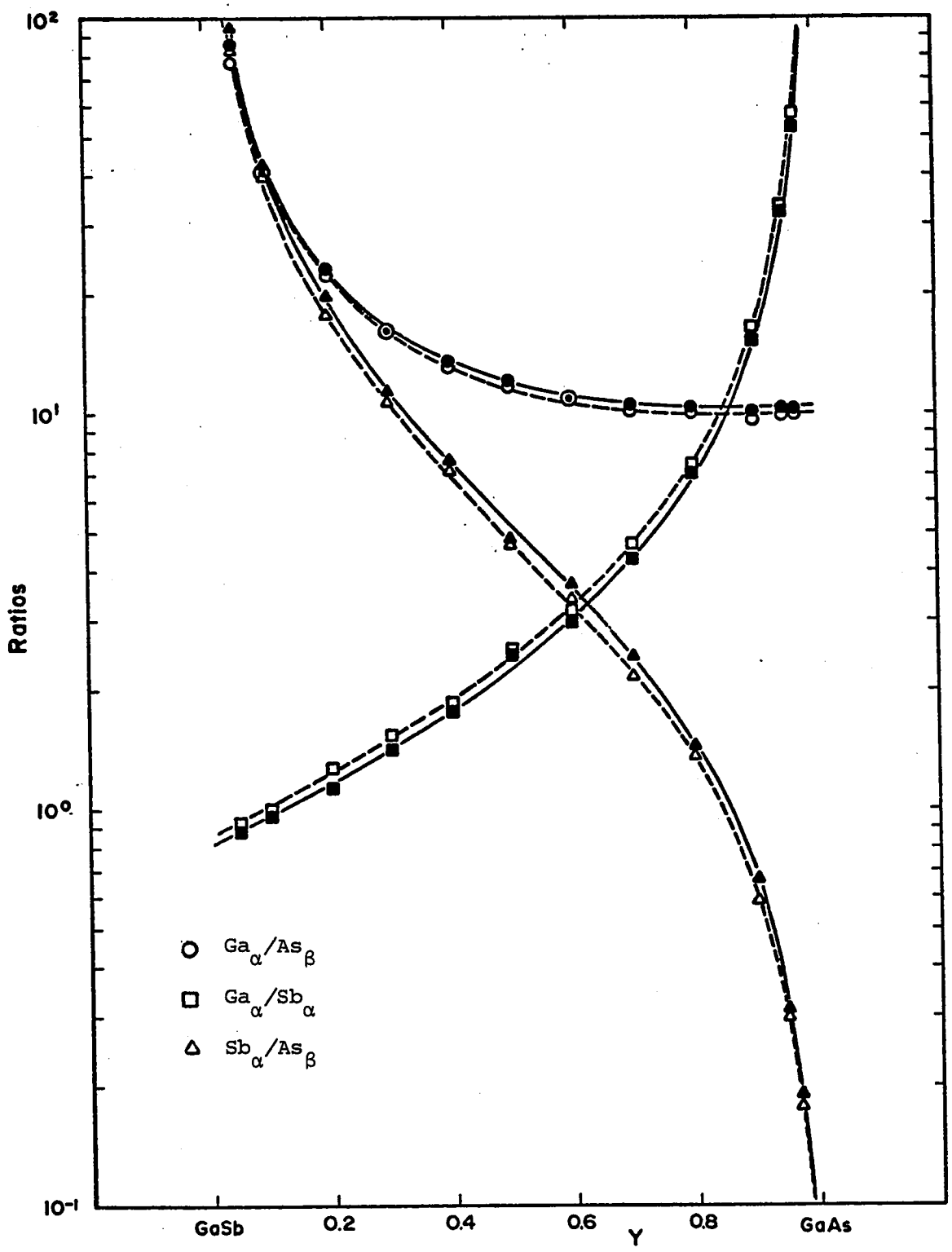

Fig. 3-13. The $GaAs_ySb_{1-y}$ system. Calibration curves for X-ray fluorescence analysis.

——— 0.10 g ------- 0.05 g

show decreasing and increasing values of the ratios Ga_{α}/Sb_{α} and Sb_{α}/As_{β} respectively. The calibration curves for the ternary system $GaAs_ySb_{1-y}$ are presented in figure 3-13.

Finally, this effect will show until a certain thickness of powder is reached and this thickness will be closely related to the penetration depth of the incident radiation. Beyond this thickness, the ratios should and do remain constant within the experimental error. As stated previously, the problem here is that no sufficient quantity of single phase material of the alloy is available to reach that thickness. Consequently, the study of ratio versus quantity of material is so important that this effect could become the greatest cause of error if not considered carefully when evaluating the composition of unknown samples.

The single phase samples were analyzed in an identical fashion as those for calibration purposes. The final analysis was done on the average values of the ratios found from three exposures (20 minutes each). The tabulated results appear in table 3-II for a number of various single phase samples. The identification of each sample is according to the growth code of the total ingot. From the calibration curves the composition corresponding to each ratio is evaluated. The average composition is then listed followed by the measured lattice constant from X-ray powder photographs. Finally, an evaluation is given for the quality of each sample regarding the homogeneity of the phase.

Table 3-II. List of samples used to determine the lattice constant-composition relation for the pseudobinary system $GaAs_ySb_{1-y}$.

Sample	Ga_α/As_β	Ga_α/Sb_α	Sb_α/As_β	y	a_{nm}	quality /5
TZF-6						
5.30 cm	0.380	0.363	0.362	0.370	0.5929	3
6.60	0.333	0.317	0.325	0.329	0.5949	3
7.40	0.255	0.241	0.249	0.252	0.5982	5
7.70	0.186	0.211	0.193	0.188	0.6011	5
8.20	0.093		0.093	0.093	0.6053	5
9.20(A")	0.030	0.030	0.030	0.030	0.6079	5
TFF-1						
1.55 cm	0.967	0.973	0.973	0.973	0.5667	5
2.05		0.967	0.967	0.967	0.5668	5
2.40		0.960	0.959	0.960	0.5668	5
3.55	0.195		0.191		0.6013	4
TZF-2						
1.10 cm		0.928	0.928	0.928	0.5679	4
5.00 (A')	0.313	0.298	0.312	0.312	0.5955	1
5.00(A")	0.265	0.265	0.267		0.5967	1
5.10(B)*	(0.550)	(0.493)	(0.492)			
5.10(A)	0.290	0.277	0.285	0.287	0.5968	3+
6.20	0.190	0.178	0.220		0.5998	3
1.90†		0.760	0.767	0.79 (0.33)	0.5721 (0.5949)	4+
(CZ)TFF-2						
2.35		0.953	0.951	0.952	0.5672	5
4.10		0.927	0.925	0.925	0.5680	5
4.70		0.920	0.920	0.920	0.5683	5
5.25(A)*	0.268	0.258	0.262		0.5996	2
5.25(A")*	0.268	0.260	0.264		0.6004	3+
5.35(A')*	0.223	0.219	0.223		0.5989	3+
5.00†		0.853	0.857	0.871 0.720	0.5695 0.5739	4

* All these samples were two-phase at least and could not be used since the detector only records the average composition of the two phases.

† These samples are two-phase but the weak one is almost unnoticeable and changes little in the composition value given from X-ray fluorescence. The values quoted here come from density considerations of the phases present. For sample TZF-2; 1.90 the strong phase (∿ 95%) is the one chosen for the graph. For sample (CZ)TFF-2;5.00, the two phases (respectively 90% and 10%) are displayed on the graph.

3.5 Lattice Constant-Composition Relation

The values of lattice constant 'a' as a function of composition 'y' for homgeneous single phase samples are shown in figure 3-14 where the estimated accuracies are ±0.0002 nm in 'a' and ±0.01 in composition 'y'. The results obtained here are in very good agreement with those of Straumanis and Kim (65S1) (also given in figure 3-14), and show that in the range $0 < y < 0.38$ the points satisfy a Vegard line but that in the range $0.70 < y < 1.00$ the lattice constant values fall well below this line.

3.6 Solid Solution in $GaAs_ySb_{1-y}$

3.6.1 Evidence of a miscibility gap

Figure 3-14 also shows the absence of any specimens in the range $0.38 < y < 0.70$ and as mentioned at the beginning of this chapter most workers including the author have been unable to find or produce single phase material in that region which now seems to indicate that a miscibility gap may exist for the pseudobinary system $GaAs_ySb_{1-y}$.

Such a possibility is substantiated by visual as well as microscopic inspections of specimens which show two regions of different colour on various cross-sectional slices. Further investigations have corroborated the presence of such a gap: a study was made of the variation of lattice constant (and hence composition, since the two can now be correlated)

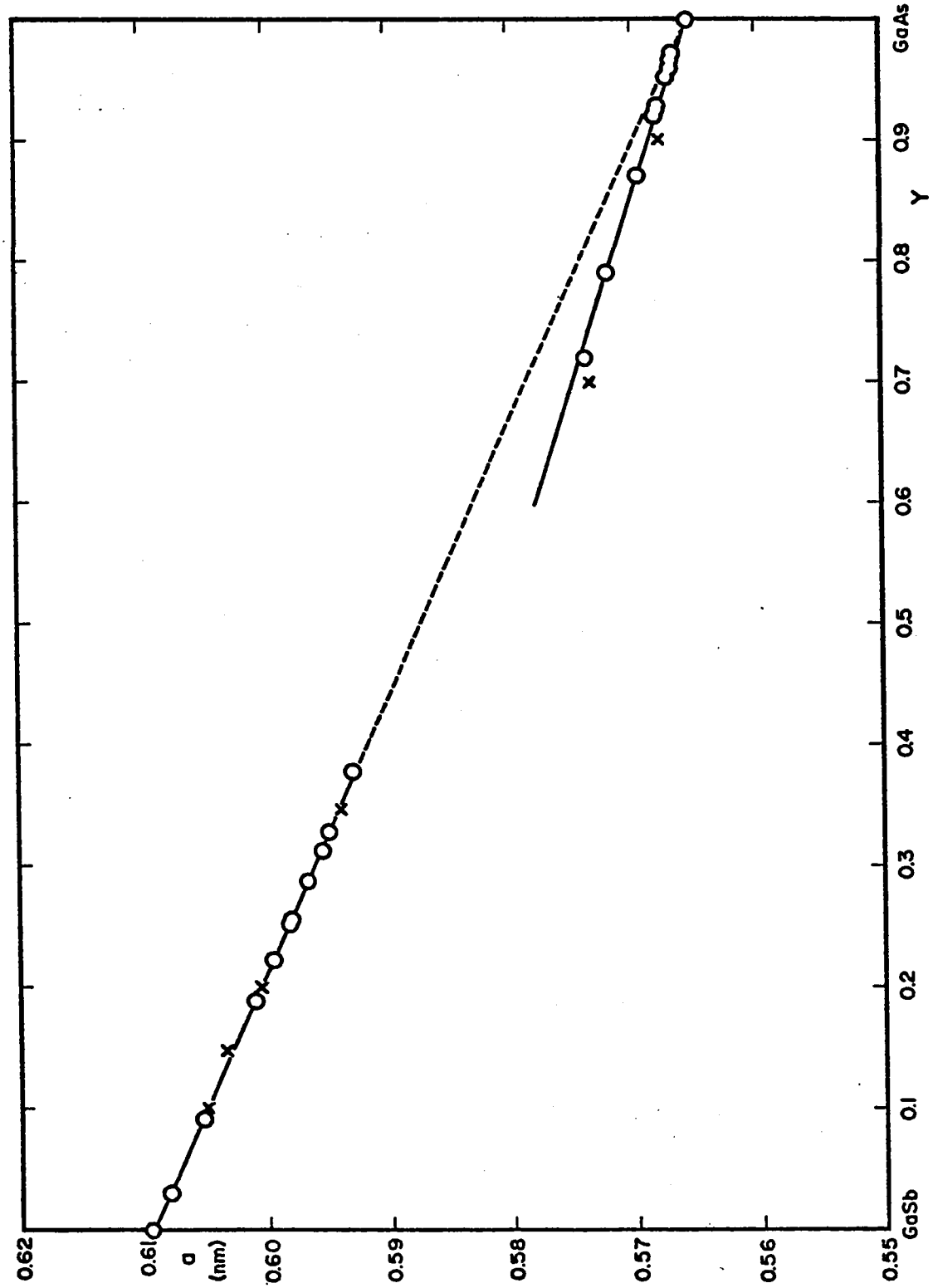

Fig. 3-14. $GaAs_ySb_{1-y}$ - variation of lattice parameter as a function of composition.

× Straumanis and Kim (65S1) O present work ------ Vegard line.

along the length of ingots produced with the horizontal Bridgman technique. In three ingots so investigated, the composition variation with position along the ingot was found to be of the general form shown schematically in figure 3-1, that is single phase behaviour throughout most of the ingot with a smooth variation in composition near the GaAs end, followed by a discontinuous change to compositions rich in GaSb. This behaviour had been interpreted as a growing fault by Rosenbaum (private communications) and associated to the difficulties encountered by Woolley (62W1) while growing alloys of $InAs_ySb_{1-y}$. However, after four different attempts to sequential growth, Rosenbaum was still unable to obtain any single phase material in the range $0.38 < y < 0.80$.

As indicated by Stringfellow (72S1) this type of variation may be expected from a system showing a peritectic reaction; the miscibility gap in the range of solid solutions corresponding to the discontinuity in the solidus curve of the phase diagram at the peritectic temperature (peritectic systems are discussed in the next chapter). Determinations of the lattice constant of specimens at the discontinuity will then reveal the limits of such a miscibility gap.

Because in the production of the ingots, the freezing interface was not vertical, the presence of the discontinuity was clearly visible and several adjacent cross-sectional slices could be cut from the same ingot. Each slice showed a GaAs-rich section characterized by a greyish blue colour and a GaSb-rich section of a light gray colour.

While these results were sufficient to indicate a peritectic behaviour, it was found that the samples could not be used directly to give accurate values for the miscibility gap. The very slow rate of growth yielded good single phase conditions over most of the ingot except close to the discontinuity where X-ray photographs displayed two-phase and occasionally multiphase behaviour. During growth, a constitutionally supercooled region is always present, but due to the large amount of supercooling that III-V solutions permit before nucleating the growth is usually relatively unperturbed. Near the miscibility gap, the solution becomes supercooled relative to the two ends of the gap and the crystal surface provides nucleation sites for both compositions.

In an effort to determine the limiting compositions at the discontinuity, small samples were taken at various positions on slices showing the two colour regions. On the X-ray photographs, faint lines corresponding to one or more subsidiary phases in addition to those of the main phase discussed above were apparent and measured whenever possible. It was found that for different ingots and therefore different growth conditions, it was impossible to duplicate the limiting compositions of the miscibility gap. Furthermore, the compositions could not be determined from X-ray fluorescent analyses as this technique only gives the average composition of a sample.

3.6.2 Growth of $GaAs_ySb_{1-y}$ with slow step-freeze

It was therefore decided to prepare a new ingot by the step-freeze technique but with a much slower growing rate. The initial com-

position was chosen as y = 0.30. The temperatures of the two zones were 1100°C and 500°C. The charge was prepared from the compounds and tellurium was added as a dopant for future use of the ingot in electrical measurements. The growth rate was 0.4 cm/day. For this ingot, a double ampoule system was used with each ampoule individually backfilled to 30 kPa of argon. The purpose of the two ampoules was to prevent oxidation of the ingot if the inside ampoule should crack. The furnace was tilted to 3.8 degrees to provide an ingot of reasonable cross-section. A horizontal furnace would have yielded a long ingot with a smaller cross-section. It would also involve longer growing periods as well as smaller surfaces to work with in the case of electrical measurements on bulk material.

The charge was left in the hot zone for a period of four days after which the recrystallization process was started by the slow pulling of the ampoule across the temperature gradient of the furnace. After 37 days, the furnace burnt out but fortunately, a good part of the ingot had travelled through the thermal gradient and the all important GaAs-rich phases were present with the sharp change in colour well defined. The standard procedures were then followed regarding cutting, sampling and X-ray photography of the cross-sectional slices. A schematic and pictorial dossier is presented in figures 3-15 to 3-17.

The double ampoule technique proved very useful as the inner ampoule cracked but retained its shape because of the outer one. This prevented the alloy from flowing out and crystallizing in a shape which would have made measurements nearly impossible. It also prevented

Fig. 3-15 Part of a cross-sectional slice showing the sharp boundary between GaAs-rich and GaSb-rich material (ingot CZ TFF-2).
a) chemical staining b) boundary through the thickness.

Fig. 3-16 Ingot TFF-73-1 showing the sharp change of phase.
a) the burning out of the furnace produced erratic growth at the end of the ingot (right)
b) a closer view of the ingot - the dark region is GaAs-rich material.

Fig. 3-17 The two faces of a slice from ingot TFF-73-1 showing the sharp boundary.
a) the crystallytes of the GaAs-rich phase are well defined (bottom).
b) the GaSb-rich phase (top) reveals the presence of GaAs-rich dendrites of the same composition as the bottom part.

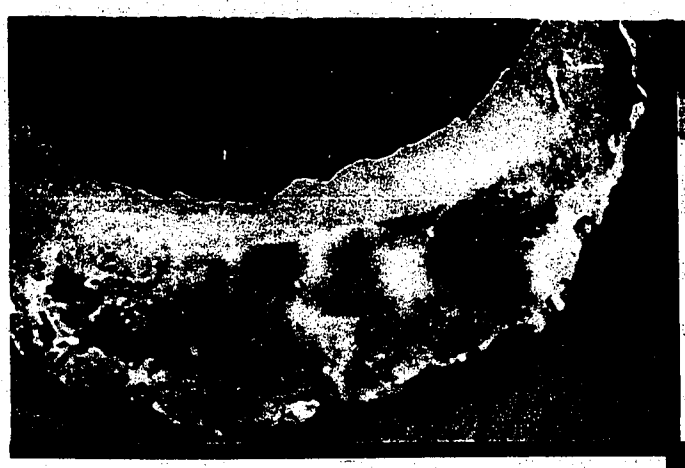

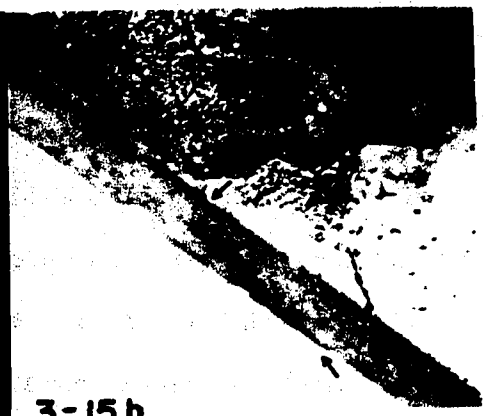

3-15b

3-16a

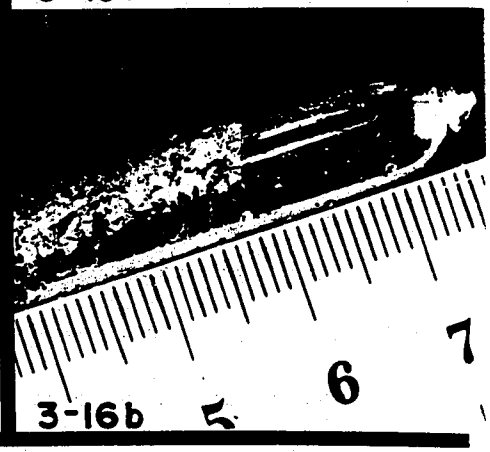

3-16b

3-17a

3-17b

oxidation of the ingot as mentioned previously. There are two possible explanations for the cracking of the inner ampoule: the tilt angle may have been too large and the weight of liquid increased the radial component of expansion thus cracking the ampoule or it may be a combination of the tilt angle too large and the burning out of the furnace as the melt then rapidly expanded upon freezing. From the shape of the resulting ingot it is more likely to be the second mechanism which took place as the first few centimetres of the ingot were correctly shaped.

3.6.3. A miscibility gap in the range $0.38 < y < 0.61$.

The final measurements involved in the determination of the limiting compositions of the miscibility gap were made on small pieces taken as close to the boundary as possible from every cross-sectional slice which displayed the two-coloured regions. Other samples taken from ingots grown by the sequential growth method were also measured; this technique does not give slices with two coloured regions but yields GaSb-rich compositions up to the lower limit of the miscibility gap (i.e. $0 < y < 0.38$).

The lattice constants of every measurable phase observed were determined and plotted on the lattice constant versus composition relation (figure 3-14). It was found that no phase, main or subsidiary, corresponding to the range $0.38 < y < 0.61$ was observed. Assuming that any phase observed in this way must represent a composition at which single phase solid solution occurs, the range $0.38 < y < 0.61$ thus represents the maximum possible limits of the miscibility gap in the

pseudobinary alloy system $GaAs_ySb_{1-y}$. Figure 3-18 shows the various phases that were observed in the afore-mentioned investigation.

The evidence collected above and the lack of experimental data strongly suggested that a detailed study of the more complex properties of the phase diagram for such an alloy system be undertaken. In the following chapters, thermodynamic properties, phase diagram determinations and other related topics are developed both theoretically and experimentally.

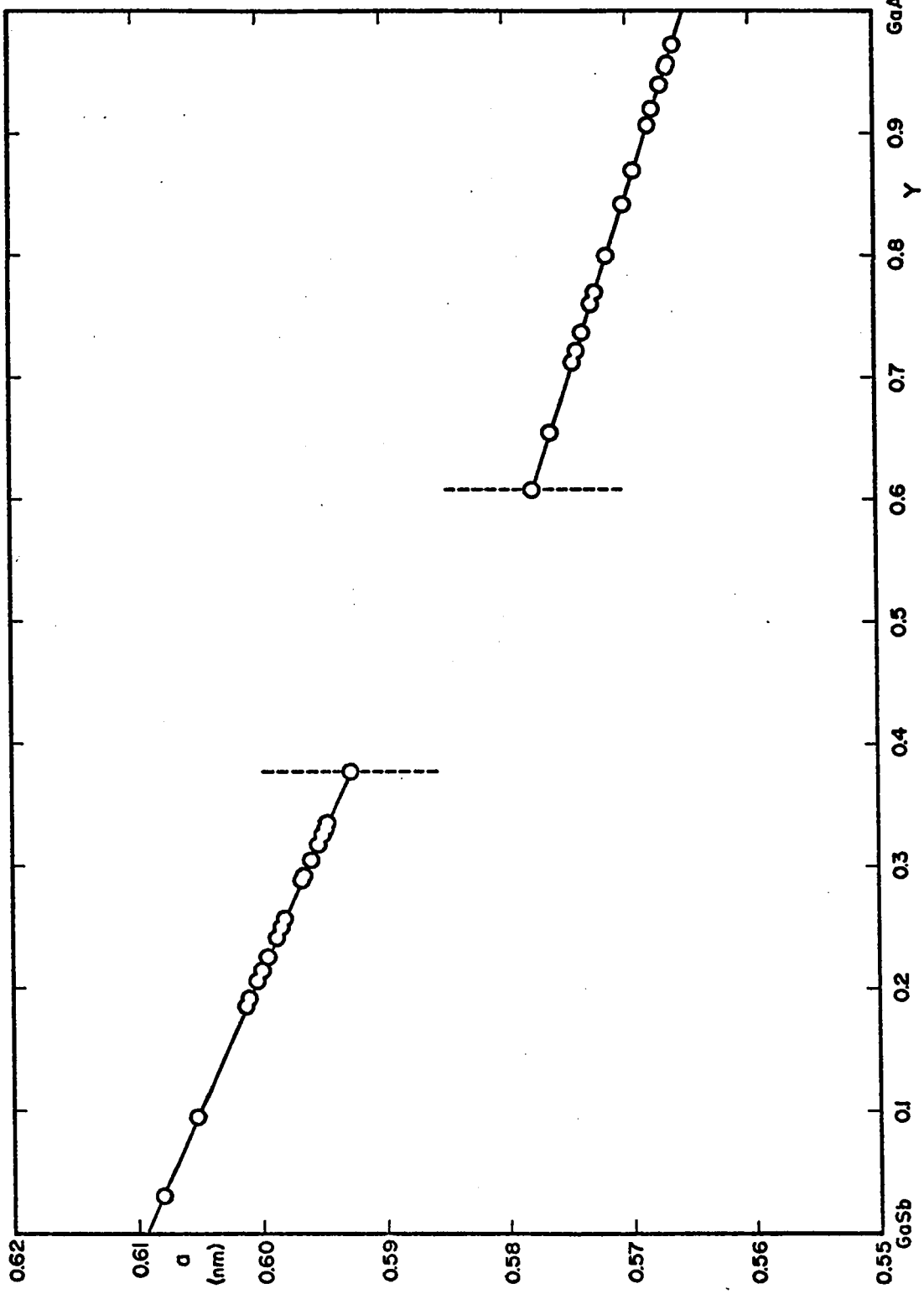

Fig. 3-18. $GaAs_ySb_{1-y}$ - representation of the limits of the miscibility gap on the pseudobinary section.

Chapter 4 Equilibrium Diagrams: general principles

4.1 Introduction

4.2 Primary Solid Solutions

4.3 Binary Systems

4.4 Free Energy

4.5 Ternary Systems

4.1 Introduction

The discussion of the physical properties, which are an integral part of 'thermodynamics' has been purposely postponed in order to devote a specific section of this work to a general study of the behaviour of alloy systems through the analyses of their respective equilibrium diagrams. In general, the structure of an alloy will depend upon the conditions under which it is cooled, but for an alloy of given composition there is at each combination of temperature and pressure an equilibrium state to which the alloy gradually approaches if it is held under the specified conditions for a sufficient time.

Since the state of true equilibrium is determined completely by the composition, pressure, and temperature, it is possible to draw diagrams which show the structure of the alloys concerned as a function of these variables: these are called 'equilibrium diagrams' or 'phase diagrams'. However in most work on metals and alloys, the structures are under atmospheric pressure and the vapour pressures are so small that it is justifiable to ignore the effect of pressure and the existence of the vapour phase, and the equilibrium of the solid and liquid phases can be studied as a function of the temperature and composition only.

It is commonly stated that the equilibrium diagram shows the structures of the alloys concerned under equilibrium conditions. The 'ordinary' equilibrium diagram, however, takes no notice of the sizes, shapes or mutual orientations of the individual crystals, although such

characteristics are of the greatest importance in determining the mechanical properties of an alloy, and must of course be taken into account when considering the condition of absolute equilibrium in the strict thermodynamic sense. The 'ordinary' equilibrium diagram shows the number and nature, and in some cases the compositions of the individual phases present in an alloy of given composition at a given temperature under conditions of what may be called 'practical' or 'ordinary' equilibrium in which effects of surfaces, sizes, shapes and orientation can be ignored.

The time taken to reach equilibrium varies greatly in different alloys and depends on whether the changes taking place involve atomic migration or diffusion over distances large compared with atomic dimensions, or merely involve a rearrangement of the atoms without long-range movement.

4.2 Primary Solid Solutions.

If AB is a hypothetical alloy system of two elements A and B, it is found that in general when the alloys are annealed to equilibrium at any one temperature the effect of the first small addition of B to A is to produce an alloy with the same crystal structure as that of the parent element A, and the resulting alloy is called a 'primary solid solution' or a 'terminal solid solution'. Such solid solutions are of two main kinds: interstitial solid solutions in which the atoms of the solute enter the interstices or holes between those of the solvent, and substitutional solid solutions in which the atoms of the solute replace

those of the solvent so that the two occupy a common lattice. Interstitial solid solutions are naturally formed only in systems where the solute atom is very much smaller than that of the solvent, and, on the other hand, substitutional solid solutions will form only when the atomic diameters of the two elements are not widely different. A primary solid solution is properly regarded as being the same phase as the parent metal, and if a physical property of such a solution is plotted as a function of the composition, the resulting curve is continuous and will usually be smooth. For systems where the atomic diameters of the two elements are nearly equal and the crystal structures are the same, a complete range of solid solution may be observed.

4.3 Binary Systems

If two elements are such that a complete range of solid solution is formed, the simplest type of equilibrium diagram is that of figure 4-1.

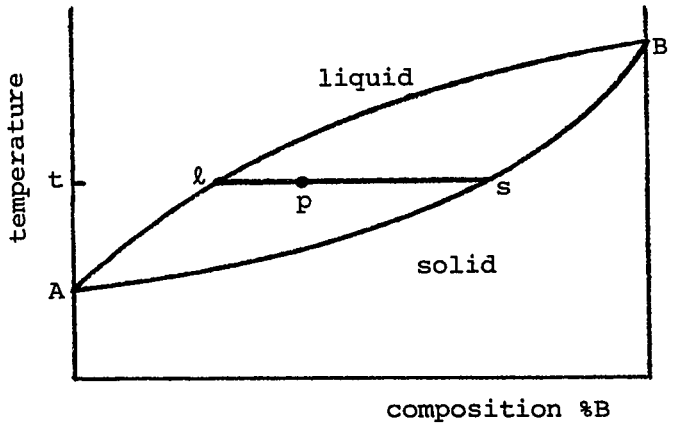

Fig. 4-1: A simple hypothetical binary system for two elements A and B.

At temperatures and compositions above the line AℓB ('liquidus curve'), the alloy is totally liquid. Below AsB ('solidus curve') the alloys are totally solid. Alloys in the region between the solidus and liquidus consist of a mixture of solid and liquid phases, and at any temperature the compositions of the two phases in equilibrium are given by the intersection of the temperature ordinate with the curve concerned. At the temperature t an alloy of composition p will consist of a mixture of liquid of composition ℓ and solid of composition s at equilibrium. The relative amounts of liquid and solid are as the ratios of ps over pℓ: this is known as the lever principle. The line sℓ is called a 'tie-line'.

The type of equilibrium diagram shown in figure 4-1 is usually confined to systems where the atomic diameters of the two elements are very nearly equal; for this purpose, the atomic diameter is usually defined as the closest distance between two atoms in the crystal of the element concerned. For a given solid solution what may be termed as the 'size factor' is the difference between the atomic diameters of the solvent and solute expressed as a percentage of the atomic diameter of the solvent, and to a rough approximation the size factor becomes unfavourable when it exceeds about 15% (17% in 64M2). In some cases, the atomic diameters have to be adjusted to allow for complicating effects such as ionization for instance.

There are also cases where the size factor is not too favourable and the equilibrium diagram looks like that of figure 4-2. where the liquidus and solidus pass through a minimum where they touch. Furthermore, systems are found in which homogeneous solid solutions split up on

cooling into two solid solutions of the same crystal structure but of different compositions, such an effect is also shown in figure 4-2 where the curve MsZs'N bounds what is known as a 'closed miscibility gap'. An alloy such as p splits into two solids of compositions s and s'. As was the case for figure 4-1, the line ss' is a tie-line and the relative amounts of the two solids formed are governed by the lever principle.

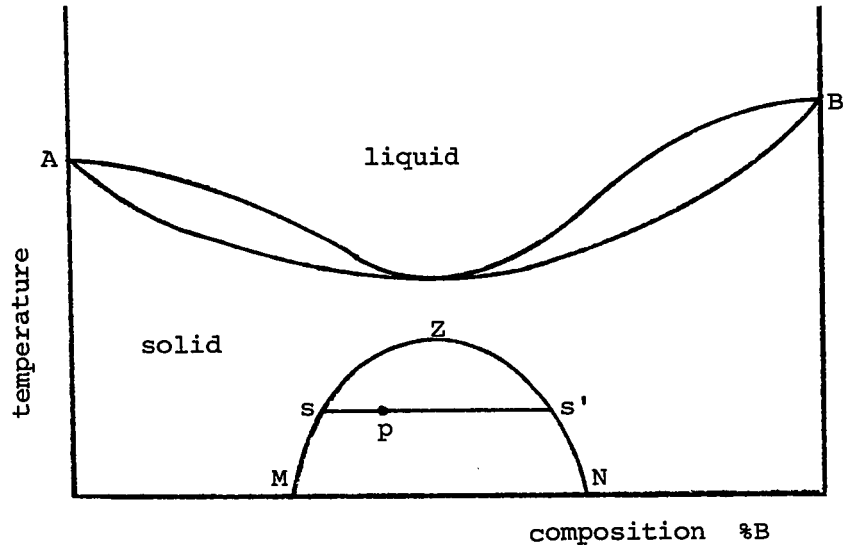

Fig. 4-2: Hypothetical binary system of two elements completely miscible in the solid state at high temperatures, but displaying a closed miscibility gap at low temperatures.

Furthermore, a stage may be reached at which the curve MsZs'N will move upward in the diagram and reach the solidus curve; the two elements are then no longer completely miscible in the solid state. The equilibrium diagram can then become of the eutectic type, or the peritectic type or combinations of either. Figures 4-3 and 4-4 show a simple eutectic system and a simple peritectic system respectively. In the

former, the melting points of each element is lowered by the addition of the other and the two liquidus curves intersect at the 'eutectic point', at this temperature, a liquid of composition E is in equilibrium with α solid solution of composition C and β solid solution of composition D (see figure 4-3). In the latter, the freezing point of one of the elements is raised by the addition of the other; at a temperature known as the 'peritectic horizontal', a liquid phase of composition P is in equilibrium with α solid of composition C and β solid of composition D, (see figure 4-4).

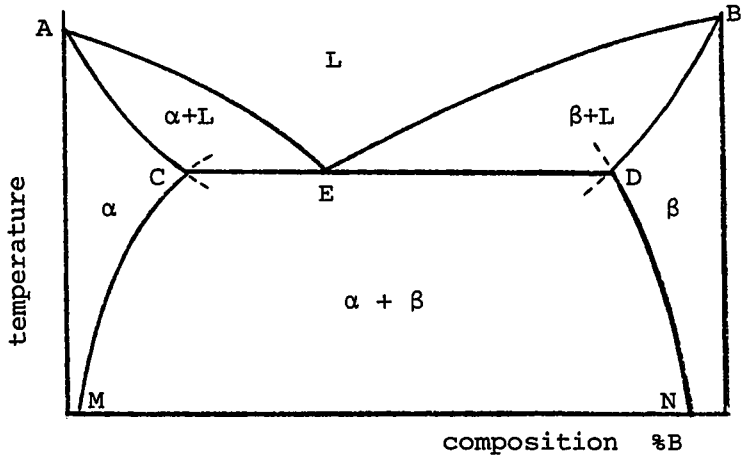

Fig. 4-3: A simple eutectic system.

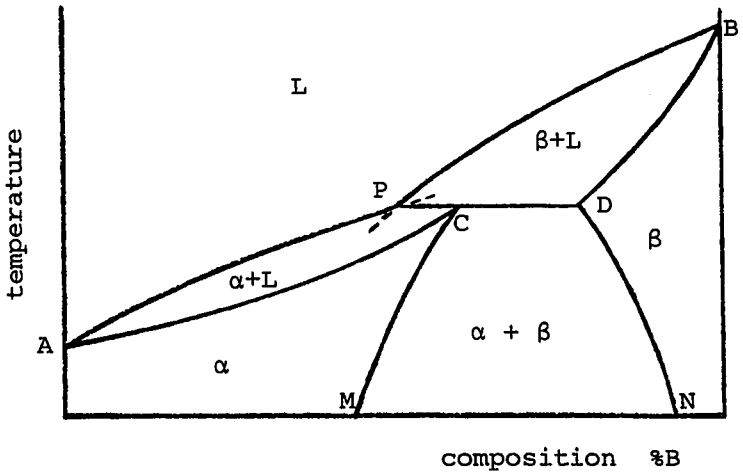

Fig. 4-4: A simple peritectic system.

Finally, in figure 4-3 the curves AC and CM represent boundaries between a single homogeneous α-phase field and the two-phase (α + L) and (α + β) fields. It is a general principle that in all cases where such intersections occur in any part of an equilibrium diagram the curves if extrapolated past their intersection must pass into two-phase regions as indicated by the dotted lines in figures 4-3 and 4-4.

4.4 Free Energy

It is possible to interpret equilibrium diagrams from the concept of free energy. In order to do so, the formalism used is the 'Gibbs free energy' defined by the equation:

$$G = U + PV - TS \qquad 4.4.1$$

where U is the total internal energy of a system of volume V at pressure P and temperature T, S is the entropy. The condition for equilibrium is that G has a minimum value. When dealing with equilibrium between solids and liquids at constant atmospheric pressure, the term PV is small compared to the others and equation 4.4.1 may be approximated by the 'Helmholtz free energy' defined as

$$F = U - TS \qquad 4.4.2$$

In the case of two elements A and B for instance, the total entropy S consists of two terms: the thermal entropy which represents the entropy attained by heating from the absolute zero to the temperature T, and the configurational entropy or entropy of mixing which results from the fact

that with two kinds of atoms, A and B, there are many alternative arrangements which are consistent with the same statistical state of randomness. In solid solution alloys a change of composition has a much greater effect upon the value of the latter and consequently it is justifiable to ignore the former and consider the condition for equilibrium when $U - TS_c$ has a minimum value (S_c is the configurational entropy).

When a solid solution is formed the configurational entropy is maximum at equiatomic composition and the relation that exists between S_c and composition has an inverted 'U-shape' symmetric form, and with infinite slopes at the end points (i.e. for the pure elements). The variation of the total internal energy with composition cannot be predicted but it is expected to be of two main types (see figure 4-5). In figure 4-5a, the resulting $U-TS_c$ curve has the lowest possible free energy, and the stable condition at all compositions will be a single phase because no splitting of the alloy into two phases can produce a free energy lower than that of a single phase. In figure 4-5b, the $U-TS_c$ curve rises to a maximum and two minima so that a tangent may be drawn to touch the latter at compositions x and y. Over the composition range outside x and y, the lowest free energy is given by a single phase but between x and y, a mixture of two phases of composition x and y will have a lower free energy than any single phase whose free energy is given by the $U-TS_c$ curve.

The curves $U-TS_c$ of figure 4-5 refer to one particular temperature only and a variation in temperature will produce a change in the positions of x and y as for instance in figure 4-5b. Figure 4-6 taken from Hume-

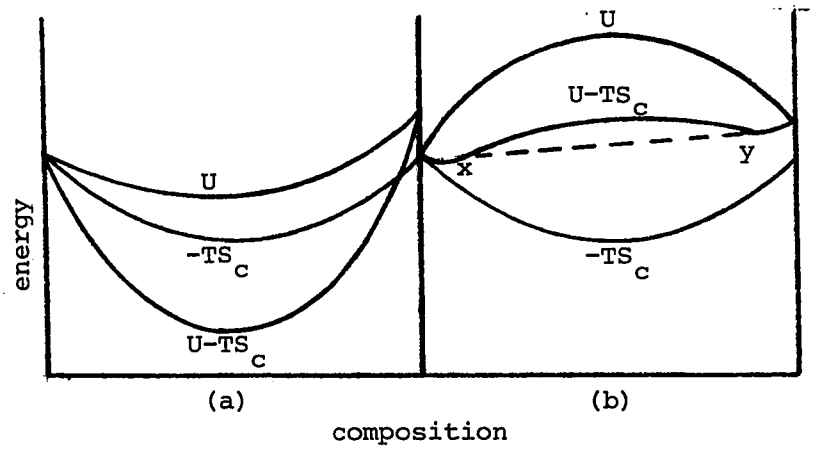

Fig. 4-5: Forms of free energy vs. composition curves for two elements with the same crystal structure.

Rothery et al. (52H1) shows how it is possible to build the solid solubility curves of a simple alloy system from free energy considerations. This technique, however, is only an interpretation,that is to say,the free energy curves are drawn here with shapes which account for the diagrams concerned. There are of course more complicated diagrams as for instance the appearance of intermediate phases of either fixed or variable compositions, phases in metastable equilibrium due to the effect of supercooling, but they too are subject to the same rules as the simpler diagrams and can be analyzed similarly in terms of the free energy concepts.

4.5 Ternary Systems

The representation of the equilibrium diagrams of a ternary system needs a three-dimensional model, since two dimensions are required to show the variations in composition, and a third dimension for the temperature. The representation used almost exclusively here is to show

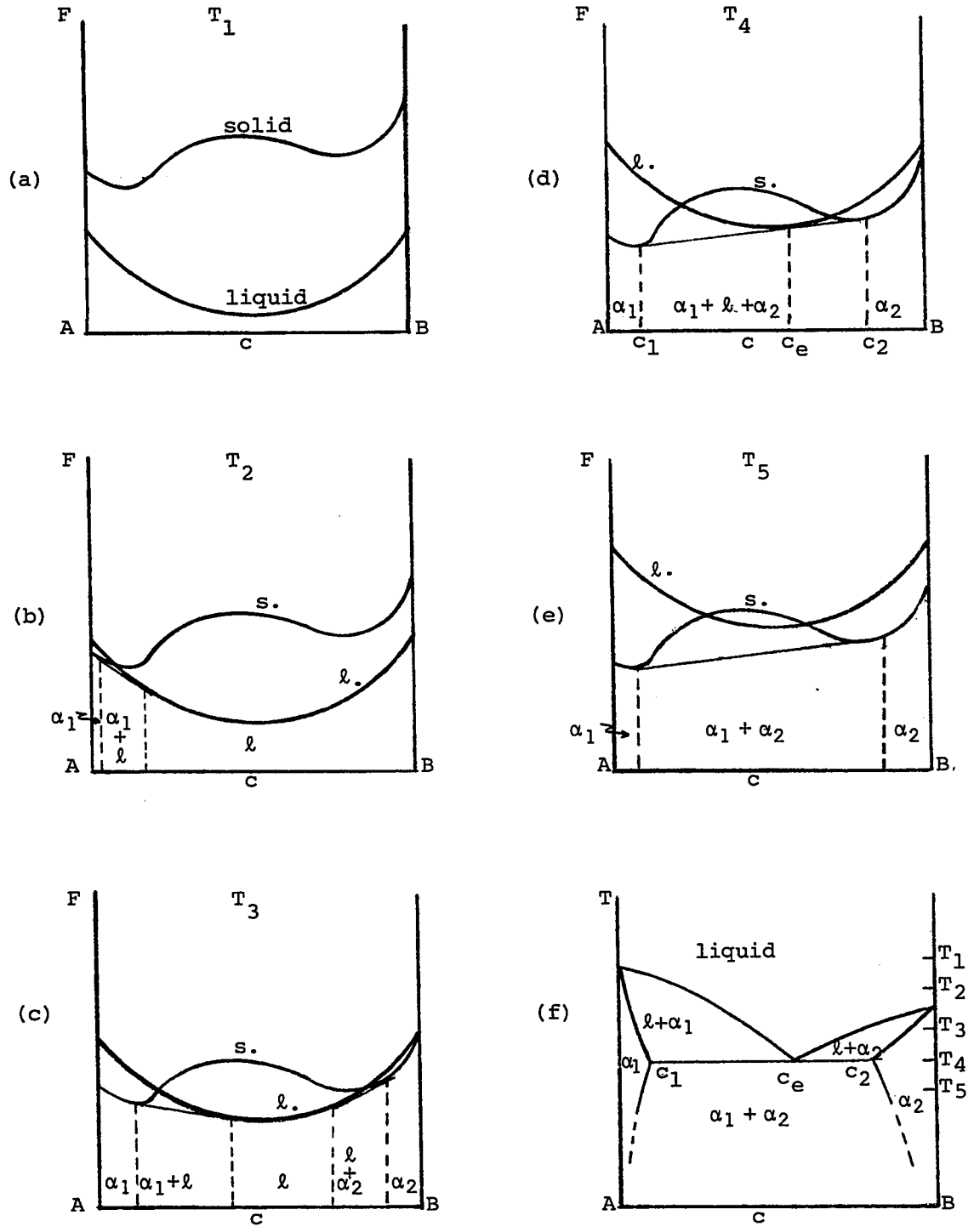

Fig. 4-6: The form of an equilibrium diagram is related to the effect of temperature on the free energy curves. In figures b to e, s. and ℓ. denote the free energy curves for the solid and liquid phases respectively.

the temperature on a vertical axis and the composition on an equilateral triangle in the horizontal plane. Such a triangle is chosen because of one of its geometrical properties which states that the sum of the length of the three perpendiculars drawn from a point P inside the triangle to the sides is equal to the height of the triangle as in figure 4-7. If, therefore, the height of the triangle is made equal to

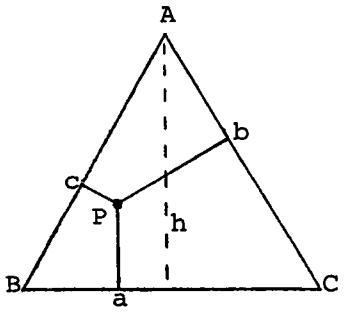

Fig. 4-7: The sum Pa + Pb + Pc is equal to the height h of an equilateral triangle.

unity, the vertices can be taken to represent the pure component elements A, B and C, and a point P inside the triangle will represent an alloy containing Pa/l of A, Pb/l of B and Pc/l of C respectively. Occasionally, however, the use of cartesian coordinates will be unavoidable especially when the compositions involve very small fractions of one or two components as an enlarged portion of the triangle would still be difficult to interpret.

In a three-component system, the liquidus is a surface rather than a line as in the two-component case since each possible composition

of the liquid corresponds to a point in the triangle. On that liquidus surface there is a line that corresponds to any particular temperature and therefore a knowledge of the liquidus surface and the solidus surface does not define which solidus composition is in equilibrium with a specified composition on the liquidus; it will then be necessary to use tie-lines to indicate the equilibrium relationships. Figure 4-8 represents a three-dimensional view of one corner of the phase diagram for a ternary system. The two partial binary liquidus define the boundaries of the liquidus surface and similarly for the solidus surface. The lines DE and FG indicate the points on the two surfaces at which the temperature has a fixed value. The solid-liquid equilibrium is then represented by the various tie-lines m_1n_1, m_2n_2.....

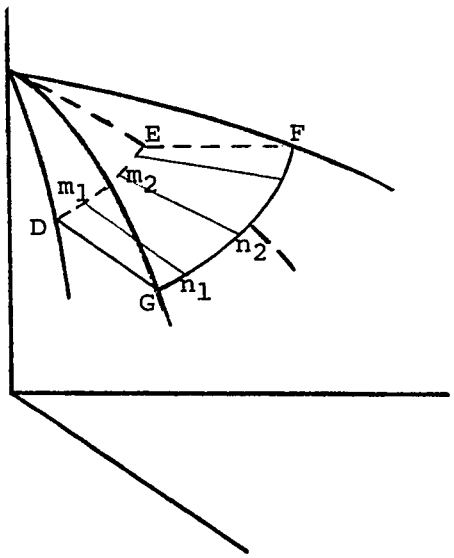

Fig. 4-8: Corner of a three-dimensional equilibrium diagram showing two partial binary diagrams. The solid-liquid equilibrium is given by the tie-lines (m_1n_1, m_2n_2...) on the isothermal surface DEFG.

The complete equilibrium diagram of a ternary system can only be represented by a three-dimensional model and usually all but the simplest cases are difficult to draw in perspective. It is therefore customary to describe ternary systems by means of plane sections through the three-dimensional model, and of those the horizontal or isothermal sections are of the greatest interest. To illustrate the use of such sections, consider a ternary system ABC composed of three binary eutectics and a ternary eutectic. Figure 4-9 gives the three-dimensional representation of such a system along with various isothermal planes. But the best representation

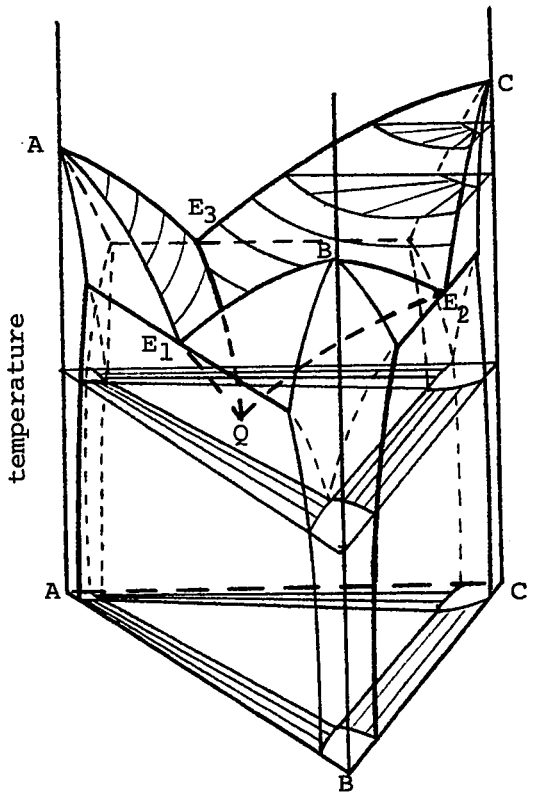

Fig. 4-9: Pictorial view of ternary system ABC composed of three binary eutectics E_1, E_2, E_3 and a ternary eutectic Q (after 52H1). Various isothermal sections with tie-lines are also represented.

is to show the isothermal plane alone and identify the various phases, the region in which they occur and the tie-lines between liquidus and solidus surfaces. The important points to consider in the case here are the eutectic points E_1, E_2, E_3 and Q. At a temperature above all four points mentioned above, the plane will look as in figure 4-10a where it is possible to recognize liquid and solid single-phase fields as well as three liquid-solid two-phase fields. The position of the three eutectic valleys is also indicated by a simple projection on the base triangle. In figure 4-10b, the temperature is above E_1 and Q but below E_2 and E_3. Four new phase fields are added to the previously existing ones: two solid-solid two-phase fields (A + C and B + C) and two solid-solid-liquid three-phase fields (A + C + ℓ and B + C + ℓ). At a temperature below E_1, E_2 and E_3 but above Q (figure 4-10c) a solid-solid two-phase field (A + B) and a solid-solid-liquid three-phase field (A + B + ℓ) are added to those of figure 4-10b. Finally, at a temperature below the ternary eutectic Q (figure 4-10d), the liquid phase vanishes and the three three-phase triangles of figure 4-10c unite to form the all solid three-phase triangle (A + B + C).

From the isothermal sections described in figures 4-10 a to d, it is possible to see that below the totally liquid region, the three-dimensional model of figure 4-9 is divided into well defined regions.

i) adjacent to each of the vertical edges of the prism there is a volume corresponding to the solid solution in the element concerned. At the higher temperatures each of these volumes is

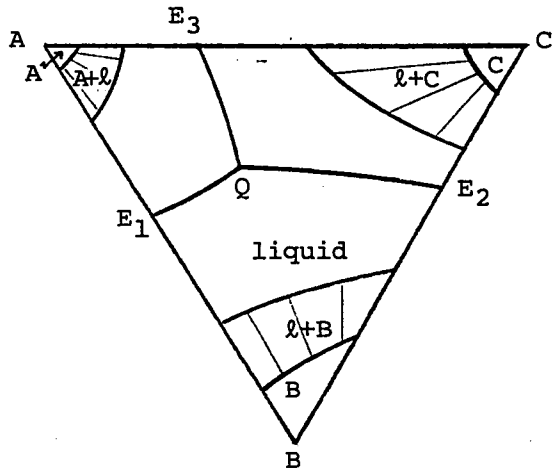

Fig. 4-10a: Isothermal section from figure 4-9 taken at a temperature above E_1, E_2, E_3 and Q.

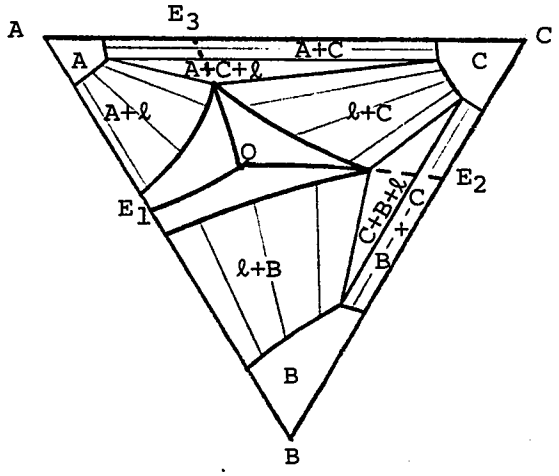

Fig. 4-10b: Isothermal section from figure 4-9 taken at a temperature above E_1 and Q, but below E_2 and E_3.

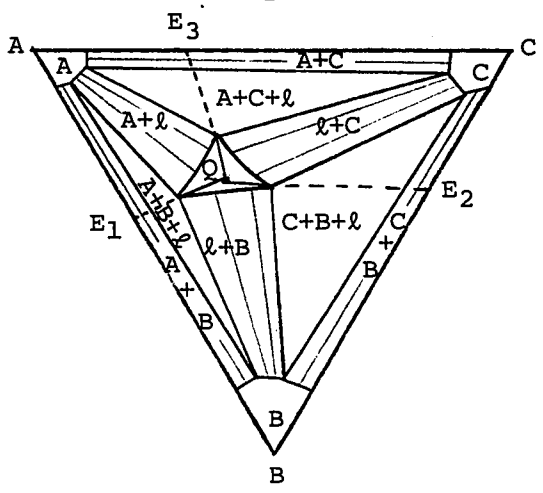

Fig. 4-10c: Isothermal section from figure 4-9 taken at a temperature above Q, but below E_1, E_2 and E_3.

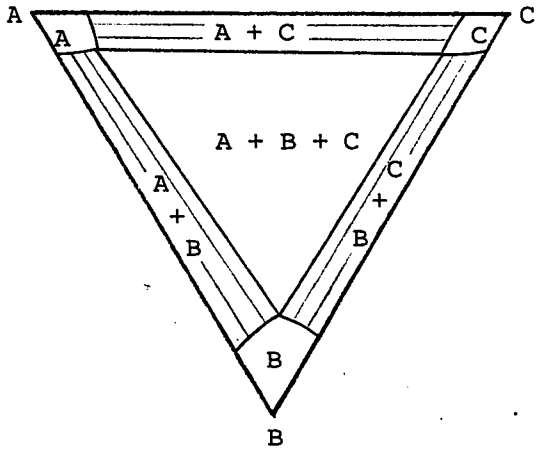

Fig. 4-10d: Isothermal section from figure 4-9 taken at a temperature below the ternary eutectic Q.

bounded by a single curved solidus surface. When the temperature falls below that of the binary eutectic E_3, the A solid surface splits into two portions which bound the two solid-solid (A + C) and solid-liquid (A + ℓ) two-phase fields respectively, and these surfaces join in the line passing through the corners of the three-phase (A + C + ℓ) triangles at different temperatures. The C and B solidus surfaces split in the same way as the temperature is lowered below the eutectic points E_2 and E_1 respectively. Finally, on passing below the temperature of the ternary point Q, the liquid phase vanishes and the volume of each single phase solid solution is bounded by two surfaces corresponding to two-phase equilibria: the A + C and A + B phase fields for the solid solution of element A and similarly for B and C.

ii) along the edges of the prism and below the temperature of the binary eutectic associated with each edge, there is a volume corresponding to two-phase solid alloys (A + B, A + C, C + B). At temperatures above point Q the inner surface of these volumes are in general curved and are ruled surfaces, that is surfaces such that horizontal lines can be drawn across them, the horizontal line at any one temperature forming one of the sides of a three-phase triangle of the type (A + C + ℓ). At temperatures below that of the ternary eutectic point Q, these surfaces are again ruled surfaces but the horizontal lines across them bound the

triangles of the three-phase solid regions (A + B + C) at the temperatures concerned.

iii) from the above considerations, it follows that each of the three-phase regions (solid + solid + liquid) builds up a volume inside the three-dimensional model, and the sides of these volumes although in general curved are ruled surfaces.

From this discussion it is then possible to look at some of the rules which apply to isothermal sections. In an isothermal section of a ternary system there cannot be more than four phases in equilibrium with one another and this regulates the various cases that follow:

i) single-phase fields: a single-phase field is represented by an area in an isothermal section. The lines bounding this area represent the compositions of the phase in equilibrium with other phases, and tie-lines may be drawn connecting the compositions of the two phases in equilibrium with one another. In the hypothetical isothermal section of figure 4-11, the area representing the W solid solution is a single-phase field. The boundary segment ab contains points which are in equilibrium with points of the single phase X (few tie-lines are shown) and similarly for the segments bc and cd for the phases Y and Z respectively. The whole boundary curve abcd will in general show abrupt changes in direction at the points b and c

where there is a change in the phase with which the phase W is in equilibrium.

ii) two-phase fields: a two-phase field in an isothermal section is represented by an area crossed by tie-lines representing the compositions of the two phases in equilibrium with one another. All alloys on a tie-line will be made of the two compositions represented by the end points and the amount of each phase will be governed by the lever principle (e.g. point p in figure 4-11).

iii) three-phase fields: in an isothermal section, three-phase fields are triangles. All alloys within the triangle consist of the same three phases whose compositions are given by the corners of the triangles. Thus in figure 4-11, alloys within the triangle Δcef are made of the three phases that follow: W of composition c, Y of composition e and Z of composition f. The relative proportions of the three phases can be obtained from the construction shown in figure 4-12. An alloy of composition P contains phases A, B, and C in the proportions of the area of the triangles ΔBPC, ΔACP and ΔAPB respectively.

Furthermore, the corners of the three-phase triangles lie on the boundaries of the single-phase areas at the points where the changes in direction occur (e.g. b and c in figure 4-11).

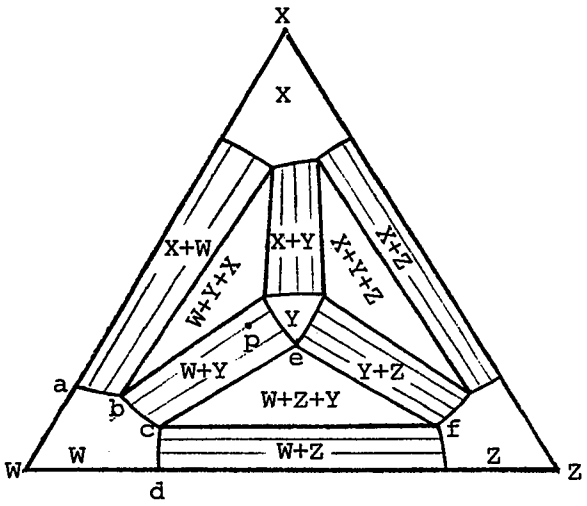

Fig. 4-11: Isothermal section of a hypothetical ternary section WXZ.

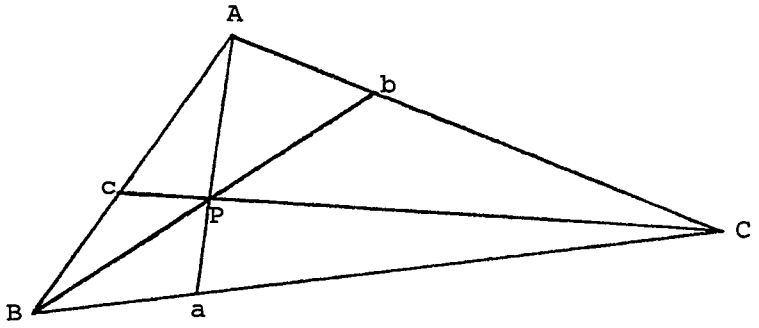

Fig. 4-12: Construction for finding the relative amounts of phases inside a three-phase triangle.

The sides of a three-phase triangle are thus the last of the tie-lines of the adjacent two-phase areas. Each corner involves the meeting of two different kinds of tie-lines and of two branches of a single-phase boundary curve. If the boundaries of the single-phase areas touching the corner of a three-phase triangle are extended, then either must lie inside the triangle or one must lie on each side of it. The angle between the extended boundaries on the side towards the triangle is less than 180^{o}. In the representation of various boundaries in figure 4-13, the above conditions are satisfied at the corners A, B and B' but the situation at C, C' and D cannot occur.

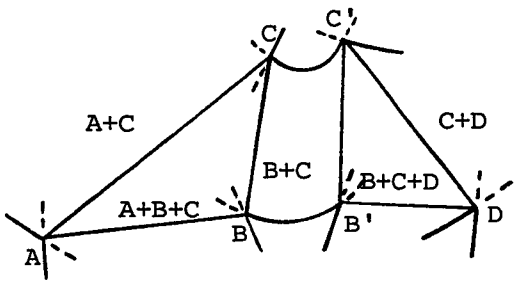

Fig. 4-13: Part of an isothermal section of a ternary system. Phase boundaries may have directions shown at A, B, B' but not those at C, C', D.

iv) four-phase invariant points: in a ternary system, the existence of four phases involves an invariant point at a fixed temperature as for instance the ternary eutectic point Q in figure 4-9.

There are other points of view, apart from horizontal isothermal sections, from which the three-dimensional model of a ternary system may be considered: vertical sections and projected diagrams are two such views. The former will not be used here as it restricts the representation by fixing the composition of one of the three components; the latter will be used, however scarcely, to represent schematically properties that vary with temperature and whose unique position in an isothermal plane is of little value. Such a projection is used in figure 4-9 to represent the position of the eutectic valleys.

Of course, the examples discussed in this chapter are relatively simple and the problem becomes more complex when a combination of multiple eutectic and/or peritectic reactions are considered or an intermediate phase within a binary system occurs for instance.

However, in the case of the alloys of concern here, the occurrence of an intermediate phase at equimolar composition for binary III-V compounds greatly reduces the complexity of diagrams as the solidus surfaces become a plane in the three-dimensional model. It is this particular property that has justified the name given to these ternary systems: 'pseudobinary alloys'.

With a working knowledge of the properties of equilibrium diagrams it will be now possible to investigate, at least experimentally, some of the thermodynamic properties of various III-V ternary systems which is the subject of the following chapters.

Chapter 5 Theoretical model for III-V ternary systems

5.1 Introduction

5.2 Fundamental Equations

5.2.1 Independent Variable

5.2.2 Thermodynamic potentials and partial molar quantities

5.2.3 Gibbs function

5.2.4 Chemical potentials and absolute activities

5.2.5 Activity coefficients

5.3 Statistical Thermodynamics

5.3.1 Distribution law and partition function

5.3.2 Configurational free energy

5.4 Ideal Solutions

5.4.1 Conditions for ideality

5.4.2 Free energy and entropy of mixing

5.4.3 Raoult's law

5.5 Regular Solutions

5.5.1 Classification of nearest neighbour pairs

5.5.2 Zeroth approximation

5.5.3 First approximation or quasi-chemical treatment

5.6 Model for III-V Ternary Solutions

5.7 Simple Solutions

5.1 Introduction

In the preceding chapters, various properties relative to the constituents of III-V ternary alloys were presented. The discussion was centred around those properties that characterize the equilibrium diagram of such systems. Particularly, the preliminary investigations on the characterization of the pseudobinary alloy $GaAs_ySb_{1-y}$ were discussed in chapter 3 but a lot more experimentation remains to be done in order to determine the various thermodynamic properties of this alloy and specify the phase diagram as little experimental data exists for the latter (62W1, 70I1, 72F1). However, before proceeding with an account of the experimental data collected toward the characterization of the phase diagram of the system mentioned above, it is a good time to introduce a theoretical approach to the problem. The model which will be proposed here deals with the predictions of phase diagrams from the various thermodynamic properties of the constituents whether these are in the form of elements or binary compounds. Furthermore, it is hoped that the early predictions of such a model will help to orientate the various experimental investigations to be carried out subsequently.

A relatively detailed analysis of the theory will be given in this chapter. The calculated results will be presented later, however, along with the experimental ones in order to facilitate comparison between theory and experiment. Such a procedure should emphasize the relative successes or failures of the theory.

The theory is presented with its implications, assumptions and a few definitions; it is not new but the treatment of some of the concepts is different from that of other workers in an attempt to stress the physical significance of each step in the treatment whenever possible. As an example, some thermodynamic parameters will be treated as varying linearly with temperature rather than with a higher order variation; also a composition dependence will not be considered. The higher order is excluded to avoid the inherent difficulty of higher order variations whose interpretation is often intricate and requires extensive computer fitting. A dependence on composition, on the other hand, would weaken the simplicity of the model, and contribute nothing but to introduce a variable that could be dealt with arbitrarily and thus confuse even more a theory that is already involved. Furthermore, it would be difficult to give a physical interpretation to a composition dependent variable.

All the models for treating phase diagrams are based on rather immutable concepts relating free energies with associated enthalpies and entropies. It is in the handling of the equations that the models differ; for instance, a very good qualitative treatment supported by references to experimental evidence is given by Hume-Rothery et al. (52H1). Stringfellow (71S1) has reported some success while using the thermodynamic properties such as energies of sublimation, molar volumes and treating the solids according to Phillips and Van Vechten spectroscopic theory of chemical bonding (70P1). But in recent years, a treatment following the quasi-chemical approach suggested by Guggenheim (35G1, 52G1) has been more widely used with various degrees of refinement by

workers such as: Antypas and James (70A1), Blom and Plaskett (71B1), Wu and Pearson (72W1), Panish and Ilegems (72P1), Joullié et al. (74J1) and Bebrick and Panlener (74B1).

The approach used in this thesis is basically of the type of the latter workers and is justified by the properties and assumptions included in the following discussion. The systems to be dealt with are ternary systems, but the solid solutions occur only on the pseudobinary sections of the composition diagram, that is to say that the end points are the stoichiometric binary compounds.

5.2 Fundamental Equations.

The first assumption is that the system is in thermal equilibrium so that the temperature is always uniform throughout the system. Under such isothermal conditions, the most important thermodynamic function is the free energy, denoted by F. In any isothermal reversible process the increase in free energy, ΔF, is equal to the work done on the system and similarly, a decrease in free energy, $-\Delta F$, is equal to the work done by the system.

5.2.1 Independent variable

The state of a liquid mixture may be completely defined by specifying the absolute temperature, the pressure and the composition of the liquid. Since this study is dealing with solids and liquids only,

a set of appropriate independent variables as T and P is defined. The composition of the mixture is conveniently described by specifying the number of moles and the mole fractions associated with each component. These are governed by the relations

$$x_i = \frac{n_i}{\sum_i n_i} \qquad 5.2.1$$

and

$$\sum_i x_i = 1 \qquad 5.2.2$$

One simple illustration is the thermodynamic function called 'molar free energy of mixing' which is the change in free energy when one mole of a mixture is formed from the constituent pure substances. For a binary mixture, this is defined as:

$$-\Delta_m F = (1 - x)F_1^o + xF_2^o - F_m \qquad 5.2.3$$

where

$x_1 = 1 - x$

$x_2 = x$

F_1^o, F_2^o = molar free energy of the pure components

F_m = molar free energy of the mixture (dependent upon x)

$-\Delta_m F$ = molar free energy of mixing (the negative sign indicates a decrease in the free energy).

5.2.2 Thermodynamic potentials and partial molar quantities

If the free energy F of any homogeneous phase is taken as a function of T, V, n_i then the following relations may be deduced

$$\frac{\partial F}{\partial T} = -S \qquad 5.2.4$$

$$\frac{\partial F}{\partial V} = -P \qquad 5.2.5$$

where S is the entropy. Another important relation is

$$\frac{\partial F}{\partial n_i} = \mu_i \qquad 5.2.6$$

where μ_i is called the 'chemical potential'. The combination of those last three equations yields

$$dF = -SdT - PdV + \sum_i \mu_i dn_i \qquad 5.2.7$$

Here the free energy is said to be the thermodynamic potential for the independent variables T, V, n_i and formula 5.2.7 is called the 'fundamental equation' for these variables. If dealing with 'partial molar quantities' like the volume for instance, then the partial molar volumes are defined by

$$V_1 = \frac{\partial V}{\partial n_1}$$

$$V_2 = \frac{\partial V}{\partial n_2} \qquad 5.2.8$$

and the total volume is related to these by

$$V = n_1 V_1 + n_2 V_2 \qquad 5.2.9$$

Analogous relations exist for the other properties such as F, S, G (Gibbs function) and H (enthalpy). It can thus be shown that for the variations in the composition of a binary mixture at constant temperature and pressure

$$(1 - x) \frac{\partial \mu_1}{\partial x} + x \frac{\partial \mu_2}{\partial x} = 0 \quad (T, P \text{ const.}) \qquad 5.2.10$$

This last formula is called the 'Gibbs-Duhem relation'.

5.2.3. Gibbs function

For solid-liquid mixtures, however, a more useful set of variables T, P, n_i yields for the thermodynamic potential, the Gibbs function G defined as

$$G = F + PV \qquad 5.2.11$$

and the associated fundamental equation for these variables written as

$$dG = -SdT + VdP + \sum_i \mu_i \, dn_i \qquad 5.2.12$$

here, the property of the entropy S is that in any reversible isothermal process the heat absorbed is $T\Delta S$. However, if the process is an irreversible isothermal one then the heat absorbed is equal to the increase ΔH of the heat function H. The relation which exists between these functions can be expressed as follows

$$G = H - TS \qquad 5.2.13$$

Inspection of equation 5.2.12 shows that when the composition of a mixture is varied at constant temperature and pressure, there is a close relationship between the functions G and μ_i. In fact, in thermodynamic terms it is said that the chemical potential is identical with the partial molar Gibbs function.

5.2.4 Chemical potentials and absolute activities

This chemical potential function has great importance in setting up a theory on the behaviour of systems in thermodynamic equilibrium. There are two important properties of chemical potentials: first, if one considers the process of transferring one mole of the substance 'i' reversibly and isothermally from a large quantity of one phase to a large quantity of another phase, then the decrease in the value of the chemical potential is equal to the net work done by the system. Second and most important here, when two phases are at the same temperature the condition for equilibrium distribution of the substance 'i' between the two phases is that the chemical potential should have the same value in both phases.

The first property relates the difference in chemical potential between two phases to experimentally determinable quantities. As an example, the saturated vapour over each phase may be assumed to behave as a perfect gas; this assumption however puts no restriction concerning the nature of the liquid or solid phases considered. The transfer of one mole of a substance 'i' from a large quantity of a liquid or solid phase α to a large quantity of another liquid or solid phase β can in

principle be performed reversibly and isothermally. The process is called an 'isothermal three-stage distillation'. The work done by the system in the three stages when the vapour is treated as a perfect gas is as follows:

i) evaporate one mole of substance i from a large quantity of the phase α against a pressure equal to the saturated partial vapour pressure p_i^α of i in the phase α $(RT - p_i^\alpha V_i^\alpha)$

ii) expand or compress the one mole of vapour isothermally from the pressure p_i^α to a pressure equal to the saturated vapour pressure p_i^β of i in the phase β $\left(RT \ln \frac{p_i^\alpha}{p_i^\beta}\right)$

iii) condense the one mole into a large quantity of the phase β by applying a constant pressure $(-RT + p_i^\beta V_i^\beta)$

By addition, the work done by the system is

$$RT \ln \frac{p_i^\alpha}{p_i^\beta} + (p_i^\beta V_i^\beta - p_i^\alpha V_i^\alpha) \qquad 5.2.14$$

and by definition, the net work done by the system is

$$RT \ln \frac{p_i^\alpha}{p_i^\beta} \qquad 5.2.15$$

where the p_i^γ's are the saturated partial vapour pressure of the substance 'i' in the phase γ. Thus, for any two phases α, β at the same temperature, the decrease in chemical potential is given by

$$\mu_i^{\alpha} - \mu_i^{\beta} = RT \ln \frac{p_i^{\alpha}}{p_i^{\beta}} \qquad 5.2.16$$

Introducing a new quantity λ_i called the 'absolute activity' defined by

$$\mu_i = RT \ln \lambda_i \qquad 5.2.17$$

equations 5.2.15, 5.2.16, and 5.2.17 yield the relation

$$\frac{\lambda_i^{\alpha}}{\lambda_i^{\beta}} = \frac{p_i^{\alpha}}{p_i^{\beta}} \qquad 5.2.18$$

Considering now the second property of chemical potentials at equilibrium where

$$\mu_i^{\alpha} = \mu_i^{\beta} \qquad 5.2.19$$

then the following holds true

$$\lambda_i^{\alpha} = \lambda_i^{\beta} \qquad 5.2.20$$

or

$$p_i^{\alpha} = p_i^{\beta} \qquad 5.2.21$$

providing the vapour is treated as a perfect gas. Otherwise, the quantity p_i is redefined as the 'fugacity' instead of the partial vapour pressure. The fugacity may be regarded simply as a partial vapour pressure corrected for deviations from perfect gas behaviour.

When developing a theory for binary mixtures it is also important to establish the relationship between the properties of the pure substances with those of the mixture. The relations governing the

chemical potentials may therefore be extended as follows:

$$\mu_1^o - \mu_1 = RT \ln \frac{\lambda_1^o}{\lambda_1} \qquad 5.2.22$$

$$\mu_2^o - \mu_2 = RT \ln \frac{\lambda_2^o}{\lambda_2} \qquad 5.2.23$$

$$-\frac{\Delta_m G}{RT} = (1 - x) \ln \frac{\lambda_1^o}{\lambda_1} + x \ln \frac{\lambda_2^o}{\lambda_2}$$

$$= (1 - x) \ln \frac{p_1^o}{p_1} + x \ln \frac{p_2^o}{p_2} \qquad 5.2.24$$

where the superscript 'o' refers to the pure substance while parameters without any superscript refer to that same substance but in the mixture. The Gibbs-Duhem relation, 5.2.10, can then be written as

$$(1 - x) \frac{\partial \ln \lambda_1}{\partial x} + x \frac{\partial \ln \lambda_2}{\partial x} = 0 \text{ (T, P const.)} \qquad 5.2.25$$

or

$$(1 - x) \frac{\partial \ln p_1}{\partial x} + x \frac{\partial \ln p_2}{\partial x} = 0 \text{ (T, P const.)} \qquad 5.2.26$$

In practice, however, it is a well known fact that for liquids and solids, the pressure, if comparable with atmospheric pressure or less, is considered small enough to make all terms in PV or VdP entirely negligible. The relations presented above will therefore be valid for all binary and pseudobinary mixtures discussed in this thesis.

5.2.5 Activity coefficients

Looking now at a solution of equation 5.2.25, the simplest form yields:

$$\lambda_1 = \lambda_1^o (1 - x)$$
$$\lambda_2 = \lambda_2^o x \qquad 5.2.27$$

or, of course

$$p_1 = p_1^o (1 - x)$$
$$p_2 = p_2^o x \qquad 5.2.28$$

and since the simplest kind of mixture which exists, satisfies these two relations, such mixtures are called 'ideal'. Very few mixtures do behave idealy but it is of interest to be able to compare them to real mixtures. In order to do so one more parameter is introduced to the already rich nomenclature: the 'activity coefficients' γ_1 and γ_2 defined by

$$\lambda_1 = \lambda_1^o (1 - x)\gamma_1$$
$$\lambda_2 = \lambda_2^o x \gamma_2 \qquad 5.2.29$$

or

$$p_1 = p_1^o (1 - x)\gamma_1$$
$$p_2 = p_2^o x \gamma_2 \qquad 5.2.30$$

Substitution of 5.2.29 into 5.2.25 gives the relation for the variations

with composition of the activity coefficients of the two species,

$$(1 - x) \frac{\partial \ln \gamma_1}{\partial x} + x \frac{\partial \ln \gamma_2}{\partial x} = 0 \text{ (T const.)} \qquad 5.2.31$$

This introduction of activity coefficients gives no quantitative information about the properties of the mixture until their values have been determined experimentally. They are, however, most convenient as they enter into all the equilibrium relations of the mixture.

5.3 Statistical Thermodynamics

The next assumptions are due to statistical considerations. The most fundamental law of statistical thermodynamics relates to a completely isolated system, that is to say a system of prescribed energy, volume and content. It is however more useful to formulate a system of prescribed temperature instead of prescribed energy. The observed equilibrium properties of such a system are correctly obtained by averaging over all accessible quantum states of the system, attaching a statistical weight $\exp(-E_i/kT)$ to each non-degenerate quantum state, with E_i being the energy of the quantum state 'i'. Of course k is 'Boltzmann's constant'.

5.3.1 Distribution law and partition function

Applying the concept of the law of distribution, the fraction of time spent by a system at given temperature and volume in the state 'i' is

$$\frac{e^{-E_i/kT}}{\sum_i e^{-E_i/kT}} \qquad 5.3.1$$

and the observed equilibrium value '$\overline{P}$' of a property 'P' whose value is 'P_i' when the system is in the state 'i' may be written as

$$\overline{P} = \frac{\sum_i P_i e^{-E_i/kT}}{\sum_i e^{-E_i/kT}} \qquad 5.3.2$$

The quantity $\sum_i e^{-E_i/kT}$ is also called the 'partition function' and is labeled Q. The usefulness of this function is that it is possible to define a function such as

$$F = -kT \ln Q \qquad 5.3.3$$

where it can be shown that F has all the properties of the thermodynamic free energy.

It often happens that the behaviour of a system with respect to some degrees of freedom is independent of that with respect to the others. The energy of the system can then be expressed as a sum of energies in the separated degrees of freedom. Therefore, in this treatment, the degrees of freedom related to the positions and motions of the centres of mass of molecules, labeled the translational degrees of freedom, are considered as separable from all other degrees of freedom. These other degrees of freedom will be referred to as internal degrees of freedom, although they include molecular rotations which are not strictly internal.

This is of course only an approximation as it implies that the rotational degrees of freedom of the molecules of each kind are the same in any mixture as in the pure substance. It does not, however, imply that the rotational degrees of freedom are the same in the liquid state as is the gas or solid state. The partition function may therefore be split into two parts, namely

$$Q = Q_{int.} \, Q_{tr.} \qquad 5.3.4$$

where the internal partition function $Q_{int.}$ relates to all internal degrees of freedom including rotations, and the translational partition function $Q_{tr.}$ relates to the motions of the centres-of-mass of the molecules. It follows that the free energy of mixing is determined entirely by the translational partition function $Q_{tr.}$, since on comparing a mixture with its constituents as pure substances all contributions to the free energy of mixing from $Q_{int.}$ will cancel.

5.3.2 Configurational free energy

In a crystalline solid, a further simplification is made to the effect that for any given quantum state of the crystal, the energy consists of two terms: a 'configurational energy' which means the energy the crystal would have if the centre-of-mass of every molecule were at rest on its lattice point, and an 'acoustic energy' term which is the energy of the vibrations of the centres-of-mass of the molecules about their lattice points. A further approximation calls for considering these two energies as mutually independent. The translational partition function can thus be written as the product of the two terms:

$$Q_{tr.} = Q_{ac.}\,\Omega \qquad 5.3.5$$

where $Q_{ac.}$ is the partition function for the acoustic modes of vibration and Ω in the configurational partition function for the molecules supposed fixed on their lattice points. The approximations discussed above imply that $Q_{ac.}$ is determined by the number of molecules of each species but is unaffected by the mixing of these molecules. Hence, the molar free energy of mixing $\Delta_m F$ of a binary mixture is determined by

$$-\frac{\Delta_m F}{kT} = \ell n\, \Omega_m - (1 - x)\, \ell n\, \Omega_1^o - x\, \ell n\, \Omega_2^o \qquad 5.3.6$$

The symbol Ω_m is the configurational partition function of one mole of the mixture while Ω_1^o and Ω_2^o refer to one mole of the pure substances respectively.

The weakness of this approach regarding crystals is the assumption of the mutual independence of $Q_{ac.}$ and Ω. Similarly for liquids, the weakness exists but there is also the fact that for liquids these functions are difficult to define since there is no lattice. Liquids are treated as if atoms were arranged on a lattice which gives rise to a structure for liquids referred to as 'quasi-crystalline'. Whereas in a crystal each atom is surrounded by a definite number of nearest neighbours, this number is not definite in a liquid. For the temperature ranges usually considered, the number of nearest neighbours has a fairly well defined average value, and, although there are fluctuations about this average, these fluctuations are not serious and the geometrical relation-

ship of each atom to its immediate neighbours is on the average very similar to that in a crystal. Moreover, the fluctuations are not sufficiently serious to disturb the regularity of the geometrical relationship between immediate neighbours for more than a rather unimportant fraction of centres in the liquid. In view of these facts, liquid mixtures will therefore be treated as quasi-crystalline, and accordingly equation 5.3.6 may be used for liquid mixtures as well as for solid mixtures.

5.4 Ideal Solutions

5.4.1 Conditions for ideality

Brief mention was made earlier of the concept of ideal solutions or ideal mixtures. The intent of course was to refer to it subsequently as a theory is being formulated in order to explain and predict the behaviour of phase diagrams. To study the conditions sufficient for a mixture to be ideal, consider a regular crystalline lattice in which each lattice point has z nearest neighbours. Next, consider two kinds of atoms A and B sufficiently similar in size and shape so that they are interchangeable on the lattice and let a crystal of the pure substance A containing N atoms have an energy $-N\epsilon_A$ when all the atoms are at rest on their lattice points. The zero of energy is defined as that of the atoms at rest at infinite separation. Neglecting interactions between pairs of atoms which are not nearest neighbours, the energy of a bond between a pair of

nearest neighbours at rest on their lattice points may be regarded as $-2\varepsilon_A/z$ and similarly $-2\varepsilon_B/z$ for a crystal of the pure substance B. If the lattice is filled partly by A and B atoms, then there will be contributions to the potential energy of the crystal from AB pairs of neighbours as well as from AA and BB pairs. Denoting the energy of an AB-bond by $(-\varepsilon_A - \varepsilon_B + \omega)/z$, this defines an 'interchange energy' ω such that: starting with two pure crystals of A and B and interchanging an interior A atom with an interior B atom, the total increase of energy is 2ω providing all atoms remain at rest on their lattice points. The energy transfers occur as follows: $z(-2\varepsilon_A/z) = -2\varepsilon_A$ of energy is removed from the destruction of z AA-bonds in crystal A and $z(-2\varepsilon_B/z) = -2\varepsilon_B$ of energy is removed from the destruction of z BB-bonds in crystal B. The replacement of each atom by one of the other kind contributes $z(-\varepsilon_A - \varepsilon_B + \omega)/z$ of energy by creating z AB-bonds. Since this is done twice, once for each sublattice, the total contribution of AB-pair creation gives $2(-\varepsilon_A - \varepsilon_B + \omega)$ of energy to the mixed crystal. Summing all the contributions to the energy one clearly sees that the total increase of energy is 2ω. If a mixed crystal is not formed then the result is still valid. This development merely clarifies the meaning of ω but the situation becomes more complex when the process of interchanging atoms is repeated since for example as the number of B atoms that set in the A lattice increases so do the chances of creating BB-bonds rather than uniquely AB-bonds. Therefore the total contribution to the energy of the system becomes difficult to estimate.

Now, a sufficient condition for the mixed crystal to be ideal is that ω should be zero. This implies that the mutual energy of an AB-

bond is equal to the arithmetic mean of the mutual energies of AA and BB-bonds. For ω to be zero also means that all configurations with the atoms at rest on their lattice points have equal energy.

If the mixed crystal contains $N(1 - x)$ atoms A and Nx atoms B, the energy when all the atoms are at rest on their lattice points is

$$- N(1 - x)\ \varepsilon_A - N\ x\ \varepsilon_B \qquad 5.4.1$$

regardless of the distribution. The number of distinguishable ways of arranging these atoms on the lattice is

$$\frac{N!}{[N(1 - x)]!(Nx)!} \qquad 5.4.2$$

and hence the configurational partition function Ω is

$$\Omega = \frac{N!}{[N(1 - x)]!\ (Nx)!}\ e^{[N(1-x)\varepsilon_A + N\ x\ \varepsilon_B]/kT} \qquad 5.4.3$$

Turning then to liquids, the quasi-crystalline approach has to be used in order to apply equation 5.4.3. to liquids. This means that a coordination number z denoting the number of atoms which are closest neighbours of a chosen atom is still used even though z may not have a well-defined value but may rather have to be regarded as an average. One further assumption is that the atoms are also sufficiently alike in size and shape to be able to pack in the same manner when mixed as in the pure liquids. Furthermore, the treatment according to separation of degrees of freedom still holds as discussed previously.

With all these assumptions, however, equation 5.4.3 may still require correction by some unspecified geometrical factor to account for the absence of a well-defined lattice, but it is assumed that this correction factor will be independent of the mole fraction and so will not affect the value for the molar free energy of mixing.

5.4.2 Free energy and entropy of mixing

The mathematical expressions for the free energy and entropy of mixing may then be deduced. The configurational term in the free energy is $-kT \ln \Omega$; using equation 4.3.9 it becomes

$$-N(1-x)\,\varepsilon_A - N x\,\varepsilon_B - kT \ln \frac{N!}{[N(1-x)]!\,(Nx)!}$$

$$= -N(1-x)\,\varepsilon_A - N x\,\varepsilon_B + NkT\,[(1-x)\ln(1-x) + x \ln x] \qquad 5.4.4$$

when Stirling's theorem is used. The corresponding values for the configurational free energy in crystals of the pure substances containing the same total number N of atoms are $-N\,\varepsilon_A$ and $-N\,\varepsilon_B$. Consequently the free energy of mixing is

$$NkT\,[(1-x)\ln(1-x) + x \ln x] \qquad 5.4.5$$

and the molar free energy of mixing $\Delta_m F$ is given by

$$\Delta_m F = RT\,[(1-x)\ln(1-x) + x \ln x] \qquad 5.4.6$$

It is useful to notice here that the formulation holds true for a quasi-crystalline liquid since the factor to be introduced into Ω for lack of a well-defined lattice was assumed independent of x. Differentiating 5.4.6 with respect to T yields the molar entropy of mixing:

$$\Delta_m S = R\,[-(1 - x)\ \ell n\ (1 - x) - x\ \ell n\ x] \qquad 5.4.7$$

5.4.3 Raoult's law

If one writes the number of molecules as N_A and N_B for $N(1 - x)$ and N_x respectively, the configurational part of the free energy becomes, according to 5.4.4

$$-N_A\varepsilon_A - N_B\varepsilon_B + kT\left[N_A\ \ell n\ \frac{N_A}{N_A + N_B} + N_B\ \ell n\ \frac{N_B}{N_A + N_B}\right] \qquad 5.4.8$$

and differentiating with respect to N_A gives the configurational contribution to the chemical potential μ_A:

$$-\varepsilon_A + kT\ \ell n\ \frac{N_A}{N_A + N_B} = -\varepsilon_A + kT\ \ell n\ (1 - x) \qquad 5.4.9$$

By putting $x = 0$, the configurational contribution to the chemical potential of the pure substance A becomes $-\varepsilon_A$. Therefore, the difference between the chemical potential in the mixture and in the pure state is

$$\mu_A - \mu_A^o = kT\ \ell n\ (1 - x) \qquad 5.4.10$$

and multiplying 5.4.10 by Avogadro's number in order to get the chemical

potential per mole yields the following relation

$$\mu_A - \mu_A^o = RT \ln (1 - x) \qquad 5.4.11$$

Returning now to a previous definition, it can be stated that the absolute activity λ is defined on the molecular scale by

$$\mu = kT \ln \lambda \qquad 5.4.12a$$

and on a molar scale by

$$\mu = RT \ln \lambda \qquad 5.4.12b$$

Therefore, the relation between the absolute activity λ_A of A in the mixture and its value in the pure substance is

$$\frac{\lambda_A}{\lambda_A^o} = 1 - x \qquad 5.4.13a$$

and similarly for B

$$\frac{\lambda_B}{\lambda_B^o} = x \qquad 5.4.13b$$

For the sake of completeness: if the vapour phase in equilibrium with the liquid or solid mixture may be regarded as a perfect gas, the partial vapour pressures p_A, p_B over the mixture are related to the vapour pressures p_A^o, p_B^o of the pure substances by

$$\frac{p_A}{p_A^o} = 1 - x \qquad 5.4.14a$$

$$\frac{p_B}{p_B^o} = x \qquad 5.4.14b$$

These last two equations are expressions of 'Raoult's law'. If the vapour phase may not be treated as a perfect gas, then equations 5.4.14 remain formally correct if each p is interpreted as a fugacity.

5.5 Regular Solutions

The last major step in the progression towards the establishment of a theory regarding the treatment of phase diagrams is a discussion about the implications of what is known as 'regular solutions'. It will be said that a regular solution is, according to Guggenheim (52G1), any mixture of atoms satisfying all the conditions for forming an ideal mixture except that the interchange energy ω, described earlier, is not zero. The atoms are thus assumed to be interchangeable on a lattice or quasi-lattice, but the configurational energy is no longer independent of the mutual disposition of the two or more kinds of atoms.

5.5.1 Classification of nearest neighbour pairs

The nature of this treatment is based on the classification of neighbouring pairs for a mixture containing $N_A = N(1 - x)$ atoms A and $N_B = Nx$ atoms B on a lattice of N sites with a coordination number z. There will be in all $\frac{1}{2}zN$ pairs of nearest neighbours of three kinds, namely AA, BB and AB pairs. If the number of AB pairs is denoted by a number zX then the number of neighbours of A atoms which are not B atoms is $z(N_A - X)$ and consequently the number of AA pairs is $\frac{1}{2}z(N_A - X)$. The number of BB pairs will similarly be $\frac{1}{2}z(N_B - X)$. For convenience, quantities related to the various kinds of nearest neighbour pairs are

displayed in table 5-I as recorded by Guggenheim.

Table 5-I

Kind of pair	Number of pairs	Energy per pair	Energy of all such pairs
AA	$z(N_A - X)/2$	$-2\varepsilon_A/z$	$-(N_A - X)\ \varepsilon_A$
AB	zX	$(-\varepsilon_A - \varepsilon_B + \omega)/z$	$X(-\varepsilon_A - \varepsilon_B + \omega)$
BB	$z(N_B - X)/2$	$-2\varepsilon_B/z$	$-(N_B - X)\ \varepsilon_B$
All	$z(N_A + N_B)/2$	-	$-N_A\varepsilon_A - N_B\varepsilon_B + X$

For a given value of X the configurational energy E_C is given by

$$E_C = -(N_A - X)\ \varepsilon_A + X(-\varepsilon_A - \varepsilon_B + \omega) - (N_B - X)\ \varepsilon_B$$

$$= -N_A\varepsilon_A - N_B\varepsilon_B + X\,\omega \qquad 5.5.1$$

and what remains , is to determine either accurately or approximately, the average or equilibrium value $\overline{X}$ of X. The equilibrium value of the configurational energy will then be given by

$$U_C = \overline{E}_C = -N_A\varepsilon_A - N_B\varepsilon_B + \overline{X}\,\omega \qquad 5.5.2$$

with the energy of mixing being $\overline{X}\,\omega$.

5.5.2 Zeroth approximation

One method of treating the problem is called the zeroth order approximation and consists of the assumption of a completely random distribution of the two kinds of atoms in spite of the non-zero energy of mixing . This leads to an average value $\overline{X}$ of X given by

$$\overline{X} = \frac{N_A N_B}{N_A + N_B} = Nx(1 - x) \qquad 5.5.3a$$

or the equivalent

$$\overline{X}^2 = (N_A - \overline{X})\ (N_B - \overline{X}) \qquad 5.5.3b$$

The resulting configurational free energy is then

$$F_c = -N_A\varepsilon_A - N_B\varepsilon_B + NkT\ [(1 - x)\ \ell n(1 - x) + x\ \ell n\ x\ ] + N\ x(1 - x)\omega$$

5.5.4

and so for the molar free energy of mixing

$$\Delta_m F = RT\ [(1 - x)\ \ell n\ (1 - x) + x\ \ell n\ x\ ] + x(1 - x)N\omega \qquad 5.5.5$$

where N is Avogadro's number. The molar total energy of mixing and molar heat of mixing are given by

$$\Delta_m U = \Delta_m H = x(1 - x)N\omega \qquad 5.5.6$$

and the molar entropy of mixing by

$$\Delta_m S = \frac{\Delta_m U - \Delta_m F}{T} = -R\ [(1 - x)\ \ell n\ (1 - x) + x\ \ell n\ x]$$

5.5.7

this last formula being identical as that of an ideal solution.

Formula 5.5.4 may be rewritten in terms of N_A and N_B to yield

$$F_c = -N_A\epsilon_A - N_B\epsilon_B + kT \left[N_A \ln \frac{N_A}{N_A + N_B} + N_B \ln \frac{N_B}{N_A + N_B} \right]$$

$$+ \frac{N_A N_B}{N_A + N_B} \omega \qquad 5.5.8$$

and the chemical potential μ_A may be obtained by differentiating with respect to N_A

$$\mu_A - \mu_A^o = kT \ln \frac{N_A}{N_A + N_B} + \left[\frac{N_B}{N_A + N_B} \right]^2 \omega$$

$$= kT \ln (1 - x) + x^2\omega \qquad 5.5.9$$

and the absolute activity λ_A becomes

$$\frac{\lambda_A}{\lambda_A^o} = (1 - x) \, e^{x^2\omega/kT} \qquad 5.5.10$$

and similarly,

$$\frac{\lambda_B}{\lambda_B^o} = x \, e^{(1-x)^2\omega/kT} \qquad 5.5.11$$

In accordance with equation 5.2.29 it is convenient to measure the deviations from ideality by means of activity coefficients γ_A, γ_B defined as the ratio of the actual absolute activity (or fugacity) to its value if Raoult's law were obeyed. Combining 5.5.10 and 5.5.11 with 5.2.29 the values of the activity coefficients are then given by

$$\gamma_A = e^{x^2 \omega/kT} \qquad 5.5.12$$

$$\gamma_B = e^{(1-x)^2 \omega/kT}$$

This formulation also satisfies equation 5.2.31.

5.5.3 First approximation or quasi-chemical treatment

Another method of treating the problem is called the first order approximation, this method becomes necessary as the assumption corresponding to complete randomness cannot be strictly correct. As $\omega/kT \to 0$, $\bar{X}$ will tend to the random value given by 5.5.3b (this involves high temperatures). At finite temperatures however, $\bar{X}$ will be less or greater than the random value according as ω is positive or negative. Equation 5.5.3b can therefore be improved by writing

$$\bar{X}^2 = (N_A - \bar{X})\,(N_B - \bar{X})\; e^{-2\omega/zkT} \qquad 5.5.13$$

this equation is a usual way of treating systems in thermodynamic equilibrium using Boltzman's statistics. Simply, the $\bar{X}$ value of the zeroth approximation is given a weighting factor $e^{-2\omega/zkT}$. The value of this factor comes from the fact that $2\omega/z$ is the energy required to change an AA-bond and a BB-bond into two AB-bonds and that $\bar{X}$, $\frac{1}{2}(N_A - \bar{X})$, $\frac{1}{2}(N_B - \bar{X})$ are proportional to the number of AB, AA and BB pairs respectively. Equation 5.5.13 is of the form expected if the several kinds of pairs of neighbours were gaseous molecular species in chemical equilibrium. Boltzman's statistics will therefore apply if one assumes that the mixture of A and B atoms reaches equilibrium similarly to gaseous systems and the approximate treatement embodied in equation 5.5.13 is

accordingly called the 'quasi— chemical' treatment.

It is convenient to introduce the abbreviation η for the quantity $e^{2\omega/zkT}$ so that 5.5.13 may be rewritten as

$$(N_A - \bar{X})\ (N_B - \bar{X}) - \eta^2 \bar{X}^2 = 0 \qquad 5.5.14$$

When dealing with the total energy and the free energy of mixing, a quantity β is defined such that

$$\bar{X} = \frac{N_A N_B}{N_A + N_B} \quad \frac{2}{\beta + 1} \qquad 5.5.15$$

and that when $\beta = 1$, the relation corresponds to the zeroth approximation. Using 5.5.3a and substituting 5.5.15 in 5.5.14 yields

$$\beta^2 - (1 - 2x)^2 = 4\eta^2\, x\,(1 - x) \qquad 5.5.16$$

having the solution

$$\beta = [1 + 4x\,(1 - x)\,(\eta^2 - 1)]^{\frac{1}{2}} \qquad 5.5.17$$

From this formulation, the configurational free energy is given by

$$F_c = -N_A\varepsilon_A - N_B\varepsilon_B + NkT\,[(1 - x)\ \ln\,(1 - x) + x\ \ln\, x]$$

$$+ \tfrac{1}{2}\, NzkT\,\left[(1 - x)\ \ln\ \frac{\beta + 1 - 2x}{(1-x)\,(\beta+1)} + x\ \ln\ \frac{\beta - 1 + 2x}{x(\beta + 1)}\right] \qquad 5.5.18$$

and the molar free energy of mixing $\Delta_m F$ by

$$\frac{\Delta_m F}{RT} = (1 - x)\ \ell n\ (1 - x) + x\ \ell n\ x + \tfrac{1}{2}z\left[(1 - x)\ \ell n\ \frac{\beta + 1 - 2x}{(1-x)(\beta+1)}\right.$$

$$\left. +\ x\ \ell n\ \frac{\beta - 1 + 2x}{x(\beta + 1)}\right] \qquad 5.5.19$$

It has been seen also that the chemical potentials are related to the absolute activities which in turn may be expressed as a function of the free energy of mixing. The relations are

$$kT\ \ell n\ \lambda_A = \frac{\partial F}{\partial N_A}$$

$$kT\ \ell n\ \lambda_B = \frac{\partial F}{\partial N_B} \qquad 5.5.20$$

which, if 4.6.8 is used, yields

$$\frac{\lambda_A}{\lambda_A^o} = (1 - x)\left[\frac{\beta + 1 - 2x}{(1 - x)(\beta + 1)}\right]^{\frac{1}{2}z} \qquad 5.5.21a$$

$$\frac{\lambda_B}{\lambda_B^o} = x\left[\frac{\beta - 1 + 2x}{x(\beta + 1)}\right]^{\frac{1}{2}z} \qquad 5.5.21b$$

and from this, the activity coefficients can be immediately written as

$$\gamma_A = \left[\frac{\beta + 1 - 2x}{(1 - x)\ (\beta + 1)}\right]^{\frac{1}{2}z} \qquad 5.5.22a$$

$$\gamma_B = \left[\frac{\beta - 1 + 2x}{X(\beta + 1)}\right]^{\frac{1}{2}z} \qquad 5.5.22b$$

These last two formulae conclude what could be termed as the first part of the theoretical analysis. It will become obvious through the remainder of this thesis that expressions for the activity coefficients were very much desired as the equations describing the conditions for equilibrium are centred around the estimation of these coefficients. The analysis presented above is due to Guggenheim's work on mixtures and it is still the basis for many investigations dealing with mixtures amenable to regular solutions. Many workers have used these principles in extending the concepts introduced here to describe the equilibrium conditions of mixtures of solid binary compounds in ternary liquid solutions. Amongst the most referred to are Ilegems and Pearson (69I1), Stringfellow and Greene (69S1), Antypas and James (70A1), Osamura et al. (72O1), Panish and Ilegems (72P1) and Joullié et al. (74J1).

5.6 Model for III-V Ternary Solutions

The model chosen to represent ternary III-V solutions is based on the assumptions that the system may be treated as a regular solution and that the quasi-chemical equilibrium approach is valid. The phase diagram is then calculated by computing the conditions for equilibrium between a ternary liquid solution A, B, C and the pseudobinary solid solution AB-AC.

As stated previously, in a solution of N_A atoms of A and N_B atoms of B, each atom is surrounded by z nearest neighbours. The energy

of the solution is regarded as a linear function of the number of the various types of nearest neighbours bonds and is therefore considered independent of temperature and composition. This energy of solution also known as interaction parameter α may be expressed for a system of A and B atoms as

$$\alpha_{AB} = z \left[E_{AB} - \tfrac{1}{2} (E_{AA} + E_{BB}) \right] \qquad 5.6.1$$

where the E_{ij} represents the interaction energy of an i-j nearest neighbour pair.

From a statistical point of view it is possible to derive the thermodynamic properties of such a model solution but it is necessary to use an approximate theory. The zeroth order regular solution approach is internally inconsistent since it assumes a random distribution of atoms even though certain configurations are energetically more favourable than others. A more reasonable approximation is the quasi-chemical equilibrium approach in which the distribution of pairs is weighted exponentially in energy, analogous to a law of mass-action. The following equations specify the thermodynamic properties of the solution

$$N_{AA} N_{BB} = \tfrac{1}{4} N_{AB}^2 \, e^{2\alpha_{AB}/zkT} \qquad 5.6.2$$

$$2N_{AA} + N_{AB} = z N_A \qquad 5.6.3a$$

$$2N_{BB} + N_{AB} = z N_B \qquad 5.6.3b$$

This approach can be used to derive the activity coefficients of A and B

in the solution. Equations 5.5.22 are the relations for the activity coefficients γ_A and γ_B as functions of the composition x, the coordination number z and a parameter β defined in 5.5.17. In here, the composition x is taken as the mole fraction of B molecules or $x = N_B/(N_A + N_B)$.

This model can also be applied to ternary III-V systems as the solid solutions are produced from two binary compounds of virtually invariant composition, therefore the equilibrium treated is between the liquid A,B,C and the mixed crystal solid solution AB-BC. The chemical potentials in the liquid phase are given by

$$\mu_i^{\ell} = \mu_i^{\ell o} + RT \ln \gamma_i N_i \qquad 5.6.4$$

where 'i' = A, B, C, $\mu_i^{\ell o}$ is the chemical potential of the pure component 'i', γ_i is the activity coefficient and N_i is the mole fraction of 'i' in the liquid. The chemical potentials in the solid phase are

$$\mu_{AB}^{\delta} = \mu_{AB}^{\delta o} + RT \ln \gamma_{AB} X^{\delta} \qquad 5.6.5a$$

$$\mu_{AC}^{\delta} = \mu_{AC}^{\delta o} + RT \ln \gamma_{AC} (1 - X^{\delta}) \qquad 5.6.5b$$

where $\mu_{AB}^{\delta o}$ is the chemical potential of the pure compound AB and X^{δ} is the mole fraction of compound AB in the solid solution. At equilibrium

$$\mu_{AB}^{\delta} = \mu_A^{\ell} + \mu_B^{\ell} \qquad 5.6.6a$$

$$\mu_{AC}^{\delta} = \mu_A^{\ell} + \mu_C^{\ell} \qquad 5.6.6b$$

Now, the chemical potential μ_{AB}^{so} of pure compound AB for a temperature below its melting point has been determined by Vieland (63V1) while considering a cycle that would involve heating the crystal from a temperature T to a temperature T_{AB}^{F} (melting point), melting it at constant T_{AB}^{F} and cool it to its initial temperature T. The expression obtained is (see Appendix B for a complete derivation of Vieland's relations):

$$\mu_{AB}^{so} = \mu_{A}^{s\ell} + \mu_{B}^{s\ell} + \Delta S_{AB}^{F}(T - T_{AB}^{F})$$

$$+ \Delta C_p \left[T_{AB}^{F} - T - T \ln (T_{AB}^{F}/T) \right] \qquad 5.6.7$$

and similarly for μ_{AC}^{so}. The term $\mu_{A}^{s\ell}$ is the chemical potential of A in a liquid of stoichiometric composition

$$\mu_{A}^{s\ell} = \mu_{A}^{\ell o} + RT \ln 0.5 + RT \ln \gamma_{A}^{s\ell} \qquad 5.6.8$$

and again similarly for $\mu_{B}^{s\ell}$. ΔS_{AB}^{F} is the entropy of fusion of compound AB and ΔC_p is the heat capacity difference between liquid and solid. If the relatively small contribution of ΔC_p can be neglected, the equilibrium conditions equations 5.6.6 may be combined with 5.6.4, 5.6.5 and 5.6.7 to yield

$$\ln \gamma_{AB} = \ln \frac{\gamma_A \gamma_B}{\gamma_A^{s\ell} \gamma_B^{s\ell}} + \ln 4 \frac{N_A N_B}{X^{\delta}} + \frac{\Delta S_{AB}^{F}}{RT} (T_{AB}^{F} - T) \qquad 5.6.9a$$

$$\ln \gamma_{AC} = \ln \frac{\gamma_A \gamma_B}{\gamma_A^{s\ell} \gamma_C^{s\ell}} + \ln 4 \frac{N_A N_C}{1-X^{\delta}} + \frac{\Delta S_{AC}^{F}}{RT} (T_{AC}^{F} - T) \qquad 5.6.9b$$

with $N_A + N_B + N_C = 1$ 5.6.9c

In order to solve equations 5.6.9 for T and X^{δ}, there remains to determine the values of the various activity coefficients. There has been various suggestions as to what form the relations should have but the model retained by most workers is still the approximation of treating the solid solution of the mixed crystals as a regular solution and the liquid solution as a mixture in quasi-chemical equilibrium.

5.7 Simple Solutions

A binary solution of constituents 1 and 2, may be called 'simple' when the excess free energy of mixing G_m^E can be approximated by a symmetrical expression of the form

$$G_m^E = \alpha x_1 x_2 \qquad 5.7.1$$

then the activity coefficients are given by the following expressions:

$$RT \ln \gamma_1 = \alpha_{12} x_2^2 \qquad 5.7.2a$$

$$RT \ln \gamma_2 = \alpha_{12} x_1^2 \qquad 5.7.2b$$

which translate to

$$RT \ln \gamma_{AB} = \alpha_{AB-AC} (1 - X^{\delta})^2 \qquad 5.7.3a$$

$$RT \ln \gamma_{AC} = \alpha_{AB-AC} X^{\delta 2} \qquad 5.7.3b$$

for a binary solution of stoichiometric compounds AB and AC. The expressions for the activity coefficients of the ternary liquid solution are, however, not so simple and have led to various approaches. Prigogine and Defay (54P1) suggested that by extension to the binary formulation the activity coefficients can be written as

$$RT \ln \gamma_A = \alpha_{AB} N_B^2 + \alpha_{AC} N_C^2 + (\alpha_{AB} + \alpha_{AC} - \alpha_{BC}) N_B N_C \quad 5.7.4a$$

$$RT \ln \gamma_B = \alpha_{AB} N_A^2 + \alpha_{BC} N_C^2 + (\alpha_{AB} + \alpha_{BC} - \alpha_{AC}) N_A N_C \quad 5.7.4b$$

$$RT \ln \gamma_C = \alpha_{AC} N_A^2 + \alpha_{BC} N_B^2 + (\alpha_{AC} + \alpha_{BC} - \alpha_{AB}) N_B N_C \quad 5.7.4c$$

Later, Darken (67D1) proposed a quadratic formalism for the representation of the excess free energy and of the activity coefficients of each component of a ternary system in the vicinity of a single component selected as a solvent. The result is identical to equation 5.6.13 except for the factor RT which does not appear. This formalism is found to be consistent with the Gibbs-Duhem equation and approaches Raoult's law for the solvent at infinite dilution and to Henry's law for each solute.

Stringfellow and Green (69S1) have formulated a somewhat different view where they start from six equations which specify the thermodynamic properties of the solution. Three of the equations are of the form of 5.6.2 and the remaining three are similar to 5.6.3 but adapted to a ternary system. Using, for the enthalpy of mixing, an expression

such as

$$\Delta H_m = x_{AB}\alpha_{AB} + x_{AC}\alpha_{AC} + x_{BC}\alpha_{BC} \qquad 5.7.5$$

and relating the activity coefficients to ΔH_m through the excess free energy of mixing, they obtained a set of equations which could be solved numerically to yield the five activity coefficients γ_A, γ_B, γ_C, γ_{AB} and γ_{AC}.

However, most other workers have used the argument of a law of mass-action to relate the number of nearest neighbour pairs to the energy of one such pair and used as an expression for the enthalpy of mixing the following relation

$$\Delta H_m = \alpha_{AB}\, x_A x_B + \alpha_{AC}\, x_A x_C + \alpha_{BC}\, x_B x_C \qquad 5.7.6$$

which yields the formalism of Prigogine and Defay for the activity coefficients in the ternary liquid solution.

This latter formalism will be the one used throughout this study. It becomes therefore possible to solve equations 5.6.9 for T and X^{δ} given the concentrations N_i of each constituent in the liquid, the activity coefficients γ's, the entropies of mixing ΔS^F_{ij} and the temperatures of fusion T^F_{ij} of the binary compounds. From the results it is then possible to construct the phase diagram of the ternary system under investigation.

The determination of various parameters, however, remains to be established and this subject is treated in the following chapter where

these parameters are determined for two specific III-V ternary systems, namely $Ga_xIn_{1-x}Sb$ and $GaAs_ySb_{1-y}$.

Chapter 6 Thermodynamic data for the III-V ternary systems Ga-In-Sb and Ga-As-Sb

6.1 Introduction

6.2 Entropies and Temperatures of Fusion

6.3 Interaction Parameters: linear variation with temperature

6.3.1 Gallium-Antimony system (GaSb)

6.3.2 Indium-Antimony system (InSb)

6.3.3 Gallium-Arsenic system (GaAs)

6.3.4 The interaction parameters $\alpha_{III-III'}$; $\alpha_{V-V'}$; $\alpha_{III-III'-V}$; $\alpha_{III-V-V'}$.

6.1 Introduction

The purpose of this chapter is to make a transition between the purely theoretical treatment of phase diagrams and the actual use of such a model. Here, the methods of obtaining the values of the various binary parameters brought forward in chapter 5 are analyzed or these values are simply presented for the case where their use has become common practice and the results are, in general, widely accepted. The parameters to be determined are: the entropies of fusion ΔS^F_{ij} as well as the temperatures of fusion T^F_{ij} of the binary compounds and finally the activity coefficients γ_i ('i' = A,B,C) in the liquid solution as the activity coefficients in the solid solution may be eliminated by substituting the γ_{ij}'s of equations 5.7.3 in equations 5.6.9

6.2 Entropies and Temperatures of Fusion

The first parameters are the entropies of fusion and the temperatures of fusion of the binary compounds of interest here namely: GaSb, InSb and GaAs. The most widely accepted values for the entropies of fusion are those of Lichter and Sommelet (69L1, 69L2) where the high-temperature heat contents of InSb and GaSb were measured over the temperature range 400K to 1450K and those of GaAs were measured over the temperature range 400K to above the melting point.

The temperatures of fusion to be used in the present calculations differ from those of Lichter and Sommelet except for GaSb. The values used here are 985K for GaSb (63H1), 798K for InSb (52L1), and 1511K for GaAs (55K2). The data are tabulated in table 6-I.

Table 6-I Entropies of fusion and temperatures of fusion of the binary compounds GaSb, InSb and GaAs

Compound	Entropy of fusion $J.mol^{-1}.K^{-1}$	Temperature of fusion K
GaSb	66.11	985
InSb	59.91	798
GaAs	69.62	1511

6.3 Interaction Parameters: linear variation with temperature

Finally, the determination of the activity coefficients of the liquid solution requires a more extensive treatment. As could be seen in the preceding chapter, they are intimately related to the interaction parameters defined in the analysis of the relationships that exist between pairs of nearest neighbour atoms. From equations 5.7.4 it is readily seen that the knowledge of the interaction parameters characteristic of each pair of constituents and of the concentrations N_i will completely determine the activity coefficients for a given temperature T. Therefore

the problem reduces to evaluating the interaction parameters and in order to do this a semi-empirical treatment has been proposed by Thurmond (64T1). This treatment is based on the fact that the α's for binary compounds have a linear dependence with temperature. Already, it is seen that this method is restrictive in the sense that it only allows the determination of the α_{III-V} parameters but not the $\alpha_{III-III'}$ or $\alpha_{V-V'}$. However, this problem is discussed at the end of this chapter.

Thurmond established this linear dependence very successfully for the compound GaAs but the method is to be used carefully as it is expected that linearity will hold when the saturated liquid phase is dilute, at temperatures far from the melting point of the compound. This is true due to the fact that the partial molar heat of mixing and excess entropy of mixing of the dilute component are in general insensitive to temperature changes, and in dilute solutions, are independent of composition changes.

The linear relationship has also been used by Ilegems and Panish (74I1), where they assume that ternary liquid solutions may be considered as 'simple' solutions. They quote evidence that binary liquid III - V systems are effectively simple over a large concentration range (72P1, 74I2).

Thurmond's analysis is based on a study of Vieland's relation for a binary diagram including a line compound (63V1)

$$\alpha_{AB} = - \frac{RT}{2(0.5)^2} \left[\ln 4x(1 - x) + \frac{\Delta S^F_{AB}}{RT} (T^F_{AB} - T) \right] \quad 6.3.1$$

where x is the mole fraction of component B and ΔS^F_{AB} and T^F_{AB} are the entropy of fusion and the temperature of fusion of the compound AB respectively. It is useful to mention that the formalism of equation 6.3.1 is not exactly that of Vieland or for that matter that of Schottky and Bever (58S1) who had previously used it. A detailed calculation shown in Appendix B relates the formalism of references (64T1) and (58S1) to equation 6.3.1 which is the formulation most widely used now.

Another point worth mentioning about this particular treatment is the approximation made during the development that the term in ΔC_p is negligible compared with the entropy term. Formally, the two terms are as follows

$$\Delta C_p \left(\frac{T^F}{T} - 1 - \ell n \frac{T^F}{T}\right)$$

and

$$\Delta S^F \left(\frac{T^F}{T} - 1\right)$$

and in order to check the validity of the approximation, the two terms have been calculated for typical temperatures and the differences computed in percentage. The results are displayed in Table 6-II where the values of Lichter and Sommelet are used for the ΔC_p and ΔS^F of the three binary compounds, GaSb, InSb and GaAs.

Table 6-II Comparison of the two terms in ΔC_p and ΔS^F of Vieland's treatment for typical temperatures.

Compound	T^F K	ΔC_p $J.mol^{-1}.K^{-1}$	ΔS^F $J.mol^{-1}.K^{-1}$	T K	$\Delta C_p(\frac{T^F}{T} - 1 - \ell n \frac{T^F}{T})$ $J.mol^{-1}.K^{-1}$	$\Delta S^F(\frac{T^F}{T} - 1)$ $J.mol^{-1}.K^{-1}$	%
GaSb	985	6.12	66.11	900	0.02	6.21	0.4
				800	0.14	15.27	0.9
				700	0.40	26.91	1.4
InSb	798	17.09	59.91	700	0.15	8.39	1.8
				600	0.77	19.77	3.9
				500	2.19	35.71	6.1
GaAs	1511	5.26	69.62	1200	0.15	18.03	0.8
				1000	0.51	35.56	1.4
				800	1.33	61.88	2.1
				600	3.13	105.69	3.0

It can now be seen from Table 6-II that the omission of the ΔC_p term is justified for temperatures not too far from the melting point with perhaps restrictions for InSb.

It is then possible to evaluate the various interaction parameters as linear functions of temperature. The relation

$$\alpha_{AB} = p + qT \qquad 6.3.2$$

which exists between α_{AB} and T is best demonstrated when equation 6.3.1 is solved for different combinations of x and T taken from the appropriate binary phase diagram data given in the literature.

6.3.1 Gallium-Antimony system (GaSb)

The experimental data available for the binary phase diagram of GaSb are from Greenfield and Smith (55G1), Koster and Thoma (55K2), Hall (63H1), and Goryunova's data in Kalyuzhnaya et al. (64K1). Table 6-III gives the values scaled from the published graphs and the values of α_{GaSb} obtained from equation 6.3.1. The latter were then submitted to a least square analysis and the resulting values of p and q are also given.

The data of Koster and Thoma were corrected for temperature by +9K as suggested by Hall, and those of Greenfield and Smith similarly by +6K to take into account the accepted value of the melting point of GaSb at 985K. The binary phase diagram of GaSb is seen in figure 6-1 while figure 6-2 shows the α_{Ga-Sb} versus T relation.

As can be seen, a wide scatter exists for temperature above 800K as it was pointed out by Thurmond that such would be the case away from dilute solutions of the mixture. However, corrections of ±5K in temperature or ±0.02 in antimony concentration brought each point to within the range of a least square analysis except for those above the eutectic composition of 0.88 antimony. For instance, one point at $x_{Sb} = 0.90$, which is above the eutectic, returned into the range when

Table 6-III Binary phase diagram data for GaSb and values of α_{Ga-Sb} from equation 6.3.1.

Source	T_K	x_{Sb}	$\alpha_{Ga-Sb} \times 10^3$ J.mol^{-1}
Greenfield and Smith (55G1)**	885	9.50×10^{-1}	15.00*
	873	9.00×10^{-1}	1.40*
	893	8.43×10^{-1}	-3.99
	915	8.00×10^{-1}	-4.56
	938	7.50×10^{-1}	-3.68
	943	7.35×10^{-1}	-3.78
	948	7.25×10^{-1}	-2.59
	953	7.00×10^{-1}	-4.20
	973	6.50×10^{-1}	8.09*
	973	6.28×10^{-1}	4.52*
	979	5.00×10^{-1}	†
	975	4.23×10^{-1}	-6.35
	963	3.50×10^{-1}	-6.77
	938	2.30×10^{-1}	-0.01*
	893	1.40×10^{-1}	-0.09
	838	0.82×10^{-1}	-2.60
	823	0.70×10^{-1}	-2.84
Koster and Thoma (55K2)***	873	9.50×10^{-1}	13.23*
	873	8.50×10^{-1}	-7.67
	903	8.00×10^{-1}	-8.05
	923	7.50×10^{-1}	-10.26
	958	6.50×10^{-1}	-9.75
	965	6.00×10^{-1}	-20.17*
	973	5.50×10^{-1}	-24.58*
	976	5.00×10^{-1}	†
	968	4.00×10^{-1}	-10.20
	945	3.00×10^{-1}	-8.42
	905	2.00×10^{-1}	-7.28
	878	1.50×10^{-1}	-6.21
	848	1.00×10^{-1}	-3.72
	793	0.53×10^{-1}	-3.51
Hall (63H1)	908	1.90×10^{-1}	-7.47
	897	1.80×10^{-1}	-9.26
	831	6.75×10^{-2}	-1.77
	727	1.42×10^{-2}	0.75
	663	0.40×10^{-2}	3.08
	603	1.07×10^{-3}	4.18
	553	2.76×10^{-4}	5.47
	528	0.64×10^{-4}	12.16*
Kalyuzhnaya (64K1)	971	4.25×10^{-1}	-66.53*
	961	3.45×10^{-1}	-16.36*
	934	2.55×10^{-1}	-10.39
	862	1.93×10^{-1}	-25.19*
	794	0.40×10^{-1}	-30.14*

$p = 23824$ J.mol^{-1} $\quad q = -32.38$ J.mol^{-1}.K^{-1}

* data point not used in least square analysis

** α_{Ga-Sb} calculated with a correction of +6K to T

*** α_{Ga-Sb} calculated with a correction of +9K to T

† value of x_{Sb} brings in an indetermination in equation 6.3.1

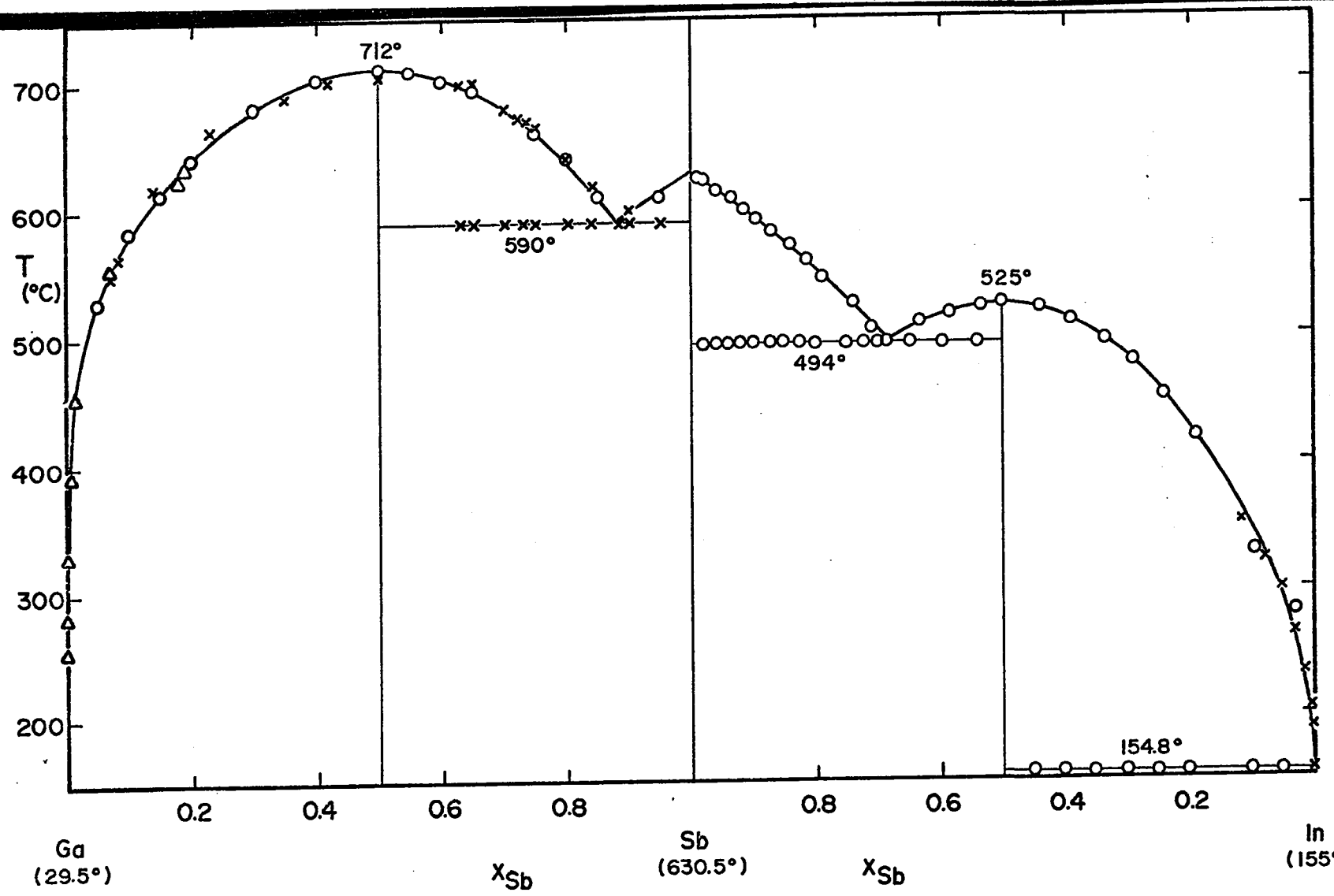

Fig. 6-1. Binary phase diagram for the two III-V compounds GaSb and InSb.

GaSb: o Ref. 55K2 (including a correction of +9°C), Δ Ref. 63H1, x Ref. 55G1.

InSb: o Ref. 52L1, x Ref. 63H1.

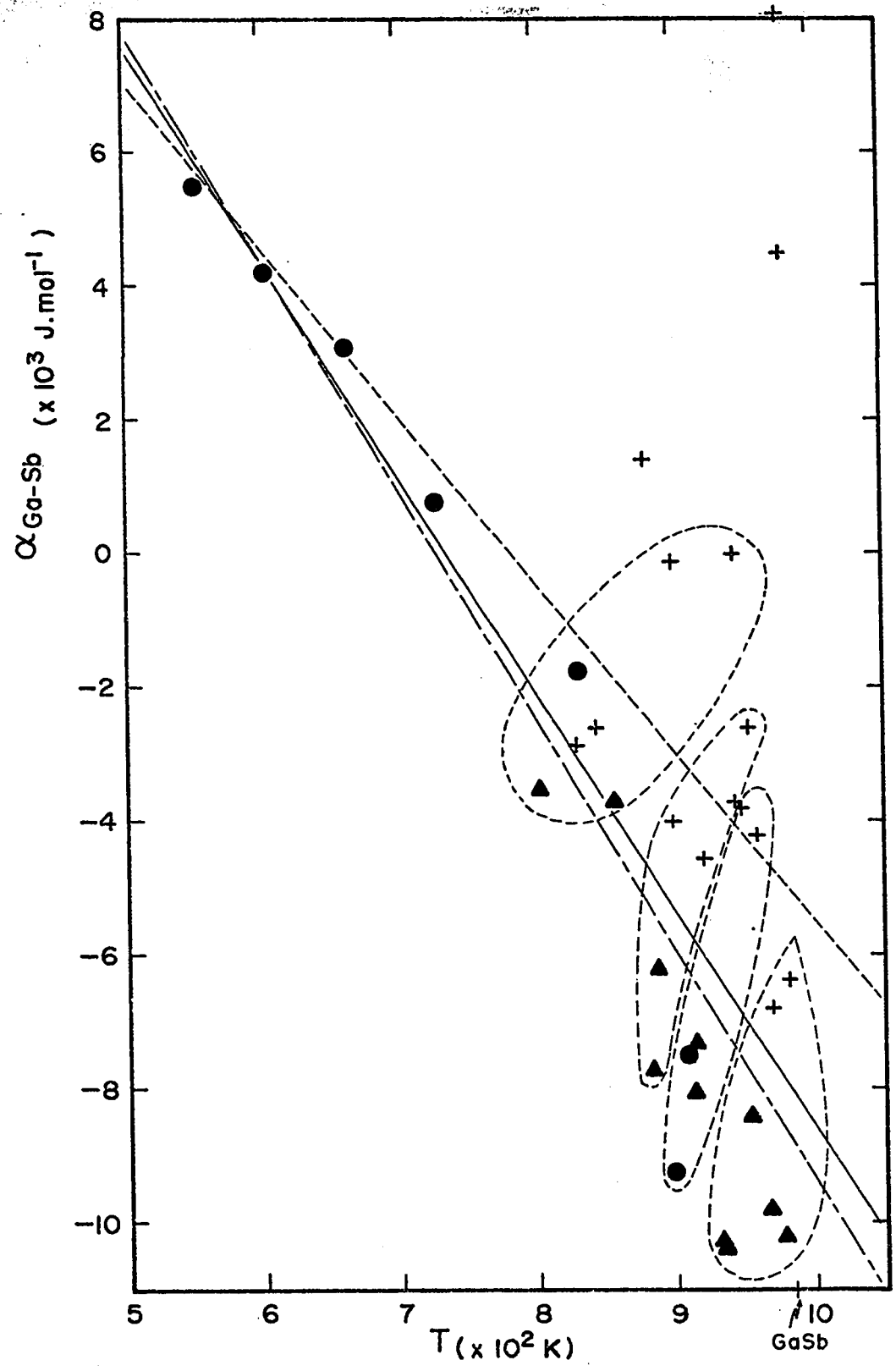

Fig. 6-2. GaSb. The interaction parameter α_{Ga-Sb} as a function of temperature. ▲ Ref. 55K2, + Ref. 55G1, ● Ref. 63H1. ——— present work (least squares fit), -----Ref. 72P1, — — — Ref. 74J1.

the $\Delta x_{Sb} = -0.02$ correction was applied. This then suggests that the high temperature data are very sensitive to either temperature or concentration variations in contrast to the low temperature points which were also tested with the corrections and found to be nearly invariant.

After such an investigation, a least square analysis was carried out to determine parameters of the linear relationship but it was decided to use a weighting factor to allow for the low density of dilute concentrations. Figure 6-2 identifies four regions which were compared with the four low temperature points, the final analysis yielded the following weighting factors:

x7 for the lowest dilute data point

x6 for the 3 remaining dilute data points.

Finally, the line corresponding to the least square analysis for 28 data points is shown in figure 6-2.

There has been a number of studies made on systems containing the binary compounds GaSb and in each case a different value for α_{Ga-Sb} is quoted. Two such values are plotted in figure 6-2 and Table 6-VI contains a longer list from the literature.

6.3.2 Indium-Antimony system (InSb)

The experimental data available for the binary phase diagram of InSb are from Pogodin and Dubinsky (49P1), Liu and Peretti (52L1) and Hall (63H1). Table 6-IV gives the values taken either directly from the published work or from a graphical analysis along with the values of

Table 6-IV Binary phase diagram data for InSb and values of a_{In-Sb} from equation 6.3.1

Source	T K	x_{Sb}	$a_{In-Sb} \times 10^4$ J.mol^{-1}
Pogodin and Dubinsky (49P1)	891	9.50×10^{-1}	4.27*
	878	9.10×10^{-1}	3.68*
	841	8.15×10^{-1}	2.82*
	803	7.50×10^{-1}	1.38*
	788	7.15×10^{-1}	0.27*
	781	6.95×10^{-1}	-0.58*
	788	6.50×10^{-1}	-1.04*
	798	5.90×10^{-1}	-1.62
	803	5.40×10^{-1}	-4.29*
	803	5.13×10^{-1}	-51.86*
	807	5.05×10^{-1}	1.32*
	803	4.60×10^{-1}	-4.29*
	798	4.10×10^{-1}	-1.62
	783	3.50×10^{-1}	-1.71
	748	2.80×10^{-1}	-2.22
	730	2.50×10^{-1}	-2.26
	663	1.50×10^{-1}	-2.00
	623	0.97×10^{-1}	-1.73
	560	0.50×10^{-1}	-1.76
Liu and Peretti (52L1)	898	9.89×10^{-1}	6.19*
	897	9.79×10^{-1}	5.34*
	889	9.58×10^{-1}	4.51*
	883	9.37×10^{-1}	4.10*
	873	9.16×10^{-1}	3.77*
	866	8.95×10^{-1}	3.56*
	856	8.68×10^{-1}	3.33*
	845	8.42×10^{-1}	3.10*
	833	8.17×10^{-1}	2.82*
	820	7.90×10^{-1}	2.44*
	800	7.39×10^{-1}	1.61*
	780	7.13×10^{-1}	0.24*
	768	6.87×10^{-1}	-1.18*
	783	6.36×10^{-1}	-1.06*
	790	5.86×10^{-1}	-1.72
	797	5.36×10^{-1}	-0.96*
	798	5.00×10^{-1}	†
	795	4.42×10^{-1}	-0.93*
	785	3.86×10^{-1}	-1.65
	770	3.37×10^{-1}	-1.79
	752	2.88×10^{-1}	-1.68
	725	2.39×10^{-1}	-1.81
	693	1.91×10^{-1}	-1.84
	602	0.95×10^{-1}	-1.95
	556	0.47×10^{-1}	-1.61
Hall (63H1)	625	1.15×10^{-1}	-1.92
	598	0.78×10^{-1}	-1.63
	573	0.50×10^{-1}	-1.38
	538	0.30×10^{-1}	-1.35
	508	1.43×10^{-2}	-1.11
	478	5.26×10^{-3}	-0.78
	463	3.48×10^{-3}	-0.73
	428	1.53×10^{-3}	-0.81

p = 4895 J.mol^{-1} q = -33.72 J.mol^{-1}.K^{-1}

* data point not used in least square analysis

** a_{In-Sb} calculated with a correction of -RK to T.

† value of x_{Sb} brings in an indetermination in equation 6.3.1

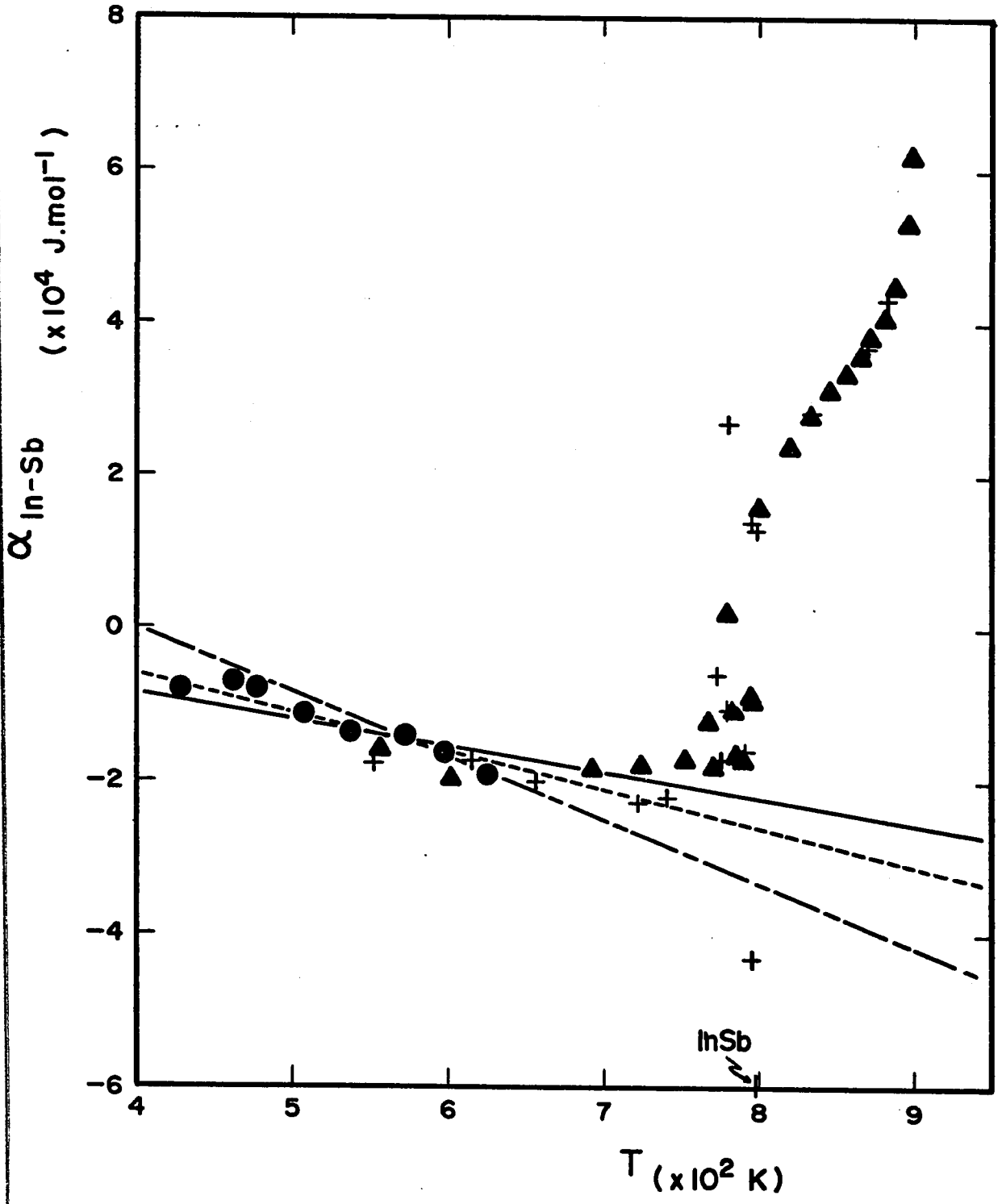

Fig. 6-3. InSb. The interaction parameter α_{In-Sb} as a function of temperature. ● Ref. 63H1, ▲ Ref. 52L1, + Ref. 49P1. —— present work (least squares fit), ---- Ref. 72P1, —— - —— Ref. 74J1.

α_{In-Sb} obtained from equation 6.3.1. The latter were also submitted to a least square analysis and the values of p and q are given.

The data of Pogodin and Dubinsky were corrected by -8K to account for their high value (806K) of the melting temperature of InSb. Figure 6-1 shows the binary phase diagram for InSb and figure 6-3 gives the α_{In-Sb} versus T relation. Here too, the wide scatter at higher temperatures was analysed in the same way as that of GaSb and again the data points above the eutectic (x_{Sb} = 0.68) could not be corrected enough since above this composition the melt is in equilibrium with solid antimony rather than with InSb. Finally, the line corresponding to the least square analysis is given in figure 6-4.

Various values of α_{In-Sb} appear in the literature and two of them are displayed in figure 6-3. A more complete list appears in Table 6-VI.

6.3.3 Gallium-Arsenic system (GaAs)

The experimental data available for the binary phase diagram of GaAs are from Koster and Thoma (55K2) and Hall (63H1). Table 6-V gives those values taken from a graphical analysis of the published data and the values of α_{Ga-As} obtained from equation 6.3.1 The latter were treated with a least square analysis in order to determine the values of p and q also quoted in the table. Figures 6-4 and 6-5 respectively show the experimental binary phase diagram of GaAs and the α_{Ga-As} versus T relation.

Table 6-V Binary phase diagram data for GaAs and values of α_{Ga-As} from equation 6.3.1

Source	T K	x_{As}	α_{Ga-As} x 10^{-4} J-mol^{-1}
Koster and Thoma (55K2)	1288	8.50×10^{-1}	-3.39*
	1338	7.84×10^{-1}	-4.78*
	1418	7.32×10^{-1}	-3.36
	1453	6.82×10^{-1}	-3.50
	1511	5.00×10^{-1}	†
	1488	3.82×10^{-1}	-3.21
	1473	3.50×10^{-1}	-3.31
	1448	3.10×10^{-1}	-5.48
	1346	1.90×10^{-1}	-3.15
Hall (63H1)	1277	1.22×10^{-1}	-2.55
	1262	1.12×10^{-1}	-2.55
	1226	8.86×10^{-2}	-2.46
	1162	1.50×10^{-2}	-2.15
	1126	3.83×10^{-2}	-2.08
	1064	2.07×10^{-2}	-1.94
	1018	1.15×10^{-2}	-1.71
	984	7.00×10^{-3}	-1.52
	964	5.60×10^{-3}	-1.56
	926	3.40×10^{-3}	-1.55
	866	1.14×10^{-3}	-.123
	827	5.31×10^{-4}	-1.06
	767	2.25×10^{-4}	-1.43*
	731	4.10×10^{-5}	-0.24*

p = 19828 J-mol^{-1} q = -36.61 J.mol^{-1}K^{-1}

* data point not used in least square analysis

† value of x_{As} brings in an indetermination in equation 6.3.1

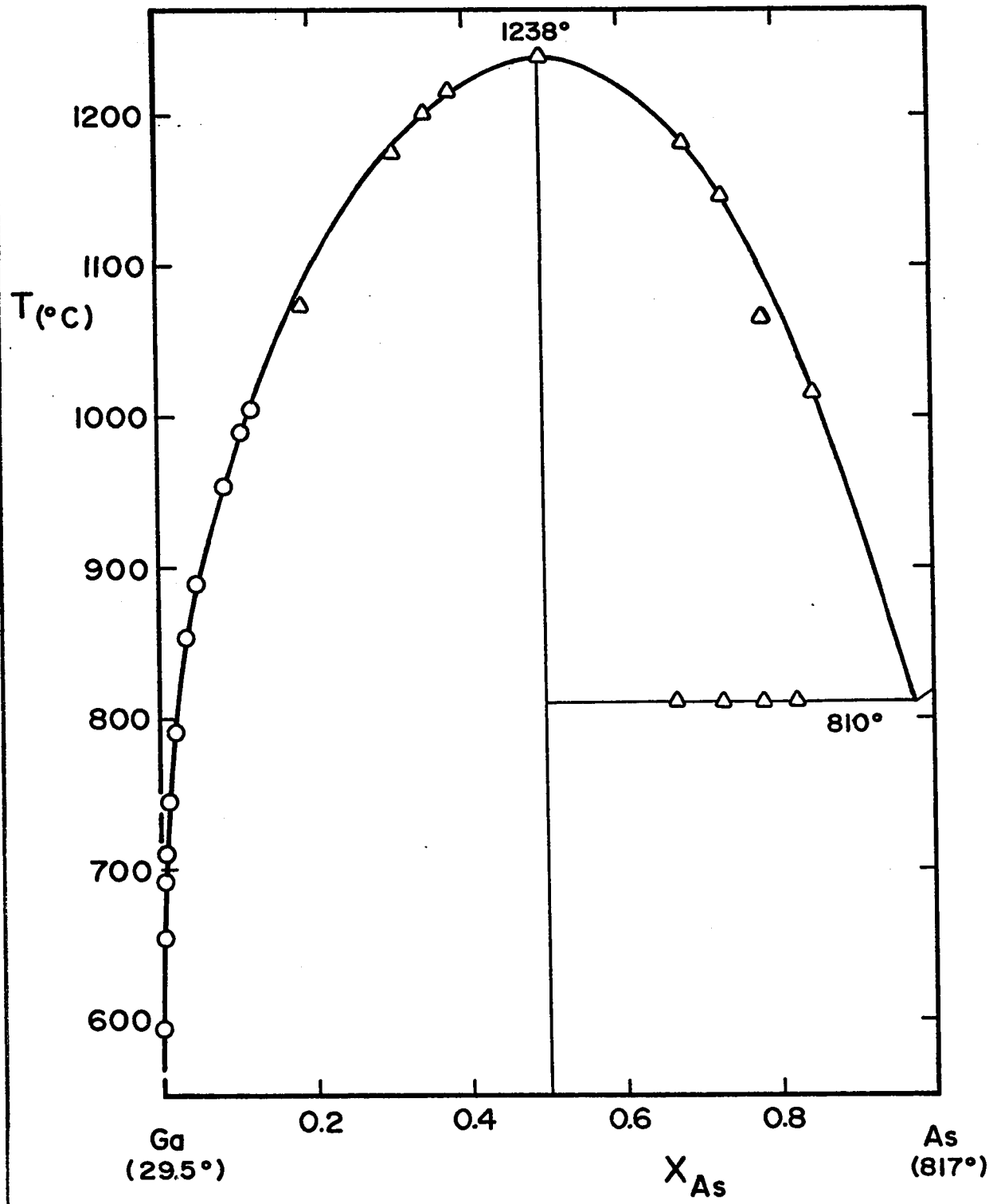

Fig. 6-4. Binary phase diagram for the III-V compound GaAs.

o Ref. 63H1, Δ Ref. 55K2.

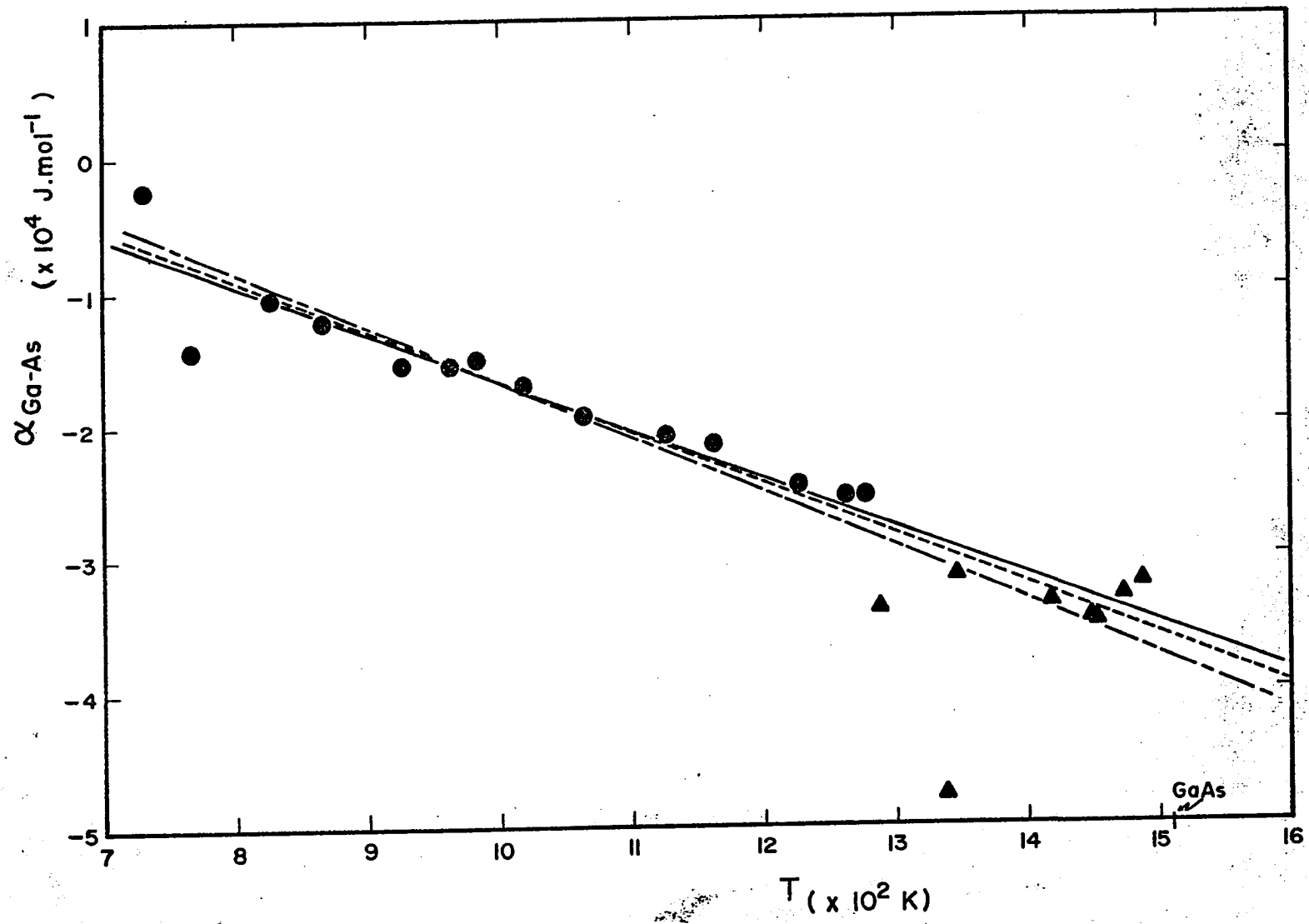

Fig. 6-5. GaAs. The interaction parameter α_{Ga-As} as a function of temperature.

● Ref. 63H1, ▲ Ref. 55K2.

—— present work (least squares fit), --- Ref. 72P1, —— – —— Ref. 72W1.

Again various values of α_{Ga-As} can be found in the literature and two of them have been plotted in figure 6-5. A more complete list is presented in Table 6-VI.

The values for the interaction parameters of binary compounds listed in Table 6-VI represent the major contributions in the related field of interest. There are, however, restrictions that were expressed by the various authors as to the validity of some values and the concerned reader may refer to each individual study. The main point which stems from the various analyses is that it is being verified more and more as well as implied by Thurmond, Arthur and Stringfellow and Greene that the quasi-chemical equilibrium treatment is questionable regarding the III - V binary systems since none has been found to behave as a regular solution. Therefore, Vieland's treatment must be considered carefully as indicated by the behaviour of the system InSb for instance. The approximation which consists of neglecting the ΔC_p term becomes disputable in light of the results for low temperatures (see Table 6-II).

6.3.4 The interaction parameters $\alpha_{III-III'}$;$\alpha_{V-V'}$; $\alpha_{III-III'-V}$; $\alpha_{III-V-V'}$

The remaining interaction parameters to be determined are those of a binary mixture of elements of the same group, and those characteristic of the ternary systems. The $\alpha_{III-III'}$ or $\alpha_{V-V'}$ may not be evaluated according to Thurmond's treatment as they do not form stoichiometric binary compounds, while the $\alpha_{III-III'-V}$ or $\alpha_{III-V-V'}$ because of their ternary nature, cannot be derived from a simple analysis. Figures 6-6 and 6-7 show respectively the binary phase diagrams for the two systems:

Table 6-VI. Various values of the interaction parameters of the binary compounds: GaSb, InSb and GaAs

Source	$\alpha_{Ga\text{-}Sb}$ J.mol^{-1}	$\alpha_{In\text{-}Sb}$ J.mol^{-1}	$\alpha_{Ga\text{-}As}$ J.mol^{-1}
Thurmond (64T1)			41672 - 46.65 T [a.]
Arthur (67A1)			21589 - 38.33 T [b.]
Stringfellow and Green (69S1)		-16652	-18326
Antypas and James (70A1)	48116 - 54.39 T [c.]		-15.48 T
Blom and Plaskett (71B1)	26024 - 33.93 T	33473 - 69.79 T	
Osamura et al. (72O1)			21422 - 33.47 T
Wu and Peasron (72W1)			24686 - 41.42 T
Panish and Ilegems (72P1)	19665 - 25.10 T	14225 - 50.21 T	21589 - 38.33 T [d.]
Joullié et al. (74J1)	25062 - 34.43 T	33472 - 83.68 T	
this study	23824 - 32.38 T	4985 - 33.72 T	19828 - 36.61 T

a. he used $\Delta S^{F}_{GaAs} = 58.6$ J.mol^{-1}

b. he used $\Delta S^{F}_{GaAs} = 69.6$ J.mol^{-1} which was unpublished data by Lichter at the time

c. they used $\Delta S^{F}_{GaSb} = 51.5$ J.mol^{-1}

d. this is Arthur's value above.

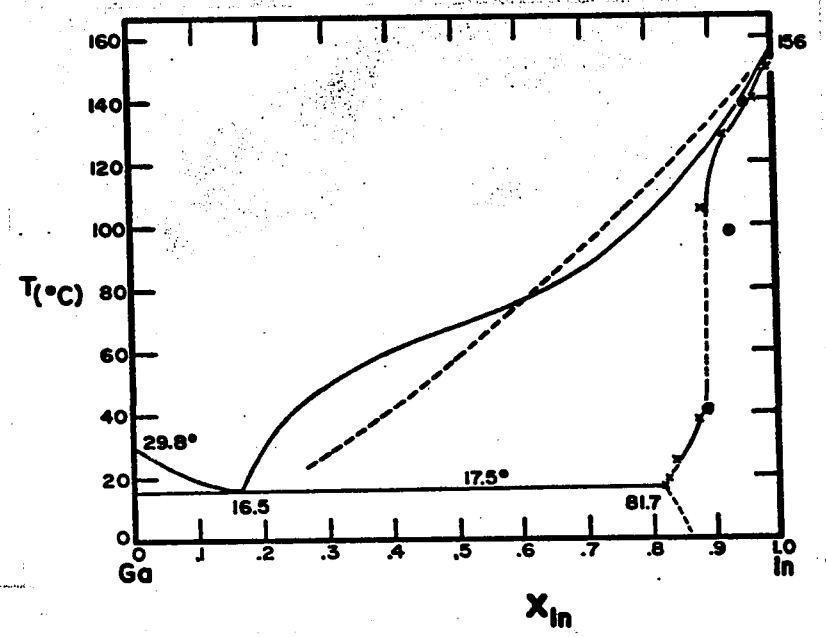

Fig. 6-6. Binary phase diagram of the Gallium-Indium system as given in Hansen (58H1).

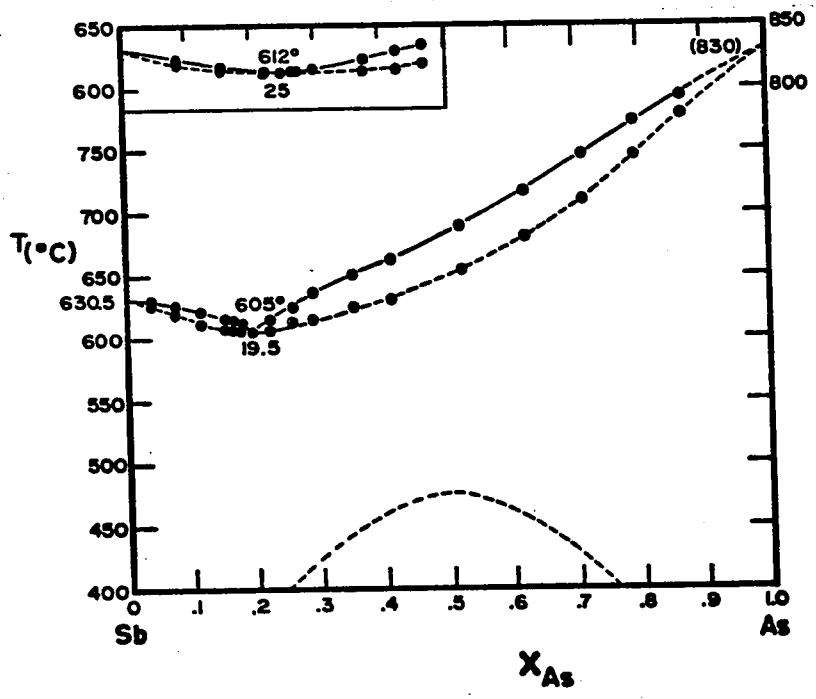

Fig. 6-7. Binary phase diagram of the Antimony-Arsenic system as given in Hansen (58H1).

Ga-In and As-Sb. The shape of the liquidus and solidus lines certainly does not allow an easy method of obtaining the interaction parameters to be foreseen a priori. As a matter of fact, their patterns only render the sketching of ternary diagrams more complicated. Nevertheless values taken from the literature are recorded in Table 6-VII. A similar situation exists for the interaction parameters of the ternary systems as a knowledge of the pseudobinary phase diagram is required in order to assign values to either the $\alpha_{III-III'-V}$'s or the $\alpha_{III-V-V'}$'s. Various values quoted in the literature are also listed in Table 6-VII.

The values of the remaining four interaction parameters used in this study do not appear in table 6-VII because the technique used to evaluate them is described in subsequent chapters. The method requires a detailed knowledge of the pseudobinary section of the phase diagram from which interrelated sets of parameters are calculated (e.g. $\alpha_{III-III'}$ with $\alpha_{III-III'-V}$).

In the chapters to follow, the ternary systems Ga-In-Sb and Ga-As-Sb are discussed in detail and the theoretical model described earlier is compared to experimental results.

Table 6-VII Various values of the interaction parameters of the III-V systems: Ga-In, As-Sb, $Ga_xIn_{1-x}Sb$ and $GaAs_ySb_{1-y}$.

Source	α_{Ga-In} J-mol^{-1}	α_{As-Sb} J-mol^{-1}	$\alpha_{GaSb-InSb}$ J-mol^{-1}	$\alpha_{GaAs-GaSb}$ J-mol^{-1}
Stringfellow and Greene (69S1)	4460 [a.]	2552 [b.]		
Antypas and James (70A1)		10042		18828
Blom and Plaskett (71B1)	4460 [a.]		6276	
Wu and Pearson (72W1)	$4602+0.67T+41.0TN_{Ga}$ [c.]			
Panish and Ilegems (72P1)	4435 [d.]	3138	7950	18828
Joullié et al. (74J1)	8368		6694	

a. from measurements of activities in Ga-In liquid alloys by Macur et al. (68M1)

b. from Shih and Peretti (56S1)

c. this relation invalidates the Gibbs-Duhem equation

d. from the heats of mixing data of Bros et al. (67B1)

Chapter 7 Phase diagram of the ternary system Ga-In-Sb

7.1 Introduction

7.2 Experimental Determination of the Phase Diagram of the Ternary System Ga-In-Sb.

7.2.1 Pseudobinary section $Ga_xIn_{1-x}Sb$ and liquidus sheet of Ga-In-Sb.

7.2.2 Solidus isoconcentration lines of Ga-In-Sb

7.3 Theoretical Determination of the Phase Diagram of the Ternary System Ga-In-Sb.

7.3.1 The interaction parameters α_{Ga-In} and $\alpha_{GaSb-InSb}$.

7.3.2 Liquidus isotherms of Ga-In-Sb

7.3.3 Solidus isotherms and isoconcentration lines of Ga-In-Sb

7.4 Discussion

7.1 Introduction

In this chapter, solidus isothermal and isoconcentration lines are determined experimentally for the ternary system Ga-In-Sb and results are compared with data predicted by the simple solution model which was presented in previous chapters. The experimental results are presented first followed by the numerical analysis. All relevant data, experimental as well as theoretical, are then plotted and compared in order to assess the predictions of the theoretical model.

7.2 Experimental Determination of the Phase Diagram of the Ternary System Ga-In-Sb.

7.2.1 Pseudobinary section $Ga_xIn_{1-x}Sb$ and liquidus sheet of Ga-In-Sb.

Preliminary investigations of the pseudobinary section $Ga_xIn_{1-x}Sb$ are due mainly to Koster and Thoma (55K1), Woolley and Smith (58W1) and Woolley and Lees (59W1). Together, these authors present enough experimental data to completely determine the liquidus and solidus lines of the pseudobinary phase diagram. The results are shown in figure 7-1. Much of the work has primarily been concentrated on the pseudobinary section since it contains all of the solid phases of interest technologically. Most of the remaining work has been concerned with the prediction of liquidus sheets and with solidus isoconcentration lines, data which are of importance in the liquid phase epitaxy technique. In

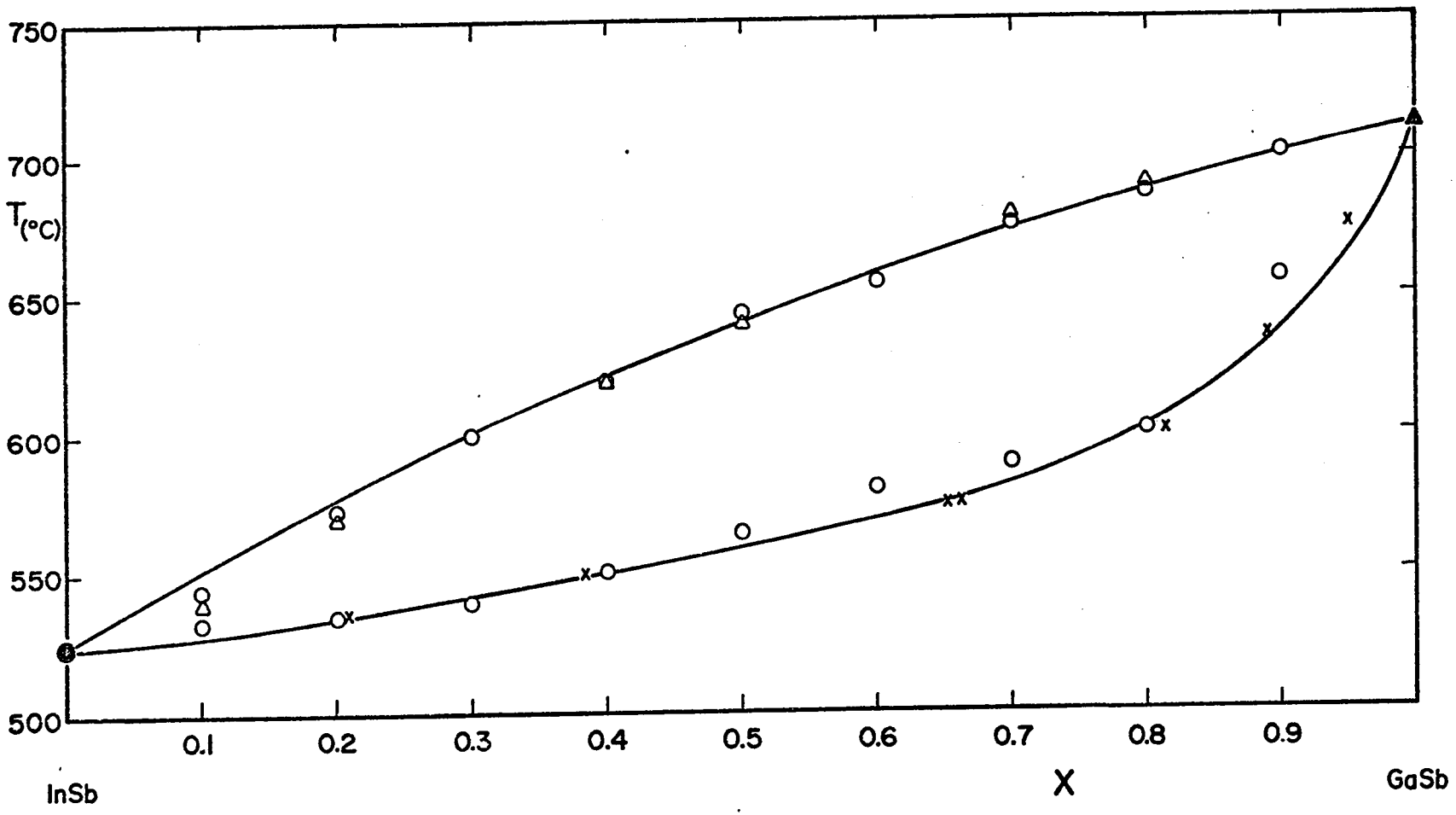

Fig. 7-1. Phase diagram of pseudobinary system $Ga_xIn_{1-x}Sb$.

○ Woolley and Lees (59W1)

✕ Woolley and Smith (58W1)

△ Koster and Thoma (55K1)

● Liu and Peretti (52L1)

▲ Hall (63H1)

——— present theoretical calculation

this latter case however, there is considerably less experimental data available. Experimental determination of the liquidus isotherms on the general phase diagram have been given by Blom and Plaskett (71B1), Antypas (72A1) and Joullie et al. (74J1), but few systematic data have been obtained on isoconcentration lines, the data available being mainly incidental results from liquid phase epitaxy work rather than designed experimental investigations of the ternary diagram.

7.2.2. Solidus isoconcentration lines of Ga-In-Sb.

The present experimental work has been the determination of solidus isothermal lines and hence solidus isoconcentration lines in the region of the diagram between the pseudobinary section $Ga_xIn_{1-x}Sb$ and the Ga-In binary. The solidus isoconcentration lines give the composition values of points on the liquidus sheet which are in equilibrium with a solid phase of given composition. In order to obtain these solidus isoconcentration lines, one must find first a suitable way of determining the tie-lines in that region of the phase diagram, the tie-lines of course give the two phases (liquid and solid) in equilibrium at a given temperature.

The experimental technique used here was that described previously for the determination of the solidus curve of the pseudobinary section and which was found to give good agreement with standard D.T.A. measurements (62W1) and also with data from 'first-to-freeze' analysis of stoichiometric melt growth samples (62T1). Briefly, a sample is prepared with a predetermined initial composition and annealed to equilibrium in

the two-phase field (i.e. between the liquidus and solidus sheets) and then quenched so that the equilibrium solid phase will freeze in and no solid diffusion will occur.

A series of starting compositions were chosen according to the configuration of the liquidus isothermal lines to ensure that the anneal temperatures would be well within the two-phase field. These liquidus isotherms were already available from the literature (71B1 and 74J1). The samples were prepared from pieces of broken ingots of Ga, GaSb and InSb. The gallium was semiconductor grade Ga (Alusuisse), the InSb was obtained commercially (n-type, polycrystalline - Cominco) and the GaSb was grown in this laboratory from the gallium described above and 59 grade antimony (Cominco). Each component was weighed to 10 μg and introduced in a quartz ampoule to form a stoichiometric mixture. The samples were prepared so that each one weighed one gram as it was found that the size of the resulting ingots was sufficient to yield enough material for the various analyses to which it was subjected. However, the overall accuracy in the mass of each ingot was estimated at 100 μg due to losses in the transfer from the weighing pan into the ampoule. Furthermore, pieces of broken ingots rather than powdered ingots were chosen in the preparation of samples for two reasons: first, the losses during transfer were minimized since each piece of ingot was handled individually, although this procedure made the weighing a very tedious exercise, and second, the broken pieces offered less oxidized surface from previous contact with air which could inhibit the melting process.

The quartz ampoules were then evacuated and back-filled with argon to a reduced pressure (approximately 35 kPa). The samples were melted by holding for one or two hours at a temperature above the melting point of the compounds (usually 800°C), quenched and transferred to an annealing furnace; this procedure also allowed examination for possible cracks of the ampoules.

The samples were then annealed to equilibrium. In the two-phase liquid solid field below the liquidus sheet, because the solid phase is very finely dispersed throughout the liquid phase, annealing for 24 hours was quite sufficient to attain this equilibrium condition. A small number of samples were annealed for times up to 20 days but showed no change from the condition observed after 24 hours annealing. Over the anneal period the temperature was kept constant at ±2°C, and its mean value determined to ±2°C by means of a calibrated Pt-Pt 13%Rh thermocouple. At the end of the anneal, the samples were rapidly quenched by plunging into an oil bath so that the equilibrium solid phase was frozen in and no solid diffusion occurred. The lines of this solid phase were easily determined in an X-ray powder photograph. The homogeneity of this solid phase was clearly demonstrated by the sharpness of the X-ray lines, the K_{α} doublet being clearly resolved, and by the fact that no variation could be observed in different X-ray patterns taken from the same quenched sample. The lattice parameter of the equilibrium solid phase and hence its composition were thus determined (62W1). The position of this solid phase on the pseudobinary section plus the composition of the initial sample clearly define the position of the tie-line on the phase

diagram.

To check that two-phase behaviour was being observed, in one or two cases further samples were investigated which lay on the tie-lines so determined and in each case the solid composition found was in good agreement with the previous value, confirming that a two-phase tie-line had been obtained.

The series of tie-lines investigated were those for the following temperatures: 380°, 430°, 475°, 525°, 550°, 600° and 650°C. To determine the liquid end of the tie-line, knowledge of the liquidus sheet is required and, as will be demonstrated in the theoretical analysis, the predicted liquidus isothermal lines are in good agreement with the available experimental data. Therefore those isotherms calculated from the simple solution model have been used here to determine the composition of the equilibrium liquid phase, being the point of intersection of the tie-line and the corresponding isothermal line. Figures 7-2 to 7-5 show the various sets of tie-lines for the temperatures mentioned above, while table 7-I contains all the relevant data: temperature, initial composition, solidus composition and liquidus composition, for the construction of those tie-lines. In addition, a three dimensional representation of the ternary phase diagram is given in figure 7-6. Various liquidus isotherms are represented along with two sets of tie-lines: 475°C and 600°C. However, the position of the eutectic valley situated in the Sb corner, is only approximate since no experimental data is available.

Table 7-I. Compositions of samples annealed in liquid-solid two-phase field at temperature T and of resulting solid and liquid phases. Values give tie-lines and points on solidus isotherms.

T °C	INITIAL COMPOSITION			SOLIDUS COMPOSITION			LIQUIDUS COMPOSITION		
	N_{Ga}	N_{In}	N_{Sb}	N_{Ga}	N_{In}	N_{Sb}	N_{Ga}	N_{In}	N_{Sb}
380°	0.050	0.550	0.400	0.050	0.450	0.500	0.05	0.82	0.13
	0.100	0.550	0.350	0.135	0.365	0.500	0.05	0.82	0.13
	0.200	0.450	0.350	0.255	0.245	0.500	0.11	0.79	0.10
	0.300	0.300	0.400	0.355	0.145	0.500	0.14	0.77	0.09
	0.350	0.300	0.350	0.435	0.065	0.500	0.19	0.73	0.08
	0.550	0.100	0.350	0.485	0.015	0.500	0.70	0.29	0.01
430°	0.050	0.550	0.400	0.050	0.450	0.500	0.05	0.76	0.19
	0.100	0.550	0.350	0.150	0.350	0.500	0.05	0.76	0.19
	0.200	0.450	0.350	0.295	0.205	0.500	0.09	0.74	0.17
	0.150	0.650	0.200	0.360	0.140	0.500	0.12	0.72	0.16
	0.195	0.550	0.255	0.365	0.135	0.500	0.13	0.72	0.15
	0.300	0.300	0.400	0.370	0.130	0.500	0.13	0.72	0.15
	0.200	0.550	0.250	0.380	0.120	0.500	0.14	0.71	0.15
	0.350	0.300	0.350	0.435	0.065	0.500	0.22	0.66	0.12
	0.450	0.200	0.350	0.470	0.030	0.500	0.42	0.51	0.07
	0.550	0.100	0.350	0.470	0.030	0.500	0.71	0.26	0.03
475°	0.050	0.550	0.400	0.065	0.435	0.500	0.03	0.70	0.27
	0.100	0.550	0.350	0.165	0.335	0.500	0.06	0.69	0.25
	0.200	0.450	0.350	0.310	0.190	0.500	0.11	0.66	0.23
	0.300	0.300	0.400	0.380	0.120	0.500	0.15	0.64	0.21
	0.350	0.300	0.350	0.435	0.065	0.500	0.25	0.58	0.17
	0.450	0.200	0.350	0.465	0.035	0.500	0.42	0.46	0.12
	0.550	0.100	0.350	0.480	0.020	0.500	0.68	0.26	0.06
525°	0.100	0.450	0.450	0.115	0.385	0.500	0.07	0.57	0.36
	0.100	0.550	0.350	0.225	0.275	0.500	0.09	0.57	0.34
	0.200	0.450	0.350	0.350	0.150	0.500	0.15	0.55	0.30
	0.300	0.250	0.450	0.350	0.150	0.500	0.15	0.55	0.30
	0.300	0.300	0.400	0.395	0.105	0.500	0.19	0.53	0.28
	0.350	0.300	0.350	0.440	0.060	0.500	0.28	0.49	0.23
	0.450	0.200	0.350	0.465	0.035	0.500	0.43	0.40	0.17
	0.550	0.100	0.350	0.485	0.015	0.500	0.66	0.23	0.11
550°	0.200	0.450	0.350	0.390	0.110	0.500	0.18	0.49	0.33
	0.300	0.300	0.400	0.400	0.100	0.500	0.21	0.48	0.31
	0.350	0.300	0.350	0.450	0.050	0.500	0.29	0.44	0.27
	0.400	0.200	0.400	0.450	0.050	0.500	0.33	0.42	0.25
	0.450	0.200	0.350	0.495	0.005	0.500	0.41	0.37	0.22
	0.550	0.100	0.350	0.495	0.005	0.500	0.63	0.23	0.14
	0.650	0.050	0.300	0.500	0.000	0.500	0.81	0.10	0.09
600°	0.250	0.350	0.400	0.425	0.075	0.500	0.24	0.36	0.40
	0.300	0.300	0.400	0.435	0.065	0.500	0.27	0.35	0.38
	0.350	0.300	0.350	0.450	0.050	0.500	0.34	0.33	0.33
	0.400	0.200	0.400	0.460	0.040	0.500	0.35	0.33	0.32
	0.450	0.200	0.350	0.480	0.020	0.500	0.44	0.28	0.28
	0.550	0.100	0.350	0.495	0.005	0.500	0.60	0.19	0.21
	0.650	0.050	0.300	0.495	0.005	0.500	0.76	0.08	0.16
650°	0.380	0.170	0.450	0.465	0.035	0.500	0.35	0.22	0.43
	0.400	0.200	0.400	0.470	0.030	0.500	0.40	0.20	0.40
	0.450	0.100	0.450	0.470	0.030	0.500	0.42	0.20	0.38
	0.490	0.110	0.400	0.495	0.005	0.500	0.49	0.17	0.34
	0.550	0.100	0.350	0.495	0.005	0.500	0.57	0.13	0.30
	0.650	0.050	0.300	0.500	0.000	0.500	0.69	0.06	0.25

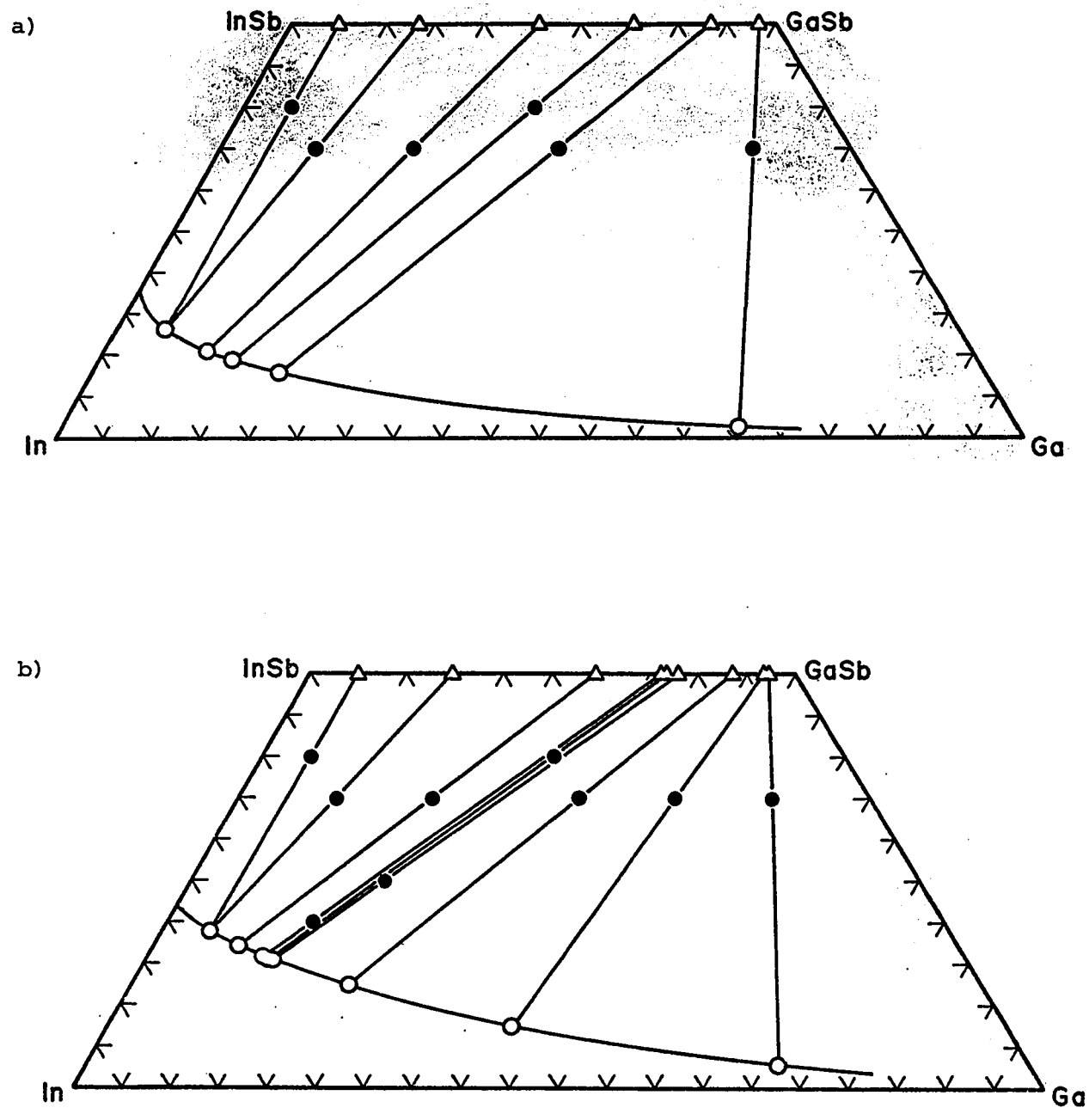

Fig. 7-2. Liquidus isotherms and tie-lines of the Ga-In-Sb system:
a) 380°C, b) 430°C.
● initial composition ○ liquidus composition
△ solidus composition

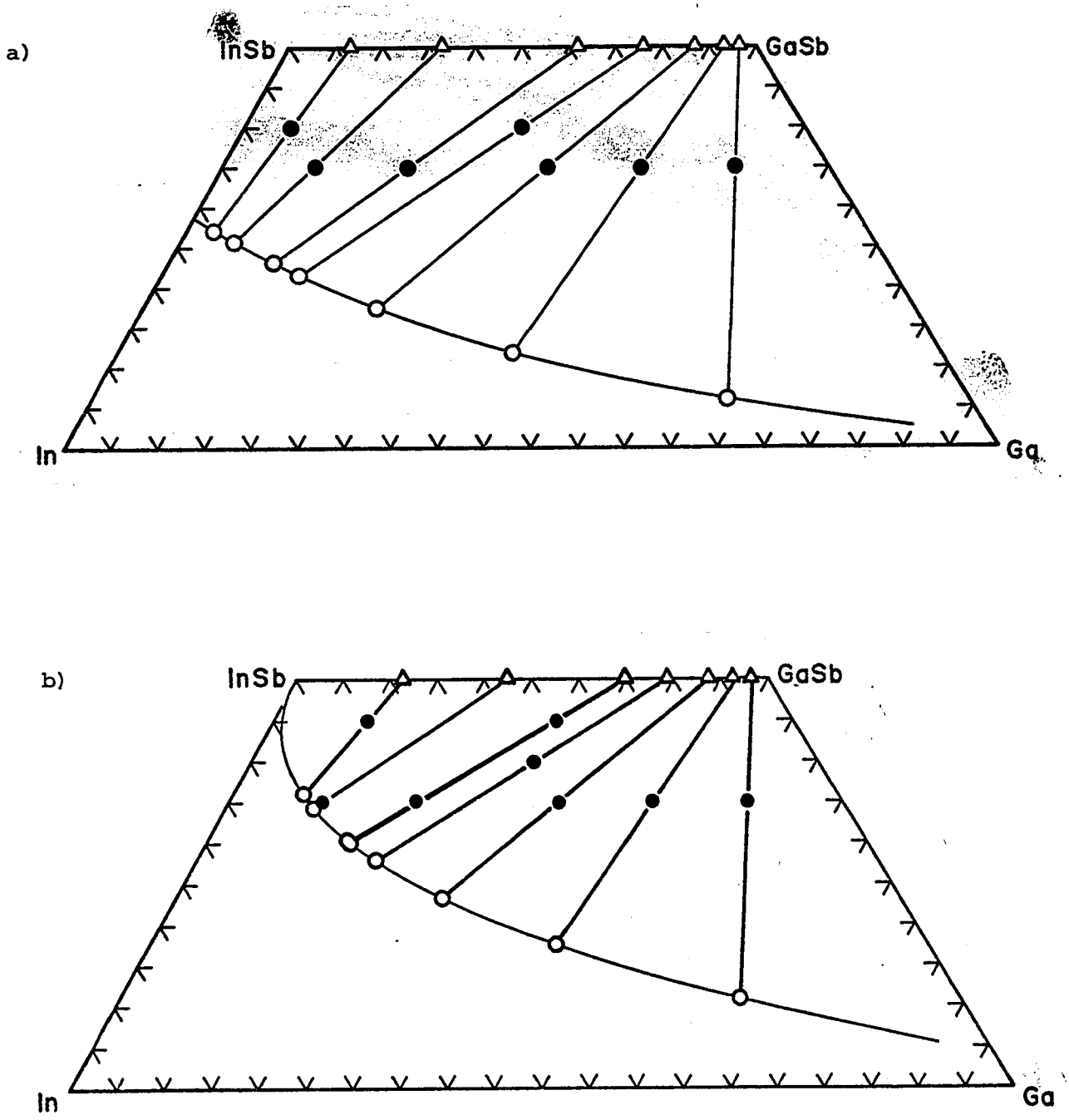

Fig. 7-3. Liquidus isotherms and tie-lines of the Ga-In-Sb system:
a) 475°C, b) 525°C.
● initial composition ○ liquidus composition
△ solidus composition

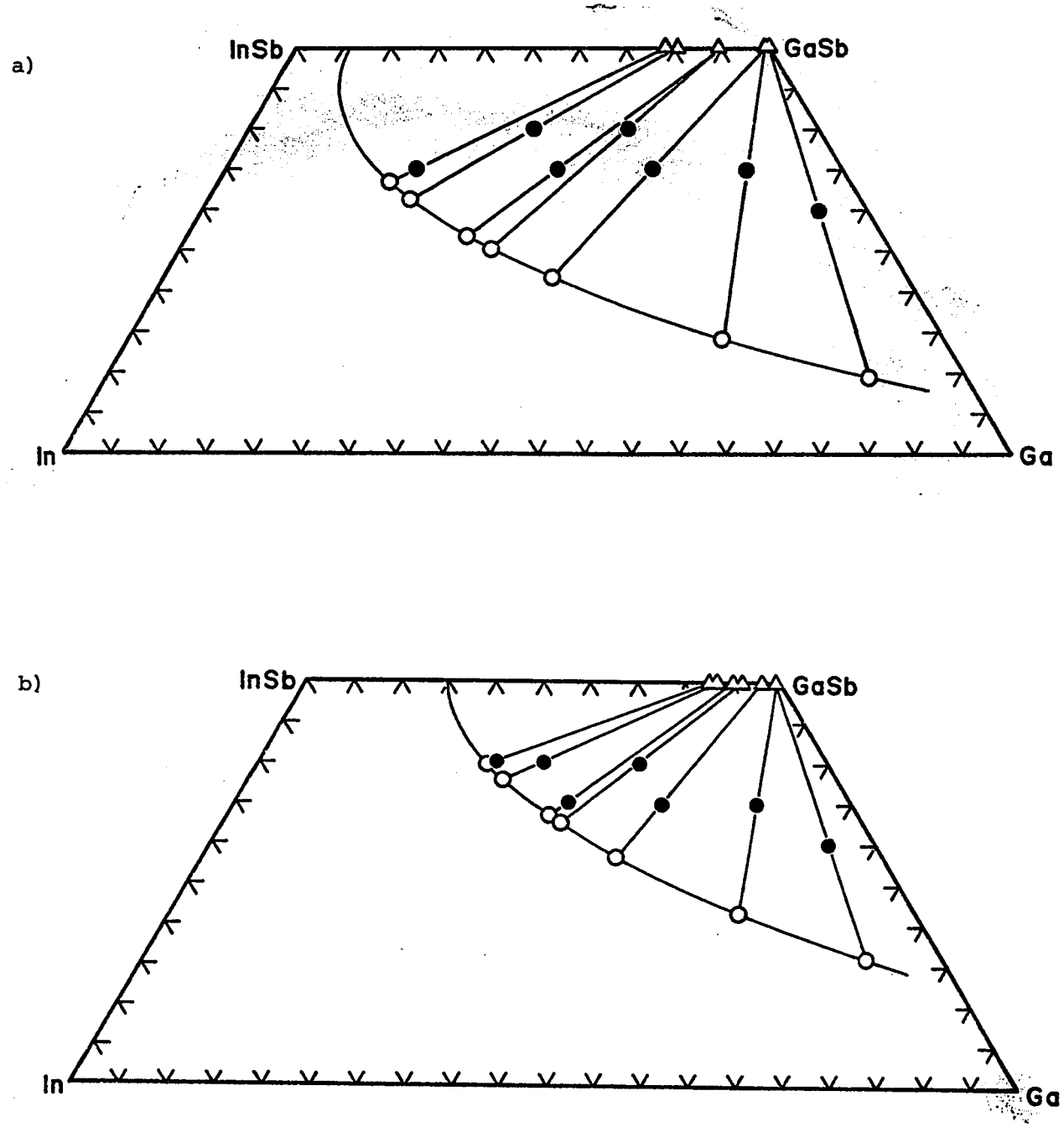

Fig. 7-4. Liquidus isotherms and tie-lines of the Ga-In-Sb system:

a) 550°C, b) 600°C.

● initial composition ○ liquidus composition

△ solidus composition

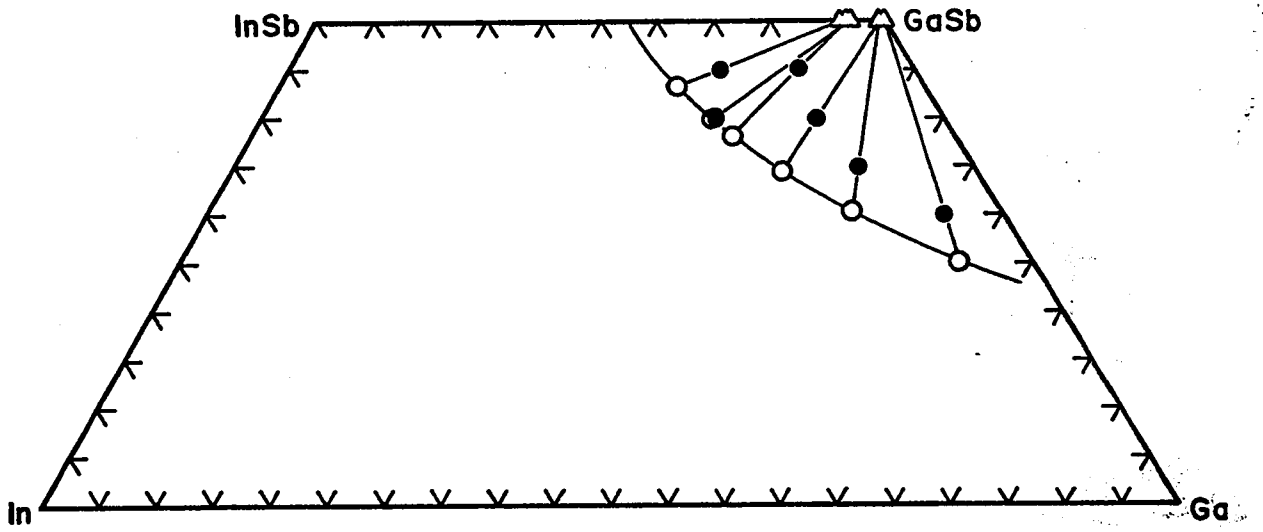

Fig. 7-5. The 650°C liquidus isotherm and tie-lines of the Ga-In-Sb system:

● initial composition ○ liquidus composition

△ solidus composition

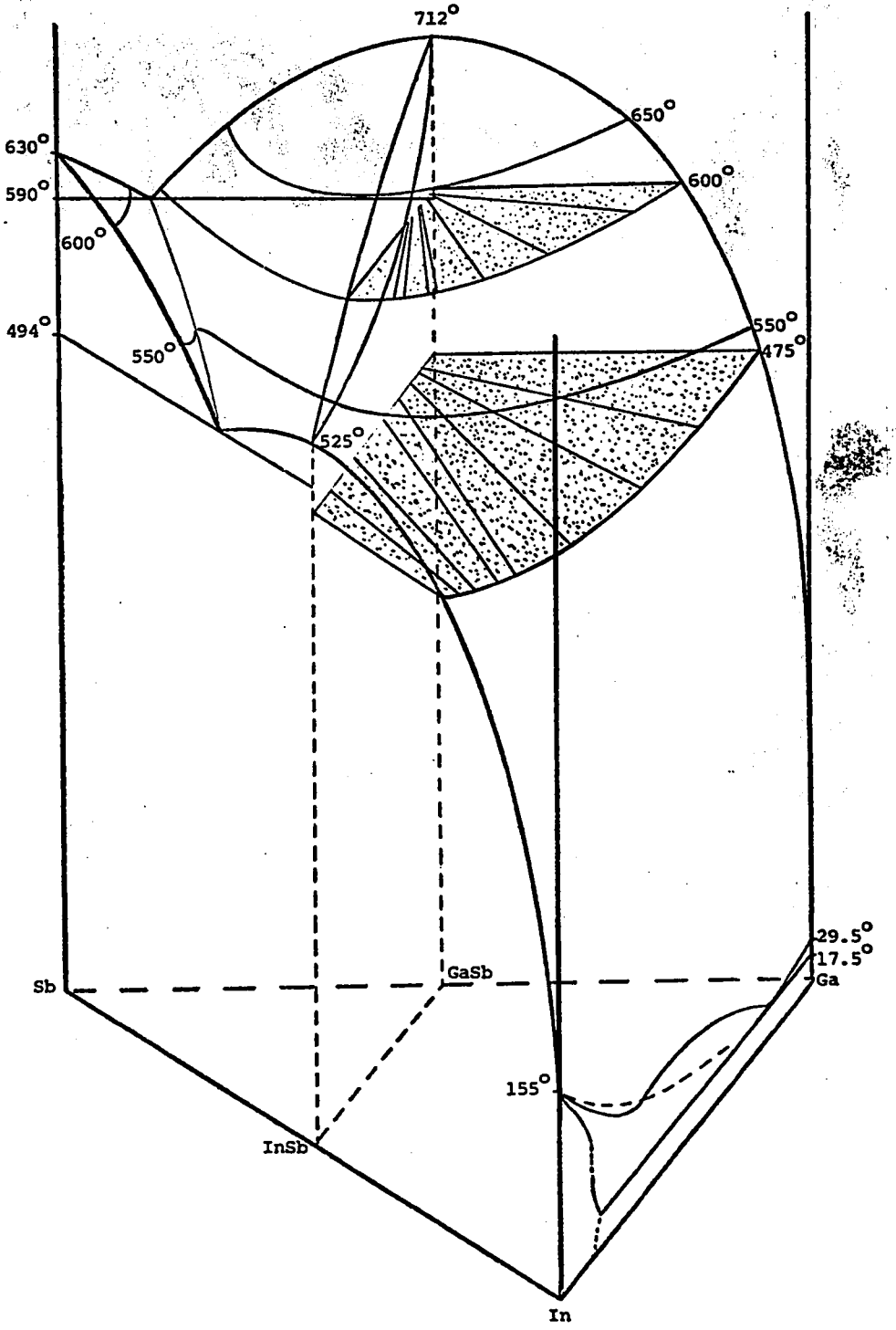

Fig. 7-6. Three-dimensional representation of the phase diagram for Ga-In-Sb. Various liquidus isotherms and two sets of tie-lines are represented in their respective planes (475° and 600°C). The position of the eutectic valley in the antimony corner is only approximate.

It is of interest to mention that, in the early stages of the research, a major difficulty arose with samples for which the concentration of antimony in the initial composition was 45%. At anneal temperatures below 500°C, the samples yielded erroneous results. In order to investigate the situation, three specimens of initial compositions $Ga_{.10}In_{.45}Sb_{.45}$ and three specimens at $Ga_{.30}In_{.25}Sb_{.45}$ were prepared and annealed respectively at 380°, 430° and 475°C. Again, in each case, the results were incompatible with those specimens with antimony concentrations less than 45%. So, more samples of the same initial compositions were prepared and the procedure was repeated twice more, again with similar results. However, since normal behaviour was resumed at 525°C and over, it was concluded that, at temperatures below 500°C, the samples with antimony concentrations of 45% were situated too close to the pseudo-binary section which contain all of the solid phases and according to an argument similar to the Lever rule, the amount of liquid phase present in the sample was insufficient to dissolve the initial solid phase and reach the desired equilibrium in the allowed time, that is, 24 hours. This conclusion, however, was not actually verified using longer anneals as there were enough samples of various initial compositions to supply data for the tie-lines needed in establishing a phase diagram.

7.3 Theoretical Determination of the Phase Diagram of the Ternary System Ga-In-Sb.

As outlined in chapters 5 and 6, the theoretical approach used

to predict the phase diagram of the ternary system Ga-In-Sb is the simple solution model. Most of the useful parameters contained in this model have already been evaluated except for the two interaction parameters α_{Ga-In} and $\alpha_{GaSb-InSb}$.

7.3.1 The interaction parameters α_{Ga-In} and $\alpha_{GaSb-InSb}$.

In previous work, the binary diagram data of Bros et al. (67B1) and Macur et al. (68M1) are usually quoted for the evaluation of α_{Ga-In} while the value of $\alpha_{GaSb-InSb}$ is usually obtained by a fit to the pseudobinary liquidus and solidus data or from the calculations of Foster and Woods (71F1). In all cases the parameter values have been assumed independent of T. Joullie et al. (74J1) determined both α_{Ga-In} and $\alpha_{GaSb-InSb}$ from the pseudobinary data by solving equations equivalent to the present 5.6.9, 5.7.3 and 5.7.4 for composition values from the liquidus and solidus curve. However, they used the data for one temperature only and again assumed that the two α's were independent of temperature.

Here, the pseudobinary liquidus and solidus data have been used to determine both α_{Ga-In} and $\alpha_{GaSb-InSb}$ as a function of temperature over the range between the melting points of the two compounds. At each temperature, appropriate composition values from the liquidus and solidus curves (figure 7-1) were inserted in equations 5.6.9, 5.7.3 and 5.7.4 and values of α_{Ga-In} and $\alpha_{GaSb-InSb}$ were determined simultaneously. The choice of values of X from the pseudobinary phase diagram was dictated by the experimental values of Koster and Thoma (55K1), Woolley

and Smith (58W1) and Woolley and Lees (59W1), but there was appreciable scatter in the graphs of α versus T for each case, as the α values seemed very sensitive to the values of X used in the calculations. In order to test this variation, the solidus compositions were allowed to vary by ±1% about the mean compositions identified by the initial solidus line and new values of α's were computed. The results are shown on figures 7-7 and 7-8 where the various solutions are plotted for each temperature used in the calculations. The variations in composition were carried out only on the solidus line and in the range $0.55 < X < 1.00$ as suggested by the steeper slope of this two-phase field boundary and no studies of variations of either the liquidus compositions or the temperature were attempted here.

From the graphs of figures 7-7 and 7-8 it was found that in each case the value of α could be written as a linear function of T and the values determined by least squares fit are given in table 7-II along with the values of the other two interaction parameters of interest, already listed in chapter 6.

Table 7-II Interaction parameters for the ternary system Ga-In-Sb

α_{GaSb}	=	23824	-	32.38T	$J.mol^{-1}$
α_{In-Sb}	=	4895	-	33.72T	$J.mol^{-1}$
α_{Ga-In}	=	12000	-	12.97T	$J.mol^{-1}$
$\alpha_{GaSb-InSb}$	=	-2816	+	11.42T	$J.mol^{-1}$

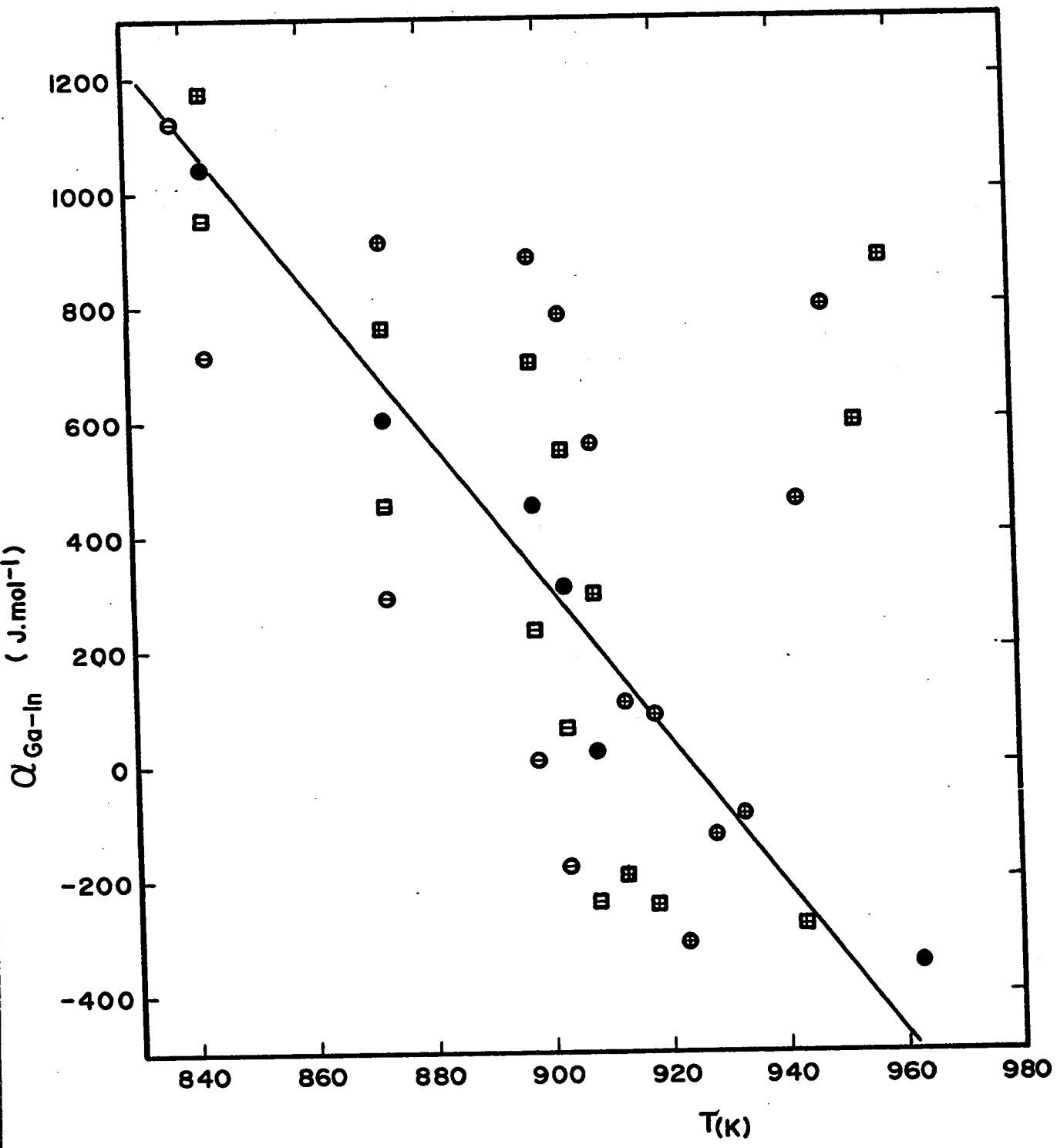

Fig. 7- 7 α_{Ga-In} vs. T. The solid circles represent the initial interpolation of the solidus line. The open squares and circles represent the corrections ±0.005 and ±0.01 respectively, of the solidus compositions. The solid line indicates the least squares fit.

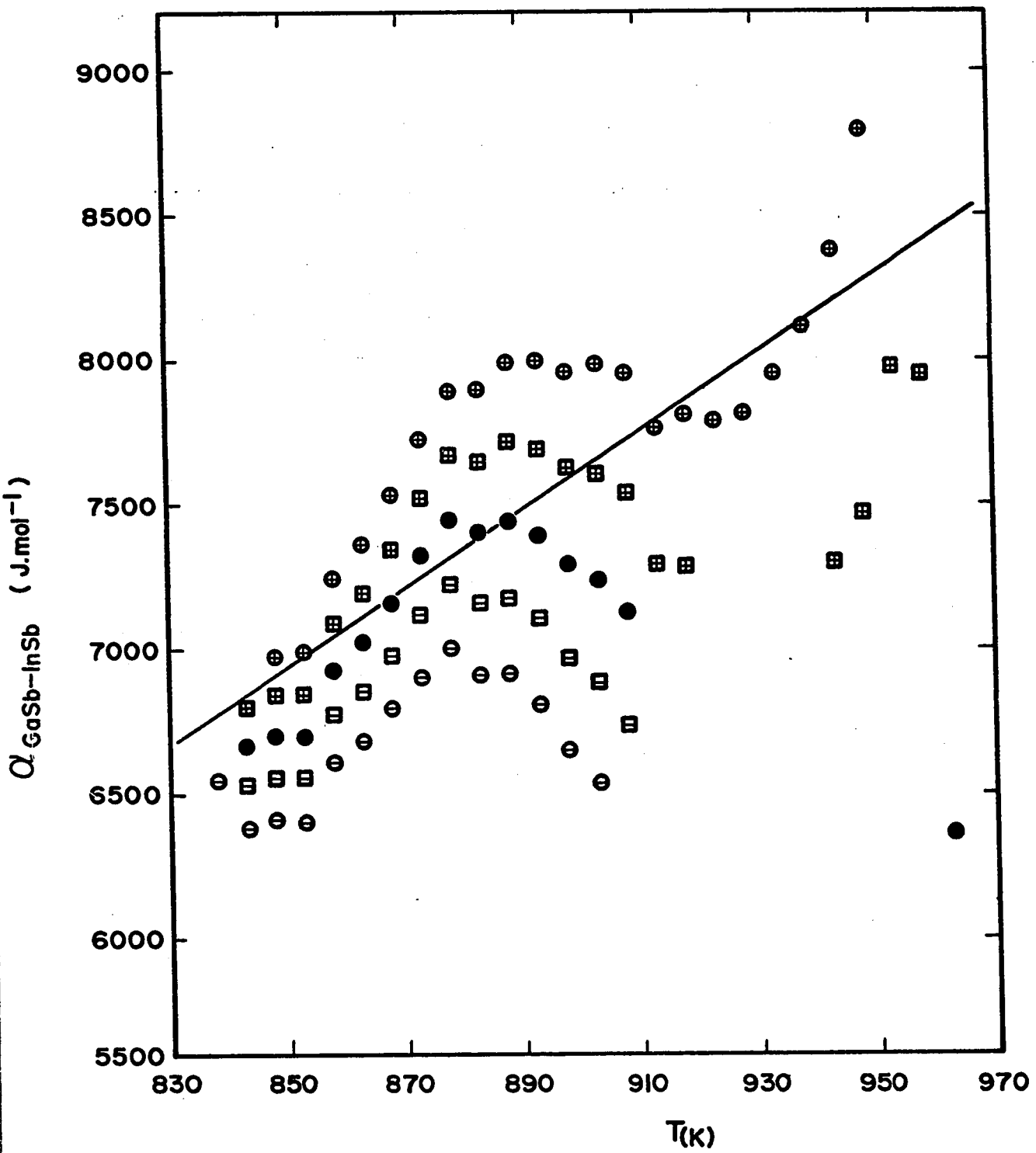

Fig. 7-8. $\alpha_{GaSb-InSb}$ vs. T. The solid circles represent the initial interpolation of the solidus line. The open squares and circles represent the corrections ±0.005 and ±0.01 respectively, of the solidus compositions. The solid line indicates the least squares fit.

7.3.2 Liquidus isotherms of Ga-In-Sb

Using the various α's derived above, equations 5.6.9, 5.7.3 and 5.7.4 were solved with sets of values of N_{Ga}, N_{In} and N_{Sb} over the whole ternary diagram to yield values of T and X. The values were then appropriately interpolated to give liquidus isothermal lines for the Ga-In-Sb system. A graph of temperature as a function of gallium concentration yielded a network of constant antimony composition and constant indium composition lines from which the isotherms could be constructed. Figure 7-9 shows the network obtained from the values of the interaction parameters listed in table 7-II. Finally, figure 7-10 gives the set of liquidus isothermal lines for the ternary system Ga-In-Sb. This set of lines defines the liquidus sheet of the phase diagram. In figure 7-10, the experimental data of Blom and Plaskett (71B1), Antypas (72A1) and Joullie et al. (74J1) also appear and it is found that over most of the composition range, the predicted isothermal lines are in fairly good agreement with experiment.

The simple solution model was also tested by other workers but with different values of the interaction parameters. Again the agreement between different sets of predicted isotherms is relatively good (figure 7-10) and after many attempts at finding the best combination by intermixing the various values of α's published, it appears that the predicted isothermal lines are not in general very sensitive to the values of α's used. Therefore the values of α's listed in table 7-II were used throughout as they involved no further fitting after their initial determination from a Thurmond like analysis (64T1) for α_{Ga-Sb} and α_{In-Sb}, and

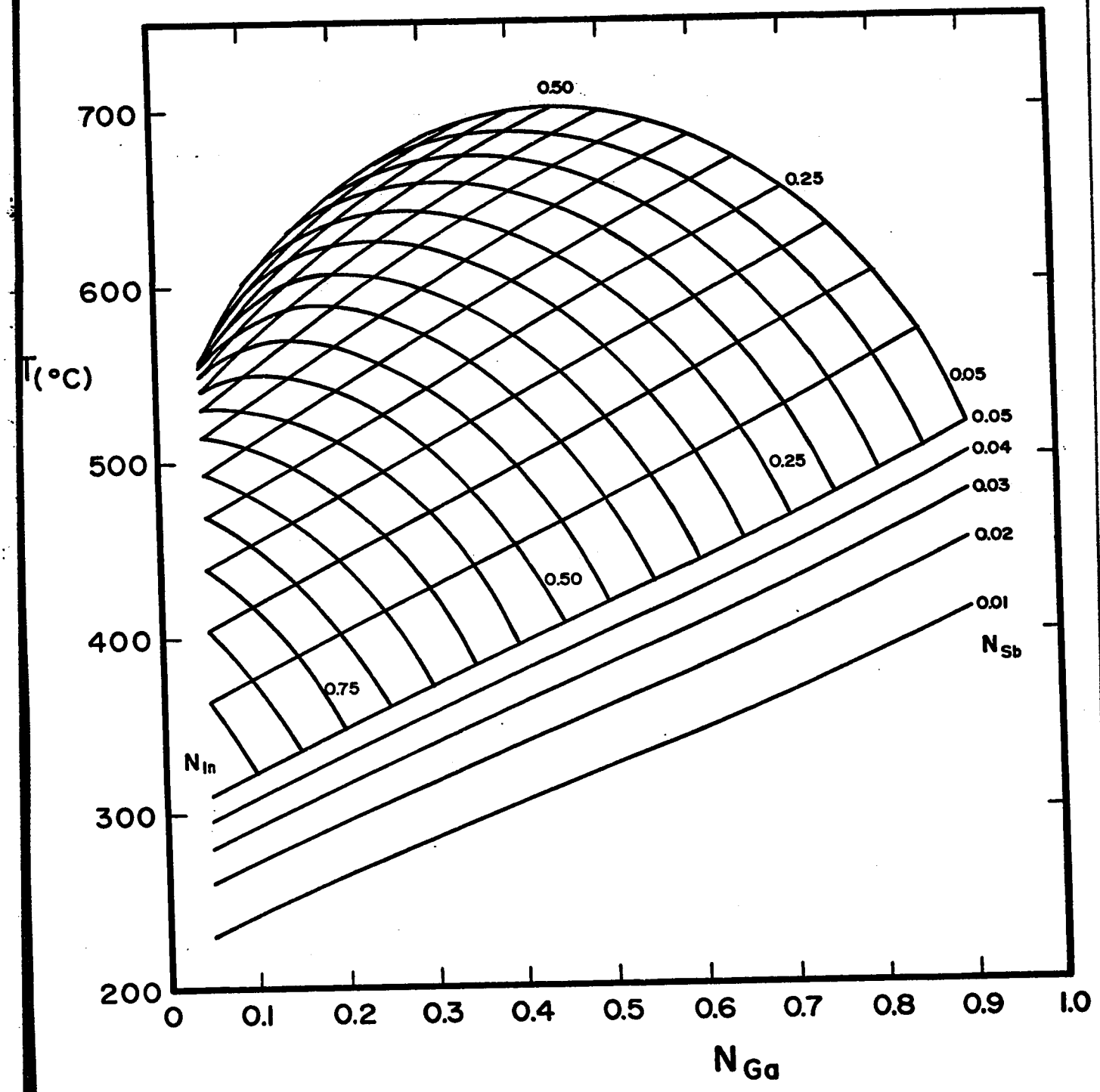

Fig. 7-9. Relationship between T and N_{Ga} from the theoretical analysis of Ga-In-Sb. The network represents the lines of constant N_{Sb} and N_{In}.

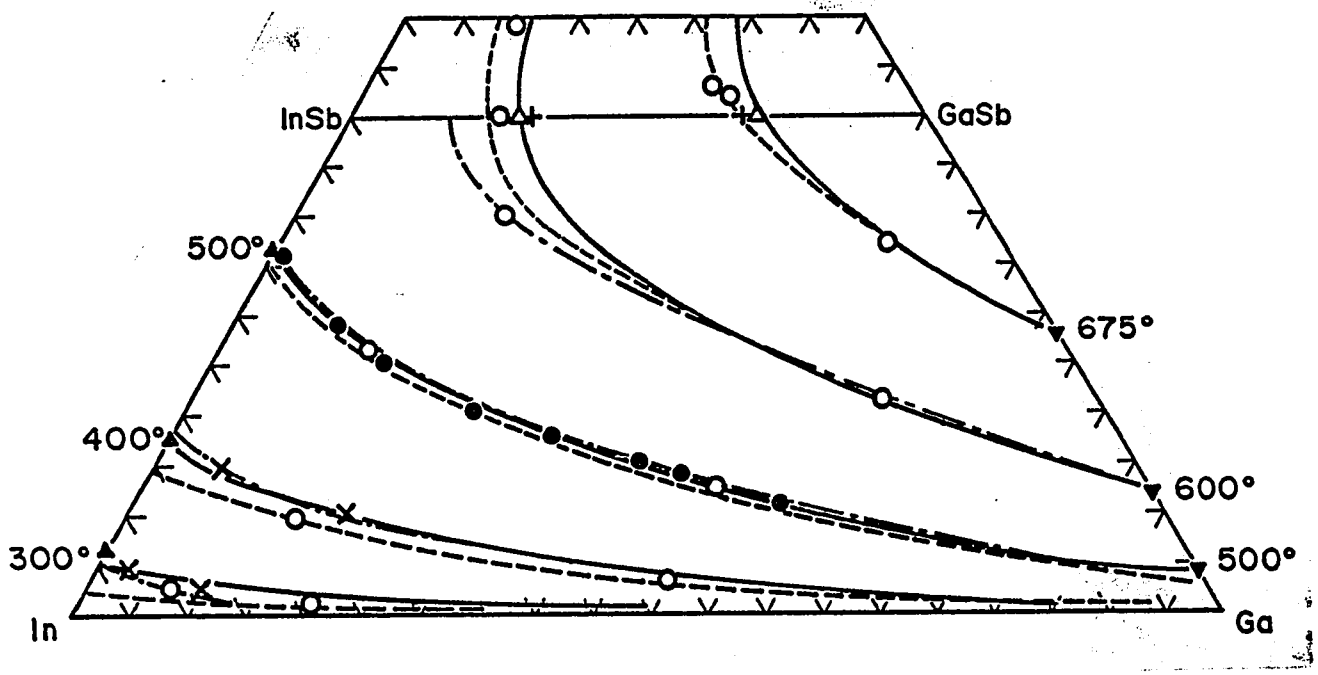

Fig. 7-10. Liquidus isotherms in the Ga-In-Sb ternary phase diagram.

(Temperatures in °C).

Theoretical calculations

———— this study

---------- Blom and Plaskett (71B1)

——·——·—— Joullié et al. (74J1)

Experimental determination

○ Blom and Plaskett (71B1)

● Antypas (72A1)

× Joullié et al. (74J1)

▲ Liu and Peretti (52L1)

△ Woolley and Lees (59W1)

+ Koster and Thoma (55K1)

▼ Koster and Thoma (55K2)

a temperature dependent relation for α_{Ga-In} and $\alpha_{GaSb-InSb}$. The main discrepancies between the present results and those of Blom and Plaskett (71B1) and Joullie et al. (74J1) are at points close to the pseudobinary section. The present results are tied to the measured pseudobinary data by the method used for determining α_{Ga-In} and $\alpha_{GaSb-InSb}$ and hence will be in better agreement with those experimental data. This will be discussed further below.

7.3.3 Solidus isotherms and isoconcentration lines of Ga-In-Sb.

From the simultaneous solutions of equations 5.6.9, 5.7.3 and 5.7.4, the solid composition X may be plotted as a function of gallium concentration to yield a set of lines of constant antimony composition resulting in the network presented in figure 7-11. From this and figure 7-9 it is then possible to plot a series of graphs of X versus N_{Ga} for constant temperature. The resulting relations give the solidus isotherms which are shown for various temperatures in figures 7-12 and 7-13. The experimental solidus isotherms can be found from the determination of the tie-lines discussed previously. From table 7-I, the concentration of the solid phase (X_{solid}) on the pseudobinary section $Ga_xIn_{1-x}Sb$ obtained from the solidus composition is plotted against the gallium concentration (N_{Ga}) of the liquidus composition. The resulting solidus isotherms are also displayed in figures 7-12 and 7-13. There is obvious disagreement between theoretical and experimental values and all attemps at varying the α-parameters failed to improve the theoretical predictions significantly.

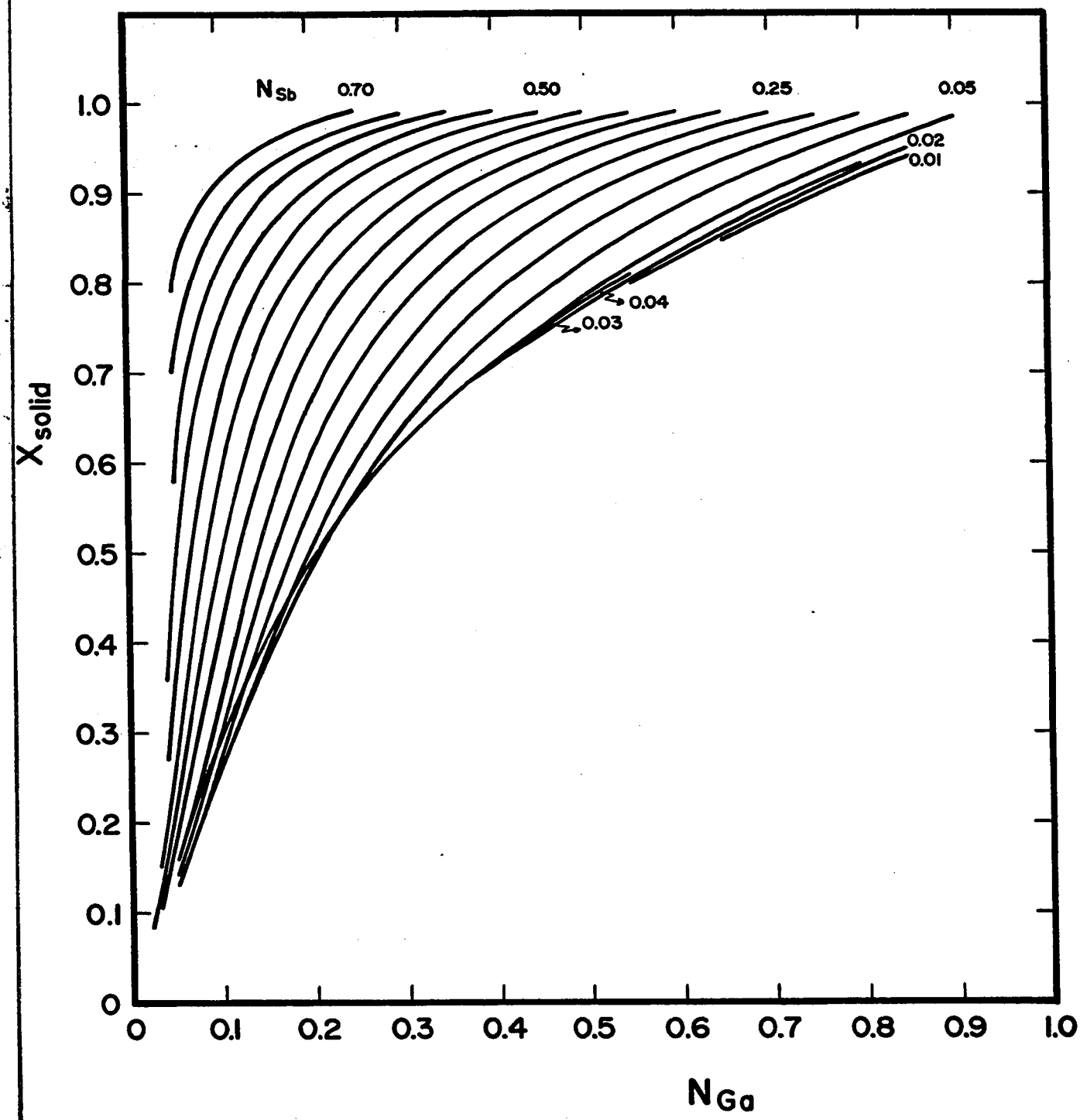

Fig. 7-11. Variation of X_{solid} as a function of N_{Ga} from the theoretical analysis of Ga-In-Sb. Lines of constant N_{Sb} are shown here.

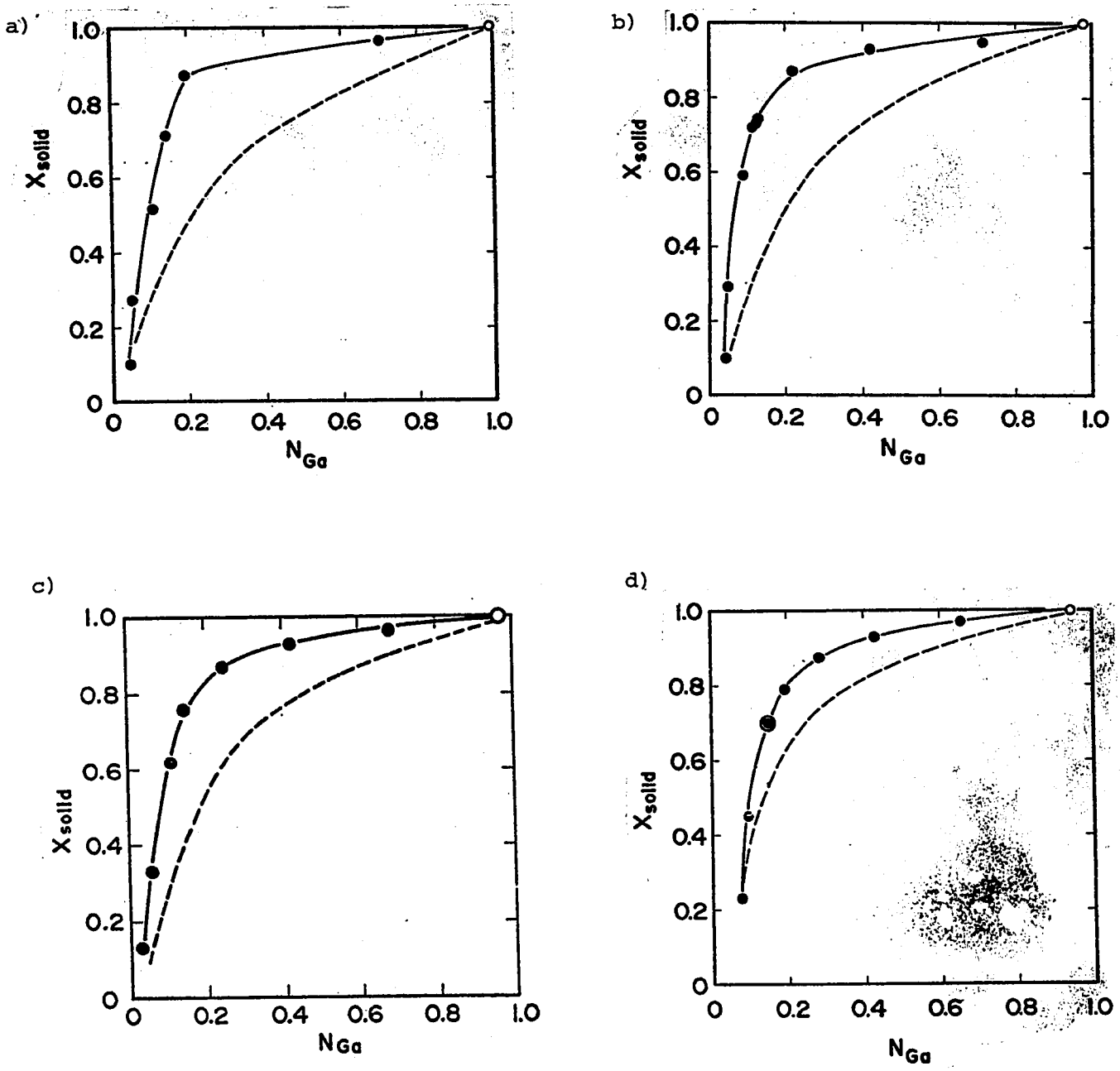

Fig. 7-12. Solidus isotherms of the Ga-In-Sb system: a) 380°C, b) 430°C, c) 475°C, d) 525°C.

—●— present experimental data

○ Koster and Thoma (55K2)

--------- present theoretical calculation

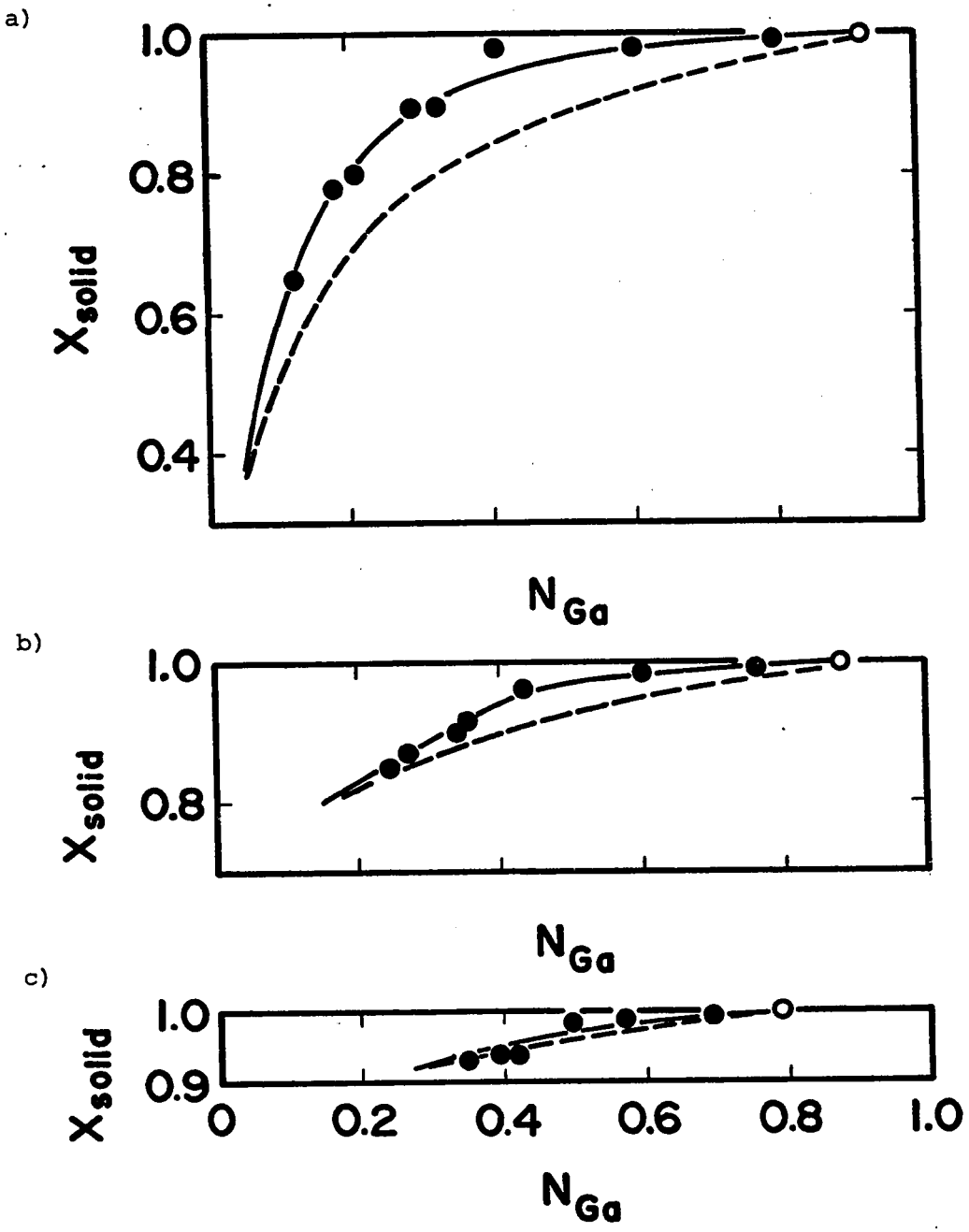

Fig. 7-13. Solidus isotherms of the Ga-In-Sb system: a) 550°C, b) 600°C, c) 650°C.

——●—— present experimental data

○ Koster and Thoma (55K2)

---------- present theoretical calculation

In order to compare the predictions of other workers, the 300°C and 500°C theoretical solidus isotherms of Panish and Ilegems (72P1) were plotted along with the results of this analysis (figure 7-14). No experimental data exist for the lower temperature, while for the higher temperature, only the points of Antypas (72A1) may be referred to. These two temperatures were chosen because they are the only two for which theoretical and/or experimental data have been published (72P1, 72A1). At 500°C, all predictions are relatively the same but at 300°C the values of Panish and Ilegems (72P1) would seem to be closer to the expected experimental solidus isotherm providing that at this temperature, the trend of having the experimental lines above the theoretical lines, as observed in figures 7-12 and 7-13, is still present.

In an effort to find a better set of interaction parameters, the values of Panish and Ilegems were introduced in this analysis, but already at about 400°C the two theoretical lines agreed and were far from the experimental results. Furthermore, above 500°C the predicted isotherms of Panish and Ilegems showed worse agreement with the experimental data than the present analysis. Values of α's from other workers were also tested but it became quickly apparent that nothing would be gained from such an exercise. In all cases, however, the solidus isotherms calculated in this study were in better agreement with the experimental results for temperatures above 550°C and this was expected of course due to the method used in determining α_{Ga-In} and $\alpha_{GaSb-InSb}$.

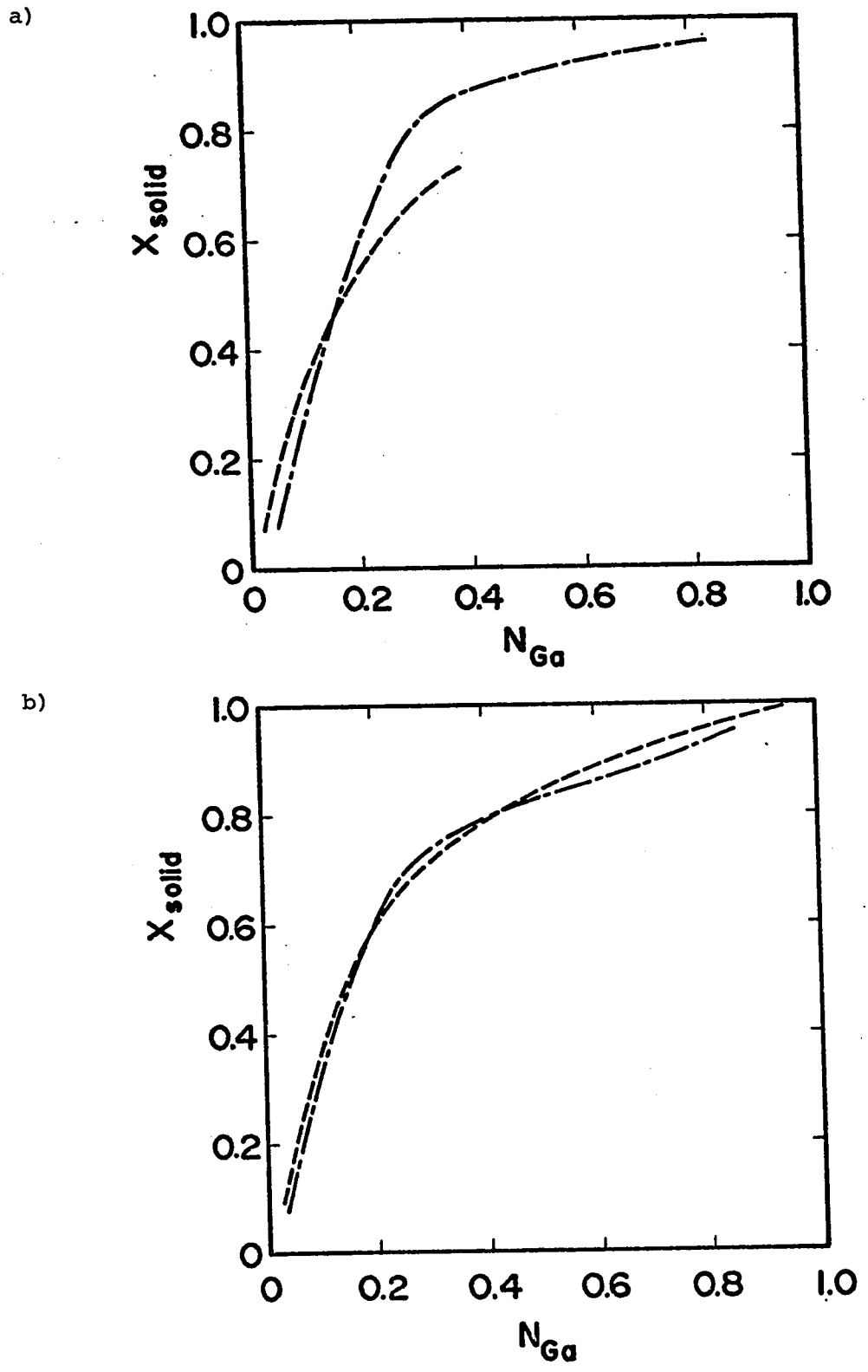

Fig. 7-14. Solidus isotherms of the Ga-In-Sb system: a) 300°C, b) 500°C.

---------- present theoretical calculation

—— - —— - calculation by Panish and Ilegems (72P1).

Finally, from these solidus isotherms and the predicted liquidus isotherms which were found to be in good agreement with experimental results (71B1, 72A1, 74J1), solidus isoconcentration lines were constructed and are shown in figure 7-15, again both experimental and theoretical values being given.

7.4 Discussion

The input data for the calculated phase diagram results are mainly in the four α parameters. Here, each has been assumed to vary linearly with temperature and its value obtained from the known data of an appropriate binary or pseudobinary section. Although previously it had been suggested that these values could be obtained from ranges of dilute solution only, it appears that consistent values of α can probably be obtained over a very wide range of composition of the relevant section as indicated by Ilegems and Panish (74I1). Comparison of the predicted data obtained with the present values of α and those of previous workers (71B1, 72P1, 74J1) indicates that the form of the liquidus isotherms is not very sensitive to the exact value of α.

In the present work, the method of determining α_{Ga-In} and $\alpha_{GaSb-InSb}$ ensures that a good fit to the data of the pseudobinary section is obtained, which was not the case in some of the previous work. In all cases, the fit to the liquidus isotherms in the range 350-500°C is good. However, the present choice of α values gives a slightly worse fit to the

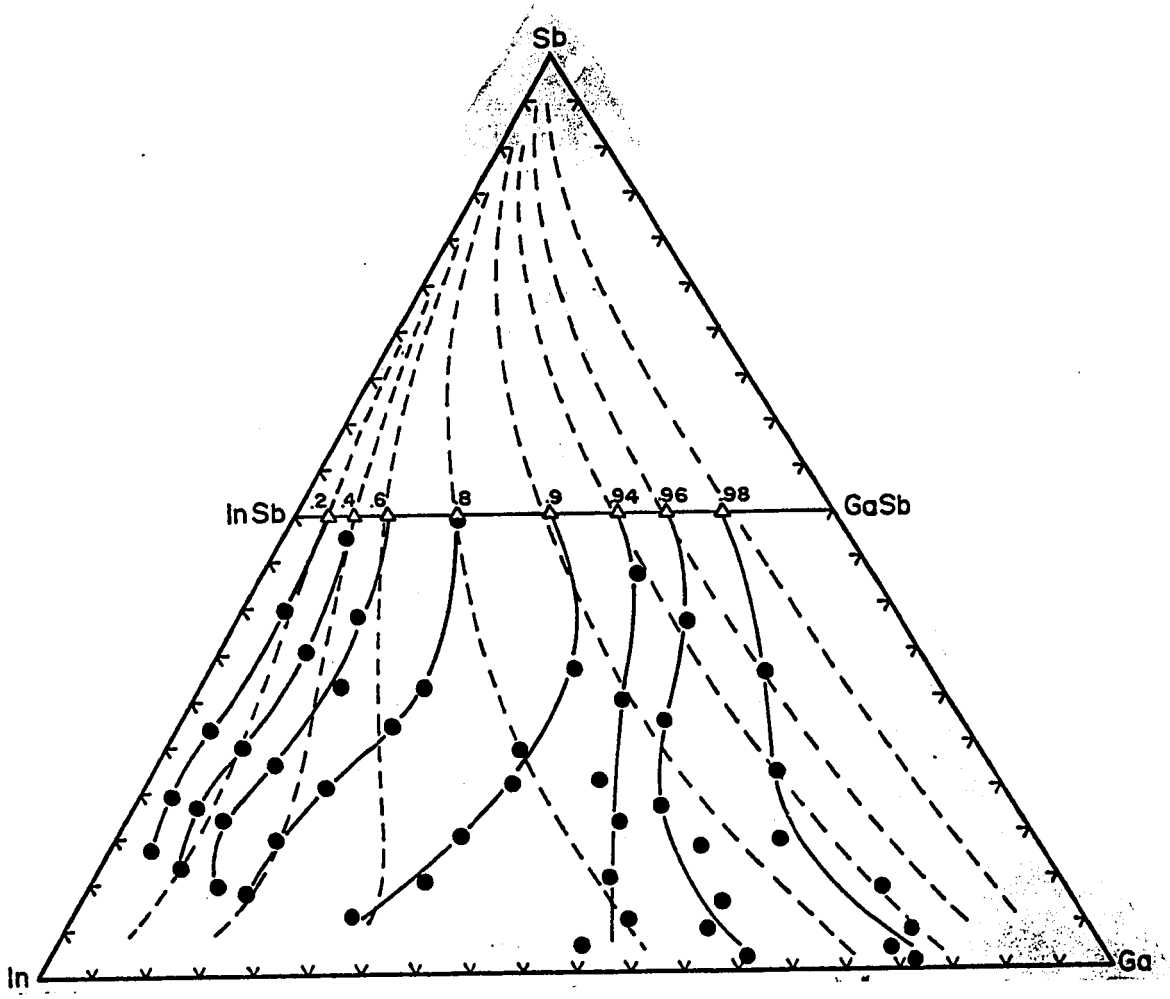

Fig. 7-15. Solidus isoconcentration lines in the Ga-In-Sb ternary phase diagram.

——●—— present experimental data

---------- present theoretical calculation

△ points from experimental pseudobinary section.

300°C liquidus isotherm data than that of Blom and Plaskett (71B1) and Joullie et al. (74J1). Thus even for the liquidus isotherms, it appears that no single set of α values gives an excellent fit over the whole range of composition considered here, but that reasonable agreement with experiment can be obtained with a careful choice of α values.

One factor which may influence the fit to experimental data in this particular case is the value of the ΔC_p term in Vieland's equation for chemical potential (63V1),

i.e.:

$$\mu_{AC}^{so} = \mu_A^{s\ell} + \mu_C^{s\ell} - \Delta S_{AC}^F (T_{AC}^F - 1)$$

$$+ \Delta C_p \left[T_{AC}^F - T - \ell n \left(\frac{T_{AC}^F}{T}\right)\right] \qquad 7.4.1$$

Throughout the analysis the ΔC_p term has been assumed to be negligible. While this is true in most cases, calculation shows that for the case of In-Sb the ΔC_p term can at low temperatures become a non-negligible part of the right-hand side of equation 7.4.1 (see table 6-II). Thus neglecting this term could have some effect on the value of α_{In-Sb} calculated and on the predicted form of the low temperature liquidus isotherms.

Thus it is clear that for the Ga-In-Sb ternary system the simple-solution model has serious limits on its usefulness. It can be used to give reasonable values of liquidus isotherms, but solidus data predicted by this method in the temperature range 300°C to 712°C are of no practial value.

In a review by Panish and Ilegems (72P1) of a number of these alloy systems, it is indicated that fair agreement between predicted and experimental values of the solidus parameters can be obtained for the ternary alloys involving phosphorus and possibly aluminum but that the agreement is poor for the heavier systems such as $Ga_xIn_{1-x}As$ and $InAs_ySb_{1-y}$. Clearly the use of the simple solution model to predict solidus data is only of value if one can predict the cases for which the model gives valid results. One possible factor in this consideration is the temperature, since it would appear that the lower the range of temperature concerned the worse is the agreement. Thus one possible reason for the discrepancy between prediction and experiment is the ΔC_p term and the associated Vieland equation. But as indicated above, the ΔC_p term is significant only below 600K and hence should have little effect even in the upper temperature range of the solid phase of the $Ga_xIn_{1-x}Sb$ alloys. However, Jordan and Weiner (75J1) have shown that Vieland's equation is exact only if α is a linear function of temperature and as has been seen above, this may not be the case here.

A second possible factor in this temperature range is that association in the liquid phase may become important (70J1). However Jordan has indicated that this effect is mainly of importance when the liquidus curve of the appropriate binary system shows a cusp around the line compound (e.g. Zn-Te, Cd-Te) and should not be important for systems showing the smooth 'convex' liquidus curves typical of most III-V combinations.

Chapter 8 Phase diagram of the pseudobinary system $GaAs_ySb_{1-y}$

8.1 Introduction

8.2 Experimental Determination of the Solidus Lines of $GaAs_ySb_{1-y}$

8.3 Miscibility Gap: variation with temperature

8.4 Discussion

8.1 Introduction

The experimental data available in the literature for the pseudobinary system $GaAs_ySb_{1-y}$ have already been quoted in chapter 3 where it has also been reported that a miscibility gap exists in the range $0.38 < y < 0.61$ of the solid solutions. In the present chapter, experimental data have been collected in order to characterize the pseudobinary section of the phase diagram and to verify its peritectic behaviour.

8.2 Experimental Determination of the Solidus Lines of $GaAs_ySb_{1-y}$.

From the findings of chapter 3, the experimental data available (62W1, 70I1, 72F1) and the theoretical calculations of Stringfellow (72S1) it was decided to investigate the properties of the phase diagram of $GaAs_ySb_{1-y}$ by annealing samples in the two-phase liquid-solid fields and rapidly quenching those samples in order to freeze in the solid phase which is in equilibrium with the liquid in the melt. From powder X-ray photographs it is then possible to measure the lattice constant of that solid phase and thus determine its composition. The method yields a homogeneous phase characteristic of the equilibrium solid and the sharp lines on the X-ray diffraction photograph are easily distinguished from the other faint and blurred lines characteristic of the phases which did not reach equilibrium before freezing out. The compositions of the equilibrium solids determine the solidus curve of the system.

Samples of various initial compositions were prepared from the stoichiometric binary compounds GaAs and GaSb. The method of preparation was the same as that for the samples of Ga-In-Sb (chapter 7). Here, however, the reduced pressure of argon inside the quartz ampoules served two purposes: first, it contributed in lowering the vapour pressure of arsenic thus reducing losses of arsenic to the sample, second, it also prevented implosions as the ampoules were taken to temperatures in excess of 1250^{o}C and it was found that at these high temperatures the quartz had a tendency to soften thus bringing up the possibility of ampoules collapsing under the ambient pressure inside the furnace.

The periods of anneal were determined experimentally and as was the case for the alloy system described in chapter 7, some samples were annealed for periods of up to 20 days. However, it was found that annealing times of three days were quite sufficient to attain the equilibrium conditions. The rest of the processing was again identical to that described in chapter 7. Again, the temperatures were measured with calibrated Pt-Pt 13% Rh thermocouples.

From Woolley's original solidus data which were available and the knowledge of peritectic behaviour, the starting compositions were selected carefully in order to provide optimum conditions in the production of equilibrium solid phases according to the Lever rule. For temperatures above the peritectic temperature the starting compositions that were chosen ranged from $y = 0.15$ to $y = 0.85$. Below this temperature, the range was $0.07 < y < 0.25$.

The experimental data are tabulated in table 8-I including the original values of Woolley: his solidus compositions, however, are corrected to account for the deviation from the Vegard line as established in chapter 3.

8.3 Miscibility Gap: variation with temperature

The next investigations were orientated towards the determination of the boundaries of the gap as a function of temperature. Preliminary trials were made with samples of initial compositions ranging from y = 0.15 to y = 0.65 with annealing times of several days as it had been already recognized that diffusion rates in the solid phase would be quite slow, but there were no accurate controls over the temperatures of anneal and the results had to be treated cautiously. The results of those preliminary tests are presented in table 8-II.

As can be seen, in most cases only one phase could be accurately determined and this follows again from the Lever rule.

Finally, all the experimental results are plotted in figure 8-1. The addition of data on the liquidus curve (70I1, 72F1) and the values obtained for the miscibility gap (chapter 3) give a reasonably complete phase diagram for temperatures above 690^{o}C.

Table 8-I Experimental solidus data for the pseudobinary system $GaAs_ySb_{1-y}$.

Initial Composition y_i	T °C	a nm	Solidus Composition y
0.85†	1170	0.5655	0.995
0.65†	1054	0.5660	0.980
0.50†	974	0.5666	0.965
0.35†	893	0.5671	0.947
0.15†	775	0.5718	0.795
0.85*	790	0.5699	0.855
0.60	800	0.5700	0.855
0.35	800	0.5701	0.850
0.60	758	0.5723	0.780
0.25	755	0.5726	0.770
0.25	750	0.5749	0.700
0.60	740	0.5951	0.325
0.07	733	0.5952	0.320
0.07	727	0.6025	0.165

† these are the original points by Woolley (62W1) but the compositions are corrected for departure from Vegard's law.

* This is an original point by Woolley which remained unpublished because of the uncertainty in temperature.

Table 8-II Experimental data for the determination of the miscibility gap in $GaAs_ySb_{1-y}$.

Initial Composition y_i	T °C	Period of anneal days	a nm	Solidus Composition y
0.15	700	57	0.6020	0.168
0.15	690	39	0.6019	0.172
0.35	690	39	0.5962	0.300
0.50	700	61	0.5961	0.304
			0.5664	0.970
0.50	715	15	0.5953	0.320
0.65	723	29	0.5952	0.324
			0.5660	0.980

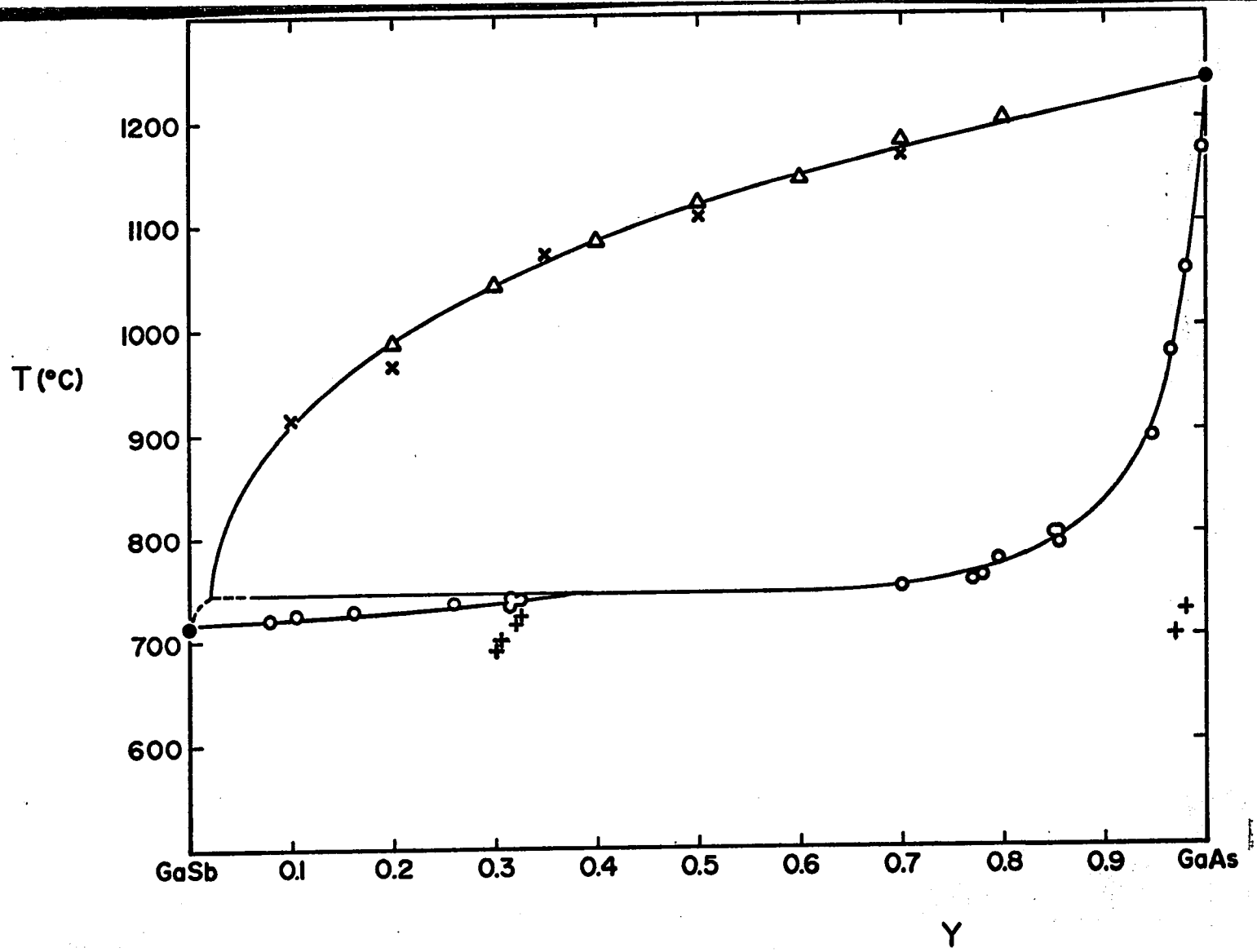

Fig. 8-1 Phase diagram for the pseudobinary system $GaAs_ySb_{1-y}$.

○ solidus data from liquid-solid equilibrium

\+ solidus data from solid-solid equilibrium

△ Ref. 72F1

× Ref. 70I1

● Ref. 69L1

8.4 Discussion

From the configuration of the phase diagram (figure 8-1) it is possible to describe the sequence followed by any sample from its initial formation to the resulting phases appearing after the annealing period. For the case of the sample annealed at 740°C (table 8-I) and with initial composition y = 0.60, the sequence is as follows: the melt upon quenching will yield a solid of composition rich in GaAs and a continuous variation of non-equilibrated phases that approach GaSb along the liquidus line. When the mixture is annealed, time becomes an important factor: if it is sufficiently long then the various phases will diffuse and produce a mixture in equilibrium which will yield the desired phases situated on the boundaries of the two-phase solid-solid field at the temperature of anneal. Every effort is made in order to ensure that the annealing time of each sample is long enough, however, if the time is too short, there will be a lack of diffusion of the phases initially formed resulting in the annealing of a mixture of different composition than the initial starting composition, but if this change in composition is small, then the new composition will still be situated within the two-phase solid-solid field and the resulting phases in equilibrium will be the same as in the case of long anneals.

For the samples annealed at 727°C and 733°C both with y = 0.07, they separate in the two-phase field below the peritectic line and the anneals yield GaSb-rich material and almost GaSb-pure material in accordance with the Lever rule. Similarly for the samples annealed at higher tem-

peratures (e.g. 755°C and above) they separate in the two-phase liquid-solid field situated above the peritectic temperature. The results for the sample annealed at 790°C (y_i = 0.85) showed the initial composition to be very close to the solidus line, however this composition is located inside the two-phase field because it was possible to detect a weak, almost GaSb-pure phase on the X-ray photograph. This is in accordance with the Lever rule and justifies the use of this sample in the determination of the solidus line.

As mentioned previously, the results presented in tables 8-I and 8-II demonstrate the advantages of annealing samples in a two-phase liquid-solid field rather than a solid-solid field as the times required to attain equilibrium conditions are much shorter in the former case. However, the investigations of the miscibility gap require that the anneals take place within the solid-solid field at this stage of the study.

In order to complete the discussion, the two samples with y_i = 0.15 show that between 690°C and 700°C, a single phase field exists since the equilibrium solid compositions of each sample are close to the initial compositions, the differences being accounted for by the experimental error. Hence, the miscibility gap does not extend to these compositions for those temperatures tested. The remaining samples in the range $0.35 < y < 0.65$ indicate that, at these temperatures, a two-phase field exists and phase separation occurs. In all cases both phases are observable but for two of the samples the GaAs-rich phase was not measured as the high angle lines were too faint on the X-ray photograph. The com-

position of this latter phase can however, be estimated to be in the vicinity of y = 0.98.

Because of the uncertainty in the annealing temperatures for samples situated within the two-phase solid-solid field the results have been supplemented by other measurements but the initial compositions of the new samples were selected away from the pseudobinary section of the composition diagram. For this technique to be successful however, a knowledge of the phase diagram of the ternary system Ga-As-Sb is required especially for the liquidus isotherms in order to allow for a proper choice of starting compositions and temperatures for the various anneals.

Since no experimental data were available on the liquidus isotherms of the ternary system Ga-As-Sb except for the pseudobinary section, and it was recognized that the simple solution model provided a reasonable set of isotherms for Ga-In-Sb, it was decided to use the theoretical predictions to obtain the phase diagram data required for the Ga-As-Sb system.

Finally, a recent study by Nahory et al. (77N1) published after the present work was completed, has given four new experimental points on the pseudobinary section (three on the liquidus and one on the solidus) and each one is in good agreement with the data already referred to or presented in this study.

Chapter 9 Theoretical analysis of the ternary system Ga-As-Sb

9.1 Introduction

9.2 Theoretical Determination of the Phase Diagram of the Ternary System Ga-As-Sb

9.2.1 The interaction parameters: α_{As-Sb} and $\alpha_{GaAs-GaSb}$

9.2.2 Liquidus isotherms of Ga-As-Sb

9.2.3 Solidus data of Ga-As-Sb

9.3 Conclusion

9.1 Introduction

Very few workers have reported theoretical analyses on the phase diagram of the ternary system Ga-As-Sb. Panish and Ilegems (72P1) and Stringfellow (72S1) have calculated the pseudobinary section $GaAs_ySb_{1-y}$ but only Antypas and James (70A1) have published results on their calculations of the ternary diagram for gallium concentrations above 50% using Darken's quadratic formalism for a ternary liquid and assuming a regular solid solution (67D2). More recently, Nahory et al. (77N1) have presented an analysis based on the simple solution model except for the treatment of one of the parameters which they have made dependent upon the antimony concentration. This analysis is examined further on.

9.2 Theoretical Determination of the Phase Diagram of the Ternary System Ga-As-Sb

In this chapter, the simple solution model described earlier is used to predict the liquidus and solidus data of Ga-As-Sb.

9.2.1 The interaction parameters: α_{As-Sb} and $\alpha_{GaAs-GaSb}$

In order to be able to use the simple solution model, it is necessary to evaluate two unknown parameters as was the case for the system Ga-In-Sb: they are the two interaction parameters α_{As-Sb} and

$\alpha_{GaAs-GaSb}$. There are various sets of phase diagram data reported for the As-Sb system (58S1, 58H1) and the values adopted for α_{As-Sb} have been somewhat arbitrary and adapted to fit the theoretical treatments used. The values listed in table 6-VII for α_{As-Sb} as well as for $\alpha_{GaAs-GaSb}$ are among the few values quoted in the literature. In addition, Nahory et al. (77N1) have used an α_{As-Sb} linearly dependent upon N_{Sb} while using the simple solution model for predicting the phase diagram.

From the experimental determination of the solidus line of $GaAs_ySb_{1-y}$ in the preceding chapter and the liquidus data available it was possible to use an approach similar to that of Chapter 7 in order to calculate the two remaining interaction parameters. The liquidus-solidus data required in the simultaneous solution of equations 5.6.9, 5.7.3 and 5.7.4 are listed in table 9-I and are taken from the lines drawn through the experimental points of figure 8-1.

The interaction parameters α_{As-Sb} and $\alpha_{GaAs-GaSb}$ were thus determined simultaneously and their values plotted as a function of temperature (solid circles on figures 9-1 and 9-2). As was the case for α_{Ga-In} and $\alpha_{GaSb-InSb}$, a study was made on the dependence of α_{As-Sb} and $\alpha_{GaAs-GaSb}$ upon the solidus compositions: these compositions were varied up to ±1% about the mean composition identified by the initial solidus line and the resulting values of the interaction parameters are plotted on figures 9-1 and 9-2 (open circles and squares). The results showed that the spread increased with increasing temperatures supporting the argument that for high temperatures the slope of the solidus line is so steep that small changes in the value of the composition bring about relatively

Table 9-I: Liquidus-solidus data of $GaAs_ySb_{1-y}$ for the calculation of α_{As-Sb} and $\alpha_{GaAs-GaSb}$.

$T_{^oC}$	liquidus composition	solidus composition
1220	0.920	0.998
1200	0.820	0.996
1180	0.736	0.994
1160	0.657	0.992
1140	0.580	0.989
1120	0.503	0.987
1100	0.430	0.985
1080	0.364	0.982
1060	0.313	0.979
1040	0.273	0.976
1020	0.238	0.973
1000	0.207	0.970
980	0.178	0.967
960	0.154	0.962
940	0.130	0.958
920	0.112	0.953
900	0.095	0.948
880	0.079	0.943
860	0.065	0.935
840	0.053	0.922
820	0.043	0.905
800	0.032	0.880
780	0.024	0.840
760	0.016	0.775

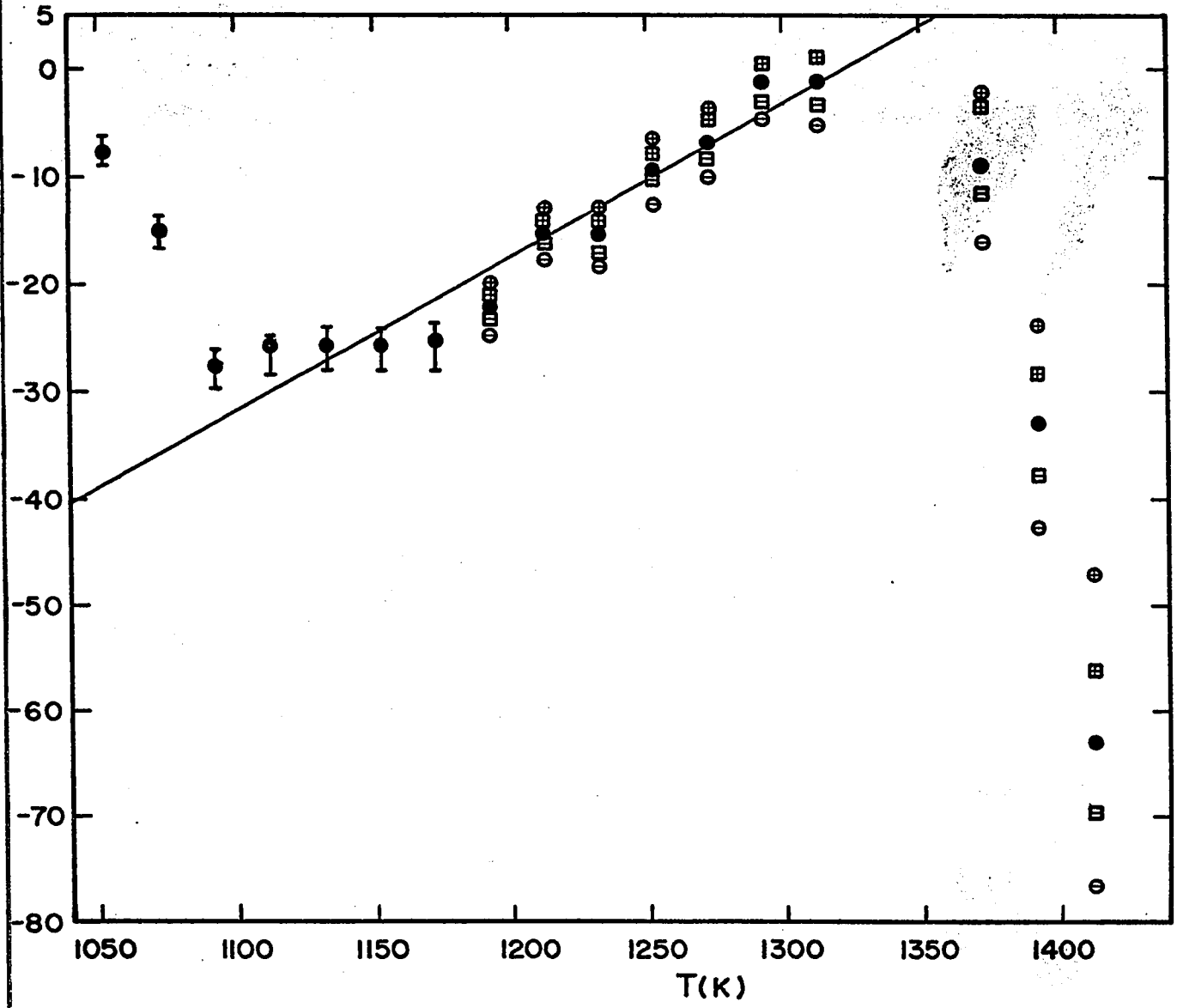

Fig. 9-1 α_{As-Sb} vs. T. The solid circles represent the initial interpolation of the solidus line. The open squares and circles represent the corrections ±0.005 and ±0.01 respectively of the solidus compositions. The solid line represents the least squares fit.

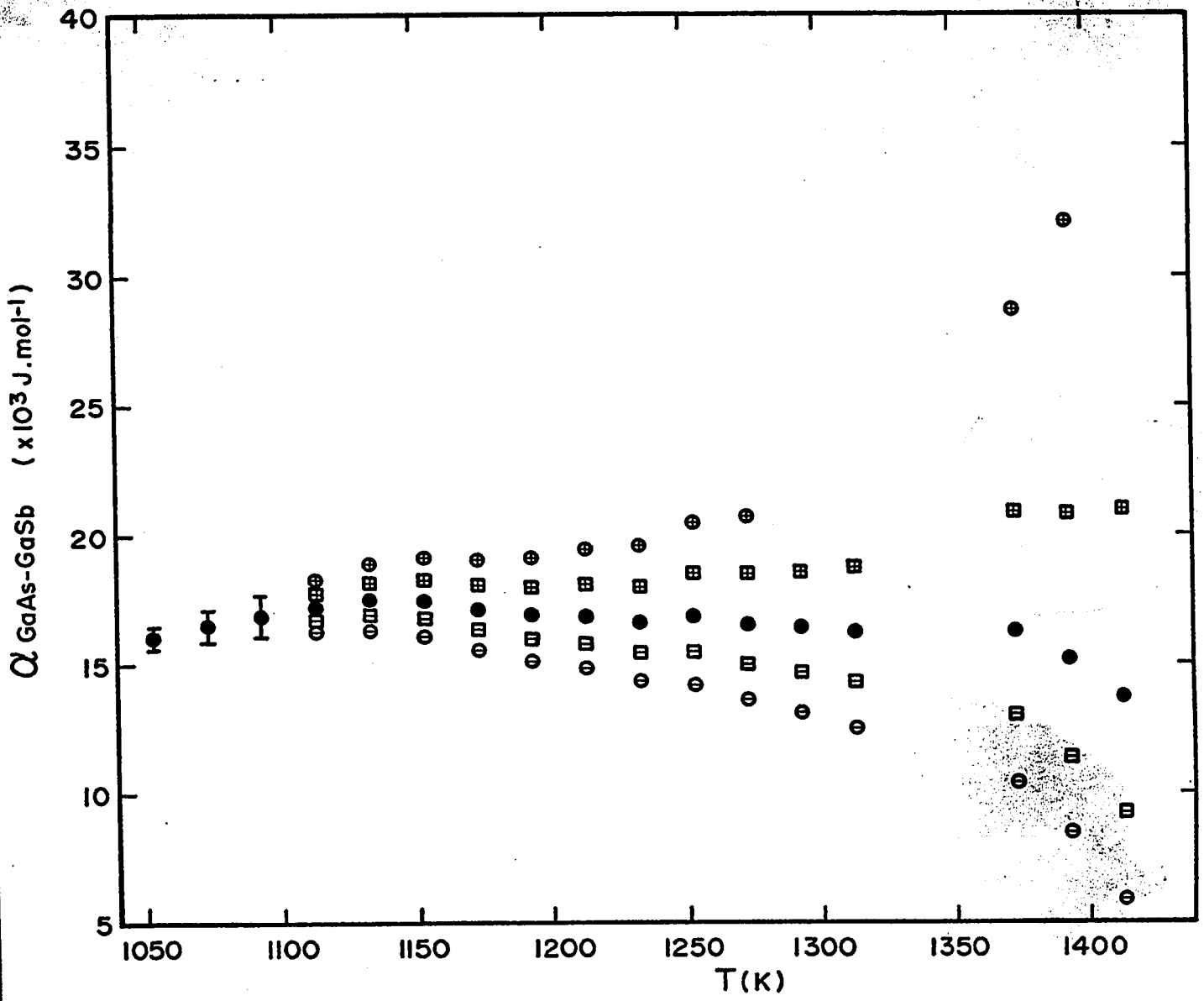

Fig. 9-2 $\alpha_{GaAs-GaSb}$ vs. T. The solid circles represent the initial interpolation of the solidus line. The open squares and circles represent the corrections ±0.005 and ±0.01 respectively, of the solidus compositions.

large variations.

Further investigations of figure 9-1 showed that α_{As-Sb} could be represented by a straight line between 1100 and 1350K. This relation was extended beyond either limit in view of the following argument: for the high temperatures, it has already been recognized that the steepness of the solidus lines can cause relatively large shifts of the points in the high temperature end of the graph and variations of 2 to 3% in composition values could raise the values in the neighbourhood of the straight line. In the lower temperature range however, α_{As-Sb} is seen to be rather insensitive to variations in solidus compositions, but the liquidus line (figure 8-1) has two features which could contribute to move considerably the two points below 1090K: first the liquidus line is very steep in this region and second, there is the presence of a 'cusp' characterized by one of the peritectic phases. These two characteristics make the choice of liquidus compositions less accurate. In view of these facts, it was therefore decided to adopt a linear variation with temperature to describe α_{As-Sb}.

In the case of $\alpha_{GaAs-GaSb}$, inspection of figure 9-2 suggested that a constant value be chosen to express this last parameter. In an attempt to obtain the proper values for the limit of the miscibility gap on the pseudo-binary section $GaAs_ySb_{1-y}$, a value of 17154 $J\text{-}mol^{-1}$ was adopted for $\alpha_{GaAs-GaSb}$ which is in good agreement with figure 9-2.

As mentioned previously, all linear variations with temperature

result from a least squares analysis and the values of the four interaction parameters used in the calculation of the ternary phase diagram Ga-As-Sb are given in table 9-II.

Table 9-II. Interaction parameters for the ternary system Ga-As-Sb.

α_{Ga-Sb}	=	23824 - 32.38T	$J.mol^{-1}$
α_{Ga-As}	=	19828 - 36.61T	$J.mol^{-1}$
α_{As-Sb}	=	14.14T - 18715	$J.mol^{-1}$
$\alpha_{GaAs-GaSb}$	=	17154	$J.mol^{-1}$

9.2.2 Liquidus isotherms of Ga-As-Sb

The appropriate equations were solved using the α's listed in table 9-II for combinations of N_{Ga}, N_{As} and N_{Sb} over the whole ternary diagram to give values of T and y. Then a graph of temperature versus N_{As} yielded a network of constant N_{Sb} as well as N_{Ga} lines which allowed for appropriate interpolations in order to get the liquidus isotherms of the ternary system Ga-As-Sb. The network is displayed on figure 9-3. The liquidus isotherms thus found are plotted on the ternary composition diagram in figure 9-4. It can be readily seen that because of the wide temperature range between the melting points of the two binary compounds, only the high temperature isotherms are represented in figure 9-4 and that the often needed lower temperature isotherms are too close to the Ga-Sb line to be distinguished from it. Here, the 700^{o}C line is the lowest iso-

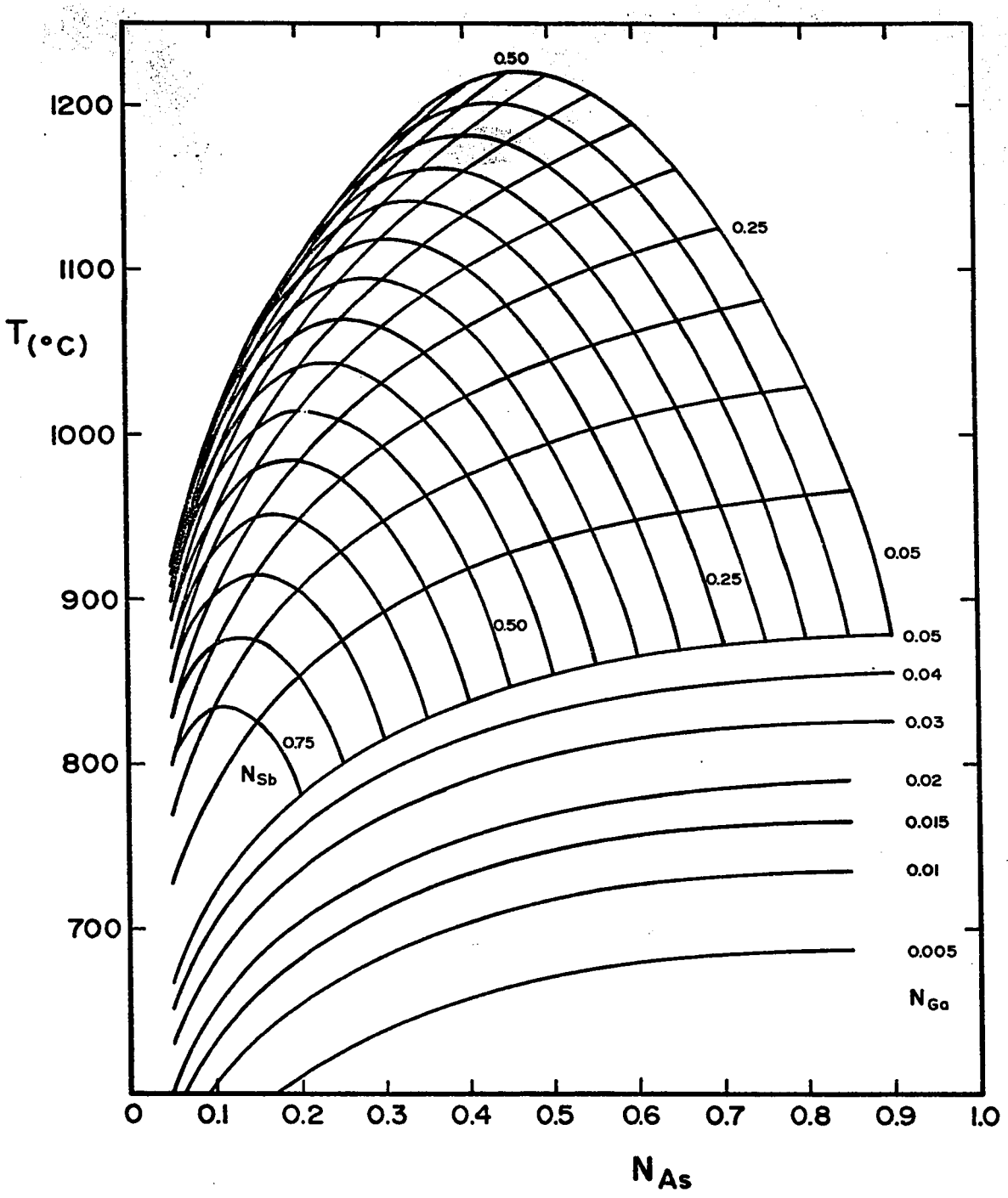

Fig. 9-3 Relationship between T and N_{As} from the theoretical analysis of Ga-As-Sb. The network represents the lines of constant N_{Ga} and N_{Sb}.

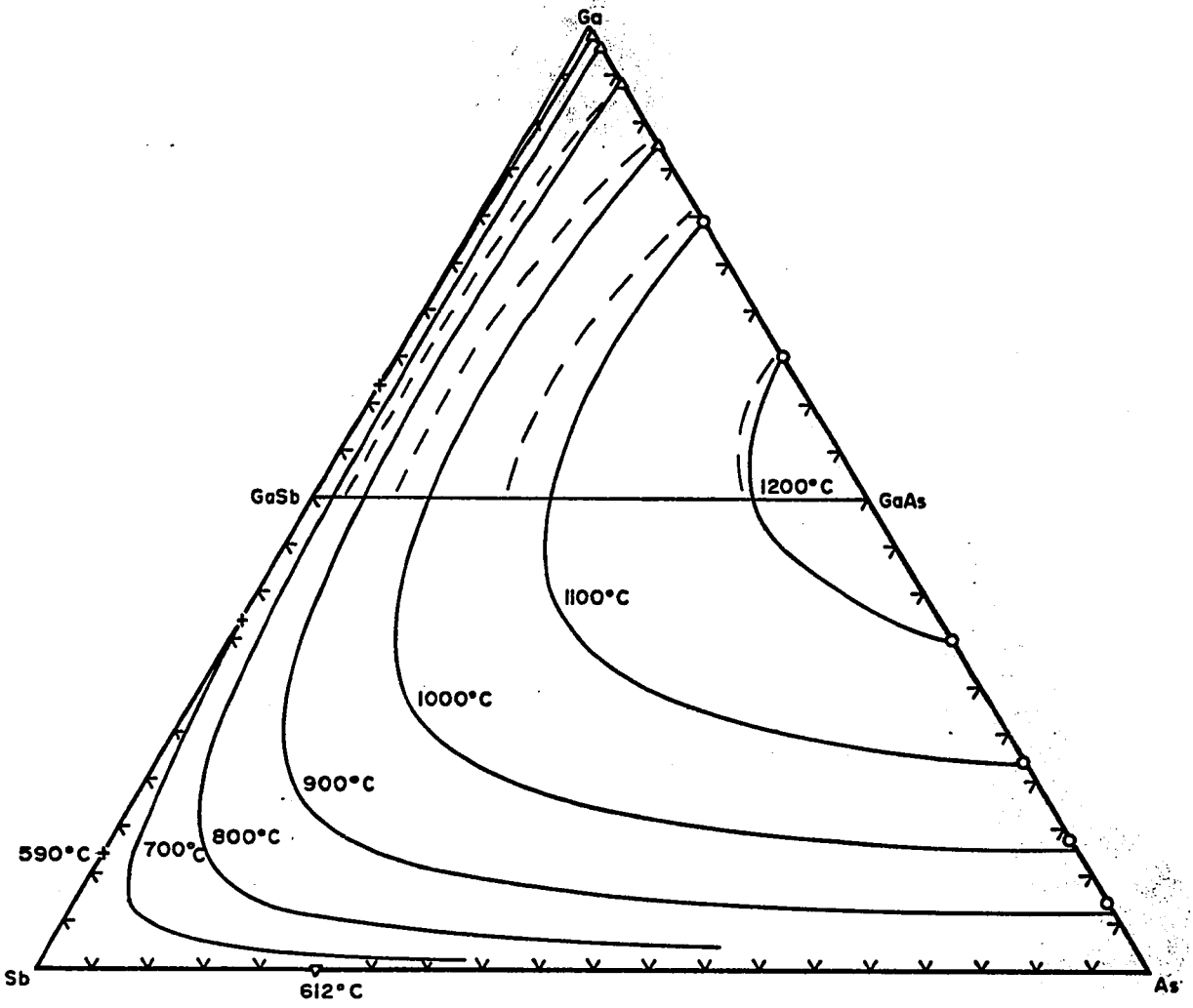

Fig. 9-4 Theoretical liquidus isotherms in the Ga-As-Sb ternary phase diagram.

———— this study --------Antypas and James (70A1)

therm plotted in the diagram. Furthermore, an undefined eutectic valley is also present in the antimony-rich corner of the diagram which makes any interpretation of data in that region or close to it very difficult.

In an attempt to clarify the story on isotherms, it was necessary to shift from triangular coordinates to cartesian coordinates and study the low temperature liquidus isotherms which occurred at very low arsenic concentrations. Such a diagram is plotted in figure 9-5 where the liquidus isotherms range from temperatures of 600°C to 850°C. The higher temperature isotherms were included to allow for comparison with figure 9-4.

As mentioned earlier, the calculations of Antypas and James (70A1) and Nahory et al. (77N1) are the only predictions available for comparison. In figure 9-4, the values of Antypas and James are plotted from graph scaling of their published work and it can be seen that they deviate from the present analysis, especially near the pseudobinary section for which experimental data are available.

In figure 9-5 the predictions of Nahory et al. have also been included with their experimental points from liquid phase epitaxy growth. Their predicted liquidus isotherms show a better fit than those of the present analysis: they chose the values of Panish and Ilegems (72P1) for α_{Ga-Sb} and α_{Ga-As}, and adjusted $\alpha_{GaAs-GaSb}$ and α_{As-Sb} so that the calculated isotherms fit all of their liquidus data as well as three equilibrium solidus points also included in their study. They have therefore assigned a value of 16746 $J.mol^{-1}$ to $\alpha_{GaAs-GaSb}$ and considered α_{As-Sb} as linearly dependent upon the concentration of antimony:

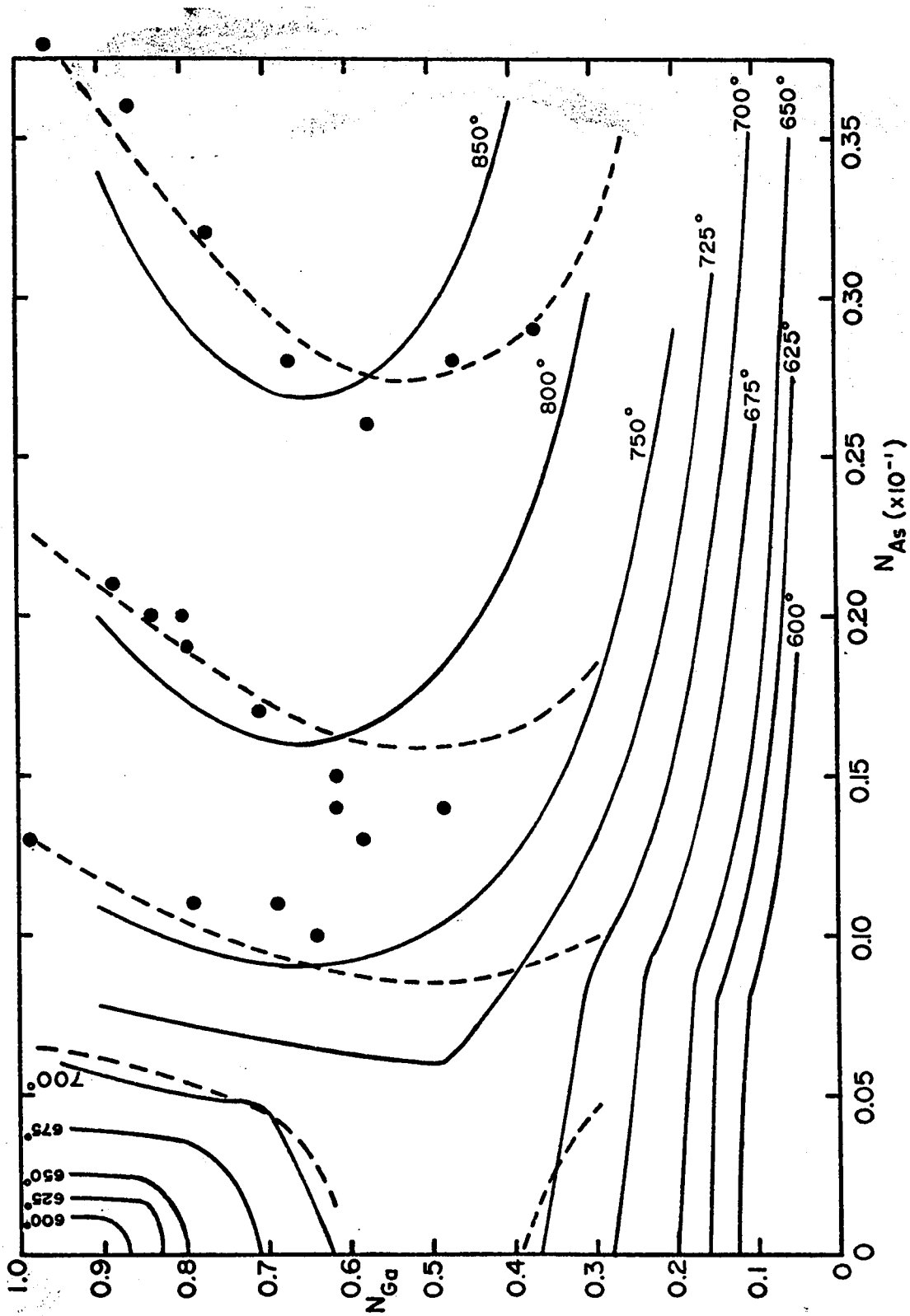

Fig. 9-5 Theoretical liquidus isotherms for low temperatures (in ^{o}C) in the Ga-As-Sb ternary phase diagram. The experimental points are from liquid phase epitaxy growth by Nahory et al. (77N1)

——— this study ---------- Nahory et al. (77N1).

$\alpha_{As-Sb} = 13807\ N_{Sb} - 7531\ J.mol^{-1}$.

In the present analysis, a dependence upon temperature was adopted instead, and the set of liquidus isotherms thus obtained is still not so far off the experimental points since the arsenic-scale in the diagram of figure 9-5 is rather large. It was, however, possible to improve the fit to the points above $N_{Ga} = 0.5$ by keeping the temperature dependence for α_{As-Sb} but increasing the value of the slope. As a matter of fact, the fit was quite good but the new value of α_{As-Sb} was then incompatible with the value found from the analysis in section 9.2.1, and therefore, the initial value (table 9-II) was kept throughout the rest of this analysis.

9.2.3 Solidus data of Ga-As-Sb

For the analysis of the solidus data it was found that a network of the type of figure 9-3 was not so useful as a plot of solid composition (y) versus N_{As} yielded values above $y = 0.9$ and thus limited the usefulness of such a network. By extending the N_{As}-scale however, it was possible to give a better representation of solidus data: figures 9-6, 9-7 and 9-8 display the y vs. N_{As} relation through the whole range of y-composition and also give the position of the miscibility gap. Three figures were needed here in order to avoid overlapping of the curves at different antimony concentrations and show the finer details of the existing relationships.

It was also possible to study the variation of the cusp mentioned earlier from the present analysis. Figures 9-9 and 9-10 show the variation

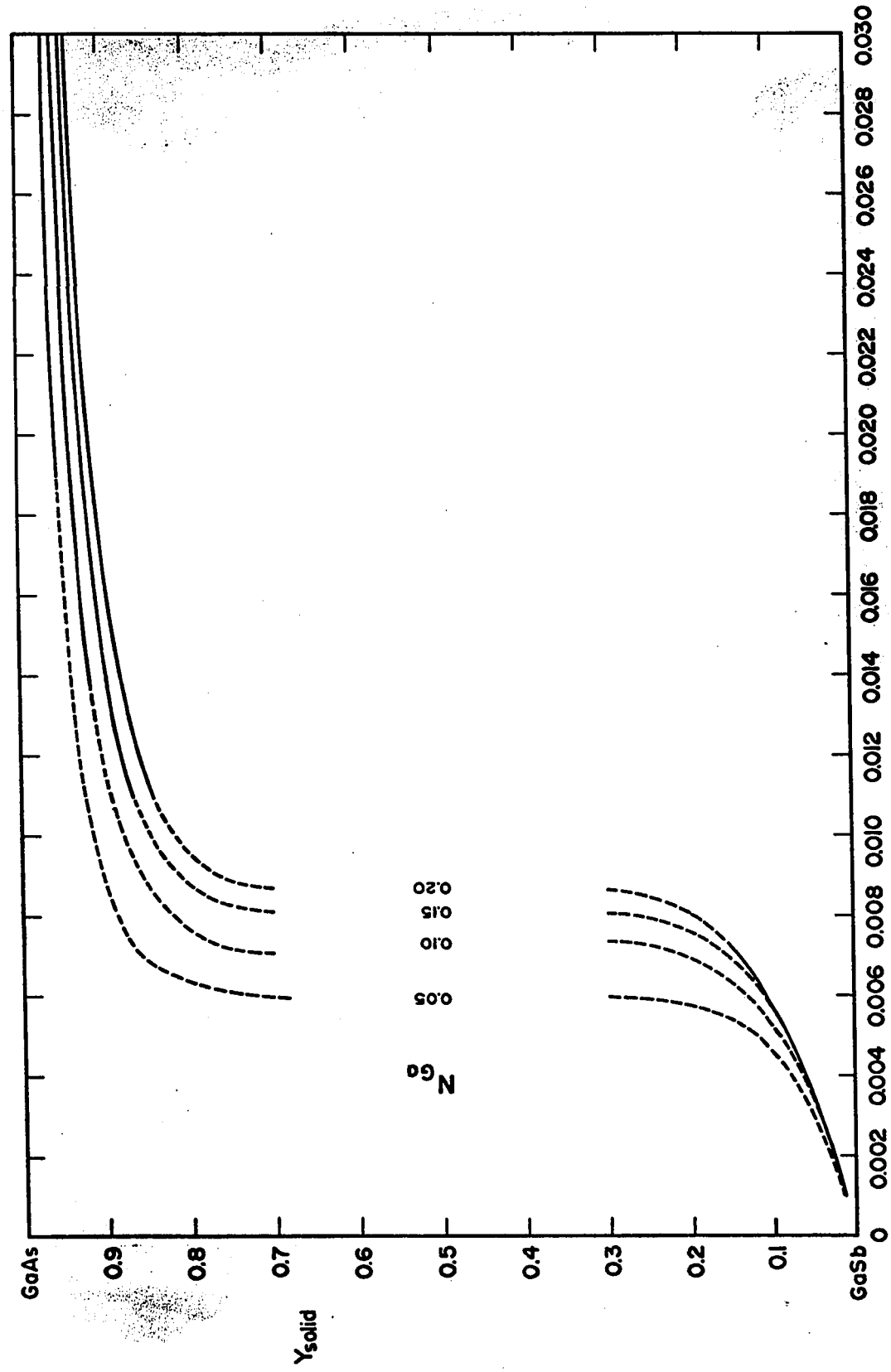

Fig. 9-6 Theoretical solidus compositions vs. N_{As} relations for various constant N_{Ga} lines.

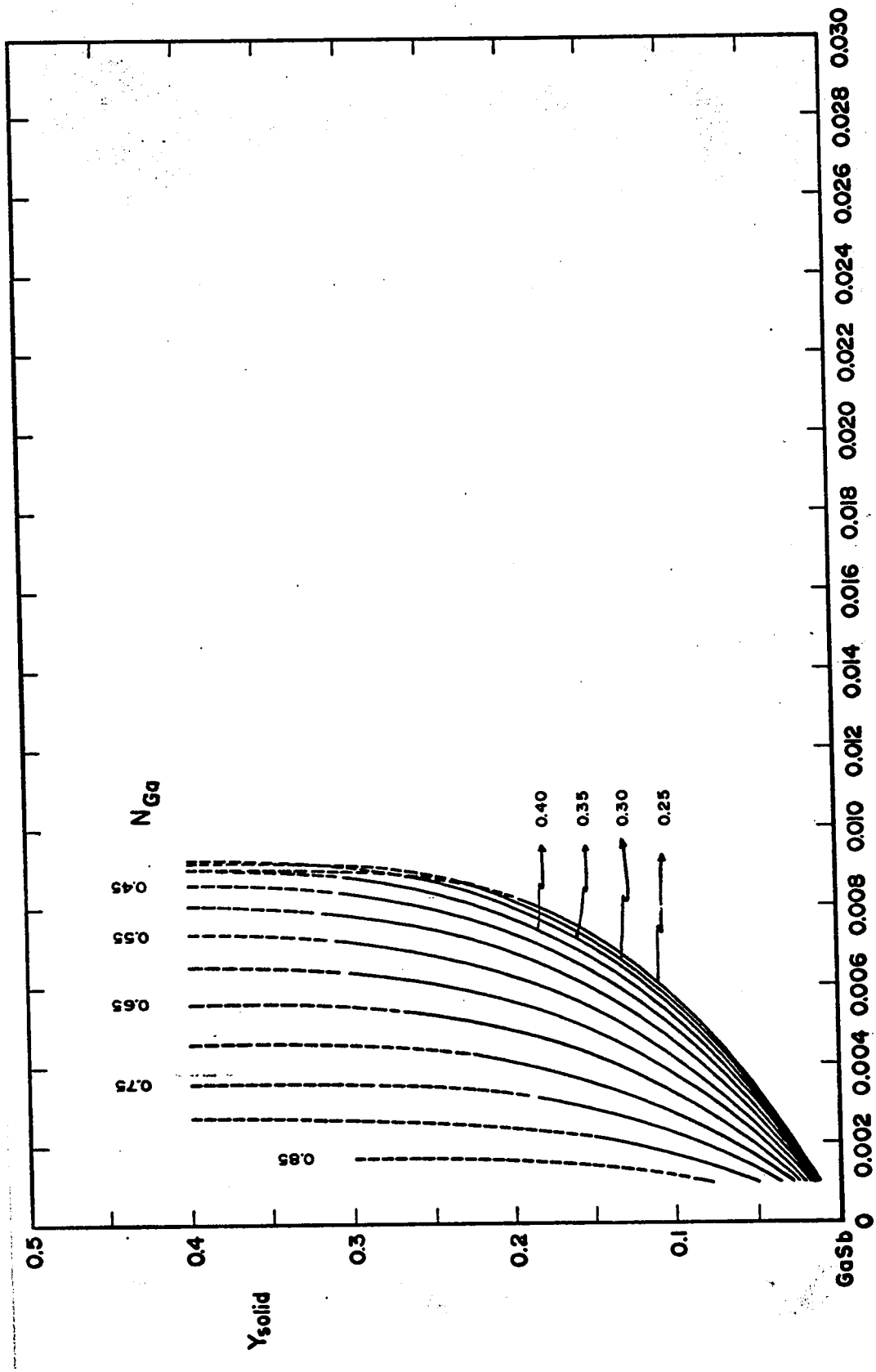

Fig. 9-7 Theoretical solidus compositions vs. N_{As} relations for various constant N_{Ga} lines ($y < 0.50$).

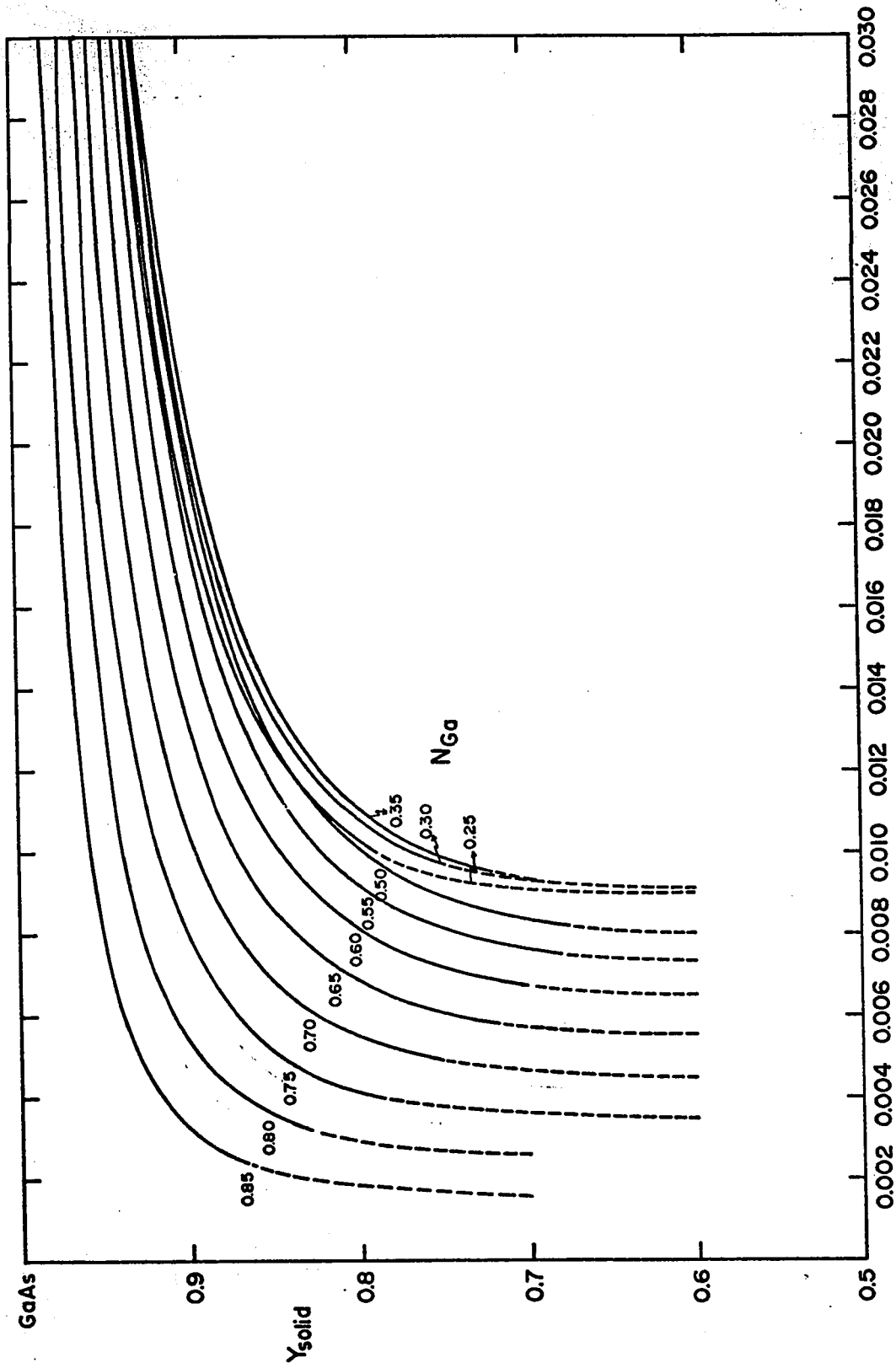

Fig. 9-8 Theoretical solidus compositions vs. N_{As} relations for various constant N_{Ga} lines ($y > 0.50$).

of T vs. N_{As} for $N_{Ga} \leq 0.50$ and $N_{Ga} \geq 0.55$ respectively. In the latter case, only a few curves were drawn to avoid overlapping. The exact composition for which the cusp occurs is given in each case by the x's. A different representation of the position of the cusp is also given in the following chapter as it makes comparison with experimental results easier.

9.3 Conclusion

There is one important conclusion that may be drawn from this study and it is the fact that it is difficult to postulate a specific variation for the interaction parameters. For this alloy system, a temperature dependence or a composition dependence can be found to be both satisfactory in explaining the experimental evidence collected so far on the liquidus properties. However, the usefulness of the simple solution model is not to be minimized as its predictions of the liquidus isotherms were most valuable in planning the kind of experimental investigations that were to follow and which are described in the following chapter.

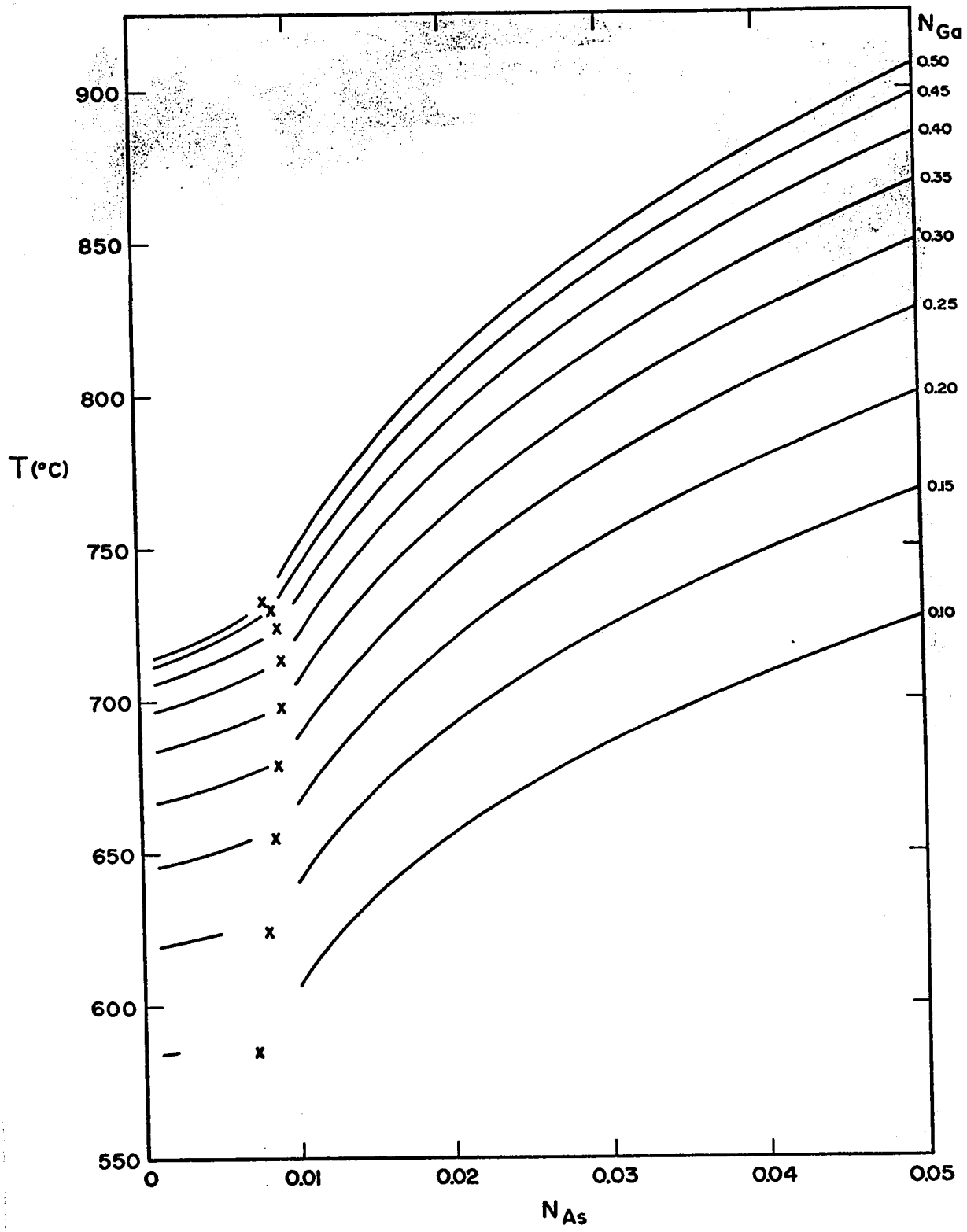

Fig. 9-9 Theoretical position of the cusp for arsenic concentrations in the range $0.10 \leq N_{Ga} \leq 0.50$.

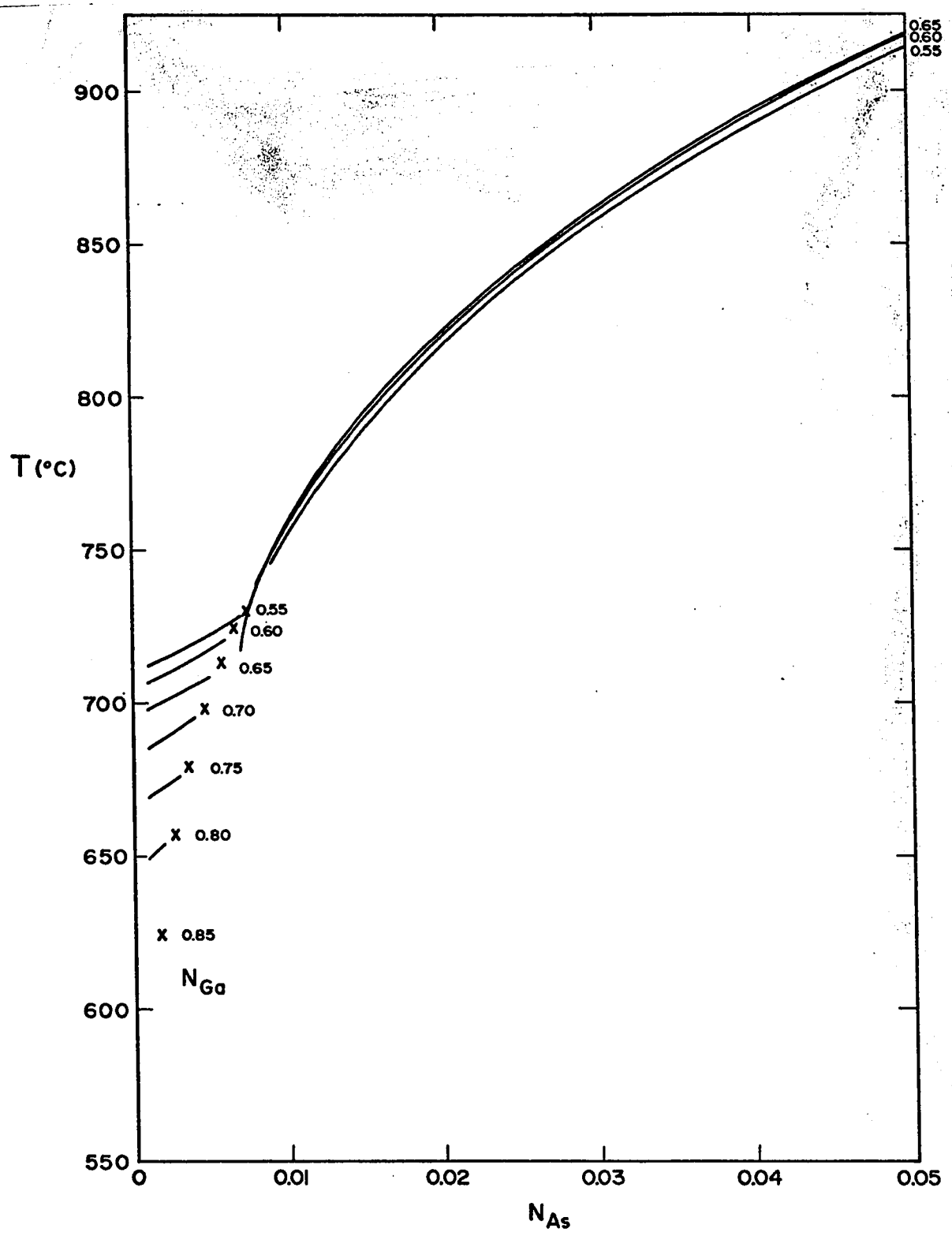

Fig. 9-10 Theoretical position of the cusp for arsenic concentrations in the range $0.55 \leq N_{Ga} \leq 1.0$.

Chapter 10 Experimental investigation of the ternary system Ga-As-Sb

10.1 Introduction

10.2 Experimental Investigation of Ga-As-Sb

10.2.1 Samples and method

10.2.2 Tie-lines, boundaries of three-phase fields and miscibility gap

10.2.3 Position of the cusp in the ternary diagram

10.3 Experimental and Calculated Pseudobinary Section $GaAs_ySb_{1-y}$

10.4 Discussion

10.1 Introduction

The observations and theoretical analysis reported in the previous chapters have demonstrated that the ternary phase diagram of Ga-As-Sb is more complicated than other ternary diagrams of III-V alloys such as Ga-In-Sb or Ga-In-As for instance. Despite the information that is becoming more and more available it is still too soon to assume that this phase diagram has been characterized completely.

The presence of a miscibility gap for the solid solutions of $GaAs_ySb_{1-y}$ suggests that three-phase fields will arise in the three-dimensional ternary diagram, and to investigate the positions of such fields it is necessary to analyze samples of initial compositions situated all over the composition triangle. This, however, will exclude compositions on the pseudobinary section as it constitutes one of the boundaries of those three-phase fields.

In this chapter, the miscibility gap is investigated further from samples with initial compositions off the pseudobinary section and various sets of tie-lines are obtained in an effort to define the boundaries of the three-phase fields.

10.2 Experimental Investigation of Ga-As-Sb.

The studies reported in this chapter toward the determination

of the ternary phase diagram of Ga-As-Sb were made at temperatures below the peritectic horizontal in order to cover the section of the diagram for which three-phase fields and a miscibility gap occur. The results thus collected are used in the determination of tie-lines present in the two-phase fields, they also complete the partial results of chapter 8 (figure 8-1) for the boundaries of the miscibility gap on the pseudobinary section, and finally, they provide valuable information about the boundaries of the three-phase fields and the position of a cusp situated on the liquidus sheet in the three-dimensional model of the phase diagram.

10.2.1 Samples and method

The samples were prepared from a mixture of GaAs, GaSb and pure antimony or gallium depending on whether $N_{Ga} < 0.50$ or $N_{Ga} > 0.50$. This technique of using binary compounds is mainly to avoid dealing with elemental arsenic which has a high vapour pressure. The preparation was carried out in the same way as described in chapter 7.

The method used here was the anneal and quench technique. The mixture was heated to a predetermined temperature where it was allowed to reach equilibrium; after sufficient time for this condition to be attained, it was then quenched in order to freeze in the solid phase which was in equilibrium in the solution. This technique was particularly well suited for the type of measurements described above since part of the mixture was in the liquid state and ensured an adequate medium for the diffusion of atoms during the period of anneal. Therefore, it allowed for equilibrium conditions to be reached at a much faster rate than if

solid-solid diffusion occurred as would be the case for instance in the investigations of a miscibility gap on the pseudobinary section.

The solid phase or phases in equilibrium thus formed were finally identified from X-ray powder photographs and the lattice constant-composition relation previously established. The state of equilibrium could also be estimated by close inspection of the diffraction lines characteristic of each phase present: diffuse lines indicating poor equilibrium conditions.

10.2.2 Tie-lines, boundaries of three-phase fields and miscibility gap

Conditions for equilibrium were investigated for various temperatures and the choice of starting compositions was dictated by an approximate determination of the boundaries of the three-phase fields given by the liquidus and solidus data of the theoretical model. Figures 10-1 a to e show the various compositions investigated, the associated tie-lines deduced from the analysis of the equilibrium conditions at different temperatures, and the boundaries of the three-phase fields. The compositions of the samples were chosen with constant gallium concentrations and such that specimens of each series would be included in either a two-phase field or a three-phase field at their respective temperatures of anneal. The analysis yielded the tie-lines of the two-phase field for known temperatures and it was also possible to determine in each case the limiting tie-line which formed the boundary of the adjacent three-phase field.

Figure 10-1e for instance, shows two such series annealed at

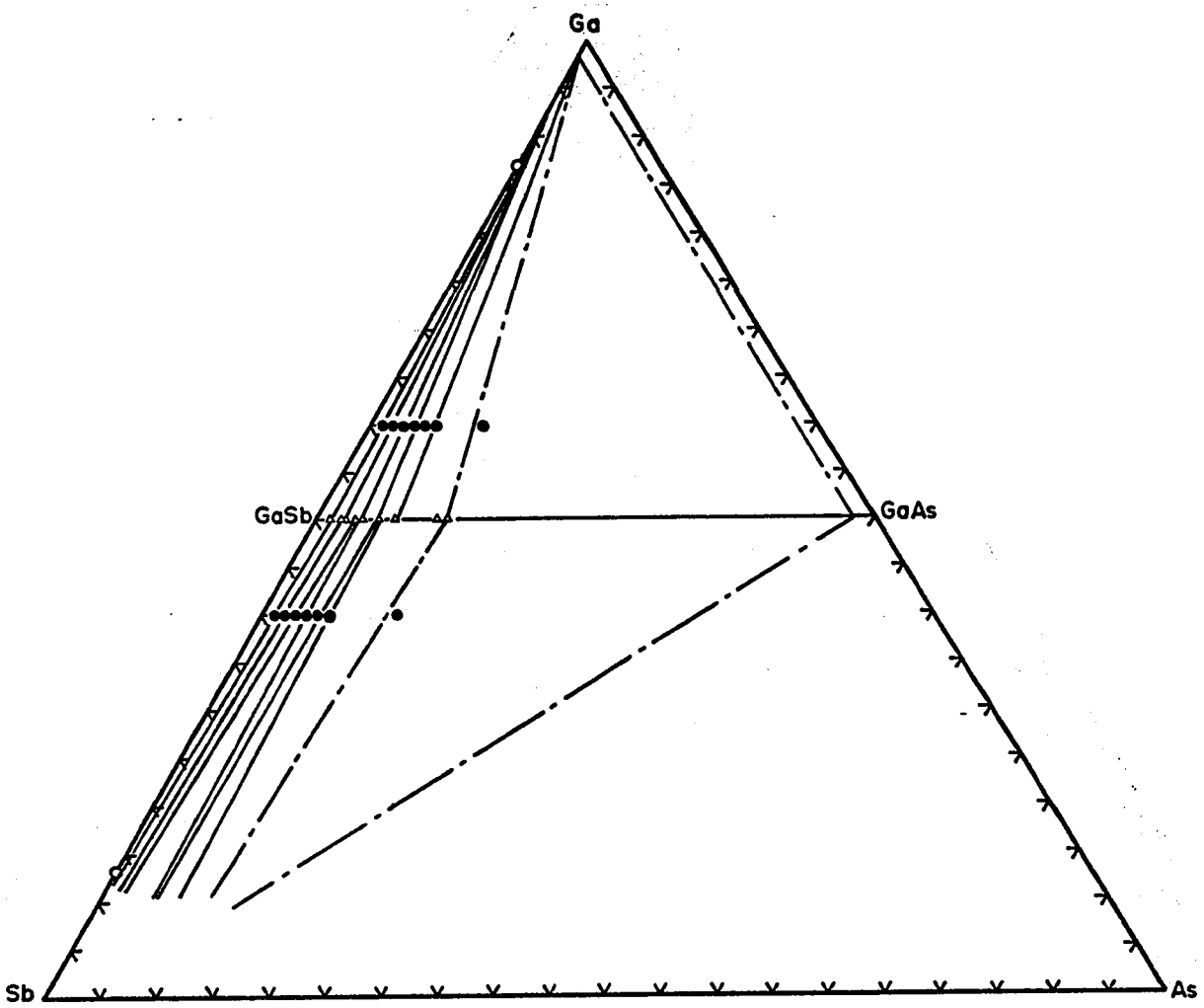

Fig. 10-1a The 600°C isothermal section of the Ga-As-Sb system. The solid lines represent the tie-lines in their respective two-phase fields and the dash-dotted lines represent the boundaries of the three-phase fields

- ● initial composition
- △ solid phase in equilibrium (GaSb-rich)
- ○ Greenfield and Smith (55G1).

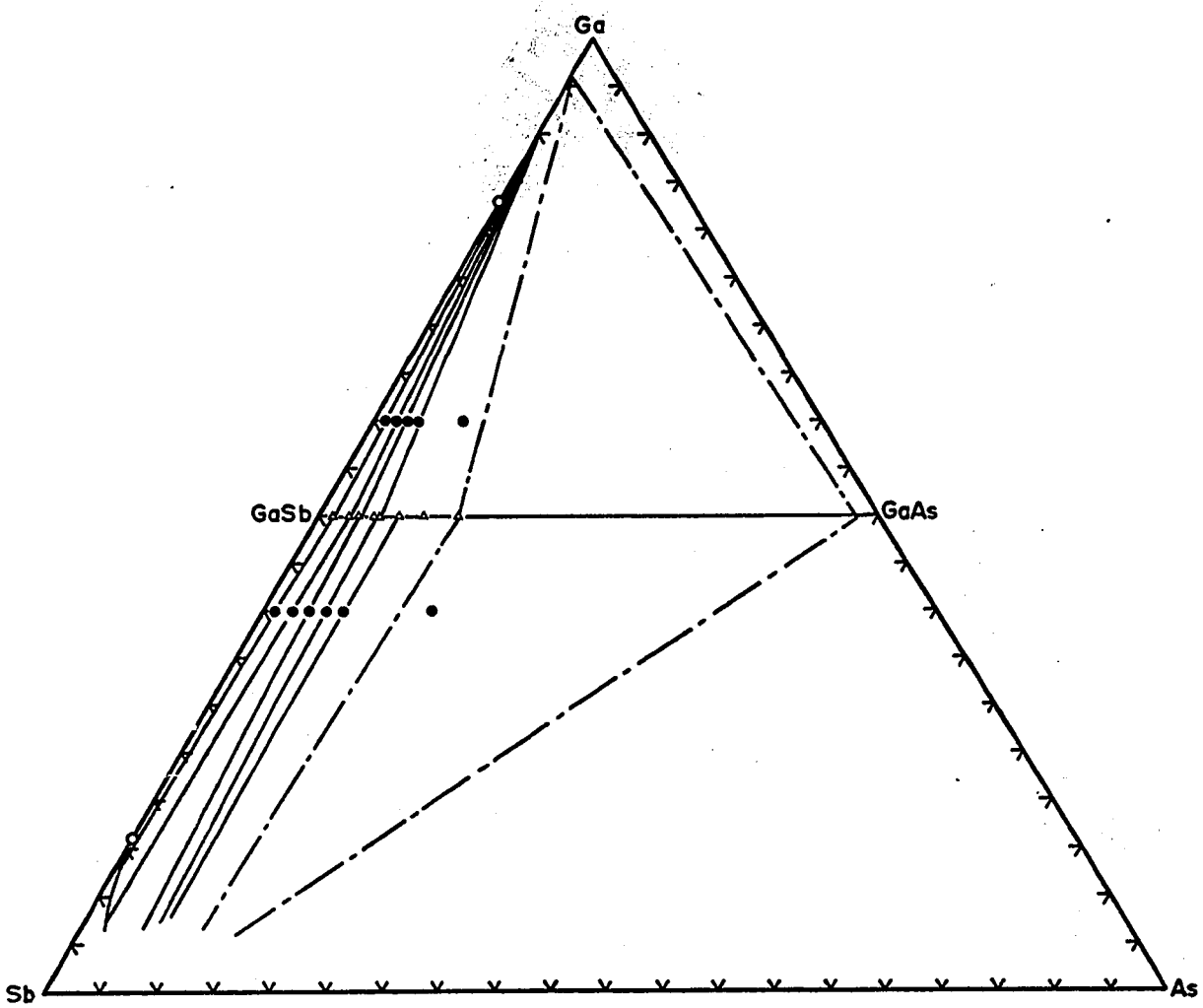

Fig. 10-1b The 625°C isothermal section of the Ga-As-Sb system. The solid lines represent the tie-lines in their respective two-phase fields and the dash-dotted lines represent the boundaries of the three-phase fields.

- ● initial composition
- △ solid phase in equilibrium (GaSb-rich)
- ○ Greenfield and Smith (55G1).

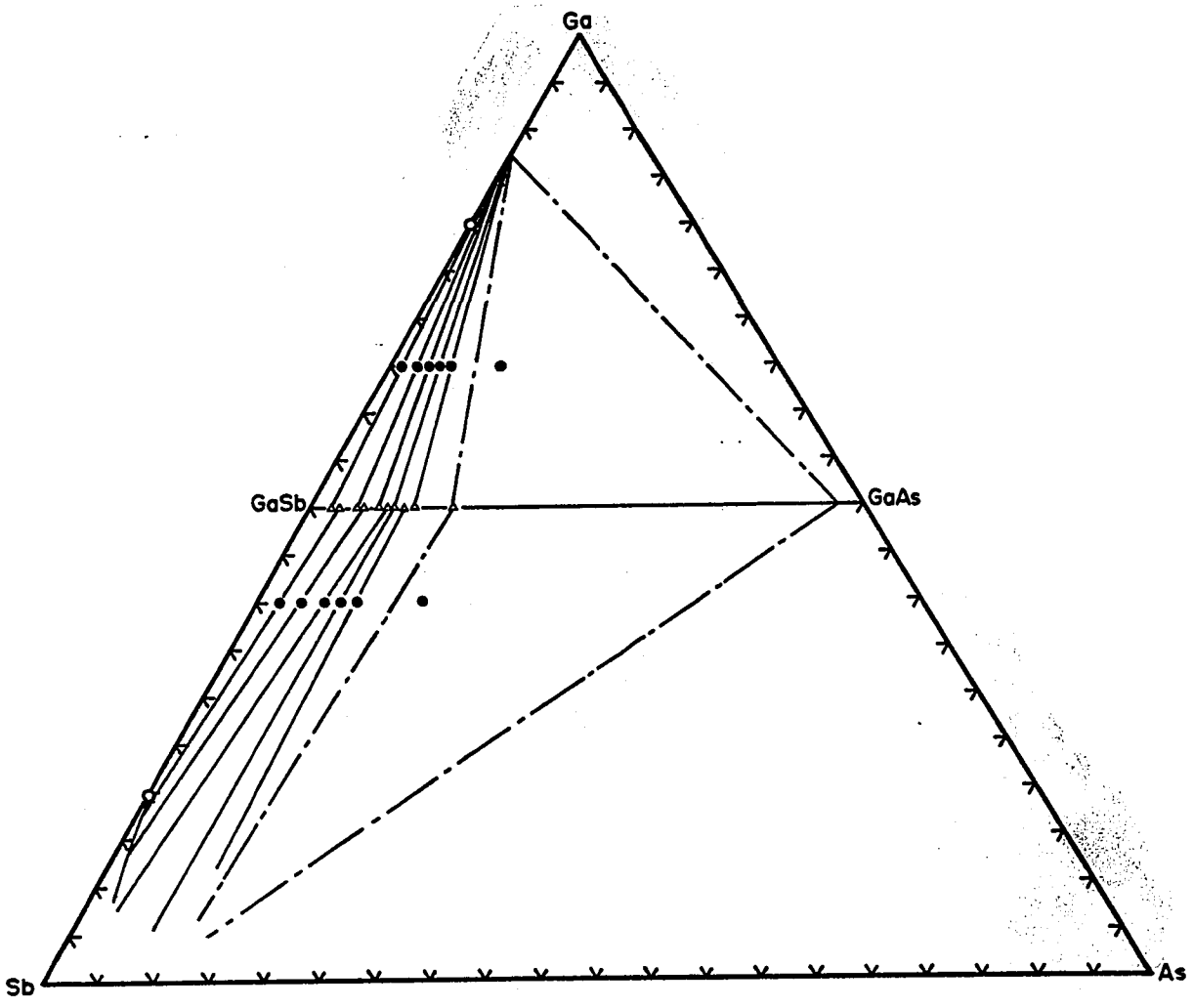

Fig. 10-1c The 645°C isothermal section of the Ga-As-Sb system. The solid lines represent the tie-lines in their respective two-phase fields and the dash-dotted lines represent the boundaries of the three-phase fields.

- ● initial composition
- △ solid phase in equilibrium (GaSb-rich)
- ○ Greenfield and Smith (55G1).

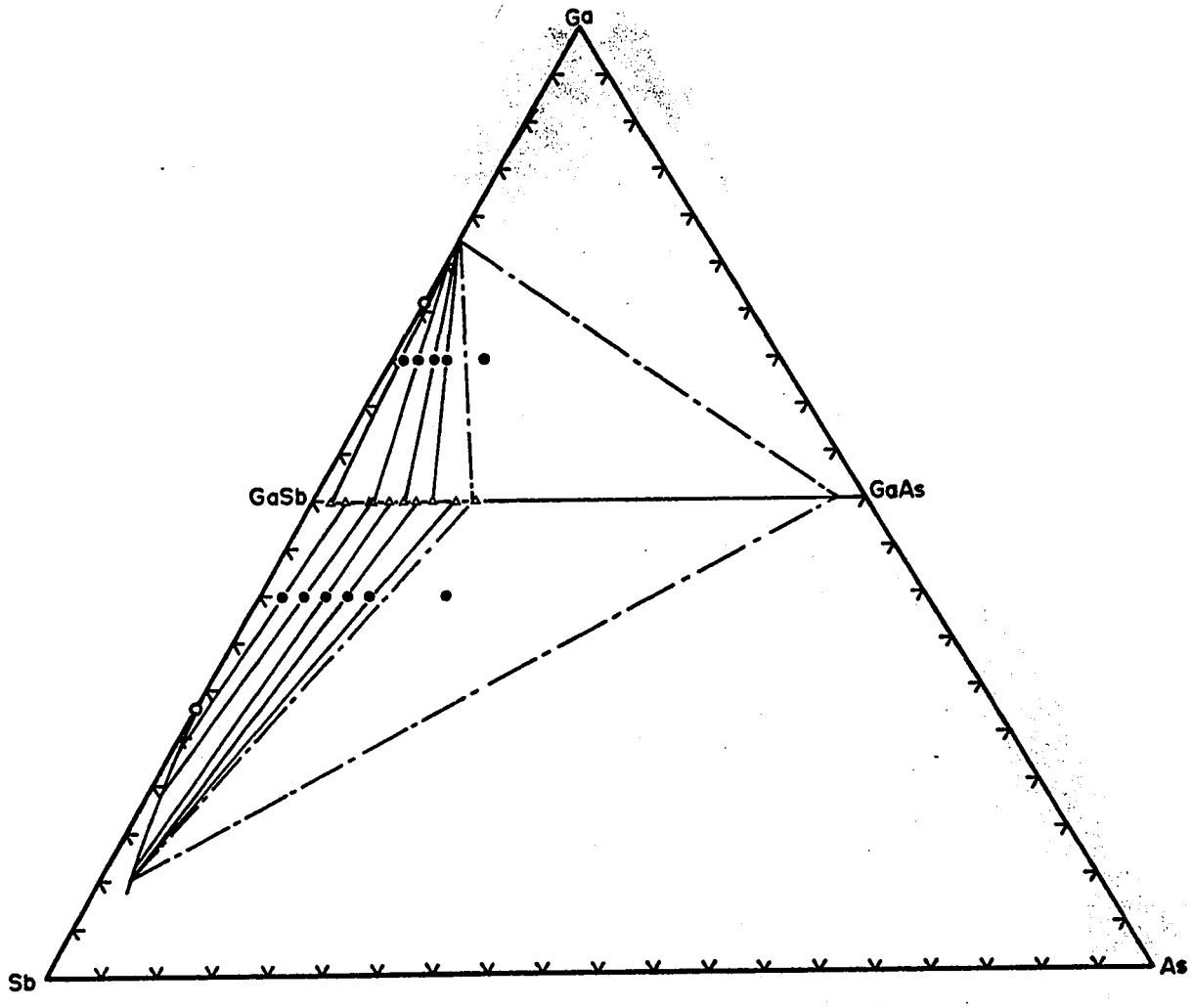

Fig. 10-1d The 675°C isothermal section of the Ga-As-Sb system. The solid lines represent the tie-lines in their respective two-phase fields and the dash-dotted lines represent the boundaries of the three-phase fields.

- ● initial composition
- △ solid phase in equilibrium (GaSb-rich)
- ○ Greenfield and Smith (55G1).

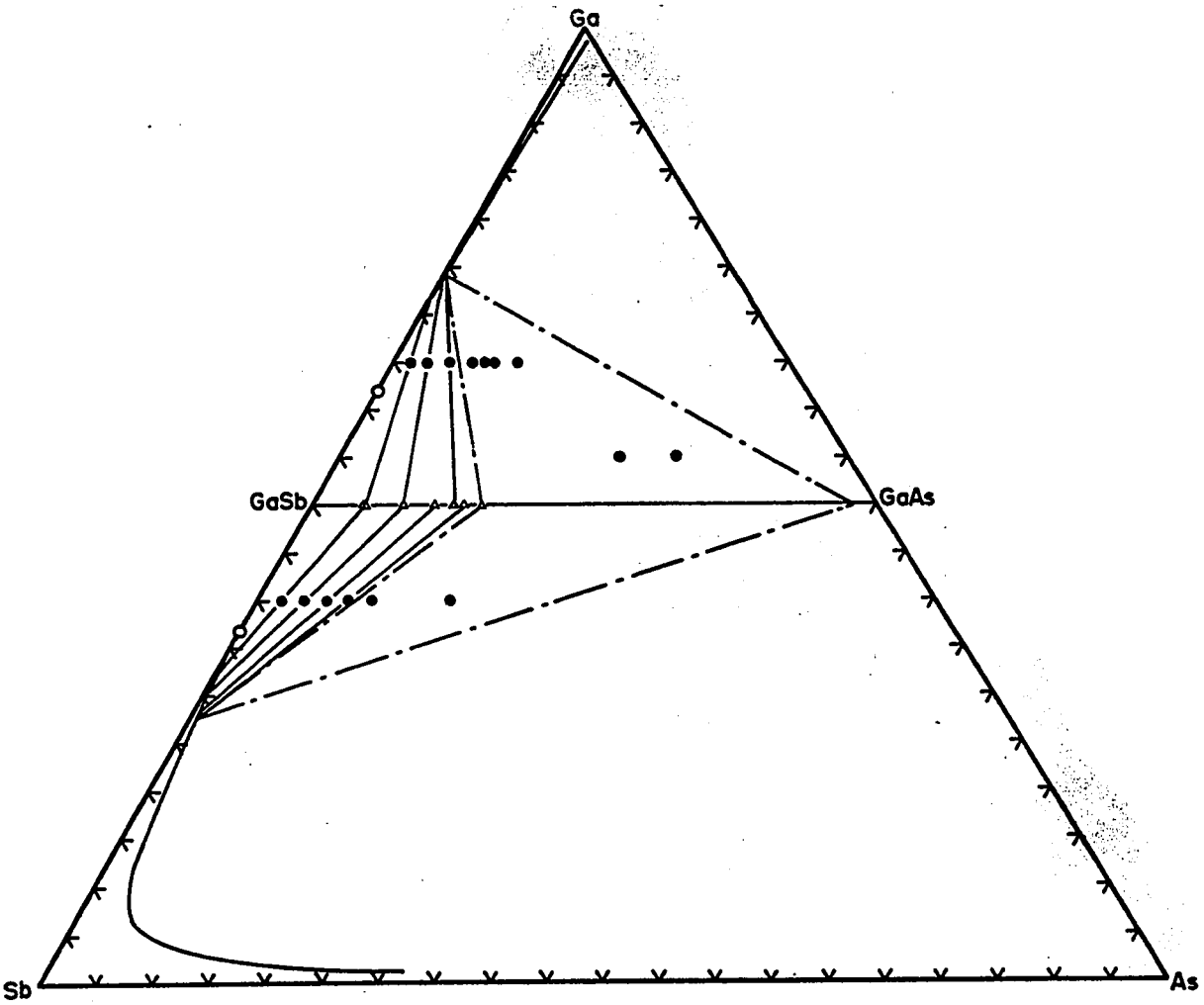

Fig. 10-1e The 700°C isothermal section of the Ga-As-Sb system. The solid lines represent the tie-lines in their respective two-phase fields and the dash-dotted lines represent the boundaries of the three-phase fields.

- ● initial composition
- △ solid phase in equilibrium (GaSb-rich)
- ○ Greenfield and Smith (55Gl).

700°C for N_{Ga} = 0.65 and N_{Ga} = 0.40. For the former, seven compositions were chosen: three samples with $N_{As} \leq 0.05$ yielded tie-lines in the two-phase field and four samples with $N_{As} \geq 0.07$ showed identical conditions of three-phase equilibrium within the experimental error. A GaSb-rich phase, a GaAs-rich phase which could not be identified clearly on the powder photograph as the diffraction lines were too weak, and finally a third phase almost GaSb-pure. This phase is due to the crystallization of the liquid phase in the equilibrated solution which drops a solid near the GaSb-pure end of the diagram. The reason for preparing more than one sample within the expected three-phase field was to verify the replication of three-phase equilibrium for samples of different compositions. A similar analysis was carried out for the series of samples with N_{Ga} = 0.40 with results confirming those of the former series. The relevant data for measurements of various series at different temperatures are tabulated in table 10-I.

There is, however, one more set of diagrams that are required in order to undertake a full analysis of the data collected and they are plots of the compositions of the solid phases in equilibrium as a function of the arsenic concentration in the initial samples. These graphs are presented in figure 10-2 a to e for each temperature investigated. At 700°C, for instance, a horizontal line has been drawn through the three-phase equilibrium data and it represents the common GaSb-rich composition in equilibrium for those two series of samples and compensates for the variations due to the temperature fluctuations of the annealing furnaces. Two lines are also drawn to join the points of each individual series of

Table 10-I Compositions of samples with constant N_{Ga} annealed at various temperatures T, and of resulting equilibrium solid phases.

T °C	Initial Composition N_{Ga}	N_{As}	N_{Sb}	a nm	Solid Composition y
600°	0.400	0.010	0.590	0.6084	0.026
	0.400	0.020	0.580	0.6076	0.045
	0.400	0.030	0.570	0.6066	0.068
	0.400	0.040	0.560	0.6063	0.073
	0.400	0.050	0.550	0.6048	0.108
	0.400	0.060	0.540	0.6047	0.110
	0.400	0.120	0.480	0.6000	0.215
	0.600	0.010	0.390	0.6084	0.026
	0.600	0.020	0.380	0.6072	0.052
	0.600	0.030	0.370	0.6058	0.084
	0.600	0.040	0.360	0.6048	0.108
	0.600	0.050	0.350	0.6058	0.084
	0.600	0.060	0.340	0.6033	0.140
	0.600	0.100	0.300	0.5991	0.235
625°	0.400	0.010	0.590	0.6084	0.026
	0.400	0.025	0.575	0.6071	0.055
	0.400	0.040	0.560	0.6064	0.070
	0.400	0.055	0.545	0.6052	0.098
	0.400	0.070	0.530	0.6032	0.144
	0.400	0.150	0.450	0.5985	0.249
	0.600	0.010	0.390	0.6083	0.028
	0.600	0.020	0.380	0.6070	0.058
	0.600	0.030	0.370	0.6065	0.069
	0.600	0.040	0.360	0.6048	0.108
	0.600	0.080	0.320	0.6013	0.188
645°	0.400	0.020	0.580	0.6075	0.048
	0.400	0.040	0.560	0.6053	0.095
	0.400	0.060	0.540	0.6034	0.138
	0.400	0.075	0.525	0.6028	0.152
	0.400	0.090	0.510	0.6022	0.166
	0.400	0.150	0.450	0.5983	0.256
	0.650	0.010	0.340	0.6079	0.036
	0.650	0.025	0.325	0.6057	0.086
	0.650	0.035	0.315	0.6041	0.123
	0.650	0.045	0.305	0.6028	0.152
	0.650	0.055	0.295	0.6013	0.187
	0.650	0.100	0.250	0.5978	0.265
675°	0.400	0.020	0.580	0.6070	0.058
	0.400	0.040	0.560	0.6049	0.105
	0.400	0.060	0.540	0.6031	0.146
	0.400	0.080	0.520	0.6011	0.190
	0.400	0.100	0.500	0.5975	0.272
	0.400	0.170	0.430	0.5972	0.279
	0.650	0.010	0.340	0.6079	0.036
	0.650	0.025	0.325	0.6047	0.110
	0.650	0.040	0.310	0.6023	0.164
	0.650	0.050	0.300	0.6001	0.214
	0.650	0.085	0.265	0.5964	0.298
700°	0.400	0.020	0.580	0.6056	0.090
	0.400	0.040	0.560	0.6026	0.159
	0.400	0.060	0.540	0.6001	0.214
	0.400	0.080	0.520	0.5976	0.270
	0.400	0.100	0.500	0.5970	0.283
	0.400	0.170	0.430	0.5970	0.283
	0.650	0.015	0.335	0.6052	0.098
	0.650	0.030	0.320	0.6025	0.160
	0.650	0.050	0.300	0.5985	0.250
	0.650	0.070	0.280	0.5957	0.312
	0.650	0.080	0.270	0.5958	0.315
	0.650	0.090	0.260	0.5956	0.308
	0.650	0.110	0.240	0.5957	0.312

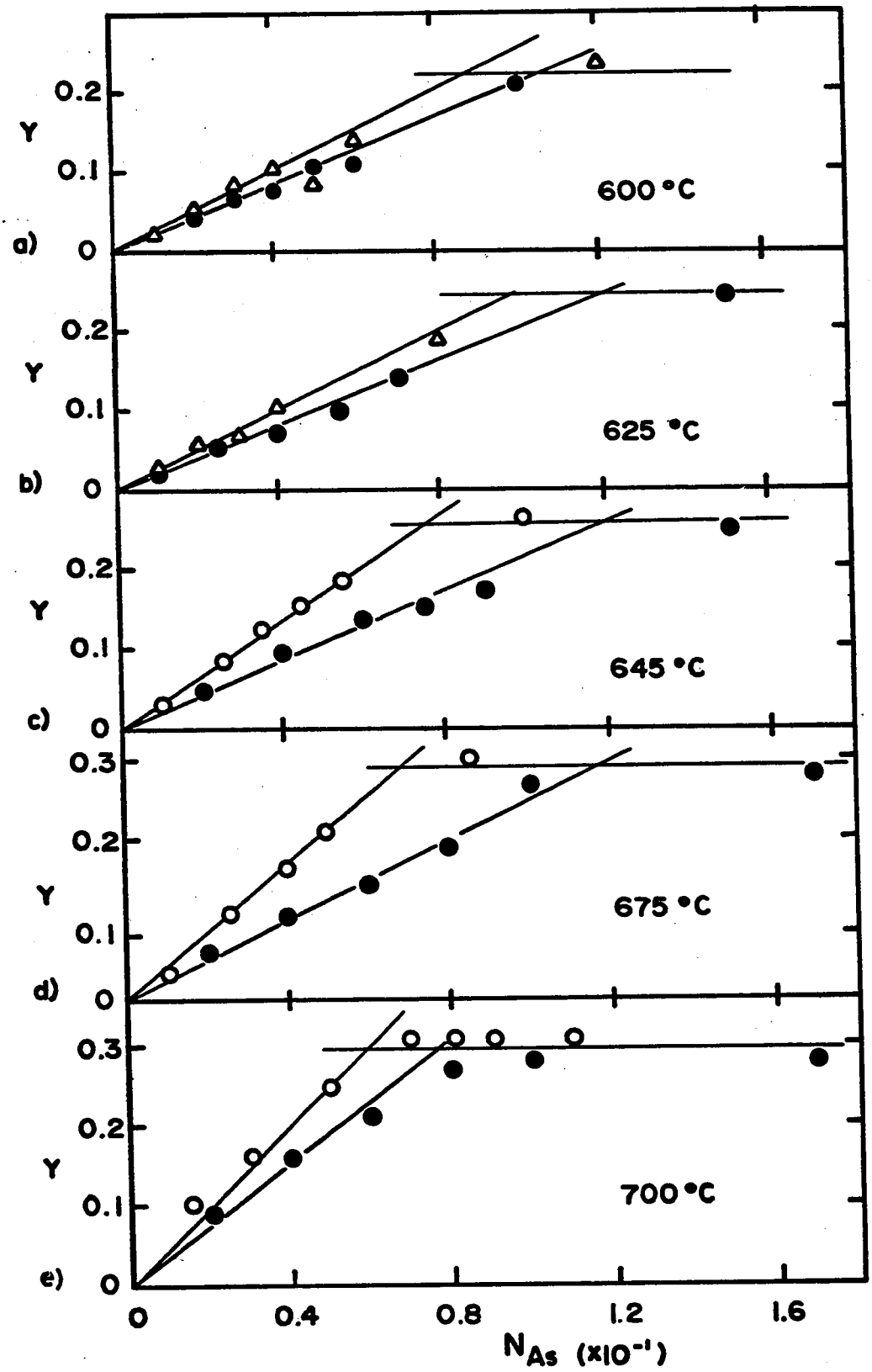

Fig. 10-2 Relations between the GaSb-rich solid phase in equilibrium and the arsenic concentration for constant values of the gallium concentration.

● N_{Ga} = 0.40 △ N_{Ga} = 0.60 ○ N_{Ga} = 0.65

samples contained in the two-phase fields: the open circles represent N_{Ga} = 0.65 and the solid circles, N_{Ga} = 0.40. From the graph it is then possible to obtain the limiting tie-line which is a boundary to the three-phase field at that temperature. The value of the common GaSb-rich composition provides one coordinate on the pseudobinary line of the ternary diagram, and the intersection of the line of each series with the horizontal line yields a value for the arsenic concentration which, when coupled to the gallium concentration of each series, supplies the second coordinate that completely locates the limiting tie-line on the section of the diagram. This limiting tie-line appears as a dash-dotted line on the diagram of figure 10-1e and on all others (figures 10-1 a to d) for these temperatures tested.

From the graphs of figure 10-2 it is also possible to obtain information about the range of the miscibility gap discussed previously. An attempt was made in chapter 8 to define the boundaries of that miscibility gap on the pseudobinary section below the peritectic temperature. But it was seen that in order to anneal samples in a two-phase solid-solid field, the times required were of the order of months and could be expected to be longer with decreasing temperatures. The method of annealing samples with initial compositions off the pseudobinary section of the diagrams was found to be a convenient way of avoiding this difficulty as it ensured the presence of a liquid in the mixture during the annealing period, and this provided an adequate medium for diffusion and greatly reduced the anneal time.

Here, the boundary of the miscibility gap in the GaSb-rich section of the diagram is obtained from the compositions of the GaSb-rich solid phases in equilibrium within the three-phase triangles as it is known that these phases only solidify on the pseudobinary section. These data points also coincide with the intersection of the limiting tie-lines and the pseudobinary plane which yielded the composition of points on the boundary of the gap at given temperatures.

The information collected from figure 10-2 however, could yield only results about the GaSb-rich section of the diagram and in an effort to complete the characterization of this diagram, further measurements were carried out within the three-phase fields but with a choice of initial compositions such that they would yield the GaAs-rich solid phase in equilibrium in the solution. It was occasionally possible to see both solid phases in equilibrium in some samples and this provided a means of checking the state of equilibrium when the GaSb-rich phase was compared to the results collected above. The data concerning these latter measurements are included in table 10-II.

Upon a rapid inspection of the data in table 10-II it becomes obvious that only the method of anneals in the three-phase triangle can be used here in the determination of the GaAs-rich boundary of the miscibility gap. The technique of tie-lines with diagrams similar to those of figure 10-2 is ruled out because of the high GaAs content of the solid phases in equilibrium. Following an argument similar to the one used for the GaSb-rich end of the diagram it can be seen that the range of com-

Table 10-II Compositions of samples annealed in a three-phase field at temperature T and of equilibrium solid phases.

T	Initial Composition			a	Solid Composition
^{o}C	N_{Ga}	N_{As}	N_{Sb}	nm	y
600°	0.550	0.170	0.280	0.5668	0.95
625°	0.550	0.200	0.250	0.5663	0.97
675°	0.550	0.200	0.250	0.5662	0.97
				0.5977	0.27
689°	0.550	0.170	0.280	0.5673	0.94
				0.5988	0.24
700°	0.550	0.250	0.200	0.5662	0.97
700°	0.550	0.300	0.150	0.5657	0.99
724°	0.550	0.170	0.280	0.5678	0.92
725°	0.550	0.200	0.250	0.5662	0.97
				0.5958	0.31
*739°	0.550	0.170	0.280	0.5739	0.72

* this point is likely to lie outside the three-phase triangle.

positions of GaAs-rich solid phases in equilibrium is so restricted that it would be impossible to plot intersections of the types in figure 10-2. Therefore, the technique of annealing samples within the three-phase fields is the only one available here. The results obtained are plotted on figure 10-3.

There is, however, one exception to the results tabulated in table 10-II. After a close reevaluation of the predicted three-phase triangle at 739°C it was found that the sample tested had an initial composition which lay possibly outside the three-phase field and therefore the results obtained would define a tie-line in the two-phase field rather than the GaAs-rich solid phase in equilibrium in the three-phase field. Nevertheless, if that tie-line is not the limiting tie-line, then it must be very close to it and it shows that the upper limit in composition for the gap at that temperature is at most y = 0.72. This result however, does not appear on figure 10-3.

From the analysis carried out for the GaAs-rich end of the diagram it is still possible to locate the position of the remaining boundary of the three-phase fields and this is treated in the following section.

10.2.3 Position of the cusp in the ternary diagram

The presence of a cusp on the liquidus sheet of the ternary diagram has been introduced in chapter 9 where its position was shown on graphs displaying the relationship between the temperature and the arsenic

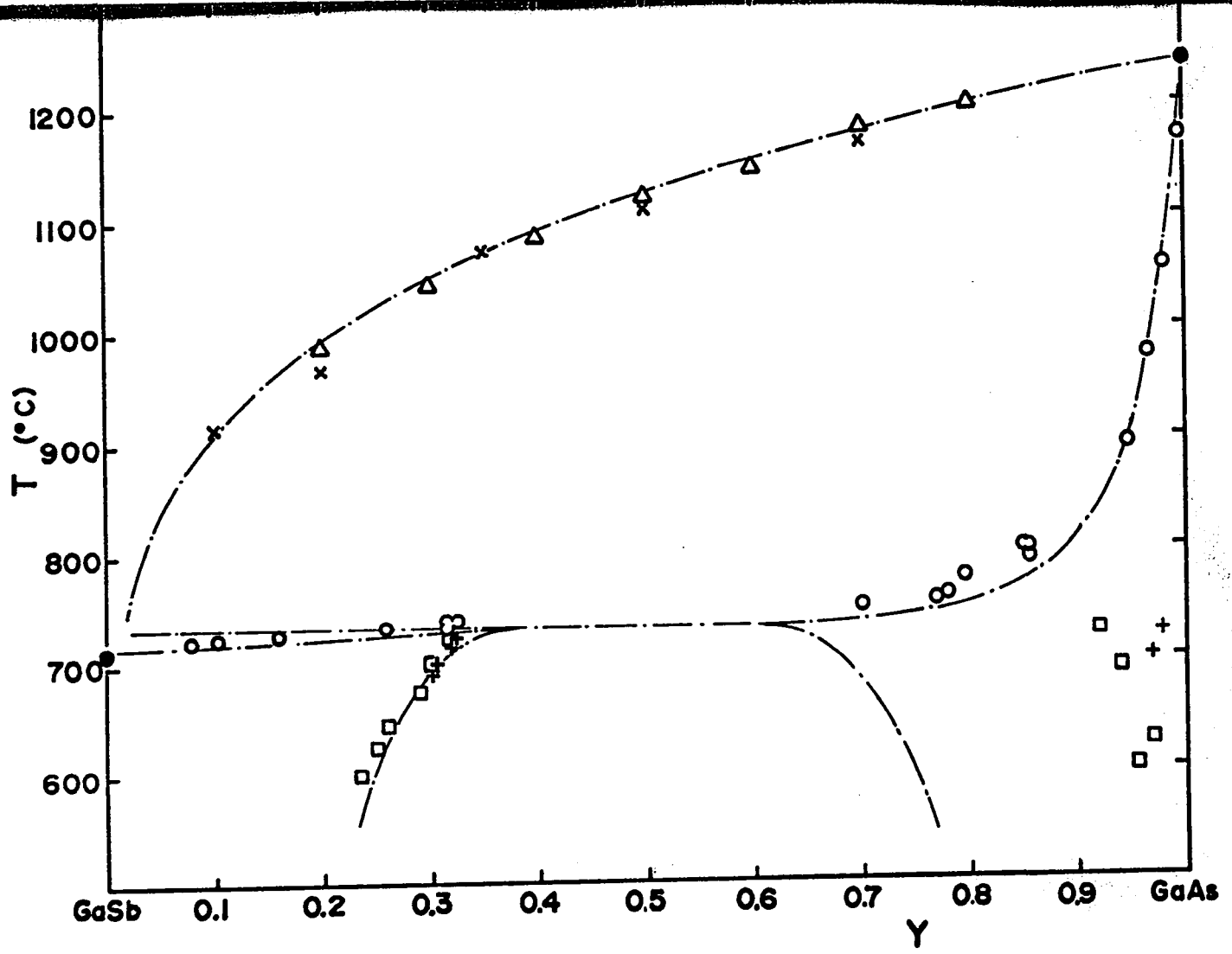

Fig. 10-3 Phase diagram for the pseudobinary system $GaAs_ySb_{1-y}$.

- ○ solidus data from liquid-solid equilibrium
- \+ solidus data from solid-solid equilibrium
- □ solidus data from liquid-solid-solid equilibrium
- —.— simple solution model
- △ Ref. 72Fl
- × Ref. 70Il
- ● Ref. 69Ll

concentration for various values of N_{Ga}. From the present analysis however, it has been found more convenient to use a different representation which yields a better overall picture of both experimental results and theoretical predictions.

The experimental results are obtained from the diagrams of figures 10-1: the position of the cusp is given by the intersection of the limiting tie-line and the relevant liquidus isotherm or, in other words, the liquidus end of the limiting tie-line. For the cases where $N_{Ga} > 0.50$, the liquidus isotherm is so close to the edge of the composition triangle that the intersection is taken to be on that edge. Below $N_{Ga} = 0.50$, this intersection can only be defined for temperatures above 675°C where the liquidus isotherms are seen to be away from the edge of the triangle (figures 10-1 d and e), but at lower temperatures, it is impossible to define clearly the liquidus end of any tie-line which falls in the Sb-rich corner of the diagram because of the presence of a eutectic valley which does not allow for a reasonable determination of the proper liquidus isotherm. Therefore, in that region of the diagram, it is impossible to define the position of the cusp.

With the experimental determination of the position of the cusp at each temperature it is then possible to draw the third boundary of the three-phase fields by joining this position on the diagram to the composition value of the GaAs-rich solid phase in equilibrium in the three-phase field on the pseudobinary plane. However, for the lower temperatures mentionned above, this boundary can only be drawn arbitrarily (figures 10-1 a to c).

Figure 10-4 shows the relations between the temperature and the gallium concentration for the cusp both experimentally and theoretically. The predicted curve T vs. N_{As} is also included to allow for locating on the ternary diagram but it is impossible to draw its experimental counterpart.

The experimental results are seen to be slightly above the calculated values for $N_{Ga} > 0.20$. Below this value, neither the tie-lines nor the boundaries of the three-phase fields can be determined accurately because of the eutectic valley and no experimental points appear in that region of the diagram. The predicted position of the cusp is also seen to be symmetrical about $N_{Ga} = 0.50$ but the presence of the eutectic valley is likely to interfere with this behaviour at low temperatures.

10.3 Experimental and Calculated Pseudobinary Section $GaAs_ySb_{1-y}$

The pseudobinary section is represented in figure 10-3 for both the experimental data collected throughout this work and the theoretical treatment of the simple solution model. The theoretical fit to the experimental results is satisfactory for the two liquid-solid phase fields except that the predictions give a peritectic temperature of 732°C rather than the experimental value estimated at 745°C. The case of the solid-solid field is different: the boundary in the GaSb-rich region is well reproduced by the calculations but the situation is different for the GaAs-rich region. The theoretical treatment used here must give symmetrical

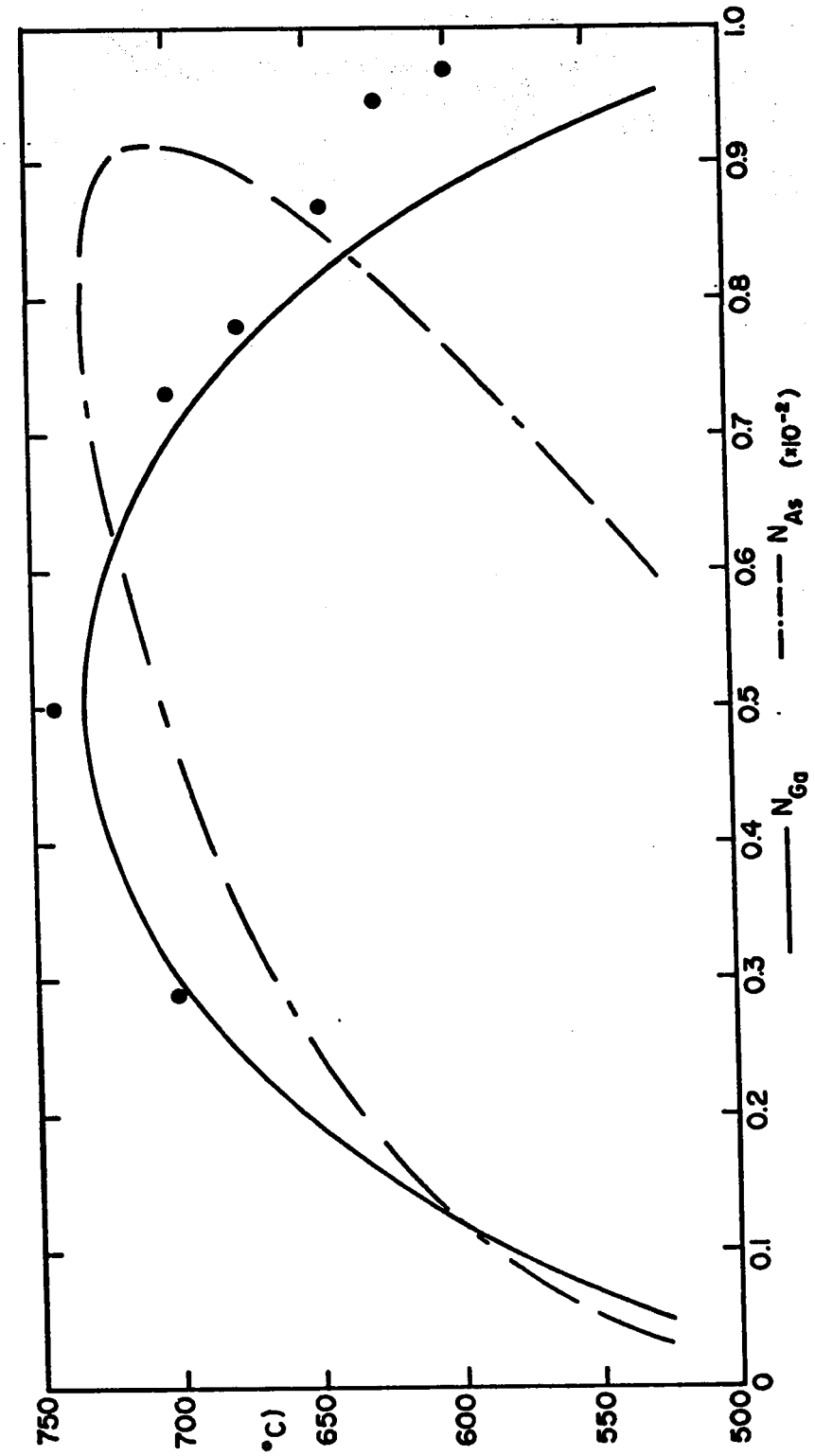

Fig. 10-4 Theoretical position of the cusp on the liquidus sheet of the Ga-As-Sb system. The solid circles are the experimental results.

boundaries about y = 0.5 for a miscibility gap and this stems from the fact that the interaction parameters (α's) are independent of composition but it can be seen that the experimental observations deviate greatly from any symmetrical behaviour about y = 0.5. Therefore, as with the Ga-In-Sb system, the simple solution model appears to give poor agreement with experimental data concerned with solid phases.

Finally, possible changes to the temperature dependence of the interaction parameters will be discussed in the following chapter as it could provide a solution for the discrepancy between experiment and theory.

10.4 Discussion

Despite the differences that were reported between the predicted and experimental results, the simple solution model still accounts for reasonable predictions: the results from the study of tie-lines are consistent with the presence of three-phase fields in the ternary diagram and with the existence of a miscibility gap in the pseudobinary section. The peritectic behaviour is predicted with the proper range of phase separation on the pseudobinary section except that the reported temperature is higher than the calculated one. The presence of a cusp on the liquidus sheet is also predicted by the model but displays symmetry about N_{Ga} = 0.50 and is slightly lower than the experimental values except for concentrations below N_{Ga} = 0.20 where it is presently impossible to conclude on the behaviour of the phase diagram due to a eutectic valley.

The main discrepancy between the present experimental results and theory is in the GaAs-rich limit of the miscibility gap. Thus the experimental data need to be considered carefully here. One possibility to be considered is that even though sharp X-ray lines were observed for these phases, equilibrium value had not been reached. In such a case, considerably longer times of annealing would be required. However, it should be noted that annealing for various lengths of time, up to several months, of samples on the pseudobinary section gave results in reasonable agreement with those from samples in the three-phase fields annealed for much shorter times. If the equilibrium values were very different from the experimental data, bigger discrepancies between different experimental results might be expected.

If, however, the simple solution model is at fault and not the experimental investigations, then a reevaluation of some of the parameters may provide the adjustments needed to reach agreement between theory and experiment. The following chapter will present new experimental data from recently published analyses and discuss possible changes in order to improve the theoretical treatment.

Chapter 11 Recent developments and suggestions

11.1 Introduction

11.2 Miscibility Gap in $GaAs_ySb_{1-y}$

11.3 The Simple Solution Model

11.4 Conclusion

11.1 Introduction

The growth technique by epitaxial layer has generated, in recent years, renewed interest for the characterization of III-V ternary systems because of their possible use as electronic devices. In the past year, experimental results have been published on the subject and it is the aim of this chapter to look at the implications of some of these results in order to compare with those already presented in this study.

11.2 Miscibility Gap in $GaAs_ySb_{1-y}$.

Nahory et al. (77N1) have disucssed the occurrence of a peritectic behaviour on the pseudobinary section $GaAs_ySb_{1-y}$. Using the simple solution approach to fit the calculated liquidus isotherms to their experimental data they have concluded that if a miscibility gap exists, then the maximum range will be $0.38 \leqslant y \leqslant 0.45$. However, they have departed from the strictly simple solution model by introducing a compositionally dependent interaction parameter similar to a previous analysis by Wu and Pearson (72W1), and they have adopted the form

$$\alpha_{As-Sb} = aN_{Sb} + b.$$

A more recent publication by Waho et al. (77W1) in a short note claims that, over the range $0.3 < y < 0.9$, homogeneous epitaxial layers can be grown by molecular beam epitaxy. These latter findings would

appear to be in disagreement with the conclusions presented here. However, the fact remains that after observations on a wide selection of $GaAs_ySb_{1-y}$ samples (in excess of 200 - different samples by the author plus all other observations by members of this laboratory), there has never been a trace of the presence of any phase in the range $0.38 < y < 0.61$ for samples grown from the melt. Nevertheless, the results of Waho et al. must be considered. One possibility is that the single phase samples they obtained represent a metastable condition. Such metastable solid solutions have been previously reported for samples of Ge-GaSb produced by very rapid cooling of small samples (Duwez et al. 60D1).

Since the annealing experiments made on samples on the pseudobinary section have shown two-phase separation and those made on samples with initial compositions off the pseudobinary section have demonstrated clearly the presence of three-phase fields, it indicates the existence of a miscibility gap, and if the results of Waho et al. represent equilibrium conditions, then this miscibility gap would have to be a closed gap rather than an open gap as indicated above. Hence, this would require that the solidus curve be a smooth curve and not show a peritectic behaviour.

If these phases reported by Waho et al. are in fact equilibrium phases and there is no peritectic behaviour of the $GaAs_ySb_{1-y}$ alloys system then the evidence of the abrupt phase change in directionally frozen ingots would have to be interpreted as follows: a closed miscibility gap would have to be situated very close to the solidus curve

so that in the range $0.35 < y < 0.70$ the temperature difference between the solidus line and the boundary of the two-phase solid-solid field would be $10^{\circ}C$ or less. When growing an ingot in a directional freeze furnace, the temperature fluctuations at the freezing interface may be such that the melt will oscillate between the two-phase liquid-solid field above the solidus curve and the two-phase solid-solid field below the boundary of the miscibility gap. This process would then contribute to the formation of two distinct phases which may be observed in ingots grown from the melt (refer to chapter 3).

Because the crystallization process is relatively slow in melt growth, the phase separation occurs within the two-phase solid-solid field as the phases tend to equilibrium and therefore it is possible that stable phases may not be formed on directionally frozen ingots if the alloy system possesses a closed miscibility gap situated near the solidus curve on the phase diagram.

Presently, members of this research group are involved with the verification of the peritectic behaviour of the alloy system $GaAs_ySb_{1-y}$. Samples with initial compositions situated on the pseudobinary section and within the two-phase liquid-solid fields are being annealed for periods of three days at temperatures that are regulated to one quarter of a degree. The first few samples have demonstrated that equilibrium had been reached in each case as the X-ray powder photographs displayed sharp diffraction lines of the solid phase in equilibrium. The preliminary result would tend to support the argument that a peritectic behaviour is

to be expected. The experimental data collected up to date are listed in table 11-I and plotted in figures 8-1 and 10-3.

Table 11-I Experimental data for the redetermination of the solidus curve of $GaAs_ySb_{1-y}$.

Initial Composition y_i	T ^oC	a nm	Solidus Composition y
0.02	720	0.6059	0.080
0.05	724	0.6050	0.105
0.15	734	0.5982	0.260
0.20	740	0.5953	0.320

11.3 The Simple Solution Model

It was recognized throughout this study that the simple solution model was rather unsuccessful at predicting the solidus data for two ternary systems namely: Ga-In-Sb and Ga-As-Sb. However, it may be possible to improve the model by attempting a reevaluation of the interaction parameter which is characteristic of the solid-solid solution. Such an analysis was suggested by the fact that one of the alloy systems studied here displayed two-phase solid-solid equilibrium and experimental data were available to test any new relationship for $\alpha_{GaAs-GaSb}$. (The author is grateful to Dr. G. B. Stringfellow for bringing this to his attention).

Strictly speaking, the simple solution model assumes that any interaction parameter is linearly dependent upon temperature but from the general principle for solid equilibrium it can be shown that this yields a symmetrical miscibility gap providing of course that such a condition prevails for the system under consideration. Equations 5.6.5 may be rewritten in the general form as follows:

$$\mu_M = \mu_M^o + RT \ln \gamma_M x \qquad 11.3.1a$$

$$\mu_N = \mu_N^o + RT \ln \gamma_N (1 - x) \qquad 11.3.1b$$

Hence if the two-phase solid-solid equilibrium is considered between the solid compositions x_1 and x_2, then the conditions for equilibrium are governed by

$$\mu_{M_1} = \mu_{M_2} \qquad 11.3.2a$$

and

$$\mu_{N_1} = \mu_{N_2} \qquad 11.3.2b$$

equations 11.3.1 and 11.3.2 combine to give

$$\ln \gamma_{M_1} x_1 = \ln \gamma_{M_2} x_2 \qquad 11.3.3a$$

$$\ln \gamma_{N_1} (1 - x_1) = \ln \gamma_{N_2} (1 - x_2) \qquad 11.3.3b$$

In the solid solution, the relation between the activity coefficients and the interaction parameter is given by

$$RT \ln \gamma_M = \alpha(1 - x)^2 \qquad 11.3.4a$$

$$RT \ln \gamma_N = \alpha x^2 \qquad 11.3.4b$$

When equations 11.3.3 and 11.3.4 are combined, the result gives

$$\alpha_1(1 - x_1)^2 - \alpha_2(1 - x_2)^2 = RT \ln x_2/x_1 \qquad 11.3.5a$$

$$\alpha_1 x_1^2 - \alpha_2 x_2^2 = RT \ln (1 - x_2)/(1 - x_1) \qquad 11.3.5b$$

Now, if there is only one solid interaction parameter for a specific system (i.e. $\alpha_1 = \alpha_2 = \alpha$), then at any given temperature provided α is independent of composition, the relation α/RT is constant. Equations 11.3.5 may therefore be rewritten as:

$$A\left[(1 - x_1)^2 - (1 - x_2)^2\right] = \ln x_2/x_1 \qquad 11.3.6a$$

$$A\ (x_1^2 - x_2^2) = \ln (1 - x_2)/(1 - x_1) \qquad 11.3.6b$$

Dividing 11.3.6a by 11.3.6b yields

$$\frac{(1 - x_1)^2 - (1 - x_2)^2}{(x_1^2 - x_2^2)} = \frac{\ln x_2/x_1}{\ln (1 - x_2)/(1 - x_1)} \qquad 11.3.7$$

Letting the two solid phases in equilibrium be symmetrical about $x = 0.5$ gives

$$x_1 = 0.5 - \delta \quad \text{and} \quad x_2 = 0.5 + \delta$$

and replacing in equation 11.3.7 makes each side identically equal to -1 thus confirming the symmetrical behaviour of x_1 and x_2 about $x = 0.5$ for any given temperature. The value of A tends to 2 as δ approaches zero.

The formalism therefore yields a symmetrical curve with a maximum at $\alpha/RT = 2$. The extent of the phase separation is obtained when $\alpha/RT > 2$, and, for the cases where $\alpha/RT < 2$, there are no real solutions to equations 11.3.6. Finally, at a temperature such that the maximum is above the solidus curve, there is an open miscibility gap that signifies a eutectic or peritectic behaviour.

However, since it is observed experimentally that the miscibility gap for the system $GaAs_ySb_{1-y}$ is asymmetrical, it becomes clear that a dependence on composition has to be investigated. In order to do so, the dependence of α_1 and α_2 is to be reconsidered. After simple algebra is applied to equations 11.3.5, the relations become

$$\alpha_1 = RT \quad \frac{[x_2^2 \ln x_2/x_1 - (1 - x_2)^2 \ln (1 - x_2)/(1 - x_1)]}{(x_2 - x_1)(x_2 + x_1 - 2x_1x_2)} \qquad 11.3.8a$$

and

$$\alpha_2 = RT \quad \frac{[x_1^2 \ln x_2/x_1 - (1 - x_1)^2 \ln (1 - x_2)/(1 - x_1)]}{(x_2 - x_1)(x_2 + x_1 - 2x_1x_2)} \qquad 11.3.8b$$

When the experimental values for the boundaries of the miscibility gap at various temperatures are substituted in equations 11.3.8, it is possible to obtain a variation for $\alpha_{GaAs-GaSb}$ as a function of composition of solid only. Figure 11-1 shows this variation which may be written as:

$$\alpha_{GaAs-GaSb} = 17200 + 9000 \ y^4 \quad J.mol^{-1}$$

A similar type of analysis was carried out on the pseudobinary section of the Ga-In-Sb system. The values of $\alpha_{GaSb-InSb}$ were taken from figure 7-8 and the corresponding temperatures were matched with the solidus compositions on the phase diagram (figure 7-1). The relation obtained for $\alpha_{GaSb-InSb}$ as a function of solidus composition is plotted in figure 11-2 along with a reasonable fit to the curve which again displays a quartic dependence upon composition of solid; the value of $\alpha_{GaSb-InSb}$ becomes

$$\alpha_{GaSb-InSb} = 1500 + 562\, x^4 \qquad J.mol^{-1}$$

The final step was then to test the values of $\alpha_{GaAs-GaSb}$ and $\alpha_{GaSb-InSb}$ deduced in the above treatment against the experimental solidus data available. For the Ga-As-Sb system, there were still large discrepancies especially near the expected peritectic temperature. For the Ga-In-Sb system, it was impossible to reproduce the experimental solidus isoconcentration lines of figure 7-15. In the latter case, a computer analysis was designed to reproduce each solidus isoconcentration line individually and the results were plotted in the form of $\alpha_{GaSb-InSb}$ as a function of temperature for various solidus compositions. The final results indicated again that there is no simple dependence of the solid-solid interaction parameter upon either temperature or solidus composition but that in fact it is likely to depend upon both in no simple manner.

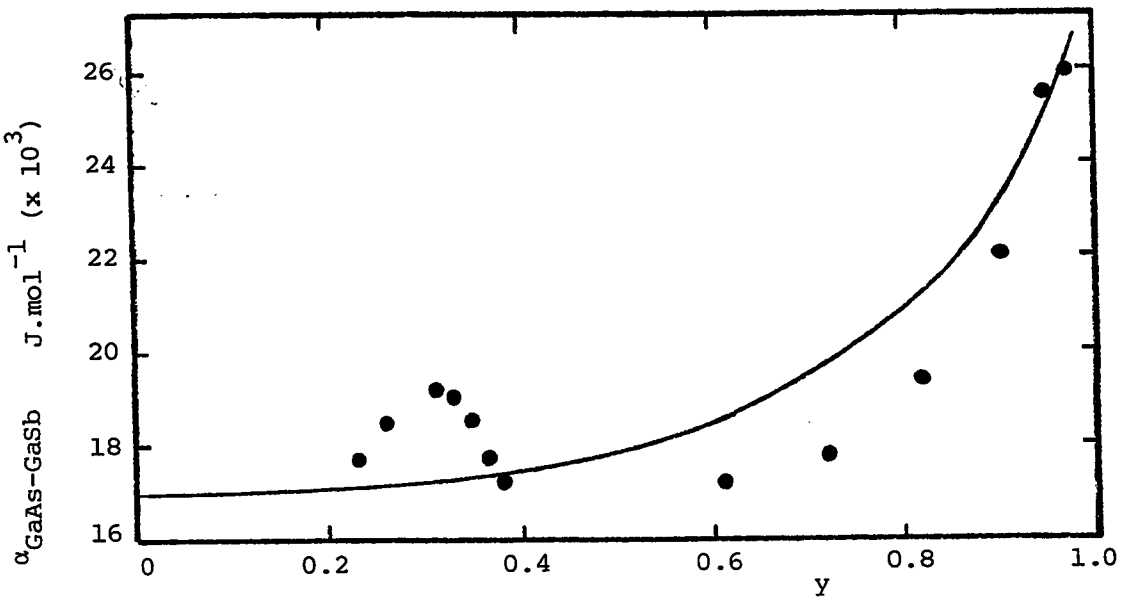

Fig. 11-1 $\alpha_{GaAs-GaSb}$ vs. y_{solid}. The solid circles are the values from equations 11.3.8. The line comes from the relation $\alpha_{GaAs-GaSb} = 17200 + 9000\ y^4$.

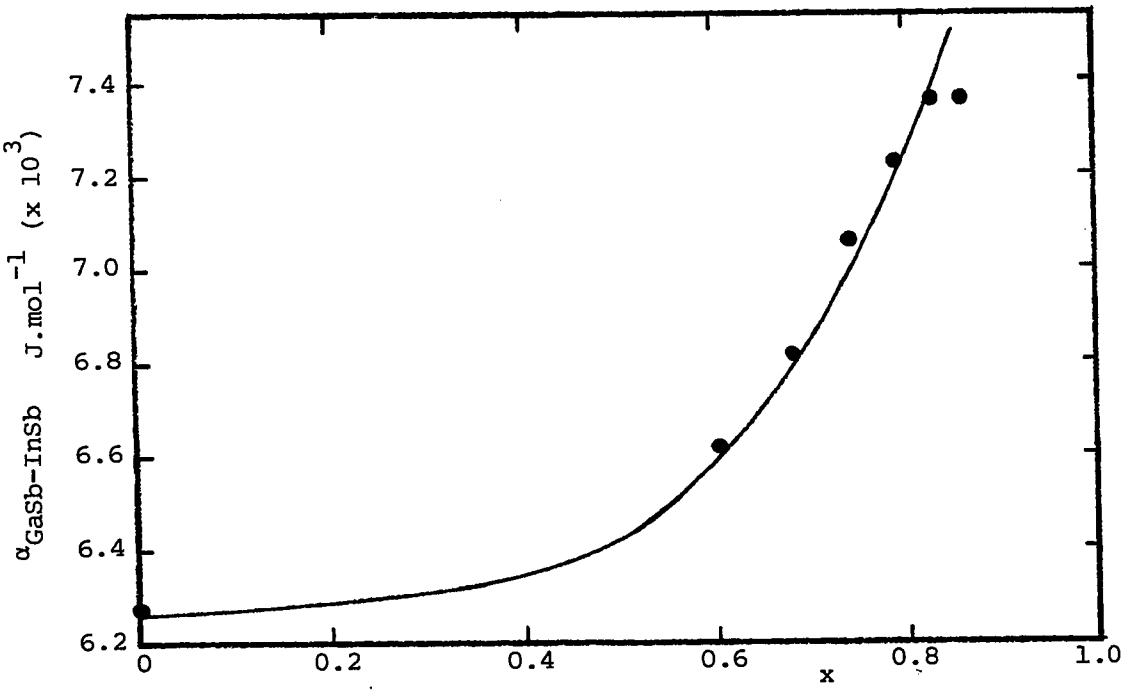

Fig. 11-2 $\alpha_{GaSb-InSb}$ vs. x_{solid}. The solid circles are the values from figure 7-8. The line comes from the relation $\alpha_{GaSb-InSb} = 6276 + 2351\ x^4$.

11.4 Conclusion

It is therefore obvious that more solid phase data are required and especially for the Ga-As-Sb system in order to proceed to a more detailed analysis of the possibilities of the simple solution model in characterizing ternary phase diagrams of III-V alloys.

Chapter 12 Summary

Investigations of the preparation of single phase specimens of the pseudobinary alloy system $GaAs_ySb_{1-y}$ have led to an extensive study of the phase diagrams of some ternary III-V systems.

The occurrence of a miscibility gap in the range of solid solutions has suggested a pseudobinary phase diagram that shows a peritectic behaviour since the gap was found to be an open gap. A departure from Vegard's law in the GaAs-rich end of that range was also observed. This behaviour therefore, is quite different from the simpler systems investigated earlier, namely: $Ga_xIn_{1-x}Sb$, $Ga_xIn_{1-x}As$ and $InAs_ySb_{1-y}$.

The analysis was then extended further to compositions off the pseudobinary section in order to characterize the ternary phase diagram of some of these alloys. The systems Ga-In-Sb and Ga-As-Sb were the object of studies both theoretical and experimental. A theoretical treatment, the simple solution model, developed by Guggenheim was reinterpreted by using new values of the interaction parameters which were also justified in this study, in an attempt to predict the ternary phase diagrams of concern here. Experimental data were also collected in order to test the theory as it was developed.

The analysis of the results revealed that the simple solution

model was rather successful at predicting the liquidus data but that for the alloys studied here it was sometimes difficult to reproduce the solidus data. It must be emphasized however, that the treatment used here was strictly the simple solution model, that is the various interaction parameters were solely dependent upon temperature (except for $\alpha_{GaAs-GaSb}$ which was chosen constant), but it has been recognized at a later stage of the research that a possible improvement to the model would be to consider the solid-solid interaction parameters as dependent upon both temperature and solidus composition. Unfortunately, this dependence does not seem to be, a priori, simple.

The reasons for carrying out the types of measurements that were described in this study are severalfold. The characterization of $GaAs_ySb_{1-y}$ was obvious in itself. For the Ga-In-Sb system, very little solidus data had been reported off the pseudobinary section and the study of solidus isoconcentration lines as well as tie-lines offered a good opportunity to supplement the ternary phase diagram. This system also proved to be quite useful in testing the efficiency of the theoretical treatment to be used later for a more complicated system: Ga-As-Sb. Finally, the characterization of the solidus isoconcentration lines was also devised to help locate starting compositions in liquid phase epitaxy growth, a project soon to be started in this laboratory.

For the Ga-As-Sb system, practically nothing had been reported on the ternary phase diagram until very recently. The presence of a miscibility gap on the pseudobinary section suggested the existence of

three-phase fields, and an investigation of the properties of the ternary phase diagram was in itself reason enough to investigate such a system. Recent developments however, have also suggested that alloys of $GaAs_ySb_{1-y}$ may be used as radiation sources for optoelectronic telecommunications.

There is of course a considerable amount of work that could be carried out on the two ternary systems studied here. More solidus data will have to be collected in each case in an attempt to improve the theoretical model. The eutectic valleys present in each diagram could be investigated and the theoretical treatment adjusted accordingly.

The peritectic behaviour should be reinvestigated by the light of the results of Waho et al., and there is still some uncertainty on the limits of the miscibility gap for $GaAs_ySb_{1-y}$. Very little is known of the high temperature isothermal sections for Ga-As-Sb and much work remains to be done in order to characterize its solidus isoconcentration lines.

However, the recent interest shown for alloys of Ga-As-Sb in optoelectronics should now favour growth of specimens by epitaxial layer and this, in turn, should provide a valuable technique in collecting experimental observations for studying the phase diagram of this and other alloy systems.

APPENDIX A Experimental techniques

A.1 Introduction

A.2 Furnaces

A.3 Quartz Ampoules

A.4 Growth of GaSb and InSb

A.5 Powdering

A.6 X-Ray Powder Photography

A.1 Introduction

The purpose of this appendix is to describe various experimental techniques used for this type of research. It is certain that not all techniques will be discussed as some of them require standard procedure: X-ray powder photographs, spark cutting or diamond saw cutting of samples, crystal growth methods are all described either in the literature or in the proper context of this work. However, sample preparation, quartz encapsulating, specimen powdering, furnace wiring along with other methods often require a special "twist" or "trick" in order to be successful. It is the wish of the author that the following descriptions may be of some use to future workers in the field.

A.2 Furnaces

Among the various equipment used in the project, furnaces had to be the most temperamental of all; built from a relatively standard design they always had a "knack" for burning out at most critical times. The melting furnaces were naturally most often subject to such defects as they were usually run at temperatures almost beyond the softening points of the heating elements. Lifetimes as short as five hours were experienced with melting furnaces running at temperatures around 1230^{o}C when preparing samples of Ga-As-Sb.

The various types of furnaces were basically constructed

following a conventional design. The element consists of a winding of Kanthal wire (1 mm in diameter) over an alumina tube (5 mm wall - 39 mm I.D.). The winding is then coated with insulating cement (Kyanex); asbestos ribbon was also introduced between two layers of cement but the lifetime of the furnace was not increased significantly on the two attempts made - the one advantage however, was that the desired temperatures were attained with less power. The heating assembly is then mounted in an aluminum box which in turn is filled with vermiculite. The one important feature in building such a furnace is in the winding of the heating element: for instance, a melting furnace will average one turn per centimetre in the middle third of the winding and two turns per centimetre in the outer thirds. The mid-section is so designed in order to maintain a uniform hot zone inside the furnace.

When these furnaces break down, it is usually due to the formation of 'hot spots' on the heating element where a high resistivity center is created thus producing very high temperatures which results in the melting of the element at that point and of adjacent turns also. The temperature is so high that in one case it was possible to observe the melting of the alumina tube. Figure A-1 and A-2 show respectively, the experimental set up of annealing furnaces with the temperature controlling units and the effect of a 'hot spot' on the heating element assembly.

Fig. A-1 Annealing furnaces assemblies.

Fig. A-2 Section of a heating element. At left, the heat released with the formation of a 'hot spot' has burnt the element and melted the alumina tube.

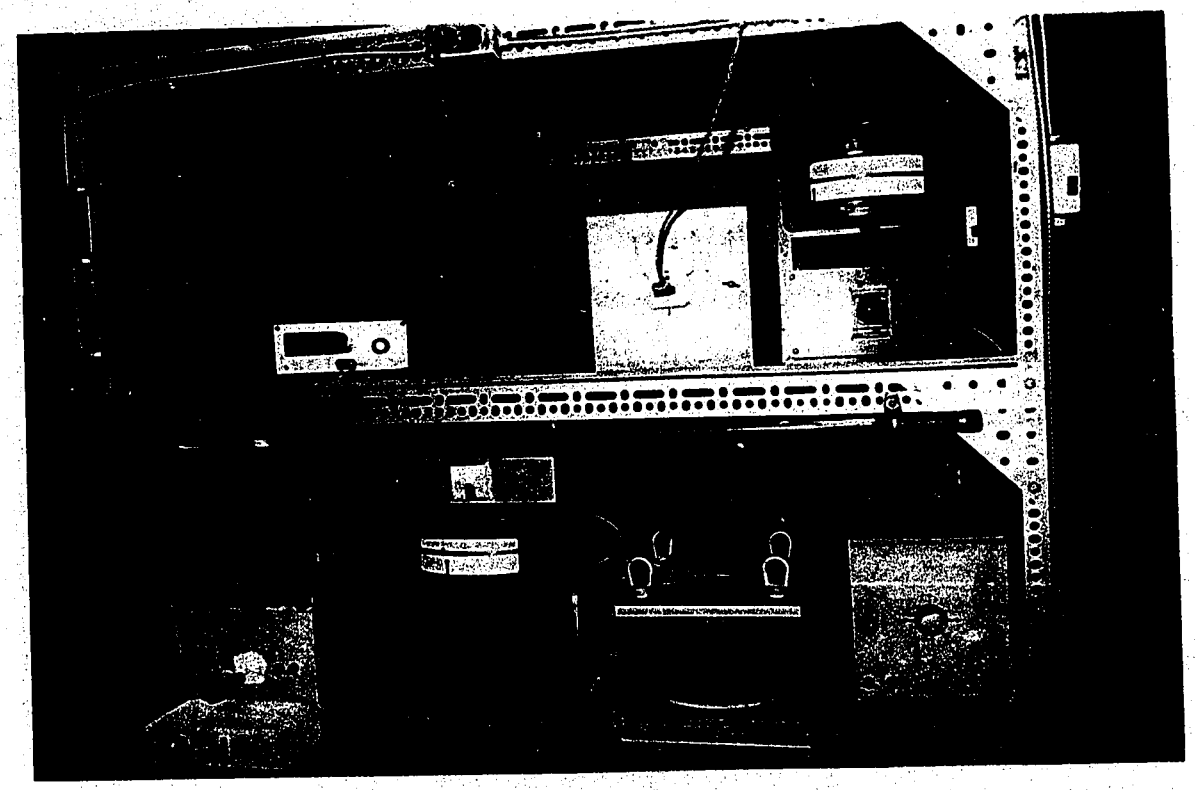

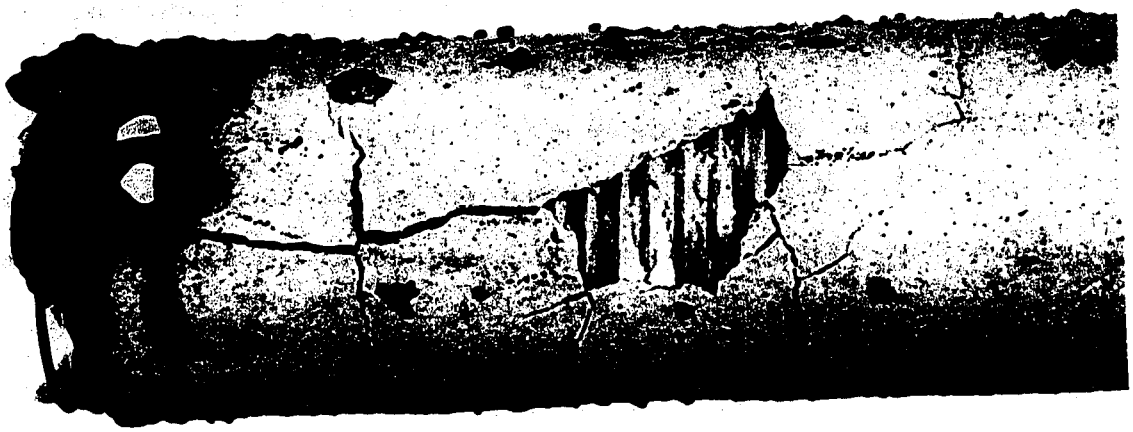

A.3 Quartz Ampoules

In order to be successful with encapsulating samples in quartz ampoules, there are a few rules to follow, and the two most important are the choice of quartz tubing and the choice of torch and flame. It was found after various attempts that according to the desired shape of sample the smallest size tube possible is best with walls strong enough to resist either the atmospheric pressure or the internal vapour pressure when the ampoules are heated. The torch and flame is also important to ensure uniform and fast sealing. In this work, an oxyacetylene torch was used for all quartz work. A flame of adequate temperature and size had to be used and this could only be achieved with the proper choice of tip and gas mixtures. In all cases, a neutral to oxidizing flame was used; more can be found in welding textbooks on the use of such torches (e.g. Lanouette et Gratton 58L1).

The presence of white oxide which forms on the outside of the ampoule may be minimized by the proper choice of flame but it can be removed by reheating the surface, however, care must be exercised in order not to melt the quartz or collapse the ampoule if it has been previously evacuated. Figure A-3 shows two ampoules after the initial melting of the charge.

Finally, whenever an ampoule has to be evacuated and back-filled with argon gas, it must be 'necked' before sealing. In this operation, the inside diameter of the tube is reduced to form a narrow neck by heating all around the section of the tube to be reduced and letting the

walls collapse; it is important here to use as little stretching as possible otherwise the walls at the neck would be too thin and the sealing operation would become virtually impossible. The ampoule is then evacuated and back-filled and under this reduced pressure, the neck is heated and the sealing is completed very rapidly. Figure A-4 shows the sequence of the 'necking' operations.

A.4 Growth of GaSb and InSb

This section is only included to provide a helpful hint when growing GaSb or InSb. When preparing these compounds by simple quenching, the quartz ampoule should be kept in a horizontal position during quenching as the charge will otherwise crack the ampoule when it freezes.

A.5 Powdering

Since most samples studied here were submitted to tests in the powder form, it was essential to design a technique that would be simple and efficient. The solution proved to be an improved method of utilizing a mortar and pestle (ceramic). The sample was initially broken into small pieces and then covered with 99% ethanol and reduced to a fine powder. This technique eliminated losses due to shattering and yielded powder grains less than 5μm (compared with 5μm aluminum oxide polishing powder).

Fig. A-3 Two samples after initial melting.

Fig. A-4 'Necking' sequence of a quartz ampoule containing a sample.

Fig. A-5 X-ray diffraction photograph of a sample of Ga-As-Sb. Lines N = 3 and 8 show the asymmetry due to poor alignment of the sample with the incident beam.

Fig. A-8 X-ray diffraction photograph of a sample of Ga-As-Sb. The low angle lines show the asymmetry and the spotted results indicate either the absence of rotation and/or the coarseness of the powder.

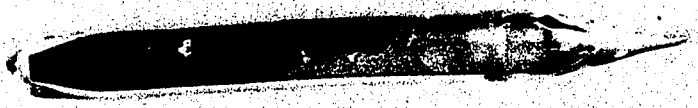

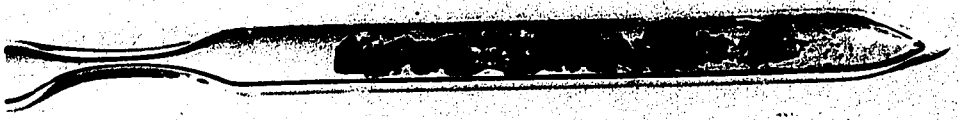

1 cm

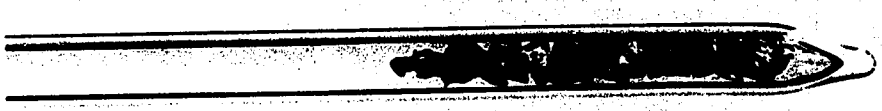

A-4

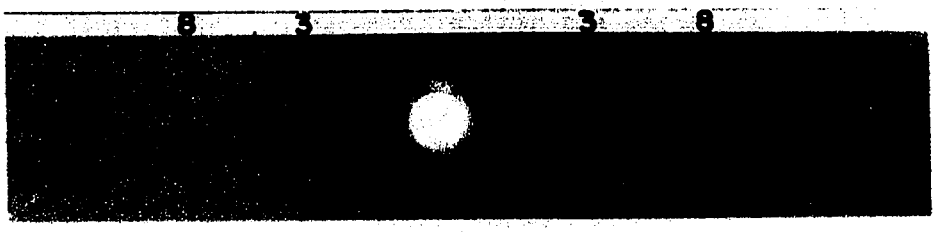

A-5

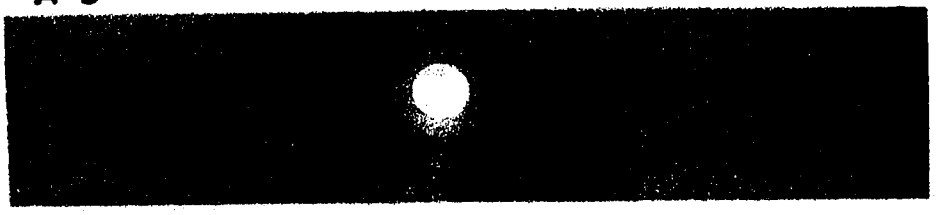

A-8

Another similar technique was used for samples with free gallium. The samples of the ternaries Ga-In-Sb and Ga-As-Sb with compositions off the pseudobinary section yielded alloys with some free gallium which made the powdering impossible as the alloy was too soft and would only deform under the action of the pestle rather than break into pieces. In order to solve that problem, the ingot was immersed in liquid nitrogen, then cracked; the pieces were then covered with more liquid nitrogen and powdered. This last method involved no greater difficulties than the first one and the grain sizes obtained were similar.

A.6 X-ray Powder Photography

The aim of this section is not to repeat a technique which is already well-known but to bring clarification on the method used to mount the samples in the camera: the powder is mixed in apiezon grease and a thin coat is applied on a quartz fiber, it is then heated (exposed to a 60 watts light bulb) in order to soften the paste and produce a smoother, more uniform layer. Because of this final step it is possible to obtain a relatively uniform atomic absorption relation from sample to sample.

There can be difficulties arising from a misalignment or improper positioning of the film inside the camera. Most of the low angle lines asymmetry comes from a misalignment of the axis of rotation relative to the incident beam of X-rays. The situation may be observed

in the photograph of figure A-5 where the low angle line N = 3 shows such a behaviour, that is, a strong line on the right but a faint doublet on the left, however the high angle lines remain unaffected. The explanation is schematized in figure A-6 where ray ① of low intensity is diffracted and ray ② of higher intensity is also diffracted to produce the observed doublet. Ray ③ is diffracted and gives a dark line. Ray ④ of low intensity is too weak to be diffracted and is absorbed by the sample thus producing the asymmetry in that low angle line.

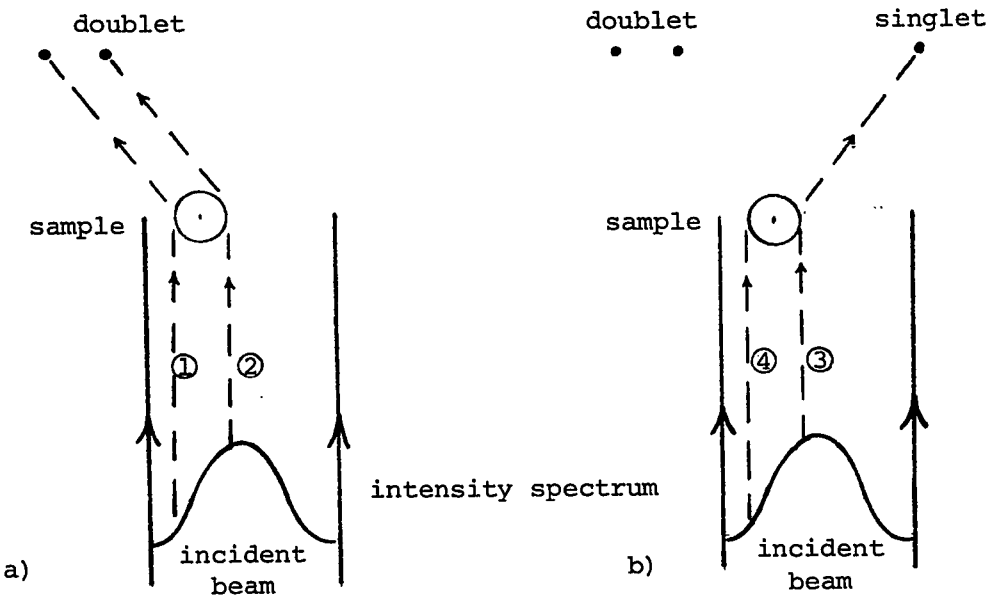

Fig. A-6 Diagram representing the X-ray paths when asymmetry of low angle lines is observed. In (a) both rays are diffracted, in b) ray ④ is absorbed completely

There are also the cases where the axis of rotation and the axis of the fiber are displaced with respect to one another: if the axis of rotation is misaligned relative to the X-ray beam then the low angle

lines will show asymmetry and variations in intensity on either side of $\theta = 0^{\circ}$. The case is schematized in figure A-7 and a typical photograph is given in figure A-8. Again, for the high angle lines the effect is very small and practically undetectable.

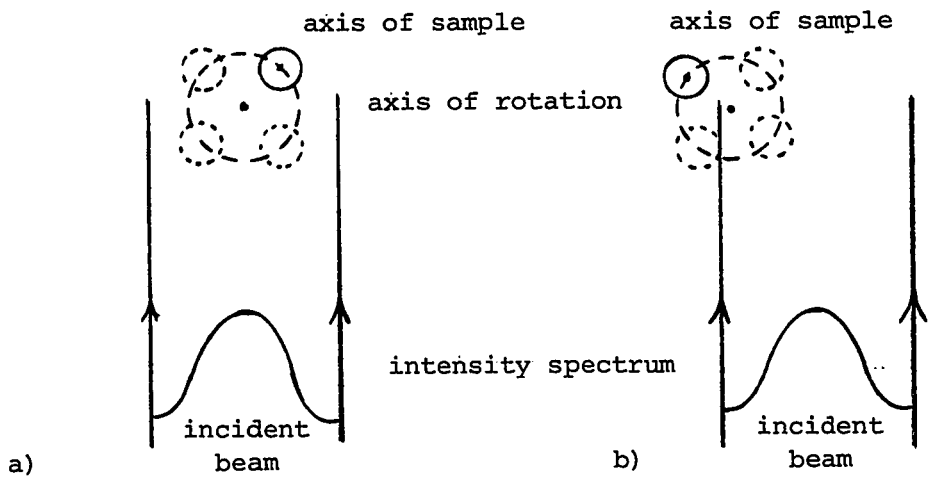

Fig. A-7 Diagram showing the axis of the fiber displaced relative to the axis of rotation. In (a) the axis of rotation is aligned with the X-ray beam and it simulates a thick sample of low density. In (b), the misalignment produces the asymmetries and variations in intensity of the low angle lines.

There are other special techniques that were used in the course of this work but it would be too long to give a full report on each one. The aim of this appendix was only to recall some of the most useful and intricate methods which made either the preparation of samples or the interpretation of results easier.

APPENDIX B Derivation of Vieland's equation for liquid-solid equilibrium

In this appendix, the formalism introduced by Vieland (63V1) is developed in detail for solid-liquid equilibrium.

The free energy change ΔF accompanying the transfer of one gram-atom of crystal AB to the melt with which it is in equilibrium at temperature T is given by

$$0 = \Delta F = 0.5 \left[F_A^o + RT \ln (1 - x) \nu_{A(1-x,\ T)} + F_B^o + \right.$$

$$\left. + RT \ln x \, \nu_{B(x,\ T)} \right] - F_c \qquad \text{B.1}$$

where F_c is the free energy of the crystal per g-atom and ν is the activity coefficient.

When a quantity of solid is heated to the melting point, melted and then cooled to the initial temperature it is possible to consider the following sequence of processes:

(1) one g-atom of crystal is heated from temperature T to the melting point T_m. ΔF_1 is given by the relations

$$\left(\frac{\partial F_c}{\partial T}\right)_p = -S_c \qquad \text{B.2}$$

and $$S_c = [S_c]_{T_m} - \int_T^{T_m} C_c \frac{dT}{T} \qquad \text{B.3}$$

where C_c is the specific heat of the crystal.

(2) the crystal is melted at T_m; $\Delta F_2 = 0$.

(3) the liquid is cooled from T_m to T. The free energy change is given as in step (1) by substituting the specific heat of the liquid.

If $C_\ell - C_c = \Delta C_p$ = constant, the sum of the free energy changes $\Sigma\Delta F$ may be expressed as follows:

for (1) $$S_c = [S_c]_{T_m} - \int_T^{T_m} C_c \frac{dT}{T} \qquad \text{B.4}$$

for (3) $$S_\ell = [S_\ell]_{T_m} + \int_{T_m}^{T} C_\ell \frac{dT}{T} \qquad \text{B.5}$$

Integrating from $T \rightarrow T_m$ in B.4 and from $T_m \rightarrow T$ in B.5 yields

$$F_1 = - [S_c]_{T_m} \int_T^{T_m} dT + C_c \left[\int_T^{T_m} \ell n\, T_m\, dT - \int_T^{T_m} \ell n T\, dT \right]$$

$$F_1 = - [S_c]_{T_m} (T_m - T) + C_c \left[(T_m - T) - T(\ell n\, T_m - \ell n T) \right] \qquad \text{B.6}$$

$$F_3 = -[S_\ell]_{T_m} \int_{T_m}^{T} dT - C_\ell \left[\int_{T_m}^{T} \ell nT \, dT - \int_{T_m}^{T} \ell n \, T_m \, dT \right]$$

$$F_3 = [S_\ell]_{T_m} (T_m - T) - C_\ell \left[(T_m - T) - T(\ell n \, T_m - \ell n \, T) \right] \quad B.7$$

Summing B.6 and B.7 gives

$$\Sigma\Delta F = \{[S_\ell]_{T_m} - [S_c]_{T_m}\} (T_m - T) - (C_\ell - C_c) \left[(T_m - T) - \right.$$

$$\left. - \; T(\ell n \, T_m - \ell n \, T) \right]$$

$$\Sigma\Delta F = \Delta S_F (T_m - T) - \Delta C_p \left[(T_m - T) - T(\ell n \, T_m - \ell n \, T) \right] \quad B.8$$

where ΔS_F is the entropy of fusion per g-atom. Now from

$$\Delta F = 0 = 0.5 \left[F_A^o + RT \, \ell n \, (1 - x) \, \nu_{A_{(1-x, \, T)}} \right.$$

$$\left. + \; F_B^o + RT \, \ell n \, x \, \nu_{B_{(x, \, T)}} \right] - F_c \quad B.9$$

which gives

$$F_c - 0.5 \, (F_A^o + F_B^o) = \frac{RT}{2} \left[(\ell n \, \nu_{A_{(1-x, \, T)}} \, \nu_{B_{(x, \, T)}} + \ell n \, x(1 - x) \right] \quad B.10$$

one can write

$$\Sigma\Delta F = 0.5 \left[F_A^o + RT \, \ell n \, 1/2 \, \nu_{A_{(0.5, \, T)}} + F_B^o + RT \, \ell n \, 1/2 \, \nu_{B_{(0.5, \, T)}} \right]$$

$$- \; F_c(T) = \Delta S_F (T_m - T) - \Delta C_p \left(T_m - T - T \, \ell n \, \frac{T_m}{T} \right) \quad B.11$$

or

$$\frac{RT}{2} \ln 1/2\nu_{A_{(0.5,\ T)}} + \frac{RT}{2} \ln 1/2\ \nu_{B_{(0.5,\ T)}} - \frac{RT}{2}\ln\ (1-x)\,\nu_{A_{(1-x,\ T)}}$$

$$- \frac{RT}{2} \ln x\ \nu_{B_{(x,\ T)}} = \Delta S_F(T_m - T) - \Delta C_p(T_m - T - T \ln \frac{T_m}{T}) \qquad \text{B.12}$$

$$\frac{RT}{2} \ln \left[\frac{1}{2}\ x\ \frac{1}{2}/(1-x)x\right] + \ln \frac{\nu_{A_{(0.5,\ T)}}\ \nu_{B_{(0.5,\ T)}}}{\nu_{A_{(1-x,\ T)}}\ \nu_{B_{(x,\ T)}}}$$

$$= \Delta S_F\ (T_m - T)\ -\ \Delta C_p(T_m - T - T \ln \frac{T_m}{T}) \qquad \text{B.13}$$

$$\ln \frac{1}{4x(1-x)} + \ln \frac{\nu_{A_{(0.5,\ T)}}\ \nu_{B_{(0.5,\ T)}}}{\nu_{A_{(1-x,\ T)}}\ \nu_{B_{(x,\ T)}}}$$

$$= \frac{2\Delta S_F}{R}\ (\frac{T_m}{T} - 1)\ -\ \frac{2\Delta C_p}{RT}\ (T_m - T\ - T \ln \frac{T_m}{T}) \qquad \text{B.14}$$

For a regular solution, the excess free energy of the melt may be expressed as

$$F^E = RT\ [(1-x)\ \ln \nu_A + x \ln \nu_B] \qquad \text{B.15}$$

or from the quasi-chemical theory of liquids (52G1)

$$F^E = x(1-x)w \qquad \text{B.16}$$

where w is an interchange energy.

Using $\overline{F}^E_A = F^E - x\ \frac{\partial F^E}{\partial x}$

where

$$x\ \frac{\partial F^E}{\partial x} = RT\ (-\ x \ln \nu_A + \ x \ln \nu_B)$$

and

$$x \frac{\partial F^E}{\partial x} = xw - 2x^2 w \quad .$$

one finds the following two solutions:

$$\overline{F}_A^E = RT \ln A \qquad \text{B.17a}$$

and

$$\overline{F}_A^E = x^2 w \qquad \text{B.17b}$$

Similarly, using

$$\overline{F}_B^E = F^E + (1 - x) \frac{\partial F_E}{\partial x}$$

where

$$(1 - x) \frac{\partial F^E}{\partial x} = RT \left[- (1 - x) \ln \nu_A + (1 - x) \ln \nu_B \right]$$

and

$$(1 - x) \frac{\partial F^E}{\partial x} = \left[(1 - x) (1 - 2x) w \right]$$

again, one obtains two solutions:

$$\overline{F}_B^E = RT \ln \nu_B \qquad \text{B.18a}$$

and

$$\overline{F}_B^E = w(1 - x)^2 \qquad \text{B.18b}$$

It is then possible to combine B.14 with B.17 and B.18 to give

$$\ln \frac{1}{4x(1 - x)} + \frac{w}{RT} \left(\frac{1}{2}\right)^2 + \frac{w}{RT} \left(\frac{1}{2}\right)^2 - \frac{w}{RT} x^2 - \frac{w}{RT} (1 - x)^2 =$$

$$\frac{2\Delta S_F}{R} \left(\frac{T_m}{T} - 1\right) - \frac{2\Delta C_p}{RT} \left(T_m - T - T \ln \frac{T_m}{T}\right) \qquad \text{B.19}$$

or

$$\ell n \frac{1}{4x(1-x)} + \frac{w}{RT}\left(-\frac{1}{2} + 2x - 2x^2\right) = \frac{2\Delta S_F}{R}\left(\frac{T_m}{T} - 1\right)$$

$$- \frac{2\Delta C_p}{RT}\left(T_m - T - T\,\ell n \frac{T_m}{T}\right) \qquad \text{B.20}$$

which in turn becomes

$$\frac{R}{2}\ell n \frac{1}{4x(1-x)} = \Delta S_F\left(\frac{T_m}{T} - 1\right) - \frac{\Delta C_p}{T}\left(T_m - T - T\,\ell n \frac{T_m}{T}\right)$$

$$+ \frac{w}{T}(x - 0.5)^2 \qquad \text{B.21}$$

$$\frac{R}{2}\ell n \frac{1}{4x(1-x)} = \left(T_m \Delta S_F - T_m \Delta C_p\right)\left(\frac{1}{T} - \frac{1}{T_m}\right)$$

$$+ \Delta C_p \ell n \frac{T_m}{T} + \frac{w}{T}(x - 0.5)^2 \qquad \text{B.22}$$

and finally, when the ΔC_p terms are neglected:

$$w = \frac{1}{(x - 0.5)^2}\left[\Delta S_F(T - T_m) - \frac{RT}{2}\ell n\, 4x(1-x)\right] \qquad \text{B.23}$$

If equation B.23 is solved for w in terms of the difference between the ideal liquidus calculated from a knowledge of ΔH_f (or $T_m\ \Delta S_F$) and the experimental phase diagram, then:

$$w_i = \frac{1}{(x - 0.5)^2}\left[\Delta S_F(T_i - T_m) - \frac{RT_i}{2}\ell n\, 4x(1-x)\right] \qquad \text{B.24}$$

$$w_{exp} = \frac{1}{(x - 0.5)^2}\left[\Delta S_F(T_{exp} - T_m) - \frac{RT_{exp}}{2}\ell n\, 4x(1-x)\right] \qquad \text{B.25}$$

subtracting B.24 from B.25 yields

$$w = w_{exp} - w_i = \frac{1}{(x - 0.5)^2} \left[\Delta S_F (T_{exp} - T_m - T_i + T_m) - \frac{R}{2} (T_{exp} - T_i) \ln 4x(1 - x)\right]$$

or finally,

$$w = \frac{\Delta S_F (T_{exp} - T_i)}{(x - 0.5)^2} \left[1 - \frac{R}{2\Delta S_F} \ln 4x(1 - x)\right] \qquad \text{B.26}$$

which is the formulation of Vieland. Equation B.26 was used by Schottky and Bever (58S1) to test for a constant w which leads to equation B.16. However, equation B.23 is the form used by most workers for the simple solution model.

REFERENCES

1935

G1 E. A. Guggenheim, Proc. Roy. Soc. (London), A148, 304.

1949

P1 S. A. Pogodin and S. A. Dubinsky, Izvest. Sektora. Fiz. Khim. Anal. 17, 204.

1952

G1 E. A. Guggenheim, 'Mixtures', Oxford University Press, Oxford.

H1 W. Hume-Rothery, J. W. Christian and W. B. Pearson, 'Metallurgical Equilibrium Diagrams', The Institute of Physics, London.

L1 T. S. Liu and E. A. Peretti. Trans. Am. Soc. Metals 44, 539.

1953

L1 T. S. Liu and E. A. Peretti, Trans. Am. Soc. Metals 45, 677.

1954

P1 I. Prigogine and R. Defay, 'Chemical Thermodynamics', Longmans, Green and Co., London.

1955

B1 J. Bednar and K. Smirous, Czech. J. Phys. 5, 546.

G1 I. G. Greenfield and R. L. Smith, J. Metals 7, 351.

K1 W. Koster and B. Thoma, Z. Metallk. 46, 293.

K2 W. Koster and B. Thoma, Z. Metallk. 46, 291.

1956

S1 C. H. Shih and E. A. Peretti, Trans. A.S.M. 48, 706.

1958

G1 G. Giesecke and H. Pfister, Acta. Cryst. 11, 369.

H1 M. Hansen, 'Constitution of Binary Alloys', McGraw-Hill, New York.

L1 Y. Lanouette et Y. Gratton, 'Le Soudage Oxyacétylénique', Service des Cours par Correspondance, Ministère de l'Education, Canada 3e Edition.

S1 W. F. Schottky and M. B. Bever, Acta. Met. 6, 320.

W1 J. C. Woolley and B. A. Smith, Proc. Phys. Soc. (London) 72, 214.

1959

W1 J. C. Woolley and D. G. Lees, J. Less Common Metals 1, 192.

1960

D1 P. Duwez, R. H. Willens and W. Klement, Jr., J. Appl. Phys. 31, 1500.

1962

C1 F. Claisse and C. Samson, 'Advances in X-ray Analysis', Plenum Press, New York, p. 335.

T1 F. A. Trumbore, P. E. Freeland and A. D. Mills, J. Electrochem. Soc. 109, 1.

W1 J. C. Woolley, 'Compound Semiconductors' (R. K. Willardson and H. L. Goering, Editors), Vol. 1, p. 3, Reinhold Publ. Corp.

1963

H1 R. N. Hall, J. Electrochem. Soc. 110, 385.

V1 L. J. Vieland, Acta. Met. 11, 137

1964

K1 A. G. Kalyuzknaya, I. K. Polushina and D. N. Tret'yakov, Russ. J. Inorg. Chem. 9, 813.

M1 O. Madelung, 'Physics of III-V Compounds', J. Wiley and Sons., Inc., New York, London, Sidney.

M2 E. G. Muller and J. L. Richards, J. Appl. Phys. 35, 1233.

P1 R. F. Potter and D. L. Stierwalt, Proc. 7th Int. Conf. Semicon. Phys. Paris, p. 1111

T1 C. D. Thurmond, J. Phys. Chem. Solids, 26, 785.

1965

S1 M. E. Straumanis and C. D. Kim, J. Electrochem. Soc. 112, 112.

1967

A1 J. R. Arthur, J. Phys. Chem. Solids 28, 2257.

B1 J. P. Bros, R. Castanet et M. Lafitte, Compt. Rend. 264, Série C, 1804.

D1 L. S. Darken, Trans. Met. Soc. AIME 239, 80.

D2 L. S. Darken, Trans. Met. Soc. AIME 239, 90.

1968

M1 G. J. Macur, R. K. Edwards and P. G. Wahlbeck, J. Phys. Chem. 72, 1047.

S1 N. N. Sirota, 'Semiconductors and Semimetals' Willardson-Beer, Vol. 4, Academic Press, New York and London.

S2 N. N. Sirota and E. Ye. Matyas, Vest. Akad. Nauk. Beloruss. SSR. 5, 106.

1969

C1 R. B. Clough and J. J. Tietjen, Trans. Met. Soc. AIME 245, 583.

I1 M. Ilegems and G. L. Pearson, 'Proceedings of 1968 Symposium on GaAs, The Institute of Physics and The Physical Society, London, p. 3.

L1 B. D. Lichter and P. Sommelet, Trans. AIME 245, 99

L2 B. D. Lichter and P. Sommelet, Trans. AIME 245, 1021.

S1 G. B. Stringfellow and P. E. Greene, J. Phys. Chem. Solids 30, 1779.

1970

A1 G. A. Antypas and L. W. James, J. Appl. Phys. 41, 2165.

I1 J. Inoue, K. Osamura and V. Murakami, Suiyokwaishi 17, 71.

J1 A. S. Jordan, Met. Trans. 1, 239.

P1 J. C. Phillips and J. A. Van Vechten, Phys. Rev. B2, 2147.

T1 M. B. Thomas, W. M. Coderre and J. C. Woolley, Phys. Stat. Sol. (a)2, K141.

V1 J. A. Van Vechten, Proc. 10th Int. Conf. Semicon. Phys. Cambridge, Mass., p. 602.

1971

B1 G. M. Blom and T. S. Plaskett, J. Electrochem. Soc. 118, 1831.

F1 L. M. Foster and J. F. Woods, J. Electrochem. Soc. 118, 1175.

P1 M. B. Panish and M. Ilegems, 'Proceedings of 1970 Symposium on GaAs'. The Institute of Physics and The Physical Society, London, p. 67.

S1 G. B. Stringfellow, J. Phys. Chem. Solids 33, 665.

1972

A1 G. A. Antypas, J. Cryst. Growth 16, 181.

F1 L. M. Foster and J. E. Woods, J. Electrochem. Soc. 119, 504.

L1 D. A. Landis, F. S. Goulding and B. V. Jarrett, Nucl. Inst. and Methods. 101, 127.

O1 K. Osamura, J. Inoue and Y. Murakami, J. Electrochem. Soc. 119, 103.

P1 M. B. Panish and M. Ilegems, 'Progress in Solid State Chemistry' (H. Reiss and J. O. McAldin, Editors), Vol. 7, p. 39, Pergamon Press, Oxford.

R1 S. D. Rosenbaum, Ph.D. Thesis, University of Ottawa, Ottawa, Ontario, Canada.

S1 G. B. Stringfellow, J. Phys. Chem. Solids 33, 665.

W1 T. Y. Wu and G. L. Pearson, J. Phys. Chem. Solids 33, 409.

1974

B1 R. F. Brebrick and R. J. Panlener, J. Electrochem. Soc. 121, 932.

I1 M. Ilegems and M. B. Panish, J. Phys. Chem. Solids 35, 409.

I2 M. Ilegems, M. B. Panish and J. R. Arthur, J. Chem. Thermodyn. 6, 157.

J1 A. Joullié, R. Dedies, J. Chevrier et G. Bougnot, Revue de Phys. Appl. 9, 455.

1975

J1 A. S. Jordan and M. E. Weiner, J. Phys. Chem. Solids 36, 1335.

1977

N1 R. E. Nahory, M. A. Pollack, J. C. DeWinter and K. M. Williams, J. Appl. Phys. 48, 1607.

W1 T. Waho, S. Ogawa and S. Maruyama, Japan. J. Appl. Phys. 16, 1875.